Nonlinear interactions and localisation phenomena in many-body ultracold atomic systems

Santiago Francisco Caballero Benítez

A thesis submitted for the degree of
Doctor of Philosophy of
The Australian National University

March, 2011

Declaration

This thesis is an account of research undertaken between October 2005 and March 2011 at The Nonlinear Physics Centre, Research School of Physics and Engineering of The Australian National University, Canberra, Australia. I was also affiliated with the Australian Research Council Centre of Excellence for Quantum-Atom Optics (ACQAO).

Except where acknowledged in the customary manner, this research presents my original results obtained under the supervision of Dr. Elena Ostrovskaya, and has not been submitted in whole or part for a degree in any university. The project that constitutes Chapter 2 was additionally undertaken under the mentoring of Dr. Rosario Paredes and Dr. Víctor Romero-Rochín, with the collaboration in the last section of Dr. Blas Rodríguez-Lara. The research introduced in Chapter 4 was performed in collaboration with Dr. Miklós Gulácsi and Dr. Joel Corney.

Santiago Francisco Caballero Benítez
March, 2011

Acknowledgements

I would like to acknowledge the excellent atmosphere to conduct research and complete my PhD in the ARC Centre for Excellence for Quantum-Atom Optics (ACQAO), the Nonlinear Physics Centre of the Australian National University (ANU). My time in both centres allowed me to develop many skills, and make invaluable friendships.

I want to thank the people who supported and guided me through my PhD, making it's completion possible. In this regard, I thank Dr. Elena Ostrovskaya who supervised me through the end of my PhD. Her brilliant guidance made possible to develop many ideas, while keeping objectives on track. Elena motivated me when I needed it the most and showed me the way to develop many skills and acquire knowledge efficiently. Her advice and ability to put things in perspective helped me greatly in those last two years, working with her was priceless. I also want to thank Dr. Miklós Gulácsí, who was my first supervisor during my PhD and took me to Australia and Germany believing in my potential to conduct research. His knowledge of many-body physics and condensed matter theory inspired me to learn as much as I could on these subjects and his patience and support have been invaluable.

I want to thank to thank Prof. Yuri Kivshar and Prof. Neil Manson, who supported me all these years and made possible my return to ANU after my recovery from illness. Their words of wisdom and encouragement helped me tremendously to get back on track and finish my PhD.

In the Nonlinear physics centre I want to acknowledge the useful discussions with Dr. Tristram Alexander and Dr. Chaohong Lee. While in the department the nice comments and wonderful sense of humour from my officemates, Jasur Abdullaev, Artur R. Davoyan, Dr. Andrey E. Miroshnichenko, Dr. Ivan Garanovich, Dr. David A. Powell, Dr. Anton Desyatnikov and Dr. Dragomir Neshev.

I wish to express my gratitude to the Max-Planck Institute for the Physics of Complex Systems (MPIPKS), where I spend more than one year of my PhD. My stay in the MPIPKS was very intense and the physics knowledge I acquired immense. The support of the people of the MPIPKS gave me while I went to visit the other "institutes" in Dresden is invaluable to me to this day. The help and friendship when I needed the most specially from Dr. Paula Riviere, Dr. Saul Ares, Dr. Sebastien Burdin and Dr. Aroon O'Brien.

When I was recovering from illness the people from the Physics Institute at the Universidad Nacional Autónoma de México (UNAM), opened the doors to me and helped me to integrate back to research. I would like to thank the support of Dr. Rocio Jáuregui, Dr. Víctor Romero-Rochín, Dr. Rosario Paredes Dr. Blas Rodríguez-Lara and Dr. Carlos Villarreal. During my stay we began a series of collaborations, which came to be a significant part of the work in my PhD thesis. To this day I deeply value their support, mentoring and friendship while I have been in Mexico.

The visit to the University of Queensland (UQ), thanks to ACQAO, made it possible to shape the BCS-BEC crossover project with the help of Dr. Joel Corney. The nice atmo-

sphere of the group in UQ allowed me to continue with that project and meet wonderful people, specially Dr. Murray Olsen and Dr. Karen Kheruntsyan.

During the long road to finish my PhD the friendship and useful dialogue with Dr. Andre Stoffel in the beginning of my PhD was very important and deeply appreciated. My life in Australia gave me the wonderful friendship of Kelly Roe, Tory Ludowici (additional thanks are in order for proof-reading the manuscript), Viktor Gal, Dr. Ryan Taylor, Dr. Amir Hadad, Andrew Connelly, Johnny Valbuena, Alex Deckers and Marc Deckers without them staying at the University House with me, I wouldn't have been able to be so productive and happy as they were my family while I was in Australia. My friends in Mexico cheered me up with their constant jokes and discussions about life when I needed them the most, specially Dr. Luis Felipe Gomez Lomeli, Brenda Rios, Federico Arriaga, La familia Capilla and Plutarco Elias Calles.

I would like to thank my family in Mexico, without the constant support of my parents Francisco and Araceli, and my sisters, Helga and Jessica, this wouldn't have been possible. Their kind words of motivation, advice, guidance and love made it possible for me to wake up everyday and complete this journey. The love and comprehension of my partner Martha Patricia Reveles Arenas, gave me the energy and happiness to get through the last two years.

Finally, all this would have not been possible without the financial support of the Mexican government by means of a CONACYT scholarship and the Research School of Physics and Engineering at ANU by means of a miscellaneous scholarship, I am grateful.

List of publications

[1] **"Intrinsic decoherence in an ultracold Bose gas confined in a double-well potential"**, S F Caballero-Benítez, V Romero-Rochín, and R Paredes. Journal of Physics B: Atomic, Molecular and Optical Physics, 43(9):095301, 2010.

[2] **"Delocalization to self- trapping transition of a Bose fluid confined in a double-well potential: an analysis via one- and two-body correlation properties"**, S F Caballero-Benítez, V Romero-Rochín, and R Paredes. Journal of Physics B: Atomic, Molecular and Optical Physics, 43(11):115301, 2010.

[3] **"Macroscopic quantum self-trapping of an ultracold BoseFermi mixture in a double-well potential"**, S F Caballero-Benítez, E A Ostrovskaya, M Gulácsí, and Yu S Kivshar. Journal of Physics B: Atomic, Molecular and Optical Physics, 42(21):215308, 2009.

[4] **"A three-site Bose-Fermi ring with a few atoms"**, Santiago F. Caballero-Benítez and Elena A. Ostrovskaya. Journal of Physics B: Atomic, Molecular and Optical Physics, 44(13):135301, 2011.

Abstract

The recent advances in trapping, cooling, and manipulation of alkali atoms have opened the possibility to create and study novel states of matter. The quantum nature of matter becomes relevant at ultracold temperatures and emergent phenomena, such as Bose-Einstein condensation (BEC), are strongly affected by the interaction between atoms and their statistics.

In this thesis we will address some of the physics in ultracold quantum gases, with Bose (Chapter 2, Refs. [1, 2] and Chapter 3, Ref. [3]) and Fermi statistics (Chapter 4), as well as ultracold Bose-Fermi mixtures (Chapter 3, Refs. [3, 4]). We will discuss phenomena driven by nonlinear interactions, such as, localisation, macroscopic quantum self-trapping, intrinsic decoherence, Mott insulating symmetry states, formation of broken symmetry states and the BCS-BEC crossover.

In this thesis new major results can be summarised as follows:

- The establishment of the relation between stationary states and decoherence originated from many-body interactions in double well bosonic systems, Chapter 2.
- The suppression or enhancement of localisation related phenomena (Superfluid and Mott-Insulator states or Macroscopic Quantum Self-trapping) in Bose-Fermi mixtures due to the presence of fermions and the interplay with many-body interactions in few site systems, Chapter 3.
- The mapping of the BCS-BEC crossover problem to a magnetic impurity problem in the BCS side of a Feshbach resonance, and the possible origin of the pseudo gap in strongly interacting ultracold fermion systems, Chapter 4.

In loving memory of Araceli and Papá Julio.

Contents

Introduction

Ultracold atomic quantum systems are dilute gases where the atoms have been trapped using electromagnetic fields [5]. The electromagnetic radiation interacts with the atoms coupling with their dipole moment and by different processes, one can confine the atoms in a region of space, with magnetic, electric and optical means or a combination of these means. Due to the confinement the process of evaporative cooling [6] can be implemented after laser cooling [7]. Thus, by lowering the trap depth, the most energetic atoms escape the trap and it is possible to reach temperatures of the order of 1-100 nK due to re-thermalisation. At these temperatures Bose-Einstein condensation (BEC) [8, 9] occurs for bosonic alkali atoms. In a Bose-Einstein condensate atoms macroscopically occupy the lowest energy state of the system. In an experiment, this is detected by a bi-modal distribution of atoms where a peak in the velocity distribution due to the fraction of the atoms that has condensed is surrounded by a thermal cloud of non-condensed atoms [see Fig. 1.1 (c)]. This new state of matter was demonstrated in 1995 by the groups of Cornell and Wieman, Hulet, and Ketterle [10–12]. The ultracold gases can be optically trapped using the Stark effect, by an intense standing wave of off-resonant light. The atoms effectively see a periodic potential, known as an optical lattice [13] [see Fig. 1.1 (a, b)]. Optical lattices present the possibility to study systems analogous to ionic lattices of solid state physics and thus study systematically microscopic models of strongly interacting particles.

In ultracold systems interactions can be manipulated by means of Feshbach resonances, and the geometry of the lattice can be controlled at will, as well as, the inclusion of defects. One can even address single sites and control the concentration of atoms across the optical lattice [15, 16]. Therefore they are ideal to mimic the physics of models of interacting particles from solid state physics, such as the Hubbard model [17] and the Bose-Hubbard model [18]. The study of these kind of models may lead to a greater understanding of the behaviour of complex phases of matter, such as the Hi-Tc superconductivity [19], quantum magnetism [20, 21] or properties of exotic phases, such as, the supersolid state [22–25] . Also, because of recent developments in the creation of artificial magnetic fields [26, 27], they could be used to investigate topological states of matter [28–30] and implement quantum computing algorithms resilient to decoherence [31, 32]. From the immediate practical point of view, applications of interacting ultracold atomic systems for metrology are currently being investigated [33–36].

The rich variety of behaviour investigated in these systems poses the difficult problem of addressing the above mentioned general questions. In order to gain some insight about the different aspects of the problems at hand, we concentrate on studying the following

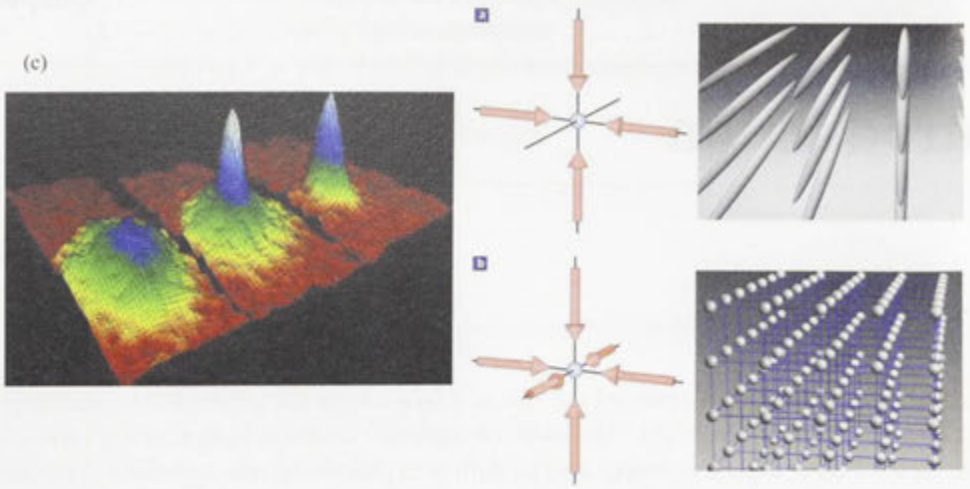

Figure 1.1: (a) In a 2D optical lattice, the atoms are confined to an array of tightly confining 1D potential tubes. (b) In the 3D case, the optical lattice can be approximated by a 3D simple cubic array of tightly confining harmonic oscillator potentials at each lattice site (Taken from [13]). (c) Images of the velocity distributions of the trapped atoms, taken by the expansion method. The left frame shows the velocity distribution just before the appearance of the Bose-Einstein condensate; the middle frame, just after the appearance of the condensate; the right frame, after further evaporation leaves a sample of nearly pure condensate. The field of view of each frame is 200 μm$\times$270μm, and corresponds to the distance the atoms have moved in about 1/20 s. The colour corresponds to the number of atoms at each velocity, with red being the fewest and white being the most. Areas appearing white and light blue indicate lower velocities (Taken from [14]).

questions regarding ultracold atomic systems:

- What are the effects of the many-body interaction in the ground-state of the system and the spectrum of excitations?
- What is the role of interactions in the formation of localised atomic states and symmetry breaking effects?

These questions are relevant to the study of ultracold atoms in the following aspects. The possibility to prepare states by manipulating interactions with useful configuration properties for the implementation of quantum computing protocols [37] and atomtronics [38–40]. Once we know the ground state and the spectrum of excitations we can formulate approximation schemes and study phenomena such as the transition from the quantum to the classical regime [41, 42], *decoherence*, understand mechanisms behind the selection of certain configurations in the ground state or formulate effective theories to explain and predict behaviour in experiments. The structure of the ground state has profound consequences on the transport properties of these systems where quantum phase transitions [43] might emerge and phenomena such as superfluidity [44] and the formation of insulating states [18, 45] are closely related.

We studied quantum degenerate systems that demonstrate a rich variety of behaviour depending on their statistics. In particular, we consider the many-body interaction in Bose systems, Bose-Fermi mixtures, and strongly interacting fermion systems. In such systems, the atoms of fermionic character (i.e. ^{6}Li or ^{40}K), or bosonic character (i.e. ^{87}Rb) are subject to a confining potential [5] in a chip [48], optical lattice [13], or magnetic trap [49]. We also assume that the interaction between atoms can be controlled by means of a Feshbach resonance [47, 50]. A Feshbach resonance occurs when, due to a external magnetic field, there is a difference in the potential seen by free atoms and bound states such that low energy particle collisions can be enhanced or suppressed [see Fig. 1.2 (c)]. The scattering length of the atoms effectively becomes dependent on the magnitude of the applied field [see Fig. 1.2 (d)] and one can manipulate the nature of the many-body interactions to be effectively repulsive or attractive [47, 50].

The systems under consideration in this thesis can be studied by analysing the following many-body Hamiltonians written in the second quantisation formalism [44].

The description of the Bose systems that we will study in Chapters 2 and 3, is based on the following Hamiltonian in second quantisation form,

$$\begin{aligned}\hat{\mathcal{H}}_{\text{bos}} &= \int_{\mathbb{R}^3} \mathrm{dx}^3 \hat{\psi}_b^\dagger(x) \left(\hat{T}_b + \hat{V}_{\text{trap}}^b\right) \hat{\psi}_b(x) \\ &+ \frac{1}{2}\int_{\mathbb{R}^6} \mathrm{dx}^3 \mathrm{dx}'^3 \hat{\psi}_b^\dagger(x)\hat{\psi}_b^\dagger(x') g_{bb}(x,x')\hat{\psi}_b(x')\hat{\psi}_b(x). \end{aligned} \tag{1.1}$$

where the fields: $\hat{\psi}_b^\dagger$ ($\hat{\psi}_b$) create (annihilate) bosonic atoms. The bosons obey canonic commutation algebra. The kinetic energy is denoted by $\hat{T}_b$ and the trapping potential is $\hat{V}_{\text{trap}}^b$, the integration is over 3 dimensional space. The interaction between bosons is a contact interaction, $g_{bb}(x,x') = g_{bb}\delta(x-x')$, which is assumed to be repulsive, and $g_{bb} \sim 4\pi\hbar^2 a_{bb}/m$, where a_{bb} is the s-wave scattering length between bosons.

The Bose-Fermi mixtures considered in Chapter 3 were studied by employing the following Hamiltonian describing fermions interacting with bosons,

$$\begin{aligned}\hat{\mathcal{H}}_{\text{mix}} &= \hat{\mathcal{H}}_{\text{bos}} + \int_{\mathbb{R}^3} \mathrm{dx}^3 \hat{\psi}_f^\dagger(x) \left(\hat{T}_f + \hat{V}_{\text{trap}}^f\right) \hat{\psi}_f(x) \\ &+ \int_{\mathbb{R}^6} \mathrm{dx}^3 \mathrm{dx}'^3 \hat{\psi}_b^\dagger(x)\hat{\psi}_b(x') g_{bf}(x,x')\hat{\psi}_f^\dagger(x')\hat{\psi}_f(x). \end{aligned} \tag{1.2}$$

where we have considered spin-polarised fermions, effectively spin-less, because they all have the same spin. The fields $\hat{\psi}_f^\dagger$ ($\hat{\psi}_f$) create (annihilate) fermionic atoms and obey anti-commutation algebra. The kinetic energy of the fermions is denoted by $\hat{T}_f$ and the trapping potential seen by the fermions is $\hat{V}_{\text{trap}}^f$, note that the trapping potential seen by the fermions and the bosons is not necessarily the same. The interaction between different species is the last term in the above expression. This inter-species interaction is assumed to be of contact nature such that $g_{bf} = g_{bf}\delta(x-x')$, can be attractive or repulsive and $g_{bf} \sim 4\pi\hbar^2 a_{bf}/m_R$, where $m_R = m_b m_f/(m_b+m_f)$ is the reduced mass and a_{bf} is the s-wave scattering length between atoms of different species.

The strongly interacting fermions described in Chapter 4 can be treated by the so-

called "single-channel model" [51],

$$\begin{aligned}\hat{\mathcal{H}}_\lambda &= \sum_{\sigma\in\{\uparrow,\downarrow\}} \int_{\mathbb{R}^3} \mathrm{dx}^3 \hat{\psi}^\dagger_{f,\sigma}(x)\left(\hat{T}_f + \hat{V}^f_{\text{trap}}\right)\hat{\psi}_{f,\sigma}(x) \\ &+ \lambda \int_{\mathbb{R}^3} \mathrm{dx}^3 \hat{\psi}^\dagger_{f,\downarrow}(x)\hat{\psi}^\dagger_{f,\uparrow}(x)\hat{\psi}_{f,\uparrow}(x)\hat{\psi}_{f,\downarrow}(x), \end{aligned} \tag{1.3}$$

alternatively, one can consider the so-called "two-channel" or atom-molecule Hamiltonian [52],

$$\begin{aligned}\hat{\mathcal{H}}_{2ch} &= \hat{\mathcal{H}}_\lambda + \int_{\mathbb{R}^3} \mathrm{dx}^3 \hat{\psi}^\dagger_b(x)\left(\hat{T}_b + \hat{V}^b_{\text{trap}}\right)\hat{\psi}_b(x) \\ &+ \int_{\mathbb{R}^3} \mathrm{dx}^3 \left\{ g\hat{\psi}^\dagger_b(x)\hat{\psi}_{f,\uparrow}(x)\hat{\psi}_{f,\downarrow}(x) + \text{h.c.}\right\}, \end{aligned} \tag{1.4}$$

where the fields: $\hat{\psi}^\dagger$ ($\hat{\psi}$) create (annihilate) atoms of different species given by their sub-indexes, where b corresponds to bosons and f corresponds to fermions. The bosons (fermions) obey canonic commutation (anti-commutation) algebra. In the case of fermions the index σ corresponds to the spin, were we consider equal number of fermions in each spin. The kinetic energy is denoted by $\hat{T}_\xi$ and the trapping potential is $\hat{V}^\xi_{\text{trap}}$ for the species $\xi \in \{b, f\}$. The interaction λ is the many-body interaction strength between fermions of opposite spin and g is the interaction strength between molecules and pairs of fermions.

The general strategy that we followed to understand the behaviour of the systems in this thesis is to start with a second quantised Hamiltonian from which we constructed a continuum model or a lattice model. We constructed a continuum model by doing the standard mean-field decoupling scheme [53–55]. In order to construct a lattice model for atoms in an optical lattice, we employed the tight-binding approximation and expanded the field operators in Bloch states using Wannier functions well localised in lattice sites [45, 51]. Once we have these representations, we took the lowest modes with the symmetries relevant to the dynamics for low energies [56]. Then, we solved the eigenvalue problem for the effective Hamiltonian, either by direct diagonalisation for arbitrary interaction strengths depending on the size of the Hilbert space or we constructed a Gross-Pitaevskii type theory [44, 53, 54] valid for large atom numbers and weak interactions. Our strategy scheme was as follows:

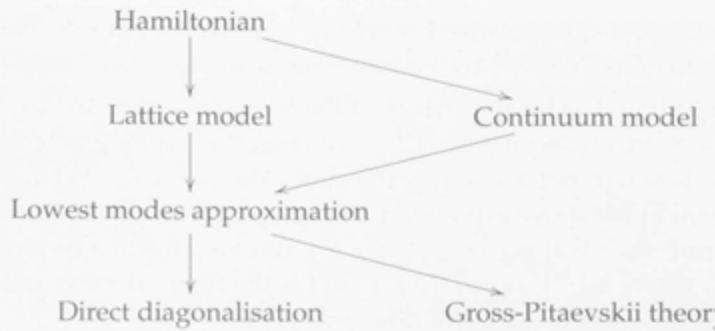

Once the eigenvalue problem was solved or the mean-field theory was constructed,

we looked at the properties of the ground state and the spectrum of excitations. Using this information, we looked at the emergence of localised states and the effect of the interaction on the formation of broken symmetry states.

The structure of the thesis is as follows. In Chapter 2 we considered systems of interacting bosons in a double-well potential. We started by analysing interacting ultracold bosons in a double-well potential, where we considered the effects beyond mean-field approximation in the dynamics of prepared states, and the formation of broken symmetry states. We considered the effect of the relaxation on stationary states and the emergence of intrinsic decoherence. We continue this Chapter with the study of a BEC inside a laser cavity, where the super-radiant transition [57] can be interpreted as a transition from localised to delocalised states. In Chapter 3, we study Bose-Fermi mixtures. We start this Chapter with the analysis of a Bose-Fermi mixture in a double well potential, using the mean-field approximation where we consider experimentally relevant parameters. We studied the effect of fermions on the formation of *macroscopic quantum self-trapped states* (MQST) [58] [see Fig. 1.2 (a,b)] and analysed possible experimental signatures of this effect. The MQST states are many-body atomic states localised in space due to the nonlinear interaction between bosonic atoms. We continued with the analysis of a Bose-Fermi mixture in a three-site ring configuration, where we diagonalised directly the Hamiltonian of the system and investigate the properties of the ground state and the formation of localised states of different atomic species with broken symmetry. We finish this Chapter with the study of a simplified model of a Bose-Fermi topological insulator [29, 30] in a double three-site ring configuration and the effect on the ground state phase diagram of a synthetic magnetic field [26, 27]. The synthetic magnetic field induces a position dependency to the kinetic energy which breaks symmetries and has consequences on the ground state configurations of atoms of different species. In Chapter 4 we analyse the Bardeen-Cooper-Schrieffer to Bose-Einstein condensation (BCS-BEC) crossover problem realised in ultracold atoms [51]. In the BCS-BEC crossover problem the atoms of fermionic character evolve from their weak coupling limit having a BCS state described by Cooper-Pairs [59], to the strong coupling regime having state described by tightly bound molecules that undergo Bose-Einstein condensation. In the crossover the interaction was controlled via Feshbach resonance. We introduce the typical Hamiltonians of the problem and consider their relationship with magnetic impurity models [60], such as the Kondo model [61] and the Anderson model [62]. We established an alternative formulation of the BCS-BEC crossover problem in terms of the single impurity Anderson model relating the magnetic impurity state with a molecular state of the crossover. We related our results to the experimental parameters of ^{6}Li and ^{40}K to describe the formation of a molecular state induced by a Feshbach resonance, the so-called Feshbach boson [63], and we give an alternative interpretation for the gap in the spectrum of excitations seen in experiments above the critical temperature for superfluidity to occur. Finally, in Chapter 5 we summarise our results and consider possible applications of our findings, and extensions to our work.

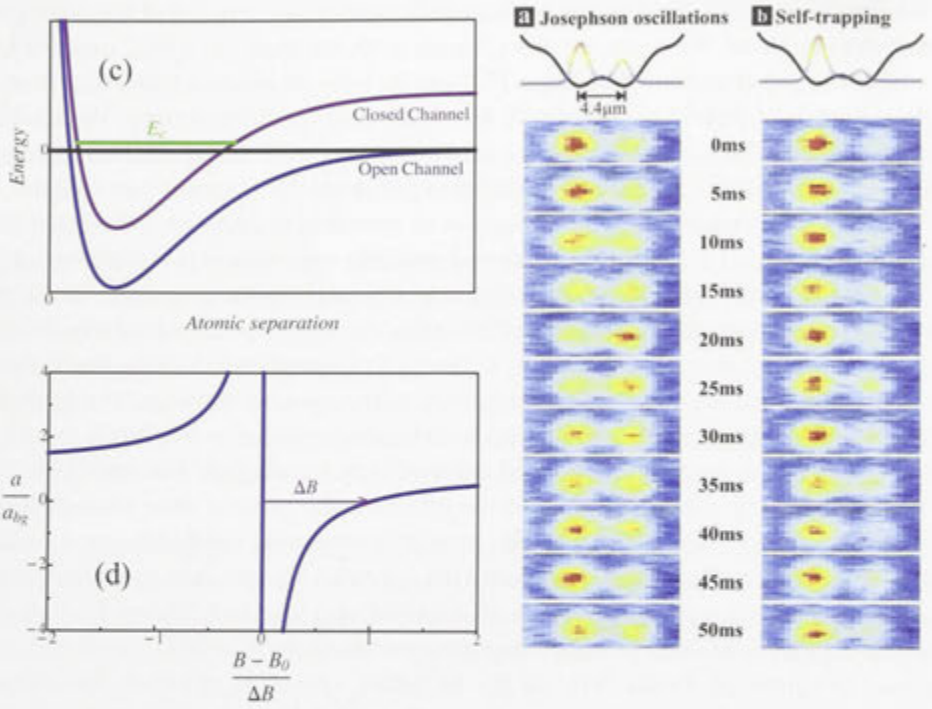

Figure 1.2: Right Panel: Weakly linked Bose-Einstein condensates in a symmetric double-well potential as indicated in the schematics. Observation of the tunnelling dynamics of two weakly linked Bose-Einstein condensates in a symmetric double-well potential as indicated in the schematics. Bose-Josephson junction in the Josephson regime (a) and the macroscopic quantum self-trapping regime (b) (Taken from [46]). Left Panels: (c) Sketch of a Feshbach resonance. The phenomenon occurs when two atoms colliding at an energy close to zero in the entrance channel resonantly couple to a molecular bound state with energy E_c supported by the closed channel potential. The resonant coupling is realised by magnetically tuning E_c near 0 if the magnetic moments of the closed and open channels differ. (d) The behaviour of the scattering length a, as a function of the magnetic field, where ΔB is the distance with respect to the resonance where $a \to 0$ (Reproduced after [47]).

Chapter 2

Interacting bosons in a double-well potential

The experimental realisation of a single bosonic Josephson junction in two weakly linked Bose-Einstein condensates (BEC) has revealed fundamental features of the dynamical nature of an ultracold interacting Bose gas in a double-well potential [46]. This system is composed of a dilute gas of alkali atoms (i. e. ^{87}Rb) below the temperature for BEC to occur. The gas is in a trap that effectively confines the gas to a quasi-one dimensional geometry where a double-well potential is seen by the atoms. This double-well potential is generated optical dipole trap consisting of two couterpropagating, focussed laser beams [46].

The study of this double-well system is important in three different aspects. The first one is the application of BEC for interferometry and metrology [64]. The second one is the study of the Bose Hubbard model [45] that describes the physics of the system. The third one is the control of quantum states to achieve atomtronics and their possible application for implementing quantum computing algorithms [39, 40].

The atomic transport has shown the existence of Josephson tunnelling or macroscopic quantum self-trapping regimes depending on the interatomic interactions, on the initial populations in the wells and the strength of the the trapping potential. What we want to understand of this system is the effects beyond mean-field approximation that occur due to the interaction between atoms and the double-well geometry. To this end we will study the Bose-Hubbard model in this geometry.

The theoretical analysis of this double well system has mainly been based on the two-mode approximation of the Bose-Hubbard model [54, 58, 65–76]. Besides providing a fairly good description of the experimental situation [46], this model has been extensively studied on its own, specially within a mean-field or semiclassical approximation. This model has lead to significant understanding of the richness of the physical problem at hand; additionally, it can incorporate asymmetric two-well potentials and external time-dependent driving fields [69]. One should also point out the relevance of this model in analysing problems in other fields, such as in nonlinear optics [77, 78].

Beyond the mean-field approximation, this model is amenable to numerical full quantum calculations, so far up to $N = 10^3$ particles [65, 68–72]. Mean field, by approximating the N-body dynamics by a set of non-linear coupled dynamical equations, is limited and incomplete since it describes the evolution of the expectation values of one-body operators only. In contrast, from the full quantum description one may, in principle, enquire

about the dynamics of one-, two-, three-, and up to N-body properties. Due to the relative simplicity of the Bose-Hubbard model model in the two mode approximation one can calculate the full N-body wave function and the full N-body density matrix (for a system up to $N = 10^4$ atoms, say). Thus, full information of the state of the system may be obtained. However, from a macroscopic point of view, most of the measurable thermodynamic and/or many-body properties, such as energy, temperature and Green's functions, in general, are given in terms of one- and two-body operators [44]. These in turn are exhaustively described by the one- and two-body reduced density matrices.

The study of the system has revealed from its mean-field treatment, the delocalised to self-trapping transition as a function of the energy and the strength of interaction between atoms [58, 66, 69, 73]. The solution in mean-field has allowed to identify this transition as a function of the energy as a classical "pitch-fork" bifurcation due to the degeneracy in configurations and the many-body nonlinear interaction [79–82]. The approaches based on direct diagonalization [68, 70–72, 74–76] have revealed that recurrences of oscillations occur in the time evolution of expectation values such as the population of the wells. These recurrences happen in between stationary values of the populations, [72, 74, 75].

We proceed as follows. Since we are dealing with a macroscopic system, we choose to describe the state of the system by specifying the number of particles N and the expectation value of the energy ε. For this to be meaningful, we must limit ourselves to states whose root-mean-square energy deviation is small; in other words, to states localised in energy. For our analysis we choose both the energy eigenstates and a well-known family of coherent states [83, 84] such that the energy requirement is satisfied. We point out here that the particular state with all particles initially in one of the wells, analysed in most of the studies with full quantum solutions [68, 69, 71, 72, 75], belongs to the family of these coherent states.

We first analyse the expectation values of the operators, $\hat{N}_1 = \hat{b}_1^\dagger \hat{b}_1$ and $\hat{J}_x^2 = (\hat{b}_1^\dagger \hat{b}_2 + \hat{b}_2^\dagger \hat{b}_1)^2$, in the energy eigenstates, where $\hat{b}_{1,2}^\dagger$ ($\hat{b}_{1,2}$) create (annihilate) atoms of the BEC in the right and left sides of the double-well. We study their values as a function of the interaction strength $\Lambda = NU/\Delta$, where $\Delta/\hbar$ is the tunnelling frequency and U the two-body interaction and N is the number of atoms. The expectation value of operator $\hat{N}_1$ corresponds to the population of one of the two wells, and the expectation value of operator $\hat{J}_x^2$ is related to the fluctuations ΔJ_x in the tunnelling since $(\Delta J_x)^2 = \langle \hat{J}_x^2 \rangle - \langle \hat{J}_x \rangle^2$ with $\langle \cdot \rangle$ the ground state average. We find that the expectation values of $\hat{N}_1$ and $\hat{J}_x^2$ in the eigenstates signal the transition from delocalisation to self-trapping. This behaviour is summarised in a phase diagram. The main result being that there exists a critical value of the interaction, such that if the interaction is greater than this value, the self-trapping transition occurs as a function of the energy of the system. Then we make a brief review of the mean-field stationary solutions to contrast and point out similarities. In particular, we show that the phase diagram separating delocalised from self-trapped states is essentially the same for direct diagonalization of the Hamiltonian and mean-field calculations [69].

We will analyse the dynamics on the expectation value of $\hat{N}_1$ and $\hat{J}_x^2$ and we will show that stationary states exist for long times. As a consequence of this stationary behaviour we consider the emergence of decoherence in the one-body reduced density matrix due to the many-body interaction, we call this "intrinsic" decoherence.

Finally, we will analyse the behaviour of a similar system, a BEC in a cavity. This kind system has very interesting physical properties. The first interesting phenomena

is the study of the transition to the "super-radiant" regime of the Dicke Model [57]. In the super-radiant regime the emission and absorption of photons by the atoms becomes coherent. Therefore, the whole system radiates like a single atom. In addition to this, the dynamical transition to a self-organized state and behaviour with the characteristics of a supersolid phase have been measured [85]. In the supersolid phase both diagonal (crystalline) and off-diagonal (superfluid) long range orders co-exist [23, 25]. We will study the behaviour of the system due to the many-body interaction and the atom-photon interaction, and the role of quantum fluctuations.

The structure of the Chapter is as follows. We study the transition from the delocalised states to the self-trapping states, comparing the results from the mean-field approximation and the calculations using direct diagonalization of the Bose Hubbard model in the two-mode approximation. Then we consider the time evolution of the system for long times with different initial conditions and we compare the results obtained using a basis of coherent states and the eigenstate basis of the Hamiltonian. It follows that, we will analyse the effect of this relaxation to a stationary state and the relation to decoherence in the system due to the many-body interaction. We will conclude the chapter with the analysis of the BEC in a cavity and a summary of our work.

2.1 The model and the effective Hamiltonian

We consider a BEC of repulsive interacting atoms (i.e. ^{87}Rb) in a one dimensional geometry confined by a symmetric double well potential. The Hamiltonian of the system can be written in second quantised form as follows:

$$\hat{\mathcal{H}} = \int \mathrm{dx}\ \hat{\psi}_b^\dagger(x)\left(T + V_{\text{trap}}\right)\hat{\psi}_b(x) + \frac{1}{2}\int \mathrm{dx}\,\mathrm{dx}'\hat{\psi}_b^\dagger(x)\hat{\psi}_b^\dagger(x')w(x,x')\hat{\psi}_b(x')\hat{\psi}_b(x) \tag{2.1}$$

where the field operators: $\hat{\psi}_b^\dagger$ (creation) and $\hat{\psi}_b$ (annihilation) obey the usual commutation algebra for bosonic fields. The kinetic energy is T and the trapping potential is V_{trap}. The many-body interaction is a contact potential, $w(x,x') = g\delta(x-x')$, with $g \sim 4\pi\hbar^2 a/m$, where the effective particle-particle interaction strength is written in terms of the (positive) s-wave scattering length a. Next, our aim is to have a simplified model that contains the essential ingredients to describe the physics of the BEC considering the effect of the many-body interaction between the atoms and the symmetry properties due to the trapping potential. Therefore, we assume that the system can be described by the lowest modes in of the field that describes the BEC. We consider that the energy of the lowest two modes is well below all other modes in the BEC. Thus, the dynamics and the energy of the BEC are mainly due to these two modes. We expand the field operators in these two modes, $\hat{\psi}_b(x) = \varphi_0(x)\hat{a}_0 + \varphi_1(x)\hat{a}_1$, where $\hat{a}_0$ corresponds to the lowest mode (symmetric) and $\hat{a}_1$ to the first excited mode (anti-symmetric). Then the Hamiltonian is:

$$\hat{\mathcal{H}} = \sum_\nu \epsilon_\nu \hat{a}_\nu^\dagger \hat{a}_\nu + \sum_{\nu,\mu,\gamma,\delta} w_{\nu,\mu,\gamma,\delta}\hat{a}_\nu^\dagger \hat{a}_\mu^\dagger \hat{a}_\gamma \hat{a}_\delta, \tag{2.2}$$

where $\epsilon_{0,1}$ are the two lowest eigenenergies of a single particle in the double well. The main assumptions that we have made and give validity to the effective theory given by (2.2) are that the two lowest energy states of the system are well below any other energy

states, and the separation between them is small.

The energy levels and the corresponding eigenfunctions are given by the solution of the following equation:

$$\left(T + V_{\text{trap}}\right)\varphi_\nu(x) = \epsilon_\nu \varphi_\nu(x),$$

and the qualitative picture of the solutions is given in Fig. 2.1, where we have that the lowest mode is symmetric and the first excited mode is anti-symmetric.

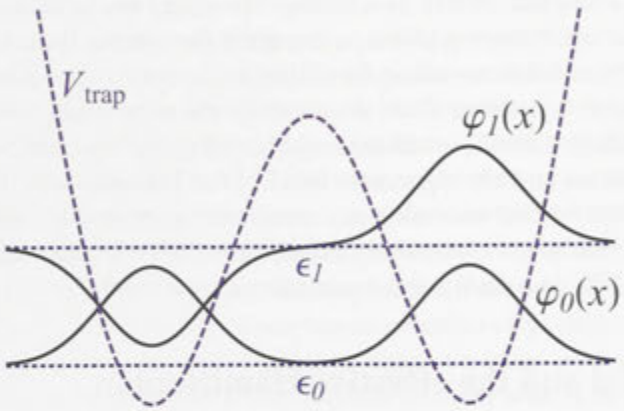

Figure 2.1: Schematics of the solutions of the single particle states of the double well potential. The lowest energy state eigenfunction (symmetric) is given by $\varphi_0(x)$ and the first excited eigenfunction (antisymmetric) is given by $\varphi_1(x)$.

The interaction term in (2.1) has been rewritten in terms of the two particle collision integral, $w_{\nu\mu\gamma\delta} = g/2 \int \mathrm{dx}\ \varphi_\nu^*(x)\varphi_\mu^*(x)\varphi_\gamma(x)\varphi_\delta(x)$, and here we assume that $g \geq 0$. Since the atom number states basis is appropriate to study the expectation value of the population of the right and left wells, we perform the following linear transformation:

$$\hat{b}_1 = \frac{1}{\sqrt{2}}\left(\hat{a}_0 + \hat{a}_1\right), \quad \hat{b}_2 = \frac{1}{\sqrt{2}}\left(\hat{a}_0 - \hat{a}_1\right),$$

and substitute in (2.2) to obtain,

$$\begin{aligned}
\hat{\mathcal{H}} &= \left(\frac{\epsilon_0+\epsilon_1}{2}\right)\left(\hat{b}_1^\dagger\hat{b}_1 + \hat{b}_2^\dagger\hat{b}_2\right) - \left(\frac{\epsilon_1-\epsilon_0}{2}\right)\left(\hat{b}_1^\dagger\hat{b}_2 + \hat{b}_2^\dagger\hat{b}_1\right) \qquad (2.3)\\
&+ \left(\frac{w_0}{4} + \frac{w_4}{4} + \frac{3w_2}{2}\right)\left(\hat{b}_1^\dagger\hat{b}_1^\dagger\hat{b}_1\hat{b}_1 + \hat{b}_2^\dagger\hat{b}_2^\dagger\hat{b}_2\hat{b}_2\right)\\
&+ \left(\frac{w_0}{4} + \frac{w_4}{4} - \frac{w_2}{2}\right)\left(\hat{b}_1^\dagger\hat{b}_1^\dagger\hat{b}_2\hat{b}_2 + \hat{b}_2^\dagger\hat{b}_2^\dagger\hat{b}_1\hat{b}_1 + 4\hat{b}_1^\dagger\hat{b}_2^\dagger\hat{b}_1\hat{b}_2\right)\\
&+ \left(\frac{w_0}{2} - \frac{w_4}{2}\right)\left(\hat{b}_1^\dagger\hat{b}_1^\dagger\hat{b}_1\hat{b}_2 + \hat{b}_2^\dagger\hat{b}_1^\dagger\hat{b}_1\hat{b}_1 + \hat{b}_1^\dagger\hat{b}_2^\dagger\hat{b}_2\hat{b}_2 + \hat{b}_2^\dagger\hat{b}_2^\dagger\hat{b}_2\hat{b}_1\right). \qquad (2.4)
\end{aligned}$$

where the interaction constants in each term depend on the overlapping between modes and are given by, $w_0 = g/2 \int \mathrm{dx}\ |\varphi_0|^4$, $w_2 = g/2 \int \mathrm{dx}\ |\varphi_0|^2|\varphi_1|^2$, $w_4 = g/2 \int \mathrm{dx}\ |\varphi_1|^4$. The relevant terms of the Hamiltonian (2.4), are the second and third terms from above, since

the first term is an energy shift and the last two terms are dropped because their contribution is considered marginal. Therefore, we will study the following effective Hamiltonian, which is the Bose-Hubbard Hamiltonian considering the two-mode approximation [70, 86, 87],

$$\hat{\mathcal{H}}_{\text{eff}} = -\frac{\Delta}{2}\left(\hat{b}_1^\dagger \hat{b}_2 + \hat{b}_2^\dagger \hat{b}_1\right) + u\left(\hat{b}_1^\dagger \hat{b}_1^\dagger \hat{b}_1 \hat{b}_1 + \hat{b}_2^\dagger \hat{b}_2^\dagger \hat{b}_2 \hat{b}_2\right), \tag{2.5}$$

where $\Delta = \epsilon_1 - \epsilon_0$ is the energy difference, or alternative $\Delta/\hbar$ is the tunnelling frequency of the two lowest energy modes and $u = (w_0 + w_4)/4 + 3w_2/2 \sim g/l^3 \sim 4\pi\hbar^2 a/m a_\perp^3$. The length $a_\perp$ is the characteristic length of the transversal direction of the anisotropic confinement, thus $U/\Delta \sim 1 - 10$ is an effective one-dimensional interaction strength [88]. We shall specify the different regimes by the dimensionless interaction parameter, $\Lambda = NU/\Delta$. We use units with $\hbar = \Delta = m = 1$.

As it has already been established, both from mean-field [58, 66, 69, 73] and full quantum calculations [68, 70–72, 74–76] , the system described by Hamiltonian (2.5) exhibits a transition from coherent oscillations to a self-trapping regime [54, 73]. The solution of the above model in the limit were $\Lambda \lesssim 1/N^2$, the non-interacting limit, is the *Rabi* regime; then as we increase the interaction the system is in the *Josephson* regime, provided that, $1/N^2 \lesssim \Lambda \lesssim 1$; while when $\Lambda \gtrsim 1$, we are in the *Fock* regime [54, 89]. The Rabi regime is equivalent to a pendulum with variable length depending on its angular momentum while in the Josephson and Rabi regimes the length is fixed. For non-interacting atoms $u = 0$, (2.5) describes sinusoidal Rabi oscillations of the populations between the two wells with frequency $\omega_R = 2\Delta/\hbar = 2$. The behaviour of the pendulum in the Fock and Josephson regimes is semiclassical while in the Fock regime the system is strongly quantum. In general the description given by (2.5) is appropriate for the BEC in a double well in the Josephson and Fock regimes [54], since g is different from zero.

The transition from delocalisation to self-trapping occurs in the Josephson regime, very close to the Fock regime. This transition has been described to occur as either when the parameter Λ is increased from zero to above a critical value Λ_c for a fixed initial condition, or for a fixed value of $\Lambda > \Lambda_c$ by varying the initial state, which is equivalent to varying the energy of the system. As a matter of fact, the experiment by Albiez et. al. [46] using Bose atoms at very low temperatures, reports the observation of a self-trapped state as a function of the initial population imbalance between wells. It proves convenient to change the representation using the Schwinger transformation [90], where we introduce the following one-body operators [70],

$$\begin{aligned}
\hat{J}_x &= \frac{1}{2}\left(\hat{b}_1^\dagger \hat{b}_2 + \hat{b}_2^\dagger \hat{b}_1\right) \\
\hat{J}_y &= -\frac{i}{2}\left(\hat{b}_1^\dagger \hat{b}_2 - \hat{b}_2^\dagger \hat{b}_1\right) \\
\hat{J}_z &= \frac{1}{2}\left(\hat{b}_1^\dagger \hat{b}_1 - \hat{b}_2^\dagger \hat{b}_2\right)
\end{aligned} \tag{2.6}$$

which are angular momentum operators and obey the SU(2) commutation relations: $\left[\hat{J}_k, \hat{J}_l\right]_- = i\varepsilon_{klm}\hat{J}_m$. The number of atoms $\hat{N} = \hat{b}_1^\dagger \hat{b}_1 + \hat{b}_2^\dagger \hat{b}_2$, is conserved. The operator $\hat{J}_x$ corresponds to the difference in population between the symmetric and anti-symmetric modes of the confining potential, $\hat{J}_y$ represents the momentum of the condensate, while $\hat{J}_z$ is the difference in population between the two wells [70]. Then, the Hamiltonian can

be written as [1] ,

$$\hat{\mathcal{H}}_{\text{eff}} = -\hat{J}_x + 2U\hat{J}_z^2,$$

where $U = u/\Delta$ and we have omitted terms proportional to $\hat{N}$, because they only introduce a constant shift to the ground state energy. From the form of the above equation it is evident that depending on the ratio U the Hamiltonian will be diagonal in different basis. When the tunnelling term ($\hat{J}_x$) is dominant, the basis corresponds to the basis where Pauli matrix σ_x is diagonal and when the interaction term ($\hat{J}_z^2$) is dominant, we have the basis where the Pauli matrix σ_z is diagonal. These considerations allow us to construct the Heisenberg equations of motion for the $\hat{J}_k$ operators, which may be transformed to their mean field counterparts by the transformation $\hat{J}_k \to NK_k$ where K_k is a c-number function of time. This approximation is valid for $N \to \infty$, $U \to 0$, but Λ finite [69], because as the number of atoms increases the system approaches the classical limit and quantum fluctuations are suppressed. For small values of the interaction strength, typically, the expectation values of one-body operators such as, $\hat{N}_1$, and two-body operators like, $\hat{J}_x^2$, oscillate following the coherent oscillations predicted by the mean-field calculation for a brief period of time, then "decay" to a stationary value for a long period of time followed by revivals, seen in the solution by direct diagonalization of (2.5) for a fixed number of atoms [69, 70]. The mean-field approximation on the equations of motion gives information on one-body properties only, and is unable to capture features such as revivals.

2.2 Density matrix of a N-body system

We work in the basis of atom number states $|N_l, N_r\rangle$, where N_l (N_r) is the number of particles in the left (right) well. These Fock states are constituted by all the different combinations of populations in each well given a total number of particles N ($N = N_l + N_r$). The evolution in time of the N-body quantum state state $|\Psi(t)\rangle$ is determined using $|\Psi(0)\rangle = |N, 0\rangle$ as the initial condition for the Schrödinger equation:

$$i\frac{\partial}{\partial t}|\Psi\rangle = \mathcal{H}|\Psi\rangle, \tag{2.7}$$

where $\mathcal{H} = \mathcal{H}_{\text{eff}}$ from (2.5). It is important to mention that such an initial condition corresponds to a particular case of the family of the so called coherent states [83, 84]. Evolution in time of the coherent states leads qualitatively to the same features for the density matrix as those that we expose below, and we will show in the following sections (see also [2]).

At the same time that we propagate the initial state over time by numerically solving (2.7), we construct the density matrix $\hat{\rho}_N(t) = |\Psi(t)\rangle\langle\Psi(t)|$ of the $N-$particle system. The study of the evolution in time of the $N-$particle density matrix leads to three qualitatively different behaviours in terms of the scaled interaction $\Lambda = UN$. For illustration purposes we select the case for $N = 20$. As indicated in the caption of Fig. 2.2, each square represents a matrix element of the N-body density matrix. First, in the

[1] This model is also a particular case of the so-called LMG model in nuclear physics, H.J. Lipkin, N. Meshkov, and A.J. Glick, Nuclear Physics, **62** 188, (1965). For recent developments in the eigenstate structure of such a model, see [86] and [87] .

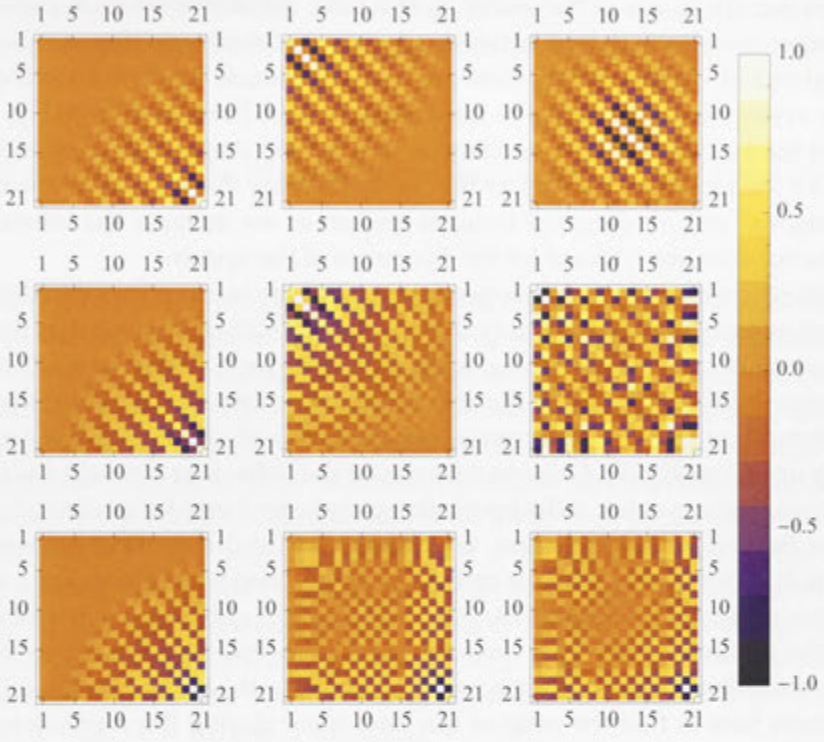

Figure 2.2: The real part of the density matrix $\rho^{(N)}$ of 20 particles for different interaction values and times, Λ=0 (top row, Rabi regime), 0.2 (middle row, Josephson regime), 2.0 (bottom row, Fock regime). Time units of each matrix correspond to 0.5 (left), 2.5 (middle), 30.0 (right). Here each square represents a matrix element of the density matrix.

non-interacting case case when $\Lambda = 0$ (Rabi regime), we observe the expected coherent oscillations for the purely tunnelling regime [58, 70]. This behaviour is reflected in the density matrix elements [Fig. 2.2, top row],which have no transition between positive or negative values from the main diagonal and there are oscillations on the main diagonal with a Rabi frequency, $\omega_R = 2$. In the second case when $\Lambda = 0.2$ (Josephson regime) we pictorially observe that the density matrix elements evolve in time from having non-interacting features (oscillations on the main diagonal), in the time [Fig. 2.2 left and middle panels]. Then the system, starts to slowly change to a stationary state characterised by checkerboard-like structures [Fig. 2.2, middle row (right)], where there is a mixture in the behaviour between positive and negative elements, with small amplitude oscillations as a function of time. Revivals are captured in the matrix elements through coloured oscillations in the main diagonal elements and are due to the finite number of atoms. Finally, in the third case, when the interaction contribution exceeds the criti-

cal value $\Lambda_c \approx 0.92$ (approximate boundary between the Josephson and Fock regime), which depends on the chosen initial condition [2], the system experiences the transition to the localised or self-trapping regime [70]. In the self-trapping regime, the particles are concentrated mainly in one of the wells. In this case, the density matrix elements have the distribution of a checkerboard lattice as a function of their sign [Fig. 2.2, bottom row (middle and right)] . In this regime there are small amplitude oscillations in the main diagonal. The system decays abruptly to the stationary state [transition from Fig. 2.2 left to middle] and the amplitude of the oscillations in the main diagonal is suppressed. From the behaviour seen in Fig. 2.2 it is clear that as we increase the interaction the symmetry between diagonal and off-diagonal terms is broken as we increase the interaction and quantum fluctuations are relevant for the dynamics of the system.

In general one can state that the property of stationarity is complicated to deduce from the information encoded in the N-body density matrix, still we can see that fluctuations due to finite number of particles play a major role as we increase the interaction, and the stationary state is characterised by the checkerboard pattern in Fig. 2.2. However, the stationary behaviour of the system can be observed directly from the expectation value of few body operators [2, 71]. One can summarise the behaviour towards the stationary state as follows. For any value of the interaction parameter Λ and for any initial condition, in particular the one we selected here, any element of the one-particle reduced density matrix starts at its value given by the initial condition, then it oscillates, for a short time following the mean-field solution [73, 76], decaying towards a *constant* value that we identify as the stationary one. After remaining in such a state for a long time , the matrix element shows revivals close but not equal, in general, to the initial condition. The main point we stress here is that the ratio of the time spent during the revivals to the time spent in the stationary state, vanishes as the number of particles increases to infinity [2]. This implies that if we observe the system at a long but arbitrary time, it will mostly be found in the stationary state. As we shall see below this leads to the phenomenon of decoherence at the level of few-body properties.

2.3 Observables and eigenstates properties

In this section we shall analyse the behaviour of the one- and two-body observables on the quantum eigenstates along the transition from delocalised to self-trapped states and we shall also briefly review the corresponding predictions of the mean-field approximation. We will point out their similarities and discrepancies. The next section will be devoted to the study of the full time quantum evolution of the quasi-classical coherent states along the transition.

As shown in the previous section, within a quantum calculation one can obtain the full N-body wavefunction $|\psi_N(t)\rangle$ and density matrix $\hat{\rho}^{(N)}(t) = |\psi_N(t)\rangle\langle\psi_N(t)|$. From the latter, one may further find the the reduced one- and two-body density matrices, $\hat{\rho}^{(1)}$ and $\hat{\rho}^{(2)}$, whose matrix elements are given by,

$$\rho^{(1)}_{\alpha\beta} = \mathrm{Tr}\left(\hat{b}_\alpha\, \hat{\rho}^{(N)}\, \hat{b}^\dagger_\beta\right) \tag{2.8}$$

and

$$\rho^{(2)}_{ab} = \mathrm{Tr}\left(\hat{b}_\mu \hat{b}_\nu\, \hat{\rho}^{(N)}\, \hat{b}^\dagger_\kappa \hat{b}^\dagger_\eta\right) \tag{2.9}$$

with the subindices α and β taking the values 1 and 2, and $a = \{\mu\nu\}$ and $b = \{\kappa\eta\}$, that is, the values $\{11\}$, $\{12\}$ and $\{22\}$. Knowledge of these two operators suffices to determine all one- and two-body properties of the system. However, even though we can calculate all the matrix elements of $\hat{\rho}^{(1)}$ and $\hat{\rho}^{(2)}$ as a function of time, we find it more illustrative to limit ourselves to the analysis of two properties, one is the number of particles in well 1, namely,

$$\hat{N}_1 = \hat{b}_1^\dagger \hat{b}_1 \tag{2.10}$$

a one-body operator. And the other is a "tunnelling correlation", i.e. a two-body operator:

$$\hat{\mathcal{C}} = 4\hat{J}_x^2, \tag{2.11}$$

where $\hat{J}_x = (\hat{b}_1^\dagger \hat{b}_2 + \hat{b}_2^\dagger \hat{b}_1)/2$ the tunnelling operator. The expectation value of this operator is related to the fluctuations in the tunnelling, or alternatively the fluctuations of the difference in the population of the antisymmetric and symmetric modes of the confining potential ΔJ_x by means of: $(\Delta J_x)^2 = \langle \hat{J}_x^2 \rangle - \langle \hat{J}_x \rangle$, with $\langle \cdot \rangle$ the ground state average.

To analyse the properties of the eigenstates of the system, we numerically solve [2] the eigensystem with $\hat{\mathcal{H}}$ given by (2.5): $\hat{\mathcal{H}}(\Lambda)|\phi_n(\Lambda)\rangle = \varepsilon_n(\Lambda)|\phi_n(\Lambda)\rangle$, where the dependence of different set of eigenstates and eigenvalues on Λ has been indicated an the sub-index n goes from 0 to N. For N particles there are $N+1$ eigenstates, the energy of the system being finite and bounded by the lowest $\varepsilon_0(\Lambda)$ and largest $\varepsilon_N(\Lambda)$ eigenenergies. In Figs. 2.3 and 2.4 we show the expectation values of $\hat{N}_1$ and $\hat{\mathcal{C}}$ in the energy eigenstates, namely, $\langle \hat{N}_1(\Lambda)\rangle_n = \langle \phi_n(\Lambda)|\hat{N}_1|\phi_n(\Lambda)\rangle$ and $\langle \hat{\mathcal{C}}(\Lambda)\rangle_n = \langle \phi_n(\Lambda)|\hat{\mathcal{C}}|\phi_n(\Lambda)\rangle$ as a function of the eigenenergy $\varepsilon_n(\Lambda)$ of the corresponding eigenstate $|\phi_n(\Lambda)\rangle$, for three values of the interaction, $\Lambda = 0.1$, $\Lambda = 1.0$ and $\Lambda = 10$, and $N = 10^3$.

From Figs. 2.3 and 2.4 we can deduce the dependence of the observables $\langle \hat{N}_1 \rangle$ and $\langle \hat{\mathcal{C}} \rangle$ on the energy eigenstates and at the same time the transition to self-trapping as Λ is varied. For $\Lambda = 0.1$ all the stationary states show, on the one hand, $\langle \hat{N}_1 \rangle_n = N/2$ while $\langle \hat{\mathcal{C}} \rangle_n$ shows a simple continuous behaviour. For obvious reasons, we call *delocalised* states those with $\langle \hat{N}_1 \rangle_n = N/2$. Thus, for $\Lambda = 0.1$ all states are delocalised. For $\Lambda = 1.0$ and $\Lambda = 10.0$ a transition from the delocalised regime to the self-trapped regime is observed. One finds that there exists a "critical" energy $\varepsilon_c(\Lambda)$, above which the average number of particles deviates from $N/2$ for equally populated wells, i.e. $\langle \hat{N}_1 \rangle_n \neq N/2$. These are the *self-trapped* states, which appear as a breaking of the symmetry $1 \leftrightarrow 2$ of the Hamiltonian (2.5). In the case of the tunnelling correlation $\langle \hat{\mathcal{C}} \rangle_n$ the transition is signalled by a cusp at $\varepsilon_c(\Lambda)$. We also performed calculations with $N = 10^4$ and found that the difference with $N = 10^3$ is almost indistinguishable, except very near the transition. Note that in Fig. 2.3 there are two isolated points near the transition; for $N = 10^4$ there are few more isolated points around the transition.

The transition is best summarised in the phase diagram of Fig. 2.5. This was obtained by the diagonalization of the Hamiltonian (2.5), considering $N = 10^3$ particles, for values of Λ ranging from $0.0 \leq \Lambda \leq 10.0$ in steps of 0.01. For each set of eigenstates we found the value $\varepsilon_c(\Lambda)$ where the delocalised to self-trapping transition occurred. This is the

[2] The eigensystem $\hat{\mathcal{H}}(\Lambda)|\phi_n(\Lambda)\rangle = \varepsilon_n(\Lambda)|\phi_n(\Lambda)\rangle$ was numerically solved by means of *Fortran*, *Mathematica* and *Matlab* diagonalization subroutines. The time evolution of an arbitrary initial state, $|\psi\rangle = \sum_n a_n|\phi_n(\Lambda)\rangle$ was performed, both, by direct evaluation of $|\psi(t)\rangle = \sum_n a_n \exp(-i\varepsilon_n(\Lambda)t)|\phi_n(\Lambda)\rangle$ with *Mathematica*, *Matlab* and by a finite-difference method within a *Fortran* code.

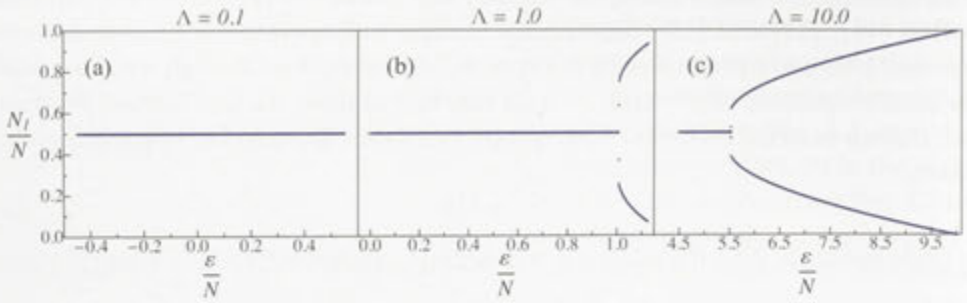

Figure 2.3: Particle population in well 1 $\langle \hat{N}_1 \rangle_n$ as a function of the energy eigenvalues ε_n for $N = 1000$ and $\Lambda = 0.1$, $\Lambda = 1.0$ and $\Lambda = 10$.

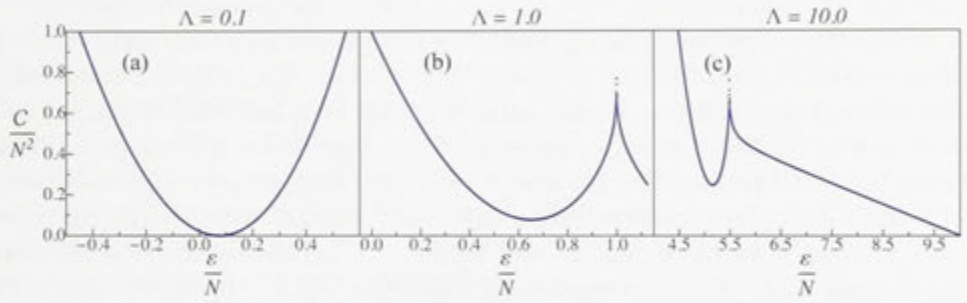

Figure 2.4: The two particle correlation $\langle \hat{C} \rangle_n$, as a function of the energy eigenvalues ε_n for $N = 1000$ and $\Lambda = 0.1$, $\Lambda = 1.0$ and $\Lambda = 10$.

(red) dotted line in Fig. 2.5. The (blue) solid lines correspond to the lowest and highest eigenenergies for each value of Λ, namely, $\varepsilon_0(\Lambda)$ and $\varepsilon_N(\Lambda)$. Hence, for $\varepsilon_n(\Lambda) \leq \varepsilon_c(\Lambda)$ the state $|\phi_n(\Lambda)\rangle$ is delocalised, while it is self-trapped for $\varepsilon_n(\Lambda) \geq \varepsilon_c(\Lambda)$. We further observe that there exists a critical value of the interaction Λ_c below which there is no transition. For $N = 1000$ we numerically find $\Lambda_c \approx 0.539$, see the inset in Fig. 2.5.

The transition from delocalisation to self-trapping in these systems has been predicted and found, both by exact diagonalization of the Hamiltonian (2.5) [68, 70–72, 74–76] and from the mean-field calculations [58, 66, 69, 73]. To highlight the similarities and discrepancies between the results of this and of the next section, we now briefly review the mean-field approximation[3]. Mean field approximation may be achieved by first setting the creation and annihilation operators as c-numbers, $\hat{b}_i^\dagger \to b_i^*$ and $\hat{b}_i \to b_i$, and further $b_i = |b_i| \exp(i\vartheta_i)$. Then, one may identify the relative population $p = (|b_1|^2 - |b_2|^2)/N$ and the phase difference $\varphi = \vartheta_2 - \vartheta_1$ as classical canonical conjugate variables. Their full dynamics is then determined by the corresponding Hamiltonian (2.5) in those variables [65, 67, 69].

The ensuing mean-field phase diagram is strikingly similar to the one shown in Fig.

[3]We follow closely the discussion and results of [69].

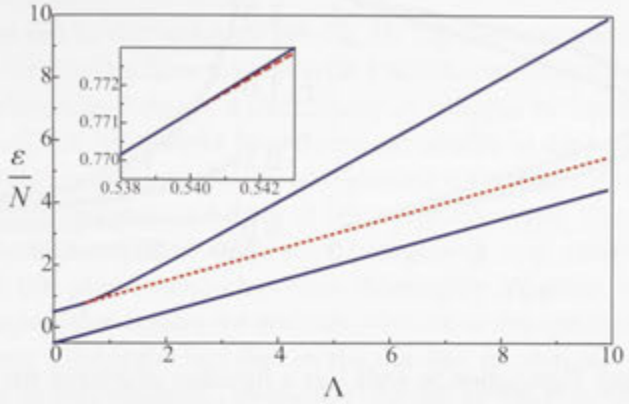

Figure 2.5: Phase diagram ε/N vs Λ for $N = 1000$ particles. The allowed states are those within the (blue) solid lines, $\varepsilon_0(\Lambda)$ and $\varepsilon_N(\Lambda)$. The (red) dotted line is the transition from delocalised to self-trapped states, $\varepsilon_c(\Lambda)$ for $\Lambda > \Lambda_c \approx 0.539$, see the inset. The states with energy greater than $\varepsilon_c(\Lambda)$ are self-trapped.

2.5 (see Fig. 1 in Ref. [69]). It is found that, for each value of Λ, there are just *two* stationary states that resemble those of $\varepsilon_0(\Lambda)$ and $\varepsilon_N(\Lambda)$ in Fig. 2.5, with the mean-field critical interaction being $\Lambda_c^{MF} = 1/2$. To be precise, for $\Lambda < \Lambda_c^{MF}$, the energies of the stationary states are $\epsilon_L(\Lambda) = (\Lambda - 1)/2$ and $\epsilon_U(\Lambda) = (\Lambda + 1)/2$, where the sub-index U and L correspond to the highest and lowest energy in the spectrum. For values $\Lambda \geq \Lambda_c^{MF}$, there are three stationary states, $\epsilon_L(\Lambda)$, $\epsilon_U(\Lambda)$ and $\epsilon_D(\Lambda) = \Lambda + 1/8\Lambda$, where D stands for the delocalised boundary. The function $\epsilon_L(\Lambda)$, for all values of Λ, essentially coincides with the function $\epsilon_0(\Lambda)$, the lowest eigenenergy shown as the lower (blue) solid line in Fig. 2.5. For $\Lambda < \Lambda_c^{MF}$, the highest eigenvalue $\epsilon_N(\Lambda)$ coincides with $\epsilon_U(\Lambda)$, while for $\Lambda \geq \Lambda_c^{MF}$, the eigenvalue $\epsilon_N(\Lambda)$ is well approximated by $\epsilon_D(\Lambda)$. In this region, $\epsilon_U(\Lambda)$ corresponds to the transition (red) dotted line in Fig. 2.5, but the mean-field stationary state turns out to be unstable [66, 67]. There are no other mean-field stationary states within those boundaries, which is one of the main differences between mean-field and the exact solution. While all the states bounded by the (blue) solid lines in Fig. 2.5 are non-stationary in the mean-field approach, they represent stationary states in the exact quantum calculation.

The mean field states are non-stationary because the population $p(\tau)$ shows coherent oscillations for any allowed initial condition and for any allowed value of the mean field (conserved) energy ϵ. Those states certainly show the transition from delocalisation to self-trapping but in the following way. For $\Lambda < \Lambda_c^{MF}$ and for a given value of ϵ, the population $p(\tau)$ oscillates between the boundary values $\pm p_+(\epsilon)$ determined by the energy. Thus, a *time average* yields $\overline{p(\tau)} = 0$, giving rise to a mean population in well 1: $N_1 = N(1 + \overline{p(\tau)})/2 = N/2$, i.e. a delocalised state. For $\Lambda \geq \Lambda_c^{MF}$ and for the energies $\epsilon_L < \epsilon < \epsilon_U$, again, the time average yields $\overline{p(\tau)} = 0$, $N_1 = N/2$, a delocalised state. However, for energies $\epsilon_U \leq \epsilon < \epsilon_D$, the time average may be accurately approximated by

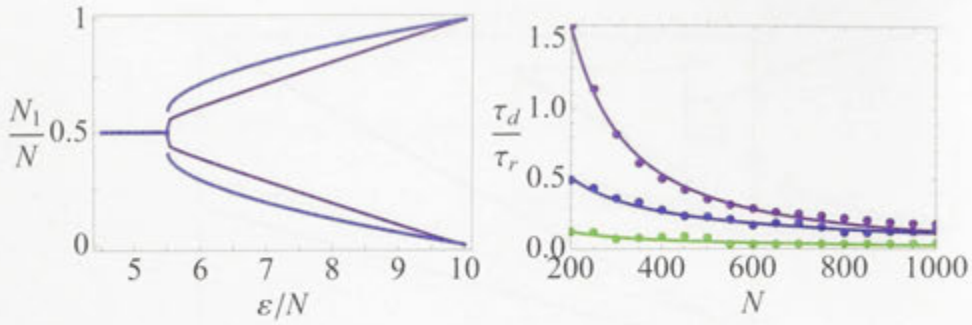

Figure 2.6: Left Panel: Population in well 1 as a function of energy for $\Lambda = 10.0$. Mean-field N_1 in purple lines. Eigenstate expectation value $\langle \hat{N}_1 \rangle_n$ in blue dots, $N = 2000$. In mean-field, for each value of the energy ϵ, there exists an infinity number of possible initial values $p(0)$ and $\varphi(0)$ for the system; all of those have the same time average value N_1, differing only in the sign of $p(0)$ for self-trapped states, $p(0) > 0$ localises in well 1, $p(0) < 0$ localises in well 2. Right Panel: The behaviour of the ratio τ_d/τ_r as a function of the number of particles for the initial state: $|N, 0\rangle$. The dots correspond to the results from the evolution in time of the eigenstates obtained from direct diagonalization of (2.5), the lines are the fits to the function $C(\Lambda)N^{\delta(\Lambda)}$. We have considered $\Lambda = 0.2$ (green). 0.8 (blue). 2.0 (purple). The parameters of the fit are: $C(0.2) = 22.7$, $\delta(0.2) = -0.98$, $C(0.8) = 71.4$, $\delta(0.8) = -0.93$, and $C(2.0) = 6175$, $\delta(2.0) = -1.56$.

[4] $\overline{p(\tau)} = p_+(\epsilon)(1 + \sqrt{1 - 1/k^2})/2$, yielding $N_1 \neq N/2$, i.e. a self-trapped state. The values of p_+ and k^2 are given by [69, 73]:

$$p_+ = \frac{1}{2\Lambda^2}\left(2\Lambda\left(2\varepsilon - \Lambda\right) - 1 + \sqrt{4\Lambda^2 + 1 - 4\Lambda\left(2\varepsilon - \Lambda\right)}\right), \tag{2.12}$$

$$k^2 = \frac{1}{2}\left(1 + \frac{2\Lambda(2\varepsilon - \Lambda) - 1}{\sqrt{4\Lambda^2 + 1 - 4\Lambda(2\varepsilon - \Lambda)}}\right). \tag{2.13}$$

In Fig. 2.6 we show a comparison of the mean-field solution and the exact diagonalization solution for the population of well 1, for $\Lambda = 10$, as a function of the energy. We find that, while the transition energy $\epsilon_c(\Lambda)$ agrees well quantitatively for both cases, there is a clear discrepancy for the population values in the self-trapped regime. The transition as a function of the energy in mean-field approximation is a classical "pitch-fork" bifurcation [79–82]. In the next section, we shall analyse the quantum dynamics of coherent states and find that, while the periods of the oscillations agree fairly well with their mean-field counterparts, the expectation values of one- and two-body properties in the basis of coherent states decay or collapse to stationary values that agree with those of the basis of energy eigenstates.

[4] The mean-field time average value may be estimated as the algebraic mean of the largest and lowest value of the elliptic Jacobi functions $\mathrm{dn}(z, q)$ (valid in the self trapped region) which are $+1$ and $\sqrt{1 - q^2}$ [69]. An exact numerical evaluation of this mean shows a deviation of few parts in 10^3.

2.4 Statistically stationary states

As already pointed out in the literature [69–72, 74, 75], the dynamical evolution of arbitrary states of the interacting Bose system with Hamiltonian (2.5) reveals, in addition to delocalised and self-trapped states, a clear decay or collapse to "stationary" states with recurrent revivals which mean-field treatments are unable to capture. The existence of these stationary states is due both to the pair-particle interaction energy and to the fact that we are looking at expectation values of few-body operators. The revivals are a consequence of the finite number of eigenstates comprising any conceivable state in this system. Although this phenomenon has been thoroughly reported, we would like here to emphasise an aspect that makes the revivals relevant to the description of the dynamics of these systems. This is the fact that as the number of particles N is increased, the relative time spent in the collapsed "stationary" region grows much faster than the time spent in the revivals intervals, such that, if one lets the system evolve for an arbitrary long time, it becomes more and more probable to find it in the stationary region.

One finds, generally, that the time *between* recurrences scales as $\tau_r = A(\Lambda)N^\alpha$ while the time *during* the recurrence, that is, the relaxation time, scales as $\tau_d = B(\Lambda)N^\gamma$. The coefficients A and B are Λ-dependent. The behaviour of the ratio $\tau_d/\tau_r = C(\Lambda)N^\delta$, with $\delta = \gamma - \alpha$ and $C = B/A$ is shown in Fig. 2.6 (right panel), where we have considered the evolution of the state $|N, 0\rangle$, for different values of Λ. From the behaviour seen in Fig. 2.6 (right panel) one can deduce that the ratio $\tau_d/\tau_r \to 0$ as $N \to \infty$. This is in marked contrast to the mean-field behaviour, as we will see below. [5]. The purpose of this section is to analyse this dynamical behaviour for a family of coherent states [83, 84] and to compare it with that of the energy eigenstates and the mean-field predictions.

The coherent states are expected to behave semi-classically and to follow quite closely the mean-field dynamics. Here, we consider the following set of coherent states [83, 84] ,

$$|\theta, \phi\rangle = \sum_{n=0}^{N} \left(\begin{array}{c} N \\ n_1 \end{array} \right)^{1/2} \sin^{N-n_1}(\theta/2)\, \cos^{n_1}(\theta/2)\, e^{-i(N-n_1)\phi} |n_1, N-n_1\rangle \tag{2.14}$$

where n_1 and $N - n_1$ are the number of particles in wells 1 and 2, and $|n_1, N - n_1\rangle$ are the $(N + 1)$ Fock states. The angles θ and ϕ determine the particular initial state. These angles may be given by fixing the expectation value of the energy and of the initial population in, say, well 1. To be precise, for given values of the number of particles N, we characterise the coherent states by their energy expectation value, $\varepsilon(\theta, \phi) = \langle \theta, \phi | \hat{\mathcal{H}} | \theta, \phi \rangle$ and leave the initial population to be adjusted by arbitrarily setting $\phi = 0$.

Taken any of these states as the initial one for the system, we evolve it numerically[2], $|\theta, \phi; t\rangle = \exp(-i\hat{\mathcal{H}}t/\hbar)|\theta, \phi\rangle$ and calculate the expectation values of $\hat{N}_1$ and $\hat{\mathcal{C}}$,

$$\langle \hat{N}_1(t) \rangle_c = \langle \theta, \phi; t | \hat{N}_1 | \theta, \phi; t \rangle \tag{2.15}$$

and

$$\langle \hat{\mathcal{C}}(t) \rangle_c = \langle \theta, \phi; t | \hat{\mathcal{C}} | \theta, \phi; t \rangle. \tag{2.16}$$

As mentioned in the first section of this chapter, the coherent state initially with the N

[5] It is worth to mention that for the initial condition $|N, 0\rangle$ analytical expressions for the collapse and revival times may be found [75] that are in agreement with our results for different values of Λ.

particles in well 1 is given by $\theta = \pi$ and $\phi = 0$. The evolution of this state has been extensively studied [58, 65–76]. Here, we shall study all possible coherent states with $\phi = 0$. It can then be shown that by varying the angle θ from $\pi/2$ to a maximum allowed value $\theta_{\max}(\Lambda)$, the energy $\varepsilon(\theta, 0)$ almost spans the whole range of values from $\varepsilon_0(\Lambda)$ to $\varepsilon_N(\Lambda)$, namely, $\varepsilon(\pi/2, 0) \gtrsim \epsilon_0(\Lambda)$ and $\varepsilon(\theta_{\max}(\Lambda), 0) \lesssim \varepsilon_N(\Lambda)$. The angle $\theta_{\max}(\Lambda)$ is calculated numerically by solving: $\varepsilon(\theta_{\max}(\Lambda), 0) = \varepsilon_N(\Lambda)$, where $\varepsilon_N(\Lambda)$ is the largest eigenvalue of the spectrum of the Hamiltonian (2.5) for a fixed number of particles and interaction strength Λ. If θ is increased beyond $\theta_{\max}(\Lambda)$ or reduced below $\pi/2$, the energy remains in the same interval $\varepsilon(\pi/2, 0) \leq \varepsilon(\theta, 0) \leq \varepsilon(\theta_{\max}(\Lambda), 0)$. However, the expectation value of the number of particles $\langle \hat{N}_1(t) \rangle_c$ registers this change, as we discuss below. The variation of this angle θ selects the probability amplitude of the components of the coherent states, namely the proportions of the states in the number state basis as a function of the energy. As the angle varies the components change and therefore the energy also. We show the behaviour of the components of the coherent state in the number basis as a function of the energy and the corresponding number state component in Fig. 2.7. As we increase the interaction and θ, states with population imbalance give the dominant contribution to the coherent state [compare the results for $\Lambda = 0.2$ (a,c) and $\Lambda = 2.0$ (b,d) in Fig. 2.7]. The dependency of θ on the energy eigenstates can be deduced from Fig. 2.8, where we show the behaviour for the parameters of Fig. 2.7. For $\Lambda = 2.0$ as we change above (below) $\theta = \pi/2$ the states that have the largest contribution to the coherent state are the ones that localise the well 2 (1) [see Fig. 2.7 (b,d)].

Figs. 2.9 and 2.11 show the time evolution of the expectation values $\langle \hat{N}_1(t) \rangle_c$ and $\langle \hat{\mathcal{C}}(t) \rangle_c$ for two arbitrary initial coherent states, see the figure caption, and for three typical values of Λ. Fig. 2.10 show the comparison of $\langle \hat{N}_1(t) \rangle_c$ with the corresponding mean-field calculations. The latter are obtained by setting the energy of the mean-field solution equal to the expectation value of the energy in the coherent state, namely, $\epsilon = \varepsilon(\theta, 0)$ for the given value of Λ.

For the case $\Lambda = 0.1$, first panels of Figs. 2.9 and 2.10, the system shows coherent oscillations initially, then it falls into a stationary value with $\langle \hat{N}_1(t) \rangle_c = N/2$ within numerical accuracy, followed by revivals at almost periodic intervals. The stationary value agrees with the mean-field time average, as shown in Fig. 2.10. For $\Lambda = 1.0$, second panels of Figs. 2.9 and 2.10, the system is already in the self trapped regime for the chosen initial condition. The mean-field counterpart does show coherent oscillations and their time average (≈ 0.855), for this value of Λ, agrees with the stationary value of the state evolved in time in the eigenstate basis (≈ 0.845).

At $\Lambda = 10.0$, third panels of Figs. 2.9 and 2.10, the system is well into the self-trapped regime and there again appear regions of coherent oscillations followed by stationary intervals in the full quantum evolution, while the mean-field calculation oscillates around an average value close but different from the stationary value of the evolution in the eigenstate basis. The discrepancy in the averages comes from the effect of quantum fluctuations, which are minimized in the coherent state basis.

We observe that the behaviour of the two-body correlation $\langle \hat{\mathcal{C}}(t) \rangle_c$ in Fig. 2.11 follows essentially the same pattern of stationary collapsed regions followed by revivals, as the population $\langle \hat{N}_1(t) \rangle_c$ in Fig. 2.9.

Because the system reaches statistically stationary states, we can describe their properties by the given values of the *mean* of $\langle \hat{N}_1(t) \rangle_c$ and $\langle \hat{\mathcal{C}}(t) \rangle_c$, namely, by their statisti-

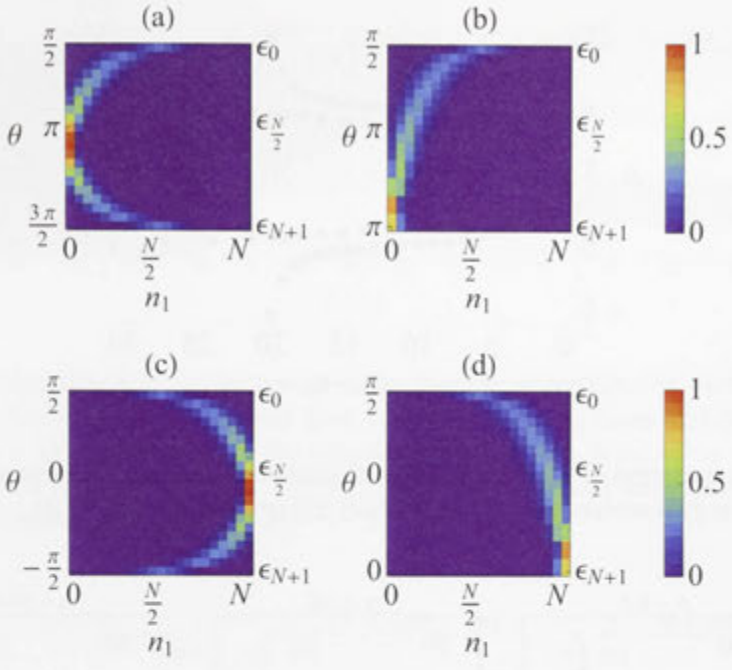

Figure 2.7: Density plot of the probabilities of the components $|n_1, N-n_1\rangle$ of the coherent states as a function of θ and the number of particles n_1 in well 1, on the right axis is the corresponding energy eigenstate ϵ_n. The parameters are: $N = 20$, (a,c) $\Lambda = 0.2$, (b,d) $\Lambda = 2.0$.

cally average values denoted as N_1^s and $\mathcal{C}^s$. This family is built in the following manner. For given values of N and Λ, and taking $\phi = 0$, we find the values of θ such that the expectation values of the energy in the coherent states span the whole interval $\varepsilon_0(\Lambda) \lesssim \varepsilon(\theta, 0) \lesssim \varepsilon_N(\Lambda)$. Then, we evaluate the time evolution of the corresponding coherent state $|\theta, 0, t\rangle$ and calculate N_1^s and $\mathcal{C}^s$. Clearly, the value of θ for a given energy is not unique. We see below that, depending on the value of θ, the coherent state can break the symmetry. If it does, it localises either near the well 1 or the well 2, once the condition for self-trapping is satisfied, i.e. for $\Lambda \geq \Lambda_c$.

Figs. 2.12 and 2.13 show the stationary values N_1^s and $\mathcal{C}^s$ for $N = 10^3$ and for $\Lambda = 0.1$, 1.0 and 10.0 as a function of the expectation value of the energy of the state. In the same graph we have included the expectation values calculated in the basis of energy eigenstates (c.f. Figs. 2.3 and 2.4). In general, we see that the stationary values from the coherent states N_1^s and $\mathcal{C}^s$ agree fairly well with the corresponding eigenstate values. Hence, we can conclude that the statistically stationary states, follow the same behaviour as the eigenenergy states. Their macroscopic behaviour is described by the phase diagram shown in Fig. 2.5. That is, there exists a critical value Λ_c, for a self-trapping transition as a function of the energy (or as a function of the initial state). Additionally, these states may be well characterised by both one- and two-body properties, that is, while the one-body properties remain constant below the self-trapping transition, two-body variables discriminate among different states. Both quantities clearly signal the transition

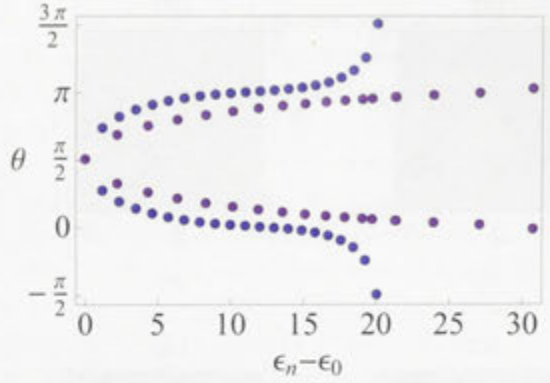

Figure 2.8: The variation of the the angle θ of the coherent state as a function of the energy eigenstates. The parameters are: $\Lambda = 0.2$ (blue), 2.0 (purple) and $N = 20$.

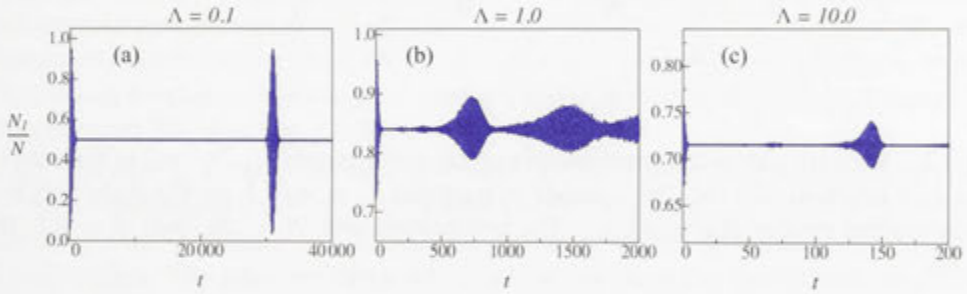

Figure 2.9: Time evolution of the expectation value of the number of particles in well 1, $\langle \hat{N}_1 \rangle_c$, calculated in the coherent states basis. Parameters are: $\phi = 0$, $N = 10^3$ and, (a) $\theta = \pi + 0.1$, $\Lambda = 0.1$; (b) $\theta = \pi + 0.1$, $\Lambda = 1.0$; (c) $\theta = \pi - 1.0$, $\Lambda = 10.0$.

point. As an additional aspect, note in Figs. 2.12 and 2.13 that the transition appears continuous for the statistically stationary states.

The transition from the delocalised to the self-trapped states displays a symmetry-breaking phenomenon. That is, the Hamiltonian is symmetric with respect to the exchange of the wells, or internal states, 1 and 2. However, the stationary states can be prepared to become localised is one of the wells depending on the angle of the coherent states θ. To be precise, one can show that for $\Lambda \geq \Lambda_c$, if $\phi = 0$ and θ yields a state localised in well 1, then $\theta = \pi - \theta$ and $\phi = 0$, localises in well 2. This is illustrated in Fig. 2.12: for $\Lambda = 1.0$ (red) solid line signals localisation in well 1 and for $\Lambda = 10.0$ (red) solid line localises in well 2.

2.5 Intrinsic decoherence

Decoherence in quantum mechanics is a process usually associated to the behaviour of a state of a system, when it interacts with its environment. If the interaction of the system

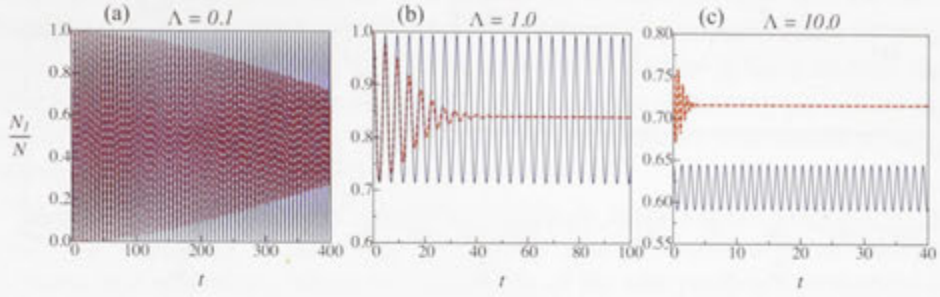

Figure 2.10: Comparison of the dynamics of the number of particles in well 1, $N_1(t)/N$ in the basis of coherent states (blue solid line) and the eigenstate basis (red dotted line) for a fixed energy ϵ. The parameters of the coherent states are $\phi = 0$, (a) $\theta = \pi + 0.1$, $\Lambda = 0.1$; (b) $\theta = \pi + 0.1$, $\Lambda = 1.0$; (c) $\theta = \pi - 1.0$, $\Lambda = 10.0$; $N = 10^3$. The corresponding energies are $\epsilon = 0.15$, 1.04 and 6.03, respectively.

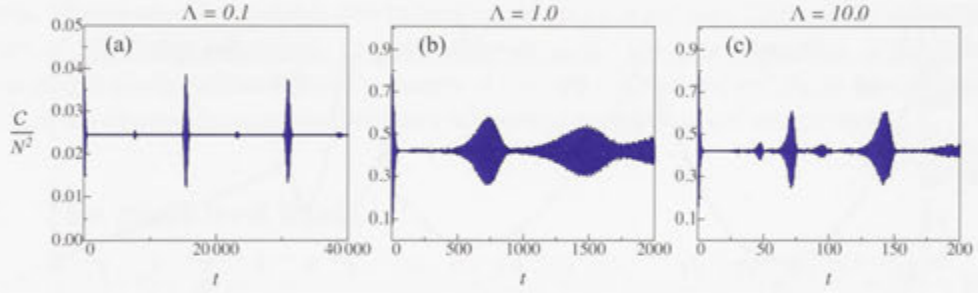

Figure 2.11: Time evolution of the expectation value of the tunnelling correlation, $\langle \hat{C} \rangle_c$, calculated in the basis of coherent states $\phi = 0$, $N = 10^3$, and (a) $\theta = \pi + 0.1$, $\Lambda = 0.1$; (b) $\theta = \pi + 0.1$, $\Lambda = 1.0$; $\theta = \pi - 1.0$, $\Lambda = 10.0$.

with its surroundings is weak, such a process is reflected by the vanishing of off-diagonal elements of the system density matrix. To describe this behaviour, one may write down master or kinetic equations for the system density matrix evolution only, in which the role of the environment is appropriately taken into account to produce the observed relaxation to a stationary state and decoherence. The environment is usually modelled as a collection of bosonic modes representing the thermal fluctuations with the environment. However, if one considers the coupled system-environment as a large composite closed system, the evolution of this composite system remains, strictly speaking, coherent in the full system plus environment Hilbert space. Thus, if attention is focused on the behaviour of the small system only, by means of the evolution of its reduced density matrix, decoherence is also observed in the sense that arbitrary initial states tend to relax, or decohere, to stationary "incoherent" states. Revivals to states close to the initial states do occur but become more improbable to observe as the environment becomes larger. Consideration of these facts, underpins derivations of master or kinetic equations for systems interacting with a thermal bath or environment [91–100].

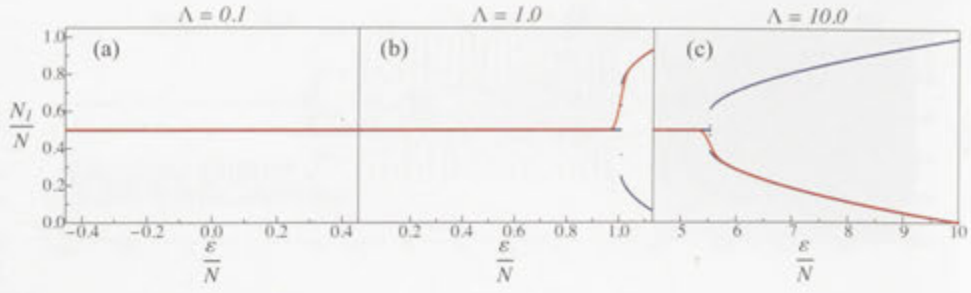

Figure 2.12: Statistically stationary value of the number of particles in well 1, N_1^s, in the family of coherent states $|\theta, 0; t\rangle$, as a function of their expectation value of the energy $\varepsilon(\theta, 0)$, for $N = 1000$, (red) solid line. For comparison, in (blue) dots line the corresponding expectation values in the energy eigenstates $\langle \hat{N}_1 \rangle_n$ (same as in Fig. 2.3). In the second panel, we show the statistically stationary states localised in well 1, while in the third panel, the statistically stationary states localised in well 2. See text.

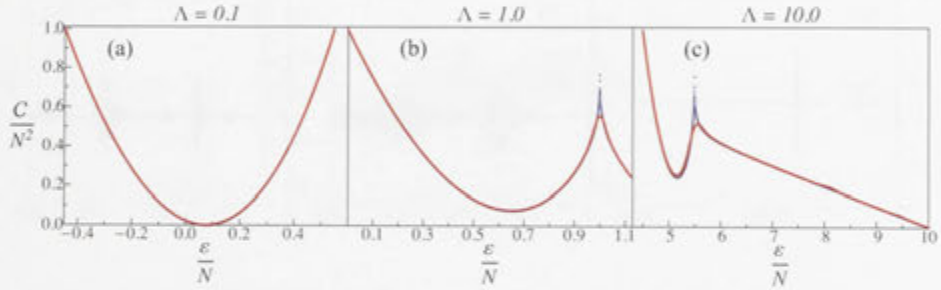

Figure 2.13: Statistically stationary value of the tunnelling correlation, $\mathcal{C}^s$, in the family of coherent states $|\theta, 0; t\rangle$, as a function of their expectation value of the energy $\varepsilon(\theta, 0)$, for $N = 1000$, (red solid line). For comparison, the corresponding expectation values in the energy eigenstates $\langle \hat{\mathcal{C}} \rangle_n$ are shown (blue dotted line) same as in Fig. 2.4.

On the other hand, according to the basic assumptions of statistical physics, a *closed* system with a large number N of degrees of freedom relaxes to equilibrium stationary states [101], manifested through the behaviour of few-body properties, such as temperature, pressure and energy [44, 101]. This is also a form a decoherence, that we will call "intrinsic". Since the mentioned properties are averages or expectation values of few-body operators, their corresponding values may be obtained by following the evolution of the appropriate reduced density matrices only. Formally, this relaxation to a stationary state is exhibited by the fact that the matrix elements of the reduced density matrices no longer evolve in time. As a consequence of this, one can always find a basis in which the off-diagonal matrix elements of such matrices vanish in the stationary state. We shall call this the *preferred* basis, in analogy to the notation used when dealing with systems interacting with its environment [41, 42, 102, 103]. In this basis, the signature of decoherence may be explicitly seen by tracking the evolution of the reduced density matrices

in the preferred basis for all times. It is important to mention, that because the number of particles is finite, the stationary state we are referring to is punctuated by recurrences to states close to the initial one. However, as we have shown in the previous section, as the number of particles is increased, the time spent in the stationary part of the evolution grows without bound with respect to the time spent in the revival intervals, such that in the thermodynamic limit the stationary state is robust.

The fact that relaxation to stationary states in large closed systems is exhibited through the dynamics of few-body properties, is also appealed to in derivations of Boltzmann-like equations, where the relaxation of the one-particle distribution function leads to a stationary state due to particle collisions.

Decoherence of a BEC in a double well potential and systems of this type in contact with external environments have already been considered using both full quantum and mean-field approaches [104–112]. We should also mention that the phenomenon of decoherence in closed systems has been recently readdressed with applications to spin systems [113, 114].

Since the system under consideration is closed, i.e. BEC in a double-well potential, decoherence cannot be traced from the information encoded in the $N-$particle density matrix. However, decoherence can be and is observed when one looks at the expectation values of few-body operators. In particular, we study the time evolution of the components of one-body reduced density matrix, $\hat{\rho}_R(t) = \rho^{(1)}$ (defined in 2.8), to investigate the effect of the interactions on the inherent relaxation towards a stationary state.

2.6 The preferred basis

Given the fact that all the information associated with any single particle property is encoded in the matrix $\hat{\rho}_R(t) = \hat{\rho}^{(1)}$ which remains unchanged over time in the stationary regime, decoherence can be formally observed by finding an appropriate basis which leads to the vanishing of the off-diagonal elements of the one-body reduced density matrix. In other words, in order to speak of decoherence in the usual sense, the reduced density matrix must be expressed in a proper basis in which the mixed state representing the stationary state becomes a completely incoherent state. Decoherence in the usual sense tells us that the system becomes classical, so that the addition of probability amplitudes approaches the limit of addition of probabilities. Namely in a quantum system described by the wave function, $\psi = \psi_1 + \psi_2$ the probability density is given by $\rho_{\mathcal{Q}} = |\psi|^2 = |\psi_1|^2 + |\psi_2|^2 + \psi_1^*\psi_2 + \psi_2^*\psi_1$. In a classical system we have that the state of the system would be given by the addition of probabilities, $\rho_{\mathcal{C}} = |\psi_1|^2 + |\psi_2|^2$. The decoherence processes are the ones that change the system from quantum to classical such that $\rho_{\mathcal{Q}} \to \rho_{\mathcal{C}}$. This is equivalent to monitoring the evolution of the off-diagonal elements of the one-body reduced density matrix , with respect to some arbitrary parameter and observing transition to a classical regime signalled by the vanishing values of the the off-diagonal elements. Equivalently, one can find the basis that diagonalises $\rho^{(1)}$, is usually called the *preferred* basis. To illustrate these ideas we select $N = 10^3$ particles and the initial condition $|N, 0\rangle$. Discussion of decoherence in few-boson systems can be found in [115].

As mentioned before, we follow the exact dynamics of the N-particle system and construct the corresponding $N-$body density matrix $\rho^{(N)}(t) = |\psi_N(t)\rangle\langle\psi_N(t)|$. From

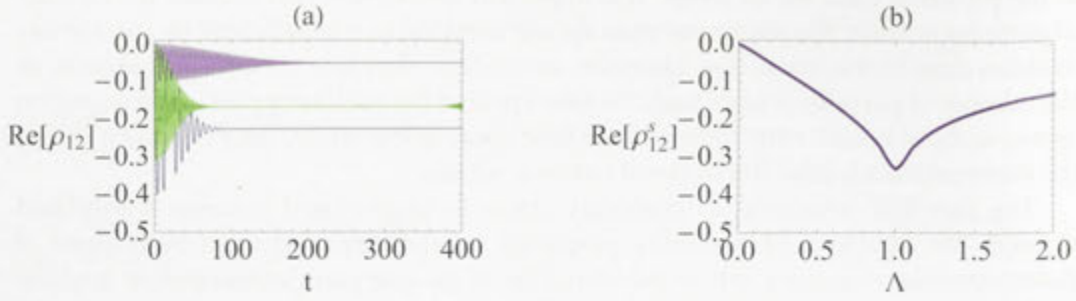

Figure 2.14: (a) Real part of the matrix element ρ_{12} as a function of t. Parameters are: $\Lambda = 0.2$ (purple), 0.8 (blue), 1.6 (green) and $N = 10^3$ particles. (b) Real part of the matrix element ρ^s_{12} as function of Λ with $N = 10^3$.

this, one can calculate the one-body reduced density matrix elements: $\rho_{\alpha\beta} = \rho^{(1)}_{\alpha\beta} = \mathrm{Tr}\left(\hat{b}_\alpha\, \hat{\rho}^{(N)}\, \hat{b}^\dagger_\beta\right)$. The single-body reduced density matrix can be generally written as,

$$\hat{\rho}_R(t) = \begin{pmatrix} \rho_{11}(t) & \rho_{12}(t) \\ \rho^*_{12}(t) & \rho_{22}(t) \end{pmatrix}. \tag{2.17}$$

In this basis the terms $\rho_{11}(t)$ and $\rho_{22}(t)$ give the particle population fraction for each of the wells, and $\mathrm{Re}[\rho_{12}(t)]$ gives the difference in population between the symmetric and antisymmetric modes per particle of the double well potential and $\mathrm{Im}[\rho_{12}(t)]$ gives the momentum per particle of the BEC. However $\rho_{12}(t)$ is not an appropriate measure of the decoherence in this basis, since the $\mathrm{Re}[\rho_{12}(t)]$ never becomes zero as shown in Fig. 2.14 (a), thus apparently showing no decoherence. Nevertheless the system does reach a stationary state, as shown in the previous section, and therefore decoherence is present. Next, we establish this result by finding the preferred basis in which the off-diagonal values of the reduced density matrix vanish as time increases.

Let $\hat{\rho}^s_R$ be the reduced density matrix associated to the stationary state that is, $\hat{\rho}_R(t) \to \hat{\rho}^s_R$ in the limit $t \gg \tau_0$:

$$\hat{\rho}^s_R = \begin{pmatrix} \rho^s_{11} & \rho^s_{12} \\ \rho^s_{12} & \rho^s_{22} \end{pmatrix}, \tag{2.18}$$

where we have already taken into account that, for the initial condition used throughout, ρ^s_{12} is real for all values of Λ. The behaviour of ρ^s_{12} is shown in Fig. 2.14 (b). We now define the *preferred* basis as that one in which $\hat{\rho}^s_R$ is diagonal. Let $\hat{U}$ be the unitary operator that performs such a diagonalization, that is,

$$\hat{\rho}^p_D = \hat{U}\hat{\rho}^s_R\hat{U}^\dagger = \begin{pmatrix} \rho^p_{D1} & 0 \\ 0 & \rho^p_{D2} \end{pmatrix}. \tag{2.19}$$

By assuming that the matrix $\hat{\rho}_R(t)$ in (2.17) is written in the representation in which the Pauli matrix σ_z is diagonal, the unitary operator $\hat{U}$ is found to be given by,

$$\hat{U} = e^{-i\frac{\theta}{2}\sigma_y}, \tag{2.20}$$

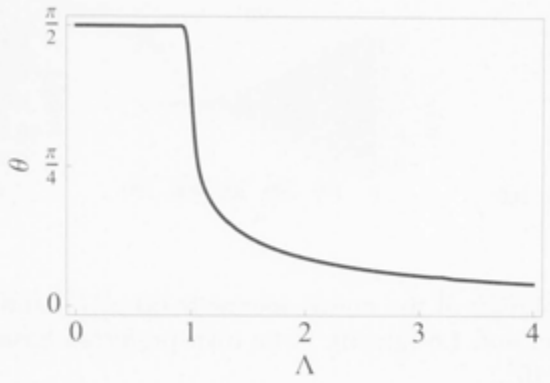

Figure 2.15: θ as a function of Λ. This angle defines the unitary transformation that diagonalizes the stationary reduced density matrix, see (2.21) Calculations were performed using $N = 10^3$.

where $\sin\theta = -\rho^s_{12}/R$, $\cos\theta = (\rho^s_{11} - \rho^s_{22})/2R$ and $R^2 = (\rho^s_{11} - \rho^s_{22})^2/4 + (\rho^s_{12})^2$. An interesting result is that, in general, the angle θ depends on Λ as discussed below. By performing such a unitary transformation on the reduced density matrix $\hat{\rho}_R(t)$ for all its temporal evolution[6], we obtain the reduced density matrix in the preferred basis. The reduced density matrix in such a basis is given by,

$$\hat{\rho}^p_R(t) = e^{i\frac{\theta}{2}\sigma_y}\hat{\rho}_R(t)e^{-i\frac{\theta}{2}\sigma_y}, \tag{2.21}$$

The matrix elements of $\hat{\rho}^p_R(t)$ are as follows:

$$\begin{aligned}
\rho^p_{11}(t) &= \frac{1}{2} + \frac{1}{2}\left(\rho_{11}(t) - \rho_{22}(t)\right)\cos\theta - \mathrm{Re}\rho_{12}(t)\sin\theta, \\
\rho^p_{22}(t) &= \frac{1}{2} - \frac{1}{2}\left(\rho_{11}(t) - \rho_{22}(t)\right)\cos\theta + \mathrm{Re}\rho_{12}(t)\sin\theta, \\
\mathrm{Re}\rho^p_{12}(t) &= \frac{1}{2}\left(\rho_{11}(t) - \rho_{22}(t)\right)\sin\theta + \mathrm{Re}\rho_{12}(t)\cos\theta, \\
\mathrm{Im}\rho^p_{12}(t) &= \mathrm{Im}\rho_{12}(t),
\end{aligned}$$

and therefore, $\hat{\rho}^p_R(t) \to \hat{\rho}^p_D$ for $t \gg \tau_0$. After we evaluate the values of θ at the stationary state, we find their dependence on Λ as depicted in Fig. 2.15. One finds that the dependence of θ on Λ shows that below a critical value Λ_c, $\theta = \pi/2$, while for $\Lambda > \Lambda_c$, θ takes values ranging from $\theta \approx \pi/2$ to $\theta \approx 0$. The critical value is $\Lambda_c \approx 0.92$ for the chosen initial state of the whole system; we recall that here we have used $|\Psi(t)\rangle = |N, 0\rangle$, namely, all particles initially in well 1. Thus, the angle θ registers the transition from delocalised to self-trapped states; one may even considered it as a kind of "order parameter" for the transition. The variation of θ indicates that the dependence of the preferred basis on Λ has two very different behaviours. For values of Λ below the transition, θ is constant and defines a unique basis for all values of Λ. Its continuous variation as a function of Λ

[6]The unitary transformation is static and the parameters for it are determined from the stationary state for different effective interaction strength values.

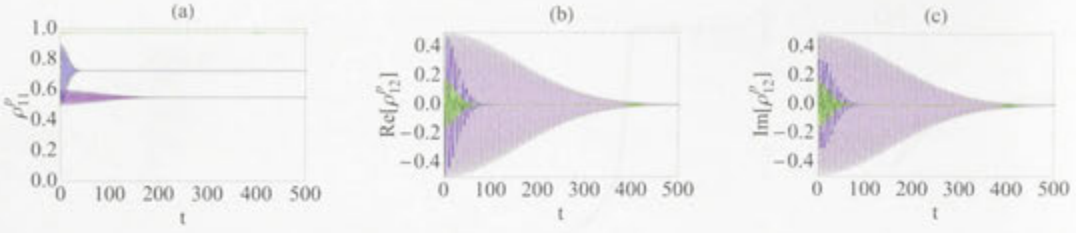

Figure 2.16: Time evolution of the matrix elements (a) $\rho^p_{11}(t)$ and (b,c) $\rho^p_{12}(t)$ for $\Lambda = 0.2$ (purple) , 0.8 (blue) and 1.6 (green), in its own preferred basis. Calculations were performed using $N = 10^3$.

above the transition indicates also a continuos change of preferred bases. For values of Λ below the transition, namely $\theta = \pi/2$ one finds that the preferred basis is that in which the tunnelling term in Hamiltonian (2.5) is diagonal, (i.e. that of the Pauli matrix σ_x) . At the transition, a sharp change occurs until in the very strong interaction regime $\Lambda \gg \Lambda_c$, $\theta \to 0$, and the corresponding preferred basis is the basis that diagonalises the interaction term (i.e. that of the Pauli matrix σ_z). One thus finds that the particle interaction plays a fundamental role in the coherence properties of this simple system.

We illustrate our results for three different values of Λ. In Fig. 2.16 we show the behaviour of the matrix elements $\rho^p_{12}(t)$ and $\rho^p_{11}(t)$ for $\Lambda = 0.2$, 0.8 and 1.6. From this figure one can see that the matrix elements that give us the information about the decoherence, $\rho^p_{12}(t)$, effectively tend to zero, while $\rho^p_{11}(t)$ and $\rho^p_{22}(t)$ become constant, and equal to ρ^p_{D1} and ρ^p_{D2}, respectively.

2.7 The Entropy

An additional and illustrative characteristics both of the stationary state and of the transition to the self trapping regime can be performed with the calculation of the von Neumann entropy defined as: $S = -\mathrm{Tr}(\rho \ln \rho)$, where ρ is a density matrix. This measure is important because is independent of the basis. The N particle density matrix $\rho^{(N)}$ is that of a pure state and therefore $S = 0$. In contrast, the entropy of the reduced density matrix changes with time and interaction strength since the single-particle state is always mixed, $\mathrm{Tr}[(\rho^{(1)})^2] \neq 1$. In Fig. 2.17 we show the von Neumann entropy of the single-particle reduced density matrix in the stationary state. One finds that for $\Lambda < \Lambda_c$ (as long as $\Lambda \neq 0$), the entropy takes its largest values ($S_{max} = \ln 2 \approx 0.69$), since the stationary states are delocalised, because $|\rho^s_{12}| = |\langle \hat{b}^\dagger_1 \hat{b}_2 \rangle| \neq 1/2$, see Fig. 2.14. Then, it displays an abrupt decay in the transition to self-trapped states. In the limit of large interactions, $\Lambda \gg \Lambda_c$, it tends to $S \approx 0$, i.e. a pure state completely localised in one of the wells. It is also important to emphasise that, the knowledge of the entropy $S(\Lambda)$ and the angle $\theta(\Lambda)$ for a particular initial state conveys complementary information on the reduced density matrix. This is clearly seen for values of $\Lambda < \Lambda_c$, for which the preferred basis is the same, namely $\theta = \pi/2$, while the entropy is different for different values of Λ, as seen in Fig. 2.17. While $\theta = \pi/2$ implies that in the stationary state the population in each well is the same, i.e. $\rho^s_{11} = \rho^s_{22} = 0.5$, it gives no information on the value of ρ^s_{12}, which varies with

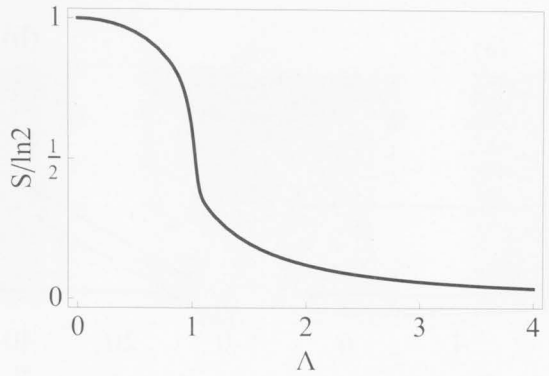

Figure 2.17: Von Neumann Entropy of a stationary state as a function of Λ. Calculations were performed using $N = 10^3$.

Λ. One the other hand, the entropy does depend on the stationary values of all the matrix elements, thus providing a measure of the coherence term, ρ^s_{12} .

2.8 BEC in a cavity

Recently the possibility to have a BEC inside a high finesse cavity has been realised and exciting physics have been explored [85]. Some of the physics of this system can be investigated using a simple model considering two harmonically confined bosonic species in different spin or angular momentum states, that are coupled to a light field . Inside the cavity the BEC is loaded and we consider that the atom decay rate and the cavity field decay rate are small compared with the atom-photon coupling. Under these assumptions effects due to quantum dissipation are negligible, and a single-mode photon can be considered. Considering two modes for the BEC, one for each species, the Hamiltonian of the system can be constructed as follows [116],

$$\begin{aligned}\hat{\mathcal{H}} &= \omega\hat{a}^\dagger\hat{a} + \epsilon_1\hat{b}_1^\dagger\hat{b}_1 + \epsilon_2\hat{b}_2^\dagger\hat{b}_2 + \frac{U_1}{2}\hat{b}_1^\dagger\hat{b}_1^\dagger\hat{b}_1\hat{b}_1 + \frac{U_2}{2}\hat{b}_2^\dagger\hat{b}_2^\dagger\hat{b}_2\hat{b}_2 \\ &\quad + U_{12}\hat{b}_1^\dagger\hat{b}_1\hat{b}_2^\dagger\hat{b}_2 + g(\hat{a}^\dagger + \hat{a}\ )(\hat{b}_1^\dagger\hat{b}_2 + \hat{b}_2^\dagger\hat{b}_1), \end{aligned} \tag{2.22}$$

where $\hat{b}$ ($\hat{b}^\dagger$) annihilates (creates) an atom, $\hat{a}$ ($\hat{a}^\dagger$) annihilates (creates) a photon, and the subindex of $\hat{b}$ refers to different species of bosonic atoms, the operator of the number of atoms is $\hat{N} = \hat{b}_1^\dagger\hat{b}_1 + \hat{b}_2^\dagger\hat{b}_2$. The photon field in a single mode is represented by $\hat{a}$, the atom-photon coupling is g, and the energy of a photon is ω. For the atoms, the inter-atomic (intra-atomic) interaction is U_{12} (U_1 and U_2) and the energy of the lowest state due to the kinetic energy and the harmonic confinement for different species (or modes) is $\epsilon_{1,2}$. In this system particle exchange due to photon absorption or emission is controlled by the coupling parameter g. The parameter $g = \lambda/\sqrt{N}$, where λ is the dipole coupling strength. Typically λ can be of the same order of magnitude other energy scales in the system, recently large coupling amplitudes have been achieved [117] due to nonlinear effects in a BEC.

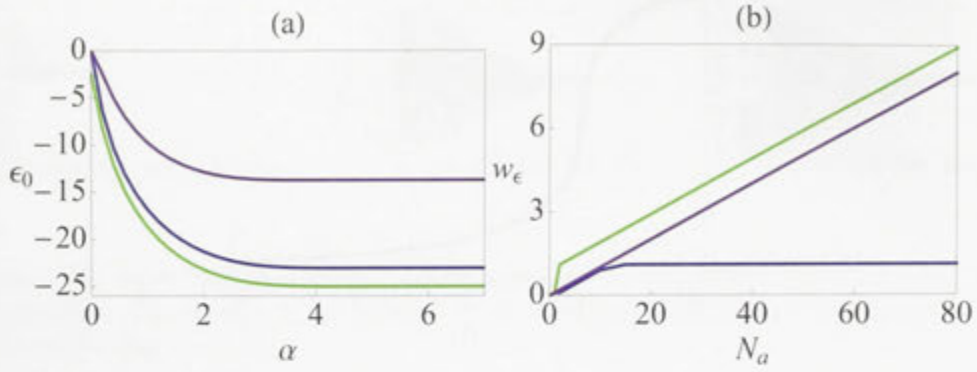

Figure 2.18: (a) The ground state energy as a function of $\alpha = N_a/N$. Parameters are: $N = 10$, $\Gamma = 10$, $\Lambda = 1$ (green), 10 (blue), 100 (purple). (b) The energy width w_ϵ of the quantised population N_1/N (2.25) as a function of the number of photons N_a. Parameters are: $N = 10$, $\Lambda = 100$, $\Gamma = 0.1$, $m/N = 0$ (green), $\pm 1/10$ (blue) and $|m/N| \geq 1/5$ (purple).

This Hamiltonian, can be mapped into as a two-site problem, similar to that considered in the previous sections. This is because having an extra species and a single mode for each species has a very similar representation to the two-site problem, as we have emphasised with the notation. Still there are some differences because now the "tunnelling" between the two modes is controlled by the photon field, and there can be an indeterminate number of photons in the system. Thus, in principle the dimension of Hilbert space is infinity. Therefore solving the above Hamiltonian relies on limiting the number of photons $N_a = \langle \hat{a}^\dagger \hat{a} \rangle$, and therefore truncating the Hilbert space. We do this by noting that after a certain number of photons (depending on the number of atoms $N = \langle \hat{N} \rangle$), the change in the ground state energy asymptotically tends to go zero [see Fig. 2.18 (a)]. In practice one can achieve this limit of negligible change in the ground state energy for $N_a \sim \alpha N$, where $\alpha \sim 3 - 5$. Using the Schwinger boson representation [90] one can write an effective Hamitonian from (2.22), as follows:

$$\hat{\mathcal{H}}_{\text{eff}} = \omega \hat{a}^\dagger \hat{a} \ + \omega_0 \hat{N} + \Delta \hat{J}_z + \frac{\Lambda}{N} \hat{J}_z^2 + \frac{\Gamma}{N} (\hat{a}^\dagger + \hat{a} \ ) \hat{J}_x, \tag{2.23}$$

where,

$$\begin{aligned} \hat{J}_x &= \frac{1}{2} \left(\hat{b}_1^\dagger \hat{b}_2 + \hat{b}_2^\dagger \hat{b}_1 \right), \\ \hat{J}_z &= \frac{1}{2} \left(\hat{b}_1^\dagger \hat{b}_1 - \hat{b}_2^\dagger \hat{b}_2 \right). \end{aligned}$$

The parameters are defined as: $\omega_0 = (\epsilon_1 + \epsilon_2)/2$, $\Delta = \epsilon_1 - \epsilon_2$, $\Lambda = (U_1 + U_2)N/2 - U_{12}N$, and $\Gamma = 2gN$. The above Hamiltonian is the Dicke model with a non-linear term ($\hat{J}_z^2$) [116]. If we would consider a system on-resonance $\omega = \Delta$, we could employ the rotating

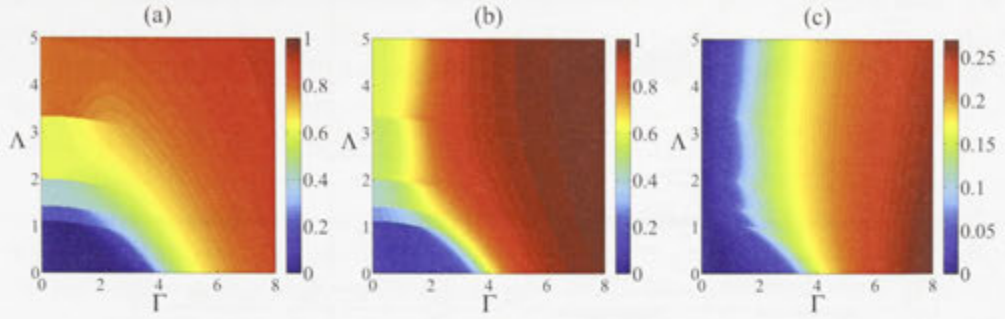

Figure 2.19: (a) Density plots of the order parameter Ψ. (b) The tunnelling correlation $\mathcal{C}$ and (c) the fluctuations in the population of mode "1", σ_1 (right) in the ground state for $N = 10$, $N_a = 30$.

wave approximation to (2.23), in this case we have [7],

$$\hat{\mathcal{H}}_{\text{eff}} = \omega \hat{a}^\dagger \hat{a} \ + \omega_0 \hat{N} + \Delta \hat{J}_z + \frac{\Lambda}{N} \hat{J}_z^2 + \frac{\Gamma}{N} (\hat{a}^\dagger \hat{J}_- + \hat{J}_+ \hat{a} \ ), \tag{2.24}$$

where $\hat{J}_\pm = \hat{J}_x \pm i \hat{J}_y$.

The ground state phase diagram can be constructed by diagonalising the Hamiltonian (2.23) in the truncated Hilbert space for a fixed number of atoms. In this system the size of a vector in the truncated Hilbert space grows like $(N_a + 1)(N + 1) \sim \alpha N^2$. The ground state phase diagram in terms of the order parameter $\Psi = 1 + 2\langle \hat{J}_z \rangle / N$ is shown in Fig. 2.19 (a). Here we have considered units relative to $\Delta = 1$, and $\omega = \omega_0 = 1$. This choice of parameters correspond to the experimentally relevant situation from [117], where the system under study is in the strong atom-coupling regime at zero detuning, $\Delta = \omega$. As the order parameter goes to zero, the system has populated one of its modes maximally, equivalently the system is "localised". In the case $\Psi = 1$ the two species are equally populated, and the system is "delocalised". Still, for this system there is no coherence between the two species such that $\langle \hat{J}_x \rangle = 0$ always. The fluctuations of $\hat{J}_x$ are small but non-zero, so that the tunnelling correlation, $\mathcal{C} = 4\langle \hat{J}_x^2 \rangle$, is a measure of the conversion between the two species [see Fig. 2.19 (b)]. Also, one can see that the fluctuations in the particle number in one of the species drop to zero in the region where we have the localised state [Fig. 2.19 (c)]. Somehow surprising is the finding that for small Γ and large Λ the fluctuations are suppressed, in clear contrast with the large Γ regime. The effect of Δ in the phase diagram is to control the size of the localisation region. As Δ approaches zero, the system is always in the delocalised regime and $\Psi = 1$, while as we increase it, the region where $\Psi \sim 0$ becomes larger. The shell structure seen in the order parameter and other quantities is characteristic of the Dicke model, when the non-linear

[7] Since our scheme of solution relies on the exact diagonalisation of the Hamiltonian by numerical means it bears no advantage to use the rotating-wave approximation, which is only valid for small atom-photon coupling. Instead we focus on the resonant case and we consider arbitrary atom-photon coupling.

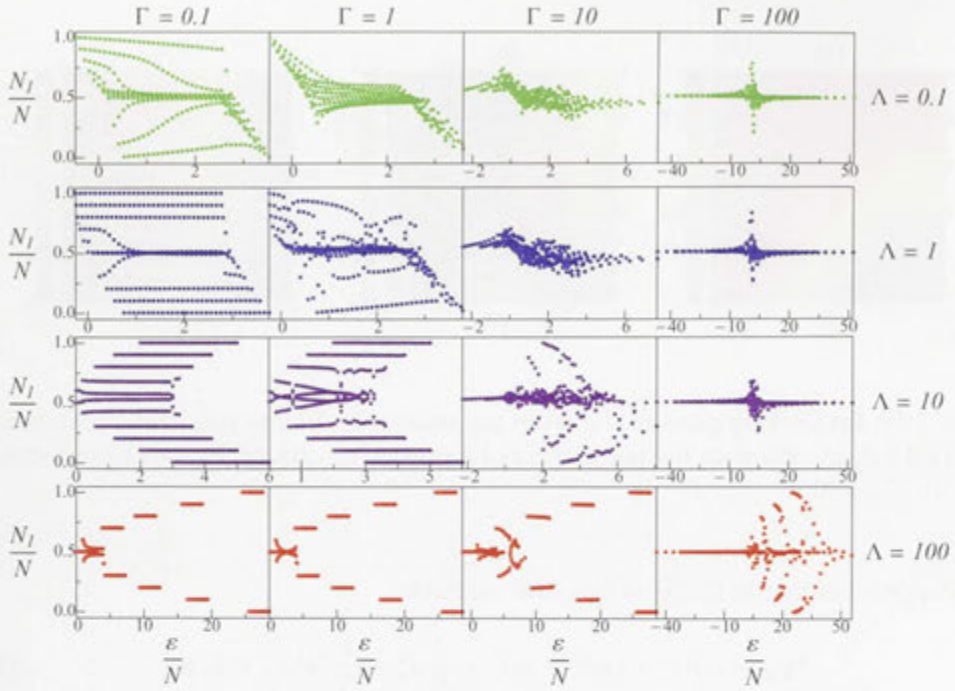

Figure 2.20: The number of atoms in mode "1" as a function of the energy eigenstates for different interaction parameters. The columns show the variation in the atom-photon coupling ($\Gamma = 0.1, 1, 10, 100$ from left to right), while the atom-atom interaction varies in the rows (same colours: $\Lambda = 0.1$(green), 1(blue), 10(purple), 100(red)).

term is absent, and is due to the photons in the system[8]. Above the first shell the system is "super-radiant" [57], the process of emission and absorption of photons by the atoms becomes coherent. Therefore the localised to delocalised transition is equivalent to the transition to the super-radiant state when $\Lambda = 0$. As we increase Λ the system is in a crossover where quantum fluctuations are suppressed below the critical value of Γ for the super-radiant transition at $\Lambda = 0$.

The characteristic dependences of one-body and two-body correlations on the energy eigenstates differ from those of the simple Bose-Hubbard double-well. For this system, there are relaxation processes with very small relaxation times but the fluctuations around the mean value of the correlations can be very large. Therefore we can't talk about statistically stationary states, because the photons induce excitations preventing the relaxation to a stationary state. Still, because $\langle \hat{b}_1^\dagger \hat{b}_2 \rangle \equiv 0$, the reduced one-body density matrix is in a preferred basis, but without a stationary state. Thus, the few-body properties of the system are strongly influenced by quantum fluctuations and the photon field [9]. We consider the behaviour with respect to the basis of eigenstates motivated by

[8] By shells we mean the different plateaus in the density plots of Fig. 2.19. In (a) these occur for $\Gamma = 0$ at $\Lambda \approx 1.2, 1.4, 2.0, 3.3, \ldots$, with $\Psi = 0.2, 0.4, 0.6, 0.8, \ldots$.

[9] In the Hamiltonian (2.22) we have not included losses, if we would include losses phenomenologically in the photon field, then relaxation to a stationary state should occur. Alternatively, one could introduce losses in the system using Heisenberg-Langevin equations i.e. [118].

the possibility of preparing the system for combinations of population of the two species, polarised states and their behaviour. Other applications of the current analysis are the evolution of a state of the system for $T > 0$, where one needs the analysis of the full spectrum of the Hamiltonian (2.23), and the finite temperature analysis of the behaviour of the super-radiant transition and the effect of the many-body interaction of the atoms.

One can see that the particle number in one of the species has a remarkably different behaviour from the single species double-well model, in the sense that the photons have induced the appearance of a series of quasi-degenerate in number stationary eigenstates. In the limit where we have an infinite number of photons one would get that the energy difference between the values of the population of the lowest mode in the BEC N_1 in Fig. 2.20 will approach zero. As a consequence, one would have a number of curves of the order of the number of atoms in the system. As seen from the ground state phase diagram the ground state energy ranges from being localised for $\Lambda \lesssim 1$ and moderate $\Gamma \lesssim 1$, to be delocalised for $\Lambda \gtrsim 1$ and $\Gamma \gtrsim 10$. In general as one increases Λ the population N_1 can only take certain quasi degenerate values for a certain energy. The variation of N_1 as we increase Λ for small atom-photon interaction changes from favouring unbalanced states to favour highly degenerate balanced configurations as a function of the energy. Above a critical energy this process reverses, see first two plots in the first column of Fig. 2.20, and unbalanced configurations are favoured. For $\Lambda \gtrsim 10$ the behaviour as a function of the energy changes, now balanced configurations occur for low energy and for high energy unbalanced multiply degenerate configurations are present [see first plot third row of Fig. 2.20]. For $\Lambda \gg \Gamma$ we have the appearance of a double ladder of unbalanced population configurations. This is because the energy levels of the Hamiltonian when the atom-photon coupling is negligible, are quantised as follows,

$$\epsilon_m = \left(\Delta + \frac{\Lambda}{N} m\right) m, \quad m = -N/2, -N/2+1, \ldots, N/2-1, N/2$$

Since the atoms de-couple and $\hat{J}_z|\Psi\rangle = m|\Psi\rangle$, the spin operator in the z component, is approximately a good quantum number. Therefore the possible populations of the atoms in mode "1" are simply,

$$\frac{N_1}{N} = \frac{1}{2} + \frac{m}{N}. \tag{2.25}$$

so the quantised structure happens at the above energies and the width of the "steps" depends on the number of photons in the system. Without photons we would get a spectrum given just by the number of particles with very localised energy levels, like in the case of the simple double well, but the photons make the state to have a width proportional to N_a [see Fig. 2.18 (b)] . Therefore these states have a shorter life-time, than the purely atomic system. The ladder structure is a consequence of the finite number of atoms and, as we increase the number of atoms, we increase the number of steps, so that in the large N limit the behaviour becomes smooth.

As one increases Γ the photons destroy these configurations due to interaction and the population of the two species become equal for $\Gamma \gg \Lambda$, see the last column in Fig. 2.20. The interaction with the photons effectively suppress the emergence of these "quantised" population states. If both interaction parameters are of the same order of magnitude, still the behaviour of the atoms is dominant, and one needs larger atom-photon coupling to reach the completely balanced state in the whole energy spectrum.

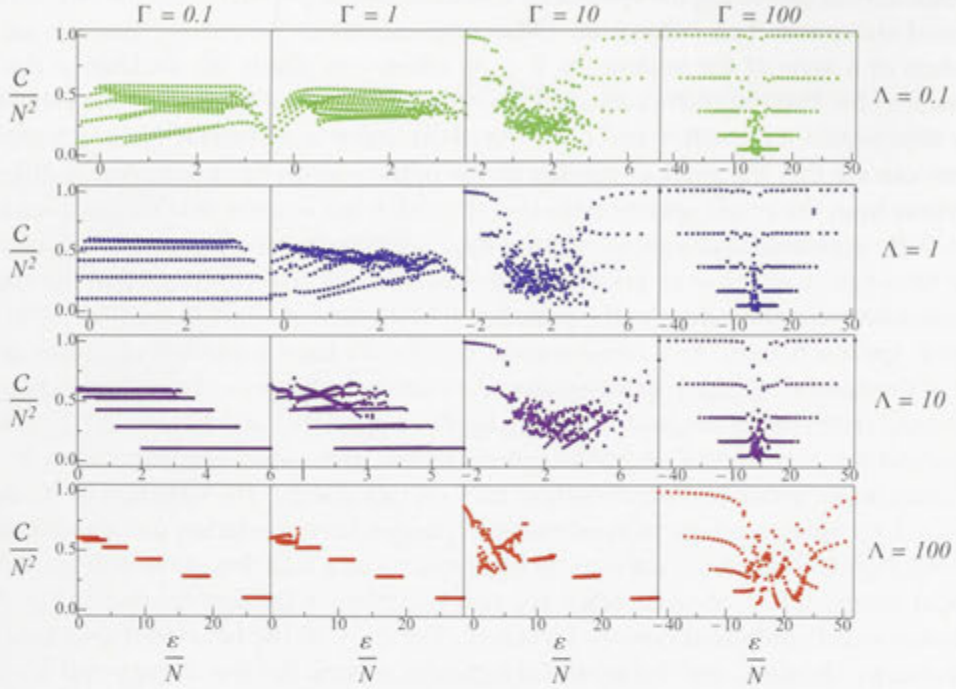

Figure 2.21: The tunnelling correlation of the atoms as a function of the energy eigenstates for different interaction parameters. The columns show the variation in the atom-photon coupling ($\Gamma = 0.1, 1, 10, 100$ from left to right), while the atom-atom interaction varies in the rows (same colours: $\Lambda = 0.1$(green), 1(blue), 10(purple), 100(red)).

The behaviour of the fluctuations in the particle number $\sigma_1 = \sqrt{\langle \hat{N}_1^2 \rangle - \langle \hat{N}_1 \rangle^2}$ and the tunnelling correlation $\mathcal{C}$ correlate with each other. The tunnelling has the same kind of behaviour as the occupancy of the higher energy modes in the sense that, as we increase the atom interaction, we observe the emergence of discretised degenerate curves [see Figs. 2.21 and 2.22 last column]. The interaction with the photons induces exchange between species (tunnelling). As one would expect, the interaction between atoms suppress the fluctuations in the population of species "1", as long as the interaction with the photons is moderate [see Fig. 2.22]. As one increases the interaction of the atoms with the photons, fluctuations are enhanced, and can be of the same order as the population of the mode [see Figs.2.22 and 2.20 last column] . The limit where we have large amplitude of the photon field such that $\hat{a} \to \beta \approx$ const. we have that the effective Hamiltonian is equivalent to the simple two-site problem, where the "tunnelling" amplitude between modes effectively depends on the photon amplitude, or alternatively we have a two site problem with the effective interaction scaled by a function of β, i.e. [119]. The behaviour of the energy spectrum in the limit of large atom-photon coupling is remarkably different from the strongly interacting atom limit and one could think of two kinds of symmetries manifesting in these extreme limits, this requires further investigation.

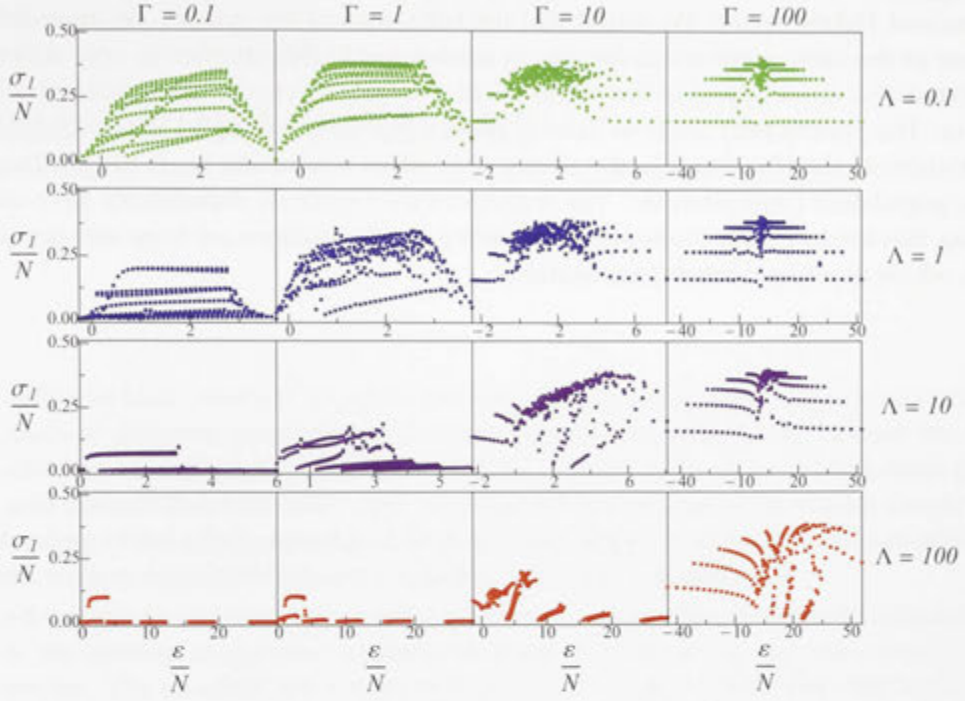

Figure 2.22: The atom number fluctuation of the atoms in mode "1" as a function of the energy eigenstates for different interaction parameters. The columns show the variation in the atom-photon coupling ($\Gamma = 0.1, 1, 10, 100$ from left to right), while the atom-atom interaction varies in the rows (same colours: $\Lambda = 0.1$(green), 1(blue), 10(purple), 100(red)).

2.9 Summary of results

We have analysed one- and two-body properties of the full quantum solution of the two-mode Bose-Hubbard fluid. We have discussed the transition from delocalised to self-trapped states, which occurs as the energy of the system is increased, provided that the pair-interaction strength is above a critical or threshold value. The full quantum solution for a large number of atoms differs from the mean-field approximation, since the latter predicts coherent Josephson-like oscillations while the exact solution shows that those oscillations decay to stationary like states in which the system spends most of its time. Since, measuring or having access to the N-body wave function appears as an impractical task in real systems, most of our understanding of macroscopic systems is based on knowledge of properties of few bodies. In this context, we argue that the decay, or relaxation, to a stationary state can be considered as decoherence, even if no interaction with an external environment is included. Such a decoherence is a consequence of the interatomic interactions.

We concluded our work in this Chapter with the analysis of another system whose representation is similar to the double well configuration, which was the BEC in a cavity. In this system we have two species coupled by a photon field under harmonic confinement. Thus, effectively the system can be treated within a two mode model with some

modifications. In this section we analysed the quantum Hamiltonian of the system in a truncated Hilbert space. We found that the behaviour of the system, yet amenable to the use of the same methods as the others considered in this chapter, is very different. We found that the coupling to the photon field strongly affects the configurations of the system. The photon field tends to destroy the analogous self-trapped states. Due to the symmetries in the Hamiltonian, the strong atom-atom interaction leads to quantisation of the population configurations. The analysis of the two-body correlations gave us the finding that for very large atom-photon coupling the fluctuations are large and get quantised, which deserves further investigation.

Chapter 3

Bose-Fermi mixtures

The ability to load ultracold quantum degenerate gases into periodic or quasi-periodic potentials of different geometries, created by optical lattices [13], has opened the way to realisation of well known condensed matter systems with atoms of fermionic [120–122] and bosonic character [123–128]. Such model systems allow us to gain deeper understanding of the fundamental problems in many body physics beyond the mean-field regime, such as transition between superfluid and Mott-insulator [51].

Self-trapping phenomena are among the most dramatic effects of atomic interactions [54] in the systems of quantum degenerate gases of restricted (e. g. one-dimensional) geometries . The so-called *macroscopic quantum self-trapping* (MQST) effect [58] manifests itself as localisation of most of the particles in the system in a particular region in space, as we have seen in the previous Chapter. The MQST and related effects in purely bosonic systems have been extensively analysed in different physical contexts, from the Josephson effect in superconductors [129] and the study of superfluid He^4 [130] to the alkali Bose-Einstein condensates [89].

In multi-site systems in the strongly interacting regime, new phenomena can emerge, such as quantum magnetism [20, 21] and the supersolid phase [22–25]. In general, these emergent phenomena belong to the class of quantum phase transitions and their mechanisms are strongly dependent both on the geometry of the lattice and the interaction between the atoms loaded into the lattice. The theoretical and experimental studies of these effects in large many-sites lattice systems are important both from the fundamental and applied points of view. For example, the physics of ultracold lattice systems where frustrations can occur is important for quantum computing [28, 31, 37, 131].

In the first sections of this chapter we will describe the effect of degenerate fermions on the self-trapping behaviour of ultracold bosons in a quasi-one dimensional symmetric double-well potential [46], in the limit of a finite number of fermions [132], which could be of the same order of magnitude as the number of bosons. In the presence of a confining potential, the fermions form a Fermi sea around the bosonic cloud (see Fig. 3.1). In order to analyse the static properties of the system we develop a quasi-analytical treatment of the system, based on a mean-field density approximation for the fermionic component and a coupled-mode theory for the bosonic component. In addition, a self-consistent numerical approach [55] is employed to analyze the self-trapping regimes in detail. We consider both attractive and repulsive interactions between bosons and fermions, which can be modified by means of Feshbach resonances [46, 132–137]. In particular, we take physical parameters corresponding to the mixture of ultracold ^{40}K-^{87}Rb atoms. We describe the effect of a Fermi sea on the formation of MQST states in the interacting bosonic

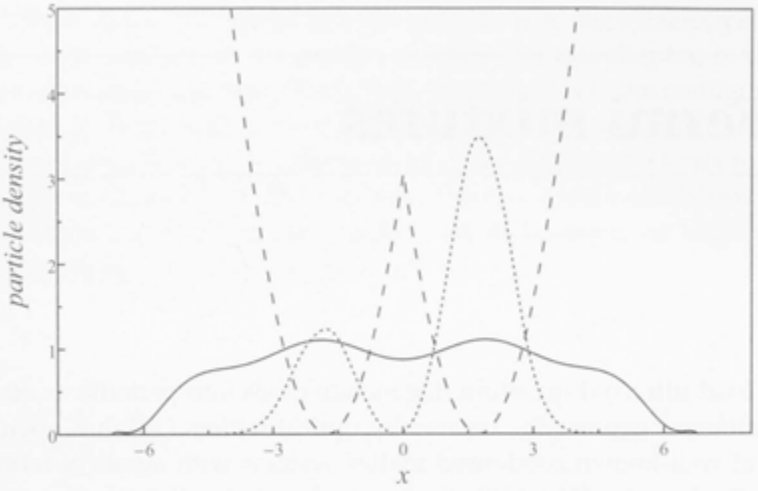

Figure 3.1: Schematics of the atomic density distribution for fermions (solid line) and bosonic condensate (dotted) in a macroscopic self-trapped stationary state formed in a one-dimensional double-well trapping potential (dashed), in the case of attractive inter-species interaction. In the repulsive case the picture is similar, however the inter-species interaction leads to the suppression of the fermionic density in the areas where the condensate density peaks.

component of the system and demonstrate, numerically, the difference in the dynamics of the systems with the attraction or repulsion between fermions and bosons. The two types of interaction between the atomic species can be achieved experimentally [133], which offers a unique opportunity to explore different MQST phases in the system.

After we address the effect of fermions in MQST, we will consider a minimal finite two-dimensional lattice model, namely a three-site ring of a Bose-Fermi ultracold mixture. Such a three-site system may be realised experimentally by engineering magnetic microtraps on an atomic chip, or by combining a harmonic potential with a triangular or Kagome lattice, as suggested in [138]. With the small number of atoms, this system lends itself to the Bose-Fermi-Hubbard model solvable by means of direct diagonalization. We consider the ground state of the system and investigate how the admixture of fermions leads to various phases, depending on the filling factor and inter-species interaction strength. In particular, we consider unusual insulating phases resulting from the inter-species interaction, which are connected to the existence of macroscopic self-trapping states in the mean-field regime [3].

In continuation to our analysis of minimal two-dimensional lattice systems, we consider a system with the essential ingredients of a topological insulator [29]. This model is a Bose-Fermi ultracold mixture in a double three-site ring configuration with four-sites. We employ direct diagonalization similar to the treatment we follow for the three-site ring, and we see the effect of an artificial position dependent vector potential applied. These artificial position dependent vector potentials have been recently realised in experiment [26, 27].

The Chapter is organised as follows: Section 3.1 introduces the second quantised and

the effective one-dimensional mean-field model for the quantum degenerate Bose-Fermi mixture trapped in a one-dimensional double-well potential. Section 3.2 presents the derivation of the coupled mode theory for the BEC cloud coupled to the Fermi sea. Section 3.3 presents the analysis of the self-trapping regimes based on the coupled-mode theory and numerical self-consistent approach for inter-species attraction and repulsion. Section 3.4 introduces the three site ring model of the Bose-Fermi mixture, and the configurations of the ground state. Section 3.5 discusses the ground state phase diagram of the system depending on the filling factors of both statistics. Section 3.6 compares the states from a homogenous variational ansatz with the results from direct diagonalisation. Section 3.7 introduces our simplified model of a topological insulator, and analyses the effect of an artificial position dependent vector potential in the ground state phase diagram. Section 3.8 summarises our work.

3.1 Bose-Fermi mixture in a double-well potential

We consider a Bose-Fermi mixture trapped in a one-dimensional symmetric double well potential. This is the quasi-one dimensional limit of a strongly elongated trap in three dimensions ($3D$) with the transverse trapping frequency $\omega_\perp$. The Hamiltonian of the system can be written in second quantised form in terms of single particle operators for each of the particle species and the inter-species interaction between bosons and fermions:

$$\hat{\mathcal{H}} = \int_{\mathbb{R}} \mathrm{d}x \left\{ \sum_{\xi\in\{f,b\}} \hat{\psi}_\xi^\dagger \hat{H}_\xi \hat{\psi}_\xi + \frac{g_{bb}}{2} \hat{\psi}_b^\dagger \hat{\psi}_b^\dagger \hat{\psi}_b \hat{\psi}_b + g_{bf} \hat{\psi}_b^\dagger \hat{\psi}_f^\dagger \hat{\psi}_b \hat{\psi}_f \right\}, \tag{3.1}$$

where the bosons and fermions in the system are represented by their corresponding field operators: $\hat{\psi}_\xi^\dagger(x,t)$ (creation) and $\hat{\psi}_\xi(x,t)$ (annihilation); $\xi \in \{f,b\}$. The field operators obey the usual commutation (bosons) and anti-commutation (fermions) algebra.

The longitudinal (x-component) single-particle part of the Hamiltonian (3.1) includes a one-dimensional double-well trapping potential: $\hat{H}_\xi = \hat{p}_x^2/(2m_\xi) + m_\xi\omega_\xi^2(|x| - x_0)^2/2$. where the trapping frequencies and the masses for each of the species are denoted by ω_ξ and m_ξ, respectively. The distance between the minima of the double well is given by $2x_0$.

The interaction strengths g_{bb} and g_{bf} in (3.1) represent the scattering between bosons and boson-fermion, respectively. These coefficients are considered to be constant in the relevant region near their resonances and approximately proportional to their s-wave scattering length. The on-site fermion-fermion interaction is Pauli suppressed. We assume that the ground-state energy of the transverse trapping potential $\hbar\omega_\perp$ is larger than both ground-state energy of the bosons and the Fermi energy of noninteracting fermions in $3D$. Within this approximation the bosonic and fermionic fields in $3D$ can be factorized in transverse and longitudinal components with the transverse field taken as the ground state of the trapping potential independent of the longitudinal behaviour and statistics. This leads to to the one-dimensional interaction coefficients $g_{bb} = 2\hbar\omega_\perp a_{bb}$ and $g_{bf} = 2\hbar\omega_\perp a_{bf}$. Where the interaction strengths have been scaled from their the $3D$ values as in [55]. In the following sections we discuss both the inter-species repulsion and attraction, and show that the sign of the interaction leads to differences in the self-trapping regimes.

Following the treatment given in [55], we derive the equations of motions from the Hamiltonian (3.1) by using the Green's function method, and perform a mean-field approximation. We define the condensate wavefunction $\psi_b^0 \approx \langle \hat{\psi}_b \rangle$, and each of the wavefunctions corresponding to the fermions, $\psi_f^n \approx \langle \hat{\psi}_f^n \rangle$. Thus, we arrive to a set of $N_f + 1$ coupled mean-field equations: N_f equations corresponding to each of the fermions and one for the BEC wavefunction [55]:

$$i\hbar\partial_t \psi_f^n = (\hat{H}_f + g_{bf}\rho_b)\psi_f^n, \tag{3.2}$$

$$i\hbar\partial_t \psi_b^0 = (\hat{H}_b + g_{bb}\rho_b + g_{bf}\rho_f)\psi_b^0, \tag{3.3}$$

where, $\rho_f = \sum_{n=1}^{N_f} |\psi_f^n|^2$, and $\rho_b = |\psi_b^0|^2$. The number of bosons (fermions) in the system is given by: $N_\xi = \int_{\mathbb{R}} \mathrm{d}x \rho_\xi$, and the ratio $r_{fb} = N_f/N_b$ defines the concentration of fermions. By introducing the scaling units of time, $2/\omega_b$, length, $\sqrt{\hbar/(m_b\omega_b)}$, and energy, $\hbar\omega_b$, the model can be cast in the following dimensionless form:

$$i\frac{m_f}{m_b}\partial_t \psi_f^n = -\partial_x^2 \psi_f^n + V_f \psi_f^n + u_0 |\psi_b^0|^2 \psi_f^n, \tag{3.4}$$

$$i\partial_t \psi_b^0 = -\partial_x^2 \psi_b^0 + V_b \psi_b^0 - \sigma |\psi_b^0|^2 \psi_b^0 + u_1 \rho_f \psi_b^0, \tag{3.5}$$

where the bosonic wavefunction and fermionic density are rescaled as $\psi_b^0 \to \psi_b^0[\hbar\omega_b/(2|g_{bb}|)]^{1/2}$ and $\rho_f \to \rho_f \hbar\omega_f/(2|g_{bb}|)$, respectively, $u_0 = g_{bf}m_f/(|g_{bb}|m_b)$, $u_1 = g_{bf}\omega_f/(|g_{bb}|\omega_b) = g_{bf}\sqrt{\kappa_f m_b/m_f}/|g_{bb}|$, $\sigma = -\mathrm{sgn}(g_{bb})$. The double-well potential for bosons or fermions, $V_\xi = m_\xi \kappa_\xi (|x| - x_0)^2/m_b$, is parametrized by the ratio of the trapping strengths, $\kappa_\xi = (m_\xi \omega_\xi^2)/(m_b \omega_b^2)$ which determines the spatial scale of the effective trapping potentials experienced by the different species of atoms.

3.2 The coupled mode theory

Numerical solutions of the model equations (3.4) are tractable when the number of fermions is small [55]. However, the current state-of-the art experiments [132] suggest that the system should be considered in the regime of moderate to large number of atoms, both for bosonic and fermionic components. We therefore consider the density of fermions ρ_f taking its stationary limit near the condensation temperature of the bosons. In this limit, the fermions can be described in the first approximation by a filled Fermi sea, where the Fermi points $\pm k_F$ are invariant upon the interaction, and Luttinger's theorem holds for the fermionic component [139, 140]. If the Fermi energy is sufficiently higher than the chemical potential of the BEC cloud, then it can be assumed that the dynamics of the fermionic cloud occurs on a much larger time scale than that of the bosons and consider the dynamics of the bosonic component under the influence of the quasi-static distribution of fermionic density $\rho_f(x)$.

Next, following the coupled-mode theory for Bose-Einstein condensates trapped in a double-well potential, developed in [56], we assume that the main contribution to the bosonic condensate wavefunction comes from the two lowest *nonlinear modes* of the double-well potential, corresponding to the symmetric ground state, $\Phi_0(x)$, and anti-

symmetric first excited state, $\Phi_1(x)$:

$$\psi_b^0 = \sum_{j=0}^{1} \Phi_j(x) B_j(t) \exp(-\mathrm{i}\mu_j t + \sigma C_j n_j t)/\sqrt{n_j}, \tag{3.6}$$

where $B_j(t)$ is the time-dependent amplitude of the relevant state ($j = 0, 1$), μ_j is its energy, $n_j = \int_{\mathbb{R}} \mathrm{d}x\ \Phi_j^2$ and $C_j = \int_{\mathbb{R}} \mathrm{d}x\ \Phi_j^4/n_j^2$. The nonlinear modes Φ_j obey the following stationary equations derived from (3.5):

$$\frac{d^2\Phi_j}{dx^2} + \mu_j\Phi_j - (|x| - x_0)^2\Phi_j + \sigma\Phi_j^3 + u_1\rho_f(x)\Phi_j = 0, \tag{3.7}$$

The equation (3.7) is equivalent to a standard mean-field Gross-Pitaevskii equation (GPE) for a BEC with a position dependent potential term modified by the nonlinear interaction with the fermionic cloud.

Substituting the ansatz (3.6) into (3.5) and using (3.7), we recover the system of two coupled equations for the mode amplitudes [56]:

$$\begin{aligned}
\mathrm{i}\frac{dB_0}{dt} &= \sigma C_0|B_0|^2B_0 + \sigma C_{01}\left(2|B_1|^2B_0 + B_0^*B_1^2\mathrm{e}^{-\mathrm{i}\Omega t}\right), \\
\mathrm{i}\frac{dB_1}{dt} &= \sigma C_1|B_1|^2B_1 + \sigma C_{01}\left(2|B_0|^2B_1 + B_1^*B_0^2\mathrm{e}^{+\mathrm{i}\Omega t}\right),
\end{aligned} \tag{3.8}$$

where: $C_{01} = \int_{\mathbb{R}} \Phi_0^2\Phi_1^2\mathrm{d}x/(n_0n_1)$, and $\Omega = 2(\mu_1 - \mu_0) + 2\sigma(C_1n_1 - C_0n_0)$. This system of nonlinear coupled equations describes the dynamical population exchange between the lowest energy states of the condensate cloud in a double-well potential. In this system of coupled equations the constants μ_j, C_j, C_{01} and n_j depend on the solution of (3.7) (see the Appendix) and therefore on the shape of the fermionic density distribution and the strength of the inter-species interaction. As shown in [56] for the case of a pure bosonic system, the dynamical system (3.8) admits phase-locked solutions corresponding to macroscopically self trapped states, characterized by the arrest of tunnelling and formation of a stationary BEC density distribution which is nonzero in each well but strongly unbalanced.

In order to analyse possible regimes of the self-trapping in the presence of the Fermi component, we will set the physical parameters of the system to those of a ^{40}K - ^{87}Rb quantum degenerate mixture [46, 132–135]. We study the system where the rescaled one-dimensional s-wave inter-species interaction parameter is attractive, $a_{bf} \approx -234\,\alpha a_0$ for ^{40}K - ^{87}Rb and for the repulsive case, we consider $a_{bf} \approx +234\,\alpha a_0$, where a_0 is the Bohr radius and α is a strength parameter. The boson-boson scattering parameter is $a_{bb} \approx 98.98\,a_0$ [132]. The double well angular frequency for ^{87}Rb is $\omega_b \approx 2\pi \times 263$ Hz (see [46]) and $\omega_f = \omega_b\sqrt{m_b/(m_f\kappa_f)}$. In a realistic experimental situation $\kappa_f \sim 1$ [141]. In the following section, we examine the difference in the self-trapping scenario for bosons caused by the different types of inter-species interactions.

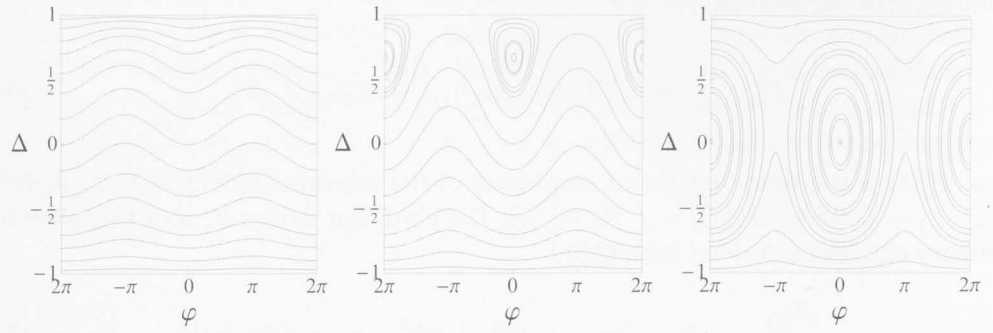

Figure 3.2: Parametric plots of the typical solutions to the system of equations given by (3.9), for $x_0 = 1.1$(left), 1.5(middle), 2.5(right) for $r_{fb} = 0$. (Reproduced after Ref. [56]).

3.3 Self-trapping regimes

Our aim is to establish the parameter space where MQST occurs in the mixed-species system. To this end, we use the ansatz, $B_j(t) = \sqrt{n_j(t)}\exp[-\mathrm{i}\phi_j(t)]$, which allows us to rewrite the system (3.8) in terms of the the difference in relative populations of the modes $\Delta = n_1 - n_0$ and the relative phase shift, $\varphi = 2(\phi_0 - \phi_1) - \Omega t$ [56]:

$$\begin{aligned}\frac{d\Delta}{dt} &= \sigma C_{01}(n^2 - \Delta^2)\sin\varphi,\\ \frac{d\varphi}{dt} &= -\delta + \sigma(C_0 + C_1)\Delta - 2\sigma C_{01}(2 + \cos\varphi)\Delta,\end{aligned} \tag{3.9}$$

where $\delta = 2(\mu_1 - \mu_0) + \sigma[(n - 2n_0)C_0 - (n - 2n_1)C_1]$, and $n = n_0 + n_1 = \text{const}$. The self-trapped states correspond to the regime where the relative phase shift is fixed to an integer of 2π, $\varphi = 2\pi m$. The difference in the population for the MQST states is given by the self-trapping parameter:

$$\frac{\Delta_{01}}{n} \approx \frac{2(\mu_1 - \mu_0)}{\sigma(C_0 + C_1 - 6C_{01})}, \quad -1 \leq \frac{\Delta_{01}}{n} \leq 1. \tag{3.10}$$

The limiting cases correspond to the situation when only the symmetric or antisymmetric mode is populated, resulting in the equal number of atoms in each well. The ultimate self-trapped state, when all the atoms are localised in one well, corresponds to $\Delta_{01} = 0$. The value of the self-trapping parameter Δ_{01} is strongly influenced by the mode coupling strengths C_{ij} and the effective energies μ_j of the nonlinear modes. In our model these can be determined semi-analytically by means of a variational approach. This approach employs an ansatz for the macroscopic wavefunction of the condensate, Φ, in the form of a linear combination of the symmetric Φ_0, and anti-symmetric Φ_1 eigenstates of the double-well potential: $\Phi(x) = \Phi_0(x) + \Phi_1(x)$, where:

$$\Phi_{0,1}(x) = A_{0,1}\left(\mathrm{e}^{-\frac{(x-x_0)^2}{2a_{0,1}^2}} \pm \mathrm{e}^{-\frac{(x+x_0)^2}{2a_{0,1}^2}}\right), \tag{3.11}$$

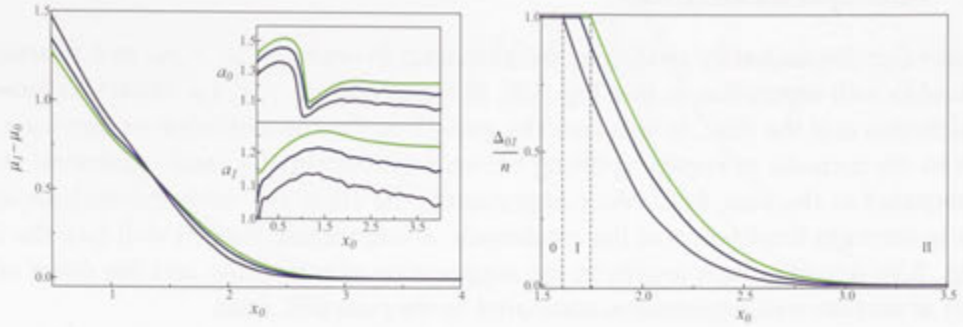

Figure 3.3: Left panel: The difference in energies, $\mu_1 - \mu_0$, as a function of the double well separation x_0, for attractive inter-species interaction. Inset: variation of the widths of the condensate wavefunctions, $a_{0,1}$, vs. x_0. Parameters are: $\alpha = 25$, $r_{fb} = 0$ (green), 2.5 (blue), 7.5 (purple). Right panel: The macroscopic quantum self-trapping parameter Δ_{01}/n as a function of the well separation, x_0, for attractive inter-species interaction. Parameters are: $\alpha = 25$, $r_{fb} = 0$ (green), 2.5 (blue), 7.5 (purple). The roman numerals stand for regions with different symmetry properties of the BEC wavefunction (see text).

and the amplitudes, A_j, and widths, a_j, are the variational parameters to be determined for each μ_j. The details of the variational calculations of the chemical potential and self-trapping parameters are presented in the Appendix. Parametric plots of the typical solutions to the system of equations given by (3.9), at different separations using the variational ansatz to calculate the corresponding mode couplings C and the effective energies μ, are shown in Fig. 3.2. The solutions clearly have a running phase for small separations and as we increase the separation, solutions with self-trapped phases appear at $\varphi = 2\pi m$ (where m an integer). The variational approach allows us to identify clearly the origin of the different behaviour in the self-trapping depending on the type of the inter-species interaction. We stress here that that width and peak density of the bosonic cloud in the ansatz are strongly dependent upon the form of the fermionic density, $\rho_f(x)$ due to extra term in the GPE, (3.7).

For each value of the well separation, x_0, the density $\rho_f(x)$ can be determined by employing a self-consistent numerical relaxation routine. Namely, we solve the eigenvalue problem for each fermion, initially without the coupling to the bosons. In the next steps, we adiabatically turn on the interaction with the bosonic cloud and calculate, iteratively, corrections to the fermionic density due to the interaction with bosons. The spatial shape of the bosonic fraction is obtained from our variational computation in the absence of coupling. The resulting fermionic density profile takes into account the feedback of the bosons on the fermions, as well as the nonlinear interaction between bosons. This approach enables for a semi-analytical treatment of the model equation (3.5) governing the behaviour of bosons in the presence of moderate to large ($N_f \sim 10^2 - 10^3$) number of fermions. Alternatively, the whole procedure can be performed numerically, with the variational solution for the BEC wavefunction replaced with that determined from the stationary mean-field model by means of a standard relaxation method [142]. In all our calculations we tested that our variational solution for the BEC component is in good agreement with the numerical solution of the stationary equation (3.7).

3.3.1 Inter-species attraction

We start our discussion by analysing the difference in energies, $\mu_1 - \mu_0$, as a function of the double well separation x_0 (see Fig. 3.3), in the case of $a_{bf} < 0$, i.e. attraction between the fermions and the BEC. In this case the growth in the concentration of fermions, r_{fb}, leads to the increase of energy splitting between anti-symmetric and symmetric states, as compared to the pure BEC. More importantly, the attractive inter-species interaction leads to stronger localisation of the condensate wavefunction in each well (see the inset in Fig. 3.3), which in turn results in the suppression of tunnelling and the onset of the MQST at smaller well separations, compared to the pure BEC case.

The behaviour of the population imbalance, $\Delta_{01}(x_0)$, is shown in Fig. 3.3. In the region marked 0 there is no self-trapping effect. In contrast, for region I, self-trapping occurs at smaller separation than in the pure bosonic system. As we increase the separation, the system moves deeper into the self-trapped regime, where the macroscopic wavefunction is completely localised in one of the two wells, and both the symmetric and antisymmetric modes are equally populated (see region II).

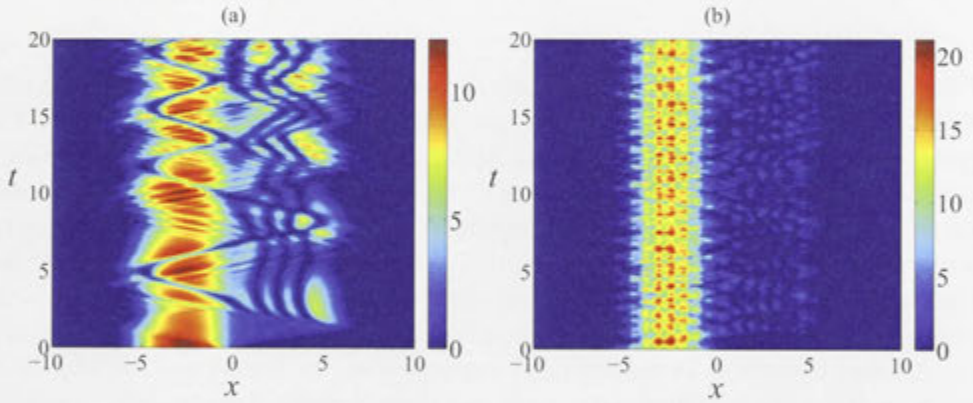

Figure 3.4: Evolution of the bosonic density $|\psi_b^0|^2$ for attractive inter-species interaction at the separation $x_0 = 2.625$ with concentrations $r_{fb} = 0.0$(a), 2.0(b), and $\alpha = 50$.

In order to test the prediction regarding the onset of the MQST, we perform numerical simulations of the propagation of the stationary solution obtained numerically for moderate number of particles ($\sim 10^2$) of each species. We can see that the effect of the fermions on the bosons is consistent with the results of our variational solution, seen in Fig. 3.4. In the case of the pure BEC for the separation considered in Fig. 3.4, self-trapping at such small well separations can not be achieved yet, thus an unbalanced state exhibits oscillations between left and right wells. The inclusion of the fermions in the system changes the behaviour of the BEC at the same value of well separation, making the cloud narrower while driving the BEC component into the self-trapping regime. The numerical simulations were done using a relaxation routine to generate the initial unbalanced solutions of the pure BEC from the Gross-Pitaevskii equation (3.7) with $u_1 = 0$. We turned on the interaction with the fermions and used the static density profiles from solving the eigenvalue problem of the stationary Schrödinger equations derived from (3.4) with the potential given at a certain separation x_0 for each fermion in the system. Finally, we let

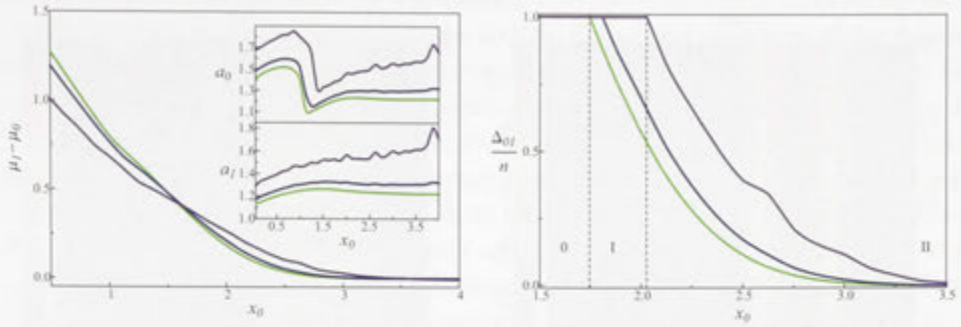

Figure 3.5: Left panel: The difference in energies, $\mu_1 - \mu_0$, as a function of the double well separation x_0 for repulsive inter-species interaction. Inset: the variation of the widths, $a_{0,1}$ vs. x_0 . Parameters are: $\alpha = 25$ $r_{fb} = 0$ (green), 2.5 (blue), 7.5 (purple). Right panel: The macroscopic quantum self-trapping parameter Δ_{01}/n as a function of the well separation, x_0, for repulsive inter-species interaction. Parameters are: $\alpha = 25$, $r_{fb} = 0$ (green), 2.5 (blue), 7.5 (purple). The roman numerals stand for regions with different symmetry properties of the BEC wavefunctions (see text).

the system evolve in time solving (3.5) by using a Runge-Kutta method in the Fourier domain and we transform back to real space at each time step.

3.3.2 Inter-species repulsion

The energy splitting between the ground and the first excited state of a BEC in the double-well potential in the case of repulsive inter-species interaction, $a_{fb} > 0$, has the opposite behaviour compared to the attractive case. In the limit of small separations, the energy difference of the mixture is smaller than that of the pure BEC [Fig. 3.5].

The dependence $\Delta_{01}(x_0)$ is shown in Fig. 3.5. The MQST states exist in all regions except from the region 0. The onset of the MQST effect in a mixture occurs at greater well separations compared to that of a pure BEC system (see region I). This is due to the fact that the presence of repulsive fermions leads to the effective broadening of the BEC wavefunction [see inset in Fig. 3.5], which extends the regime of enhancement of inter-well tunnelling to larger well separations. Therefore localisation of an unbalanced state is achieved only for larger values of well separation compared to the pure bosonic case. Our numerical simulations of the dynamics of the mixed cloud confirm that, in the case of inter-species repulsion for a moderate number of particles ($N_f \sim 10^2$), the self-trapping regime is suppressed, as compared to the purely bosonic case, and the bosonic cloud suffers from broadening, see Fig. 3.6.

3.3.3 Signatures of self-trapping

The nontrivial nature of the self-trapping in the case of the mixture of the BEC and the degenerate Fermi cloud can potentially be explored in an experiment with a double-well potential, similar to that presented in [46]. In an experiment, however, one would measure the difference in atom numbers between the BECs occupying two different wells of the potential, ΔN, rather than the populations of two nonlinear modes $\Phi_{0,1}$. Possi-

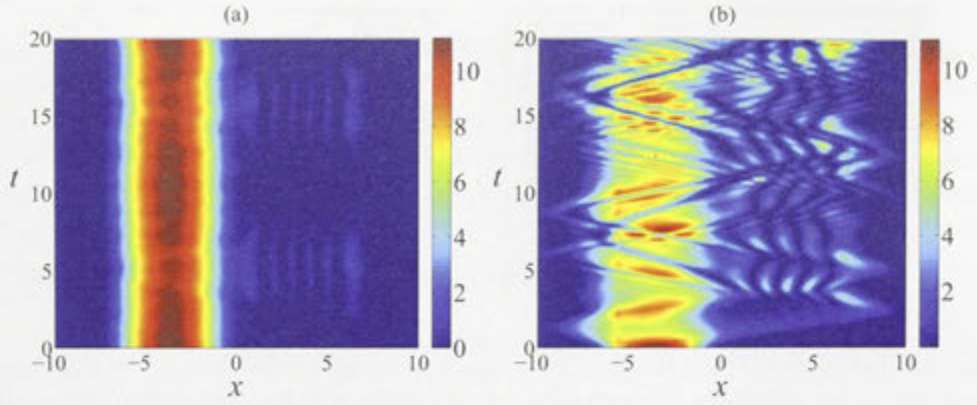

Figure 3.6: The order parameter $|\psi_b^0|^2$ for repulsive interaction at the separation $x_0 = 3.625$ with concentrations $r_{fb} = 0.0$(a), 2.0(b) and $\alpha = 20$.

ble results of such a measurement are shown in Fig. 3.7, as predicted by (a) variational results, and (b) numerical simulations. It can be seen that, in contrast to the case of a pure BEC (green line), the mixture with the attractive inter-species interaction facilitate the self-trapped state for smaller separations (blue line) and the repulsive interspecies interaction shifts the onset of self-trapping to larger separation values (purple line). The population imbalance, $\Delta N/N_{Tot}$, where N_{Tot} is the total number of BEC atoms, is a function of well separation [see Fig. 3.7 (a)] given by:

$$\frac{\Delta N}{N_{Tot}} = \left(\frac{n^2 - \Delta_{01}^2}{n^2 + \Delta_{01}^2}\right) \frac{\mathrm{erf}(y)}{(1 - \exp(-2y^2))^{1/2}}, \quad y = \frac{x_0}{a_1} \tag{3.12}$$

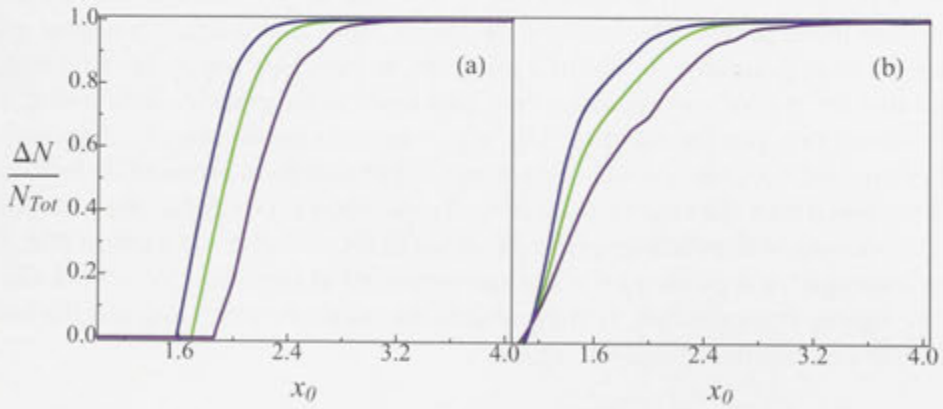

Figure 3.7: (a) Variational result of the relative population imbalance between the two potential wells in a self trapped state for attractive fermions (blue), repulsive fermions (purple) and pure bosons (green), the system with fermions has a concentration $r_{fb} = 7.5$ as a function of well separation. (b) Time averaged population imbalance between two potential wells, where an initially unbalanced state has been evolved over time. Parameters are the same as in (a).

Finally, we note that the effect of the fermions on the MQST is detectable for as long as the amount of fermions is not very large, so that the spatial structure of the fermionic density is still affected by the double-well nature of the potential. For a very large Fermi sea the fermionic density is nearly homogeneous across the spatial extent of the trap, which results in the homogeneous shift of the energy levels for the bosonic component. The effect of the fermions for fixed number of bosons on the MQST parameter at a fixed separation disappears as the concentration of fermions grows, and the value of the self-trapping parameter, Δ_{01}/n, asymptotically approaches that corresponding to the pure BEC system for that separation. As an example, for the repulsive mixed system at the separation $x_0 = 2$ and $\alpha = 5$ the MQST parameter differs from that of a pure BEC by 10% of its value when the number of fermions exceeds the number of bosons by the factor of 10^2.

3.4 The three-site ring model and the ground state configuration

We consider a mixture of ultracold bosons and fermions in a ring configuration of three sites. This system can be realized experimentally on an atomic chip or using optical lattices [138]. In the limit of small number of atoms this system can be described by the Bose-Fermi-Hubbard model and the ground state of the Hamiltonian can be obtained by direct diagonalization. In our model the atoms of different species are able to "hop" between nearest neighbour sites emulating the kinetic energy that they have and the bosons interact on-site while we consider spin-polarized fermions with on-site interactions excluded by the Pauli principle. The different species in the mixture interact, i.e. via Feshbach resonance, and have an effective attractive or repulsive many-body interaction.

We will obtain the ground state configuration of the model and construct its ground state phase diagram for different interaction parameters. We will see the effect of interactions in emergence of localised phases which are different from the regular "Mott-Insulator" phases of the pure Bose system [45]. We will show the effect of interactions on the superfluid order parameter, and the relation of these new phases with the enhancement of quantum fluctuations in certain parameter regimes.

Based on the standard Bose-Fermi Hubbard model (see, e.g. [143]), the Hamiltonian for the three-site ring can be written as follows:

$$\mathcal{H} = \mathcal{H}_b + \mathcal{H}_f + \mathcal{H}_{bb} + \mathcal{H}_{bf}, \tag{3.13}$$

where,

$$\mathcal{H}_\xi = -T_\xi \sum_{<l,m>} \left(\hat{\xi}_l^\dagger \hat{\xi}_m + \hat{\xi}_m^\dagger \hat{\xi}_l \right), \tag{3.14}$$

$$\mathcal{H}_{bb} = \frac{U_{bb}}{2} \sum_{l=1}^{3} \hat{n}_l^b \left(\hat{n}_l^b - 1 \right), \tag{3.15}$$

$$\mathcal{H}_{bf} = U_{bf} \sum_{l=1}^{3} \hat{n}_l^b \hat{n}_l^f. \tag{3.16}$$

Here $\hat{b}^\dagger$ ($\hat{b}$) are the creation (annihilation) operators for the bosons and $\hat{f}^\dagger$ ($\hat{f}$) the creation

(annihilation) operators for the fermions; the number operators are: $\hat{n}^{\xi} = \hat{\xi}^{\dagger}\hat{\xi}$, $\xi \in \{b, f\}$. The nearest neighbour tunnelling coefficient is T_{ξ}, the intra- and inter-species interaction strengths are $U_{bb} > 0$ and U_{bf}, respectively.

In general, one can write a state vector of the system as follows: $|\bar{\Psi}\rangle = |\bar{\Psi}\rangle_f \otimes |\bar{\Psi}\rangle_b = |n_1^f, n_2^f, n_3^f\rangle_f \otimes |n_1^b, n_2^b, n_3^b\rangle_b$, where, $n_1^f + n_2^f + n_3^f = N_f$, and $n_1^b + n_2^b + n_3^b = N_b$.

In the case of inter-species repulsion $N_f = 1$ and $N_b = 3$, the states corresponding to the lowest energy levels are the ones with the following on-site particle distributions:

$$\begin{aligned} |1\rangle_+ &\rightarrow |1,0,0\rangle_f \otimes |0,3,0\rangle_b, \\ |2\rangle_+ &\rightarrow |1,0,0\rangle_f \otimes |0,1,2\rangle_b, \\ |3\rangle_+ &\rightarrow |0,0,1\rangle_f \otimes |0,2,1\rangle_b, \\ |4\rangle_+ &\rightarrow |1,0,0\rangle_f \otimes |1,1,1\rangle_b, \end{aligned}$$

where $|1\rangle_+$, $|2\rangle_+$ and $|3\rangle_+$ have six-fold degeneracy, while $|4\rangle_+$ is a triplet. These states are schematically shown in Fig. 3.8 and the corresponding energies are plotted in Fig. 3.9 (left).

For attraction with $N_f = 1$ and $N_b = 3$ (see Fig. 3.8 and Fig. 3.9 (right)), the lowest-lying energy states are as follows:

$$\begin{aligned} |1\rangle_- &\rightarrow |0,0,1\rangle_f \otimes |0,0,3\rangle_b, \\ |2\rangle_- &\rightarrow |1,0,0\rangle_f \otimes |2,0,1\rangle_b, \\ |3\rangle_- &\rightarrow |1,0,0\rangle_f \otimes |1,0,2\rangle_b, \\ |4\rangle_- &\rightarrow |0,1,0\rangle_f \otimes |1,1,1\rangle_b, \end{aligned}$$

where the states with symmetry $|1\rangle_-$ and $|4\rangle_-$ are triplets and $|2\rangle_-$ and $|3\rangle_-$ have six-fold degeneracy. Similar ground state configurations occur at incommensurate filling, as shown in Fig. 3.10.

As the bosonic interaction strength changes, the ground state of the system is changing symmetry. The hierarchy of the lowest lying energy levels corresponding to different states is shown in Fig. 3.9 for the commensurate and in Fig. 3.11 for incommensurate filling of bosons. In the case of commensurate filling, for a fixed value of the inter-species interaction and growing U_{bb}, the ground state structure evolves from a mixture of degenerate states (a) and (b) to the state (f) (in Fig 3.8) in the case of inter-species repulsion, and from (d) to (e) and (f) in the case of inter-species attraction. Similarly, in the case of incommensurate filling, the ground state evolves from a mixture of states (a) and (b) to (c) and to the mixture of degenerate states (c) and (f) (see Fig. 3.10) for inter-species repulsion, and from (d) to (e), to the mixture of states (c) and (f) for the attractive inter-species interaction.

The energy spectrum of this small scale system exhibits a gap, Δ, given by the energy difference between the ground state and first excited manifold [see Fig. 3.12 (a)]. For the commensurate filling of bosons this gap opens up at sufficiently strong boson repulsion for both repulsive and attractive inter-species interaction, as well as for $U_{bf} = 0$ [see Fig. 3.12 (b)], and its magnitude is proportional to the interaction strength. It is reminiscent of the gap in the excitation spectrum of bosonic systems in lattices that indicates superfluid (SF) to Mott-insulator (MI) transition. Indeed, using the exact diagonalization of the Hamiltonian (3.13) and extracting characteristic behaviour of tunnelling correlations and

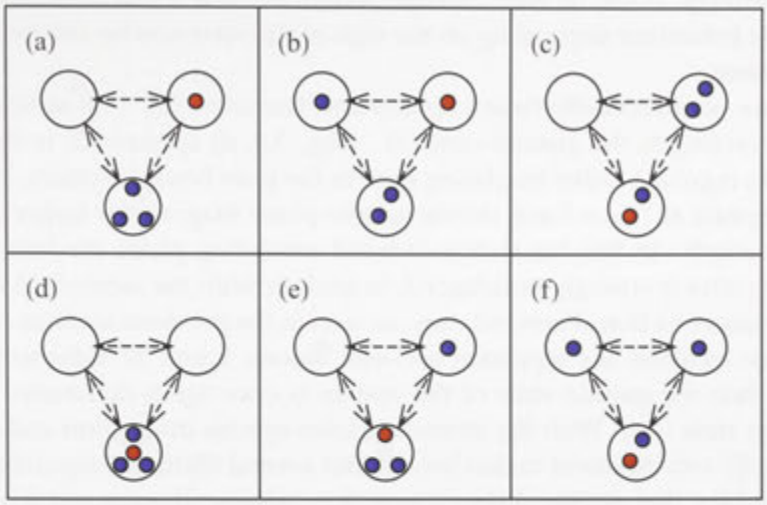

Figure 3.8: Schematics of the on-site state configurations of three bosons (blue circles) and one fermion (red circle), with the lowest energy. The figures correspond to the states: (a) $|1\rangle_+$, (b) $|2\rangle_+$, (c) $|3\rangle_+$, and (f) $|4\rangle_+$ for repulsive inter-species interaction, and (d) $|1\rangle_-$, (e) $|2\rangle_-$, (c) $|3\rangle_-$, and (f) $|4\rangle_-$ for inter-species attraction.

particle number fluctuations, we can construct the phase diagram of the ground state and examine the transition to the insulating states in our small-scale Bose-Fermi system.

3.5 Phase diagram

The typical characteristic quantity for different quantum phases of an ultracold quantum degenerate gas in a the lattice system is the spatial (tunnelling) correlation for the bosonic component η_b and the tunneling correlation of the fermionic component η_f, given by $\eta_\xi = |\langle \hat{\xi}_i^\dagger \hat{\xi}_{i+1} \rangle| / n_{\text{avg}}^\xi$, $\xi \in \{b, f\}$, where $n_{\text{avg}}^\xi = N_\xi/3$. The boson tunnelling correlation can be used to construct the phase diagram of the model, depending on the interactions. In a bosonic lattice this quantity tends to zero when the system is in the Mott-insulator regime, and approaches one when the system is in the superfluid regime. Similarly, in our small, finite, mixed-species system, this quantity can be used to delineate between an insulating and a superfluid state. The fermion tunnelling correlation measures the mobility of the fermion in the system. When its value is close to one, the fermion is mobile, and when it is zero, the fermion is pinned to one of the sites.

3.5.1 Commensurate boson filling

As a start, we analyse the components of the ground state for the system with a commensurate number of bosons, $N_f = 1$ ($n_{\text{avg}}^f = 1/3$), and for the fixed inter-species interaction strength $|U_{bf}| = 10$. The boson tunnelling correlation for $N_b = 3, 9$ is shown in Fig. 3.13. Due to the small number of particles, there exists a distinct crossover region between the SF ($\eta_b = 1$) and insulating ($\eta_b = 0$) regimes [138], where $0 < \eta_b < 1$. When this quantity is closer to either of the two extreme values, we will refer to it as a SF- or MI-enhanced

regime, respectively. It can be seen that the system exhibits a rich phase diagram with an asymmetric behaviour depending on the sign of the inter-species interaction and the number of bosons.

For the case of attraction between bosons and fermions, $U_{bf} < 0$, a new insulating phase corresponding to the ground state $|1\rangle_-$ (Fig. 3.8, d) appears. It is strikingly different from the regular MI-like insulating state in the pure bosonic system, $|4\rangle_\pm$ (see Fig. 3.8), which appears at $U_{bf} = 0$ and dominates the phase diagram for larger inter-species interaction strength. In this interaction-induced insulating phase the bosonic occupation of the ring sites is strongly unbalanced, in analogy with the mean-field macroscopic self-trapped states of a Bose-Fermi mixture, as seen in the previous sections of this Chapter [3]. As one increases the repulsion between bosons, a new SF enhancement region appears and then the ground state of the system is once again dominated by the regular insulating state $|4\rangle_-$. With the increasing inter-species interaction and the number of bosons, the SF enhancement region breaks into several filaments separated by the insulating states $|2\rangle_-$ that appear due to interaction between bosons and fermions. This change in the structure of ground state can also be followed in Fig. 3.9 (left). Due to the change of symmetry of the ground state at the points where different configurations become degenerate (level crossings in Fig. 3.9) we have the appearance of SF-enhanced regions where η_b has a local maxima lines.

In the case of inter-species repulsion, $U_{bf} > 0$, the system is superfluid for small U_{bb}. In Fig. 3.9 (a) one can clearly see that the ground state in this region is superposition of degenerate states $|1\rangle_+$ and $|2\rangle_+$, which is a typical sign of frustration. Insulating regions appear for larger inter-species interaction and are dominated by the $|2\rangle_+$ state [see Fig. 3.13 (b)]. For large U_{bb} transition to the regular insulating state $|4\rangle_+$ occurs.

For both signs of inter-species interaction, the behaviour in the regions where $U_{bb} \sim U_{bf}$ is SF-enhanced. The effect of increasing the number of bosons is to scale up the regions of SF behaviour and introduce additional insulating regions due to inter-particle interactions. The appearance of the gap in the energy spectrum (Fig. 3.12) correlates exactly with the insulating regions in the phase diagram.

While the phase diagrams in Fig. 3.13 (top) are based on the behaviour of the bosonic

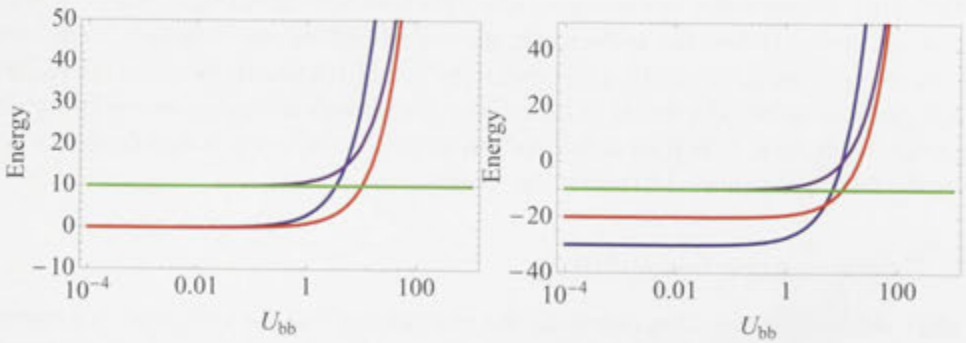

Figure 3.9: The energy of the states with the largest contribution to the ground state as a function of U_{bb} for inter-species (left) repulsion and (right) attraction with the fixed magnitude $|U_{bf}| = 10$. States with different symmetries are in different colours as: $|1\rangle_\pm$ (blue), $|2\rangle_\pm$ (red), $|3\rangle_\pm$ (purple), $|4\rangle_\pm$ (green).

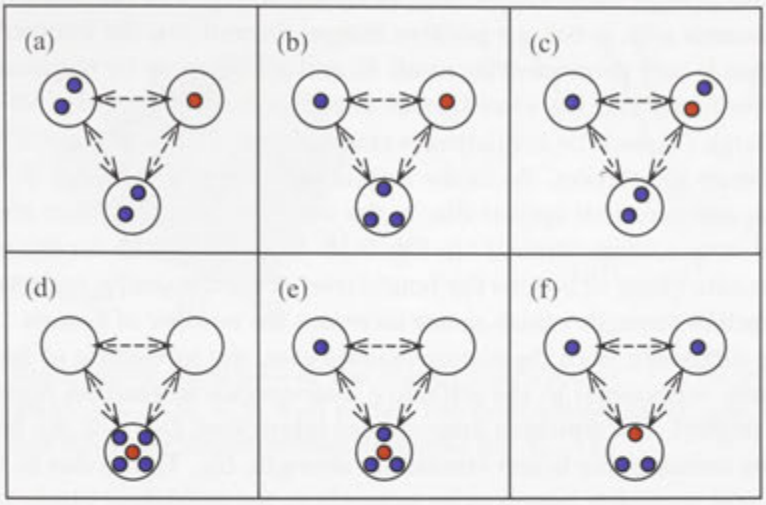

Figure 3.10: Schematics of the on-site state configurations of four bosons (blue circles) and one fermion (red circle), contributing to the lowest energy band. The panels (a), (b), (c), and (f) correspond to repulsive inter-species interaction and (d), (e), and (f) – to inter-species attraction.

fraction, it is useful to examine the tunnelling correlation of the fermion in the system. As seen in Fig. 3.13 (bottom left), in the region corresponding to the regular bosonic insulating state, (i.e. for $|U_{bb}| \gg 1$) and for low inter-species coupling, the fermions are free to hop between the ring sites, which can also be deduced from the symmetry of the $|4\rangle_{\pm}$ state [see Fig. 3.8]. In the mean-field picture [3] this behaviour reflects the fact that the effective interaction-induced potential seen by the fermion is weak and completely symmetric. As one increases $|U_{bf}|$, the fermions localise and no tunnelling is possible. In contrast to the regular insulating phase, the bosonic insulating phases that arise purely due to the inter-species interaction and correspond to symmetry-broken states (e.g. $|1\rangle_{-}$ or $|2\rangle_{+}$), naturally give rise to the regions of suppressed tunnelling of the fermion.

To characterise the interaction-induced insulating phases further, we look at the boson number fluctuations in the system given by $\sigma = \sqrt{\langle \hat{n}_i^b \hat{n}_i^b \rangle - \langle \hat{n}_i^b \rangle^2}/n_{\text{avg}}^b$, see Fig. 3.13 (bottom right). As expected from the MI behaviour, the fluctuations in the regular insulating phase (with the $|4\rangle_{\pm}$ symmetry) approach zero as one increases the strength of repulsion between bosons. In contrast, for attractive inter-species interaction the interaction-induced insulating region at low values of U_{bb} is dominated by fluctuations, which can be taken as a signature of the new insulating state.

3.5.2 Incommensurate boson filling

It has been noted (see, e.g. [138, 144]) that for a few-particle pure bosonic system at incommensurate filling a small superfluid fraction is always present, therefore no insulating state can occur. We find that this is indeed the case in our system with no fermions (or $U_{bf} = 0$). The insulating phases in this case occur only in the presence of fermions, with non-zero inter-species interaction strength. For the repulsive inter-species interaction the

insulating phase at large U_{bb} is suppressed, as shown in Fig. 3.14 (a), which is typical for $N_b = 3m + 1$ bosons with m being a positive integer. In contrary, the interaction-induced insulating region is very prominent for small N_b and is broken up by regions of enhanced superfluidity for larger N_b. For inter-species attraction both the regular MI-like insulating region at large U_{bb} and the insulating region at lower values of U_{bb} are retained due to the inter-species interaction. As in the case of commensurate filling, at large U_{bb} the new insulating domains that appear due to the inter-species interaction are dominated by the ground state configuration (f) in Fig. 3.10. In general, both for incommensurate and commensurate filling of bosons the boundaries of the insulating regions are pushed to larger interaction strength values as one increases the number of bosons.

In striking difference from the commensurate case, the tunnelling of fermions is almost completely suppressed in the attractive inter-species interaction region, $U_{bf} < 0$ [see Fig. 3.14 (right)]. For repulsive inter-species interaction, $U_{bf} > 0$, the fermion gains mobility as one increases the boson interaction strength, U_{bb}. This is due to the fact that, for larger U_{bb} and repulsive inter-species interaction, the insulating phase is dominated by the state (c) in Fig. 3.10 [see also Fig. 3.11 (left)]. In this case the fermion is always able to hop between the sites with lower bosonic occupation numbers. In contrast, in the case of inter-species attraction the insulating phase is dominated by the state (f) in Fig. 3.10 [see also Fig. 3.11 (right)] and the fermions are pinned to a site with the highest occupation of bosons. For weaker inter-species interaction, $U_{bf} < U_{bb}$, the fermion is delocalised as in the commensurate case.

3.5.3 Role of the fermion filling factor

So far, we have considered one fermion interacting with N_b bosons. Therefore, the results presented above are also applicable to a mixture of two bosonic species (see, e.g. [145]) with a single atom in one of the components. In the case of $N_f \neq 1$, the Bose-Fermi-Hubbard model is still valid for the fermion filling factor less than 1 (the system with no fermions is equivalent to the system with three fermions), and the fermion statistics influ-

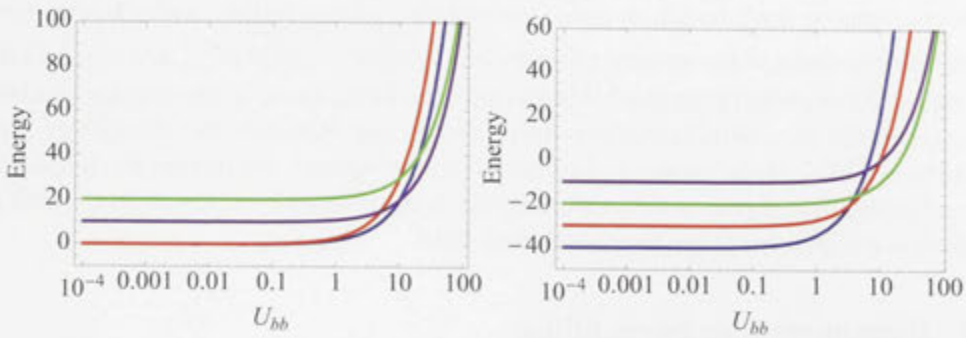

Figure 3.11: The energy of the states with the largest contribution to the ground state as a function of U_{bb} for inter-species (left) repulsion and (right) attraction with the fixed magnitude of inter-species interaction $|U_{bf}| = 10$. Energies of states with different symmetries shown in Fig. 3.10 are for repulsion (a) blue, (b) red, (c) purple, (f) green and for attraction (d) blue, (e) red, (c) purple, (f) green.

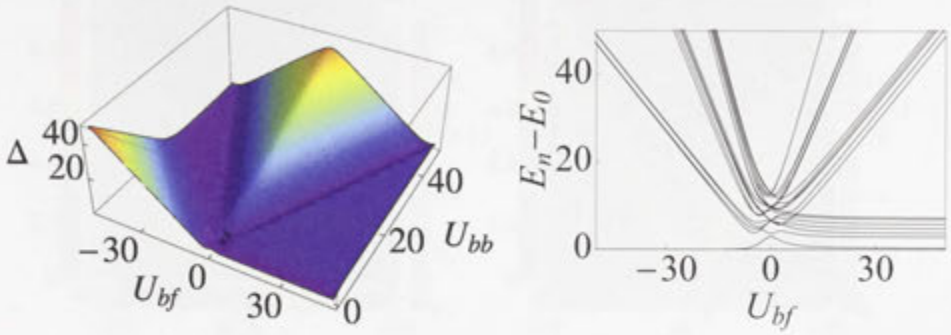

Figure 3.12: Right panel: Structure of the energy spectrum vs. U_{bf} for commensurate filling of bosons ($U_{bb} = 1$, $N_b = 3$). Left panel: The dependence of the gap, $\Delta = E_1 - E_0$ on the intra- and inter-species interaction strengths for $N_b = 3$.

ences the ground state configuration. In particular, the system is particle-hole symmetric for $1/3$ and $2/3$ filling of fermions. This fact is reflected in the behaviour of the phase diagram, so that the case of $1/3$ fermion filling with repulsive inter-species interactions corresponds to the case of $2/3$ fermion filling with attractive inter-species interaction. For example, in the case of $2/3$ filling of fermions the interaction-induced insulating regions appear for repulsive rather then attractive interaction between species, as seen in Fig. 3.15. Other characteristic properties of the system, such as the behaviour of the fermion tunnelling correlations and bosonic number fluctuations, are qualitatively the same as for $N_f = 1$. If one would consider larger fillings of fermions then one needs to move away from the single band picture of the standard Bose-Fermi-Hubbard model. One needs to include additional bands depending on the number of fermions and the number of sites due to the Pauli principle and additional couplings between bands must be considered [146–149].

3.6 A variational solution

In order to gain deeper understanding of the system and verify the non-trivial nature of the inhomogenous phases, we performed mean-field calculations using the following SU(3) coherent state ansatz [1] [138],

$$|\Psi_v\rangle = \frac{1}{\sqrt{N_b! N_b^{N_b}}} \hat{F}_f \hat{F}_b^{N_b} |0\rangle,$$

[1] The coherent state ansatz is equivalent to using a Hartree-Fock state, or alternatively to do mean-field theory.

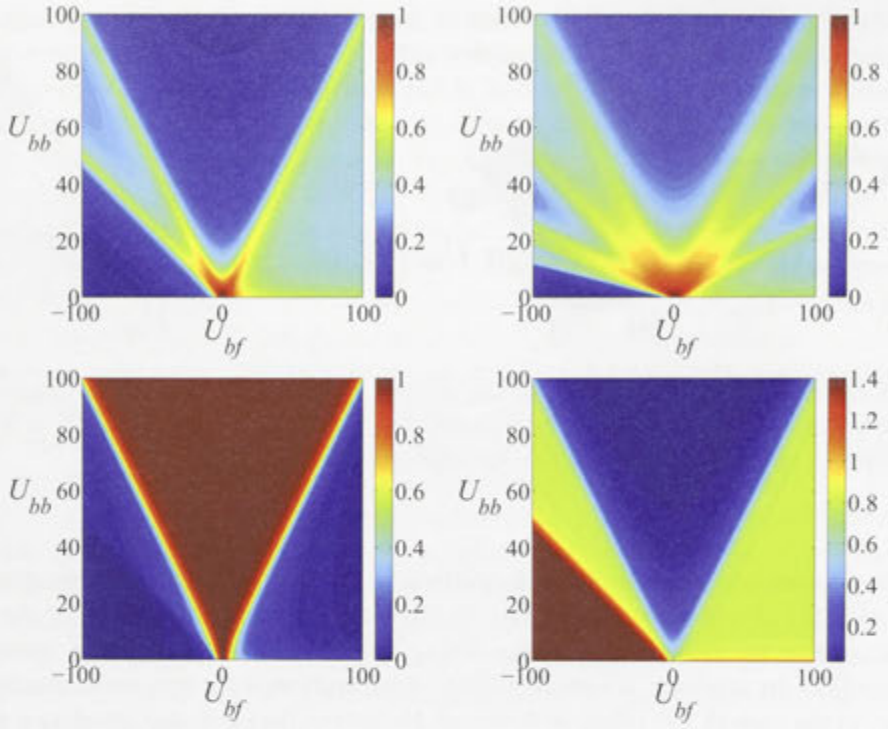

Figure 3.13: Top panels: Density plots of the boson tunnelling correlation, $\eta_b(U_{bf}, U_{bb})$, for (left) $N_b = 3$ and (right) $N_b = 9$. Bottom panels: Density plots of the (left) fermion tunnelling correlation, $\eta_f(U_{bf}, U_{bb})$ and (right) boson number fluctuations, $\sigma(U_{bf}, U_{bb})$ for $N_b = 3$.

where,

$$\hat{F}_f = \sum_{l=1}^{3} \psi_{f,l} \hat{f}_l^\dagger, \tag{3.17}$$

$$\hat{F}_b = \left(\sum_{l=1}^{3} \psi_{b,l} \hat{b}_l^\dagger \right)^{N_b}, \tag{3.18}$$

with, $\psi_{\xi,l}, \xi \in \{b, f\}$ as variational parameters, and $|0\rangle$ the vacuum state, conserved quantities are: $\sum_{l=1}^{3} |\psi_{b,l}|^2 = N_b$ and $\sum_{l=1}^{3} |\psi_{f,l}|^2 = 1$. The classical Hamiltonian can be derived as, $H = \langle \Psi_v | \mathcal{H} | \Psi_v \rangle$, we have:

$$H_b = -t_b \sum_{<l,m>} \left(\psi_{b,l}^* \psi_{b,m} + \psi_{b,m}^* \psi_{b,l} \right) + \frac{U_{bb}}{2} \left(\frac{N_b - 1}{N_b} \right) \sum_{l=1}^{3} |\psi_{b,l}|^4, \tag{3.19}$$

$$H_f = -t_f \sum_{<l,m>} \left(\psi_{f,l}^* \psi_{f,m} + \psi_{f,m}^* \psi_{f,l} \right), \tag{3.20}$$

$$H_{bf} = U_{bf} \sum_{l=1}^{3} |\psi_{b,l}|^2 |\psi_{f,l}|^2. \tag{3.21}$$

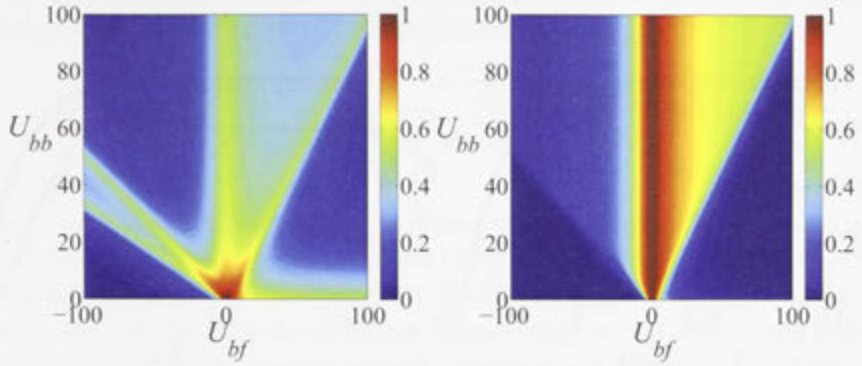

Figure 3.14: Density plot of the (left) boson and (right) fermion tunnelling correlation for $N_f = 1, N_b = 4$.

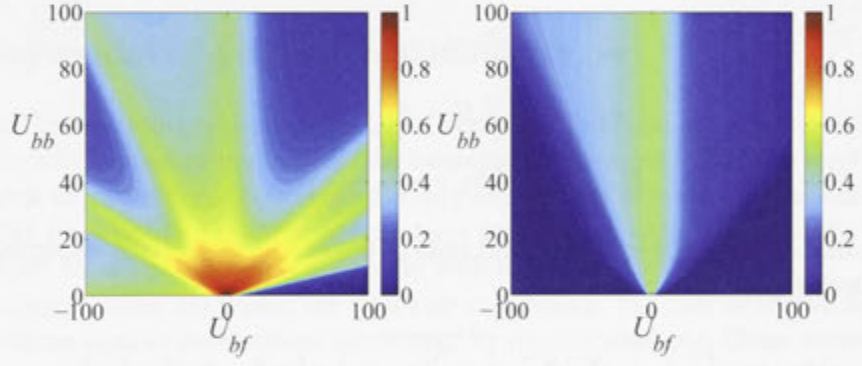

Figure 3.15: Density plot of the (left) boson and (right) fermion tunnelling correlation for $N_f = 2, N_b = 10$.

One can derive the equations of motion for the above Hamiltonian, $i\frac{d\psi_{\xi,l}}{dt} = \frac{\partial H}{\partial \psi^*_{\xi,l}}$, one gets,

$$i\frac{d\psi_{b,l}}{dt} = -t_b \sum_{l \neq m} \psi_{b,m} + U_{bb}\left(\frac{N_b - 1}{N_b}\right)|\psi_{b,l}|^2\psi_{b,l} + U_{bf}|\psi_{f,l}|^2\psi_{b,l}, \tag{3.22}$$

$$i\frac{d\psi_{f,l}}{dt} = -t_f \sum_{l \neq m} \psi_{f,m} + U_{bf}|\psi_{b,l}|^2\psi_{f,l}. \tag{3.23}$$

We look at solutions of the form $\psi_{\xi,l} = A_{\xi,l}\exp(-i\mu_\xi t + \phi_{\xi,l})$, $\xi \in \{b, f\}$. The stationary homogenous solutions are, $A_{b,l} = \sqrt{N_b/3}$ with $\phi_{b,l} = \phi_b$ and $A_{f,l} = 1/\sqrt{3}$ with $\phi_{f,l} = \phi_f$.

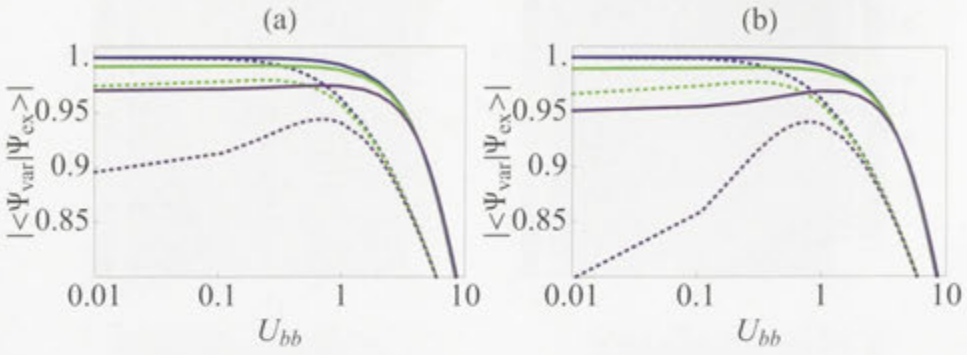

Figure 3.16: The fidelity of the variational ansatz $|\langle\Psi_{\rm var}|\Psi_{\rm ex}\rangle|$, for (a) repulsion and (b) attraction between bosons and fermions with $|U_{bf}| = 0$ (blue), 1 (green), 2 (purple). The number of bosons in the system is: 3 (solid), 9 (dotted).

For the ground state we have:

$$\mu_b = \frac{U_{bb}}{3}(N_b - 1) + \frac{U_{bf}}{3} - 2t_b \tag{3.24}$$

$$\mu_f = \frac{U_{bf}}{3}N_b - 2t_f \tag{3.25}$$

$$E_{\rm var} = \frac{\mu_b}{2}N_b + \mu_f - \frac{U_{bf}}{3}N_b \tag{3.26}$$

The state that corresponds to the ground state of the variational ansatz, using the multinomial theorem, can be written as:

$$|\Psi_{\rm var}\rangle = \left(\frac{1}{3}\right)^{\frac{N_b+1}{2}} \sum_{n_i^f}\sum_{n_i^b} \sqrt{\frac{N_b!}{n_1^b!n_2^b!n_3^b!}}|n_1^f, n_2^f, n_3^f\rangle_f \otimes |n_1^b, n_2^b, n_3^b\rangle_b,$$

where the sum over n_i^f goes over all the combinations given by $n_1^f + n_2^f + n_3^f = 1$ and the sum over n_i^b goes over the combinations given by $n_1^b + n_2^b + n_3^b = N_b$. The agreement between the variational solution and the exact energies is good for small interaction $U_{bb} < 1$, at fixed U_{bf}. As long as the inter-species interaction strength is small compared to U_{bb} the variational ansatz gives a good estimation of the ground state energy. Still, if we look at the variation of the ground state energy for fixed repulsion U_{bb} and we vary U_{bf}, the agreement with the variational ansatz breaks down from the start. The system is very sensitive to the variation of U_{bf}. From the exact solution, in the case of $U_{bf} > 0$ for fixed U_{bb} we see that the ground state energy saturates as we increase the inter-species interaction. This doesn't happen for the variational ansatz. We see the competition of the interaction energy with the kinetic terms, which when $U_{bf} \gg U_{bb}$ compensate each other. In contrast, for the attraction between bosons and fermions in the exact solution, we see that the ground state energy decreases. This is because the interaction energy is negative thus the total energy has monotonic character and no saturation, the effective interaction energy and kinetic energy have the same sign. Therefore in the case of attraction

qualitative agreement can be achieved with the variational solution. The fidelity of the variational ground state $|\langle\Psi_{\rm var}|\Psi_{\rm ex}\rangle|$, calculated as follows:

$$\langle\Psi_{\rm var}|\Psi_{\rm ex}\rangle = \left(\frac{1}{3}\right)^{\frac{N_b+1}{2}} \sum_{n_l^f}\sum_{n_l^b}\sqrt{\frac{N_b!}{n_1^b!n_2^b!n_3^b!}}C(n_1^f,n_2^f,n_3^f,n_1^b,n_2^b,n_3^b),$$

where the C's are the amplitudes corresponding to components of the ground state from the solution by direct diagonalization of the Hamiltonian (3.13). The fidelity can be seen in Fig. 3.16 for repulsion (a) and attraction (b). Here we can see that, as we increase the interactions, the fidelity goes down rather dramatically depending on the inter-species interaction strength, and the increment in the number of bosons (see Fig. 3.16).

From the results of the variational ansatz we learn that, as we increase the interactions the broken symmetry states start to play a major role in the behaviour of the system. The variational ansatz can be used to search for unbalanced solutions such that: $A_{\xi,1} \neq A_{\xi,2} \neq A_{\xi,1}$. Solutions of this type for $U_{bf} \neq 0$ can have energies lower than their homogenous counterparts. The possibility to use these states to extend the validity of the variational solution requires further investigation.

3.7 Toy model of a topological insulator

Motivated by the robustness of topological states for their use in quantum computing [31, 37], it is of interest to understand the behaviour of systems with these kind of states and the role of interactions. Following the very recent work of Stanescu, Galitski and Das Sarma [29], on simplified models that can have topological states similar to the Haldane model [150], we study a Bose-Fermi system with these characteristics.

Topological states are useful for quantum computing, because as shown by Kitaev [31] are robust against decoherence introduced by the environment. These states are protected by an energy gap that isolates a sector of the Hilbert space and therefore arbitrary controlled unitary operations on them can be performed. The robustness of combinations of these states forming a qubit happens because as one applies a unitary operation the result only depends on the topology of the braiding of qubits and small fluctuations in the operation have negligible effect [32].

In this section we will understand the effect of the artificial vector potential in the behaviour of the insulating states, the superfluid phase and the quantum fluctuations in a simplified model. Besides from affecting the structure of the phase diagram as compared with the system without vector potential, we will see how, the vector potential breaks the particle-hole symmetry of the fermions.

We construct our model by having 4 sites, two triangles, where we have a position dependent vector potential. This vector potential generates an effective magnetic field with opposite flux in each triangle, see Fig. 3.17. This kind of vector potential can be generated in optical lattices artificially by means of dressing the atoms in an optical field that couples different spin states [26, 27], or by moving the atoms in a spatially varying laser field [30, 151–153].

This has the consequence that the hopping amplitudes acquire a position dependent phase. We propose the following extension of the Bose-Fermi ring as a simplified small

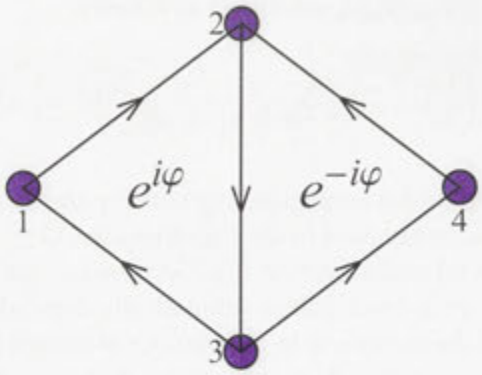

Figure 3.17: Schematics of our two dimensional topological insulator Bose-Fermi system.

scale version of an interacting topological insulator,

$$\mathcal{H} = \mathcal{H}_b + \mathcal{H}_f + \mathcal{H}_{bb} + \mathcal{H}_{bf}, \tag{3.27}$$

where,

$$\mathcal{H}_\xi = -T_\xi \sum_{<l,m>} \left(e^{i\varphi_\xi(l,m)} \hat{\xi}_l^\dagger \hat{\xi}_m + e^{-i\varphi_\xi(l,m)} \hat{\xi}_m^\dagger \hat{\xi}_l \right), \tag{3.28}$$

$$\mathcal{H}_{bb} = \frac{U_{bb}}{2} \sum_{l=1}^{4} \hat{n}_l^b \left(\hat{n}_l^b - 1 \right), \tag{3.29}$$

$$\mathcal{H}_{bf} = U_{bf} \sum_{l=1}^{4} \hat{n}_l^b \hat{n}_l^f. \tag{3.30}$$

where for simplicity we have chosen: $\varphi_\xi(1,2) = \varphi_\xi(2,3) = \varphi_\xi(3,1) = \varphi_\xi(4,2) = \varphi_\xi(3,4) = \varphi$ and $\varphi_\xi(l,m) = -\varphi_\xi(m,l)$. This simplified model has the essential ingredients for the emergence of topological states [29].

We construct the ground state phase diagram of the model by calculating the tunnelling correlation η_b, as a function of the interactions for fixed number of bosons, with different fermion filling factors and different φ in Fig. 3.18. We can see that, as expected from our results in the previous section in the case where $\varphi = 0$ (real hopping amplitudes), the system has the particle-hole symmetry in terms of the fermion filling, so that we recover the behaviour seen in attraction for $1/4$ filling for repulsion in $3/4$ filling, and vice-versa.

For $\varphi \neq 0$ and in particular, when $\varphi = \pm\pi/2$ (imaginary hopping amplitudes), the particle hole symmetry in the fermion filling is broken. Now we have that for $1/4$ filling for inter-species repulsion the region where the system is superfluid extends to larger intra-species interaction values as compared to the $\varphi = 0$ case (compare Fig. 3.18 (a) and (d)). As one increases the number of fermions, now in addition to the $1/4$ and $3/4$ filling cases we also have the half-filled case [Fig. 3.18 (b) and (e)], which are robust against

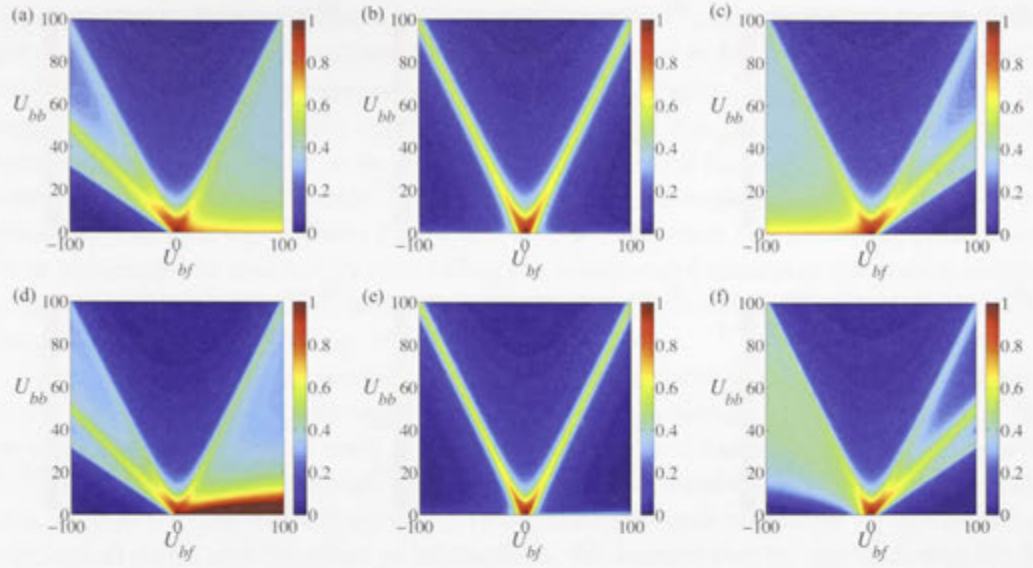

Figure 3.18: Density plots of the boson tunnelling correlation η_b, for $\varphi = 0$ (top panels) and $\varphi = \pi/2$ (bottom panels) with $N_f = 1$ (a,d), 2 (b,e), 3 (c,f), and $N_b = 4$.

the vector potential applied, so that the effect of the phase is to marginally suppress the superfluid region in the whole phase space, as it happens with other fillings. In the case of $3/4$ filling now the system presents strong suppression of the SF enhanced region corresponding to attraction (compare Fig. 3.18 (c) and (f) for small U_{bb}).

The suppression and enhancement of the superfluid components in the system at different fermion fillings as compared to the $\varphi = 0$ situation correlate with the enhancement of fluctuations for U_{bb} small (see Fig. 3.19). This increment in fluctuations correlates with the behaviour seen in η_b due to the symmetry breaking. In generally the boundaries with the localised states are marginally shifted to lower values of the interactions (see Fig. 3.18).

3.8 Summary of results

In conclusion, we have analysed the formation of self-trapped states in a BEC cloud mixed with degenerate fermions and confined in a one-dimensional double-well potential. Our semi-analytical approach is reliable in the limit of moderate to large number of fermions ($N_f \sim 10^2 - 10^3$) . The properties of the bosonic macroscopic wavefunction are analysed by means of a variational method, which allow us to comprehensively describe the spatial properties and symmetry of the self-trapped state and identify the reasons for enhancement or suppression of self-trapping. The self-trapping regimes in the Bose-Fermi mixture are predicted to be markedly different for repulsive and attractive inter-species interaction and highly sensitive to the fermion concentration. For the attractive interaction, the growth of the fermionic fraction leads to the MQST at smaller well separations. This is due to the effective *suppression of tunnelling* due to the narrowing of the bosonic wavefunction. In the repulsive case, the growth in the fermionic fraction has

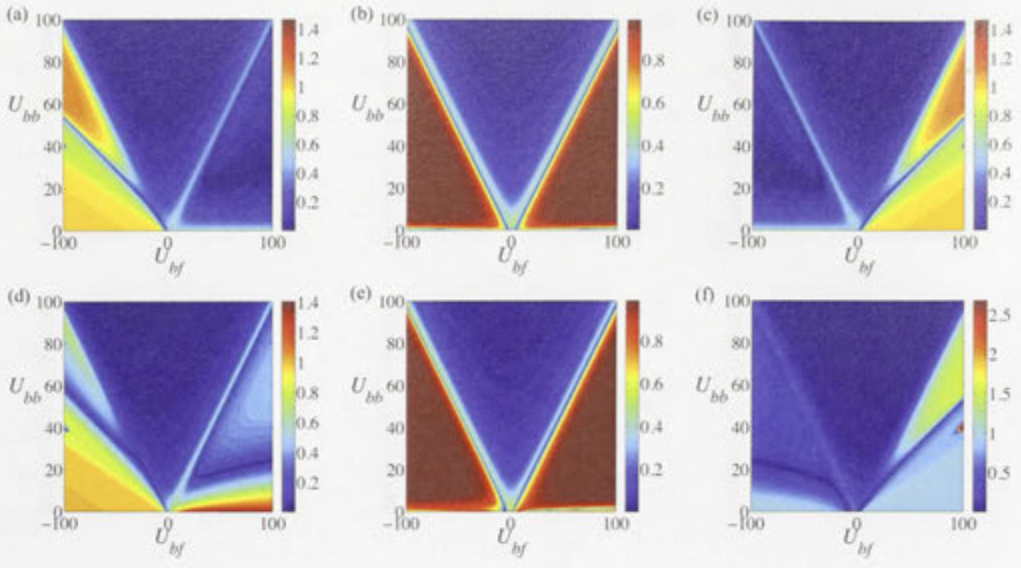

Figure 3.19: Density plots of the fluctuations σ_b, for $\varphi = 0$ (top panels) and $\varphi = \pi/2$ (bottom panels) with $N_f = 1$ (a,d), 2 (b,e), 3 (c,f), and $N_b = 4$.

a stronger effect on the dynamics of bosons and promotes the onset of the MQST regime to greater well separations, as a result of the *tunnelling enhancement* due to the fermion-induced broadening of the BEC wavefunction. In both attractive and repulsive cases, the effect could be accentuated by enhancing the strength of the interspecies interaction via Feshbach resonance.

Both the enhancement and the suppression of self-trapping in the BEC cloud mixed with degenerate fermions may signal the existence of the new regimes of the dynamics and switching of BECs in atomic waveguides and nonlinear interferometers with mixed atomic species. They are expected to have profound consequence for the formation and dynamics of the self-trapped gap states in the Bose-Fermi mixtures loaded into periodic potentials. Beyond the mean field, as we found in our later work on the ring configuration, these effects have implication for the onset of the superfluid to Mott insulator (MI) transition in a lattice potential [18, 45, 126, 154], leading to the in-homogeneous suppression of the MI regime, and the appearance of new insulating states.

We also have analysed the ground state of a small-scale system of quantum degenerate bosons and fermions in a three-site ring configuration. We have restricted the consideration to the fermion filling factor less or equal than one, which as allowed us to employ a standard Bose-Fermi-Hubbard Hamiltonian. By examining the tunnelling correlations and particle fluctuations in the system, we have found that the system admits mobile and insulating states that are analogous to the superfluid and Mott insulator states in infinite lattices. The novel insulating states identified in this small-scale system for both commensurate and incommensurate filling of bosons, are purely due to the inter-species interactions and can be controlled by controlling the interaction strengths and the number of fermions injected into the system.

Further we have considered an extension of this model. This extension was a simpli-

fied model with the ingredients of a topological insulator. In this model we see the effect of the inclusion of an artificial position dependent vector potential. The vector potential introduces a phase dependence into the hopping amplitudes, and as a consequence, the hopping amplitudes can take complex values. Due to this, the vector potential breaks the symmetry with respect to the fermion filling. We find that the suppression and enhancement of superfluid components in the system is strongly dependent on the vector potential. This strongly affects the region where the system has insulating phases and these phases can be selected by controlling the number of fermions in the system and the artificial vector potential. We find that there is enhancement of the quantum fluctuations due to the symmetry breaking.

The results of our "toy model" may be useful for the study of topological insulators in the sense that many-body interactions have been considered. The properties of the ground state of this small scale system can be used to construct representations with the correct symmetry properties and study the effect of interaction in topological invariants, such as the Chern numbers [155]. This can help to understand the categorisation of topological states and the effect of interactions. We learned that by manipulating the interactions and the vector potential one can generate insulating states that could be useful for the implementation of quantum computing protocols. Still, the study of the configurations of the ground state and the robustness against decoherence of the states with localised fermions, need to be further investigated.

Canonical transformations and the BCS-BEC crossover

Motivated by the theoretical work of Eagles [156] and later Leggett [157] with the objective of understanding the strong coupling limit of the theory of Bardeen-Cooper-Schrieffer (BCS) on superconductivity [59], the possibility of a crossover to a Bose-Einstein condensate (BEC) has been a important problem to address. The implementation of the crossover regime is performed with ultracold fermions and it is one of the most challenging problems in physics both theoretically and experimentally. In the BCS-BEC crossover, ultracold atoms of fermionic nature, i.e ^{6}Li and ^{40}K, that constitute the system interact by means of a Feshbach resonance. A Feshbach resonance happens because the magnetic moment of two colliding atoms is different from a molecular state, therefore by applying a constant magnetic field one can select the components of the system. This is due the fact that the interactions between atoms only depend on the spin of the valence electrons of the colliding atoms [50]. As the intensity of the magnetic field changes the atoms either behave closer to Cooper pairs (BCS side of the resonance) or to a BEC of molecules (BEC side of the resonance).

The BEC of molecules is the macroscopic occupation of the lowest energy state at temperatures below a critical temperature where the system can be described as a collection of tightly bound molecules of two fermionic atoms of opposite spin. These molecules behave as a collection of point like bosons. The Cooper-pairs are extended objects in space where two fermions of opposite spin and opposite momenta pair, as a consequence of the many-body interaction and the behaviour of the atoms near Fermi energy in the Fermi surface that contains them. Because of the interaction via the Feshbach resonance in the BCS side, the atoms form Cooper-pairs and a pairing gap Δ_{BCS} forms in the energy spectrum. As this gap opens, the Cooper-pairs condense in the lowest energy state giving rise to a coherent state. This coherent state is a superfluid, a fluid that can flow without friction. As one increases the temperature the pairs break and the gap vanishes while superfluidity ceases to happen.

Due to properties of the bound states on either side of the resonance, the BCS limit is often referred to as the weak coupling limit and the BEC of molecules is the strong coupling limit [157]. In either limit, the system has well defined properties, while in the region near the resonance, also known as unitary limit, the description becomes problematic. The limit is called unitary limit because the effective interaction strength coming from the two-body scattering amplitude when the scattering length diverges is one. The ground state near the unitary limit is a strongly interacting superfluid of pairs, with a

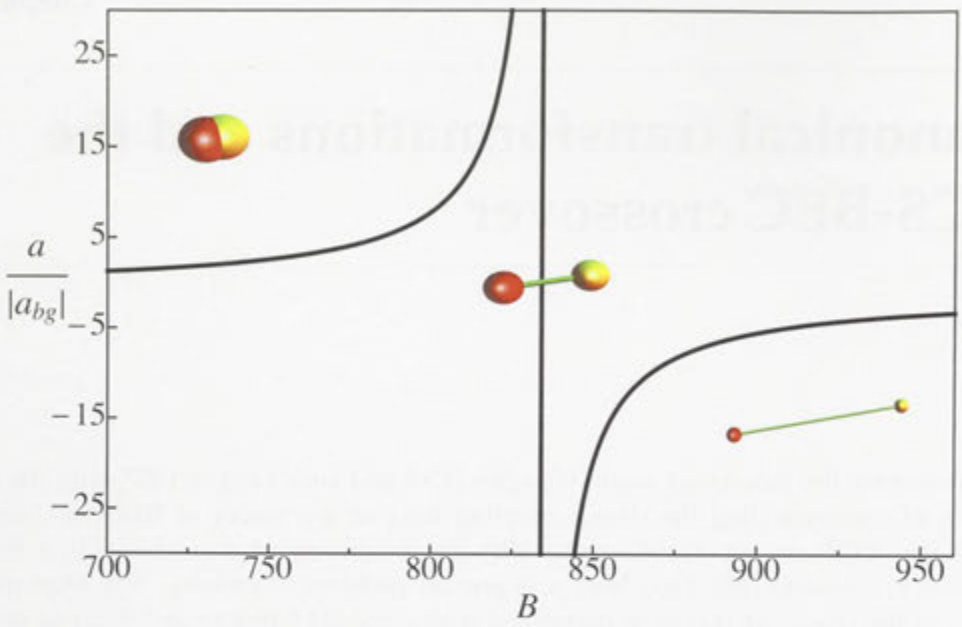

Figure 4.1: The behaviour of the scattering length as a function of the magnetic field for the broad resonance of ^{6}Li, and a qualitative description of the regimes in the BCS-BEC crossover. The many-body interaction is $\lambda = 4\pi\hbar^2 a/m$. On the left we have the BEC limit of the molecules, at resonance where $B \approx 834$ we have the unitary limit and on the far right we have the extended Cooper pairs of the BCS limit.

size of the order of the inter-particle spacing of constituent fermions. In essence, the system has two different objects, Cooper-pairs and molecules that transform into each other depending on the many-body interaction. As one moves across the Feshbach resonance the Cooper-pairs collapse to molecules and the molecules break into correlated pairs. In the limit when the interaction becomes singular and changes sign we have the system in a state where strong correlations are dominant, see Fig. 4.1.

Experimental findings in these ultracold neutral systems have confirmed the formation of BEC of molecules from fermionic atoms below a certain temperature with an interaction controlled by a Feshbach resonance [158, 159]. The existence of a pairing gap in these systems [160] lead to the search of a superfluid state, sometimes referred to as Hi-Tc superfluidity. This is because of having a high critical temperature compared with the Fermi Energy of the system [161]. The confirmation of the superfluidity came from the observation of quantum vortices. This quantum vortices form a characteristic pattern, the so-called Abrikosov lattice, analogous to the phenomena seen in type II superconductors, when a magnetic field is applied [162]. There have been also measurements that contrast the thermodynamical properties of the strongly interacting system with those of a non-interacting system [163]. In the limit where the system is at the resonance, corresponding to the singular point of the scattering length, it is thought that the thermodynamic properties of the system can be described by a re-scaled version of the non-interacting Fermi gas [164, 165]. This universality hypothesis implies that the energy of the system is pro-

portional by a universal function to the energy of the non-interacting system. This universal function only depends on the ratio of the temperature with the Fermi temperature, and is independent of the microscopic details of the model used to describe the system. Still one finds that provided this holds, the system has anomalous exponents in its thermodynamic properties [166] in the sense that they do not correspond to either bosonic or fermionic degrees of freedom. Recently [167, 168], studies in ^{40}K have shown that the system presents a dispersion relation for its excitations above the critical temperature with a contribution referring commonly in the literature as a pseudo gap or a normal state excitation gap [19]. The dispersion relation is given by $E_{\mathbf{k}} = \sqrt{(\epsilon(\mathbf{k}) - \mu_a)^2 + \Delta_{\mathrm{BCS}}^2 + \Delta_{pg}^2}$, where the pseudo gap is Δ_{pg}, $\epsilon(\mathbf{k}) = \hbar^2|\mathbf{k}|^2/(2m)$, and μ_a is the chemical potential of the atoms. The importance of this finding is linked to the fact that in BCS theory a superconductor should have a vanishing gap in the energy spectrum as one increase the temperature above the critical one, $E_{\mathbf{k}} \to \epsilon(\mathbf{k}) - \mu_a$. This suppresses the superconducting state [44], and therefore in the analogous neutral atom system one could expect the same for the superfluid behaviour [51]. Still instead, there is a non vanishing contribution in the dispersion relation above the critical temperature, $E_{\mathbf{k}} \to \sqrt{(\epsilon(\mathbf{k}) - \mu_a)^2 + \Delta_{pg}^2}$. This fact remains a mystery, with many different interpretations of its origin, and is a common feature of the Hi-Tc superconductors [19]. Due to these similarities, ultracold strongly interacting fermions are thought to be the analogous neutral system to the Hi-Tc superconductors. This has strongly motivated research in the field since ultracold atoms have the advantage of being very clean systems, where interactions can be manipulated at will. Therefore, one could use ultracold atomic systems to study the properties of this kind of strongly correlated ground states [51].

Theoretical approaches to understand the crossover problem are based mainly in the study of either the single channel model or the two channel model [169]. The two-channel model description is based on molecular bound-states, or Feshbach bosons (FB's) corresponding to a bosonic channel interacting with a collection of free atoms in a fermionic channel. The single channel model, constructed in terms of fermions only, is primarily based on the BCS mean-field picture of Leggett [157], using an ad-hoc, many-body interaction which becomes singular at the Feshbach resonance and changes sign. Essentially, these two approaches map to each other in the limit of enslaved bosons, or a broad resonance [50, 52]. In the limit of enslaved bosons, the molecules are defined in terms of the pairs of the atoms. The common goal of these theories is to interpolate between the BCS and BEC limits. Other treatments involve the Hubbard model with negative U (attraction) to represent the pairing present in the problem where they use Monte-Carlo methods to find the ground state energy and the energy of the bound state representing the molecules [170]. This approach was originally suggested by Nozieres and Schmitt-Rink [171]. A number of studies have been considered doing numerical simulations of the BCS Hamiltonian extended to the strong coupling regime. These studies concentrate in the behaviour of the bound state energy as a function of the interaction based on Jastrow functions for a variational ansatz of the ground state and Monte-Carlo methods to calculate the ground state energy [172–175]. These approaches, give insight to the relevant scaling properties of the energy in the system, but unfortunately they don't answer questions regarding the possible mechanisms responsible for the pairing or the spectrum of excitations.

One of the most difficult questions to answer is what happens near the unitary limit, when the system is at the resonance. This is because the regular perturbation theory in powers of the gas parameter $n^{1/3}a$, with $n = k_F^3/(3\pi^2)$ which is proportional to product of the Fermi momentum k_F and the scattering length a, ceases to be valid when the Feshbach molecules form and the fermions are strongly interacting. In this limit, the scattering length diverges, therefore, there is no good perturbation parameter and the Fermi energy is thought to be the most important parameter that controls the behaviour of the energy of the system [176]. This is because expansions of the energy in terms of powers of this dimensionless quantity are not convergent. For example, the well known results of Huang, Yang and Lee [177, 178], state that the energy per particle can be written as follows,

$$\frac{E}{N} = \frac{3}{5}\epsilon_F \left(1 + \frac{10}{9\pi}k_F a + \frac{4(11-2\ln 2)}{21\pi}(k_F a)^2 + \cdots\right) \tag{4.1}$$

where ϵ_F is the Fermi energy, the term proportional to $k_F a$ is due to the two-body collisions and the terms proportional to higher powers than one of $k_F a$ are due to the many-body processes and they are the energy due to correlations [44]. The expansion in (4.1), is only valid in the limit were $k_F a \ll 1$ and positive scattering length, $a > 0$, since as noted in [179] the gas would collapses for $a < 0$. Therefore, there is not a small perturbation parameter in the theory in this sense, and correlations are dominant. In principle, many questions remain open upon the nature of the system in this regime, since the properties seem to be a mixture of fermionic and bosonic behaviour [166, 180]. One of the problems is that there is no satisfactory model Hamiltonian that represents the mixed character of the low energy effective degrees of freedom, they are neither purely bosonic nor purely fermionic fields. Beyond the aforementioned interpolation scheme based on [157], alternative theories are scarce and one needs to assume usually a BCS type theory modified by a regularised many-body interaction and Feynman diagram resumations to renormalise the interaction and recover the correct two-body physics.

The two channel model has some of the essential ingredients needed to address the BCS-BEC crossover problem. The approximation of this model in the limit where a single bound-state exists, while neglecting the interaction between atoms has been recently mapped by Falco and Stoof [181] to the anisotropic Kondo model [60]. In this representation, the FB and the atoms map into spin and pseudo-spin variables in a restricted Hilbert space of double occupancy. This representation can be readily identified with Cooper-pairing in the sense of Anderson's random phase approximation (RPA) for the superconducting state [182]. The pseudo-spin variables are defined in terms of the creation and annihilation of the fermions of different spin, this is the so-called Abrikosov representation for spins in terms of pseudo-fermions [183]. In Falco and Stoof treatment, the magnetic detuning with respect to the Feshbach resonance that controls the position in phase space of the model, shifts the chemical potential of the FB only, and acts as an external field in the Kondo model picture. This external "magnetic" energy in the Kondo picture is proportional to the detuning from the Feshbach resonance. In the absence of the external field, at the resonance, due to the mapping in spin and pseudo spin representation, the interaction between Cooper-pairs and FB has the same properties as the one of the Kondo model considering fermionic carrier and spin channels. In this sense, flipping a local spin and creating a bound-state are equivalent descriptions, while fermion carriers correspond to the free atoms. In the Kondo picture, the energy cost of the scat-

tering favours the formation of certain ground state configurations, where the scattering between spins and carriers is correlated. Incoming carriers can only interact with certain local spin configurations and this local spin configurations promote the interaction with only particular carriers, generating feedback. This ultimately results in the well known Kondo problem as one decreases the temperature below the Kondo temperature [184]. The Kondo problem is region of the parameter space of the Kondo model where perturbation theory breaks down. Perturbation theory doesn't work because there is a non-physical divergency at the Kondo temperature, because high energy contributions due to the interactions become dominant below this energy scale. Therefore, physical quantities such as the resistivity become infinity. In the two-channel picture, from the many-body perspective, the interactions between the Cooper-pairs and the FB occur in analogous manner to the Kondo model. This is because a FB will be created or destroyed depending whether or not a Cooper-pair will have the same energy and vice-versa, thus the processes induce correlations. In this respect, the mapping done by Falco and Stoof gives the possibility to understand in a clear picture, the nontrivial nature of the many body process involved.

However, when one neglects the interaction between Cooper-pairs, one removes the important length scale which affects the possible processes to take place. Such description only seems appropriate in the limit close to the resonance on the BEC side of the crossover, once the molecules have been formed, since the interaction between Cooper-pairs is not accounted for in the theory. An alternative more consistent description, could be the one given by the *single impurity Anderson model* (AM) [62]. This model, besides from being purely fermionic in nature, can be used to understand the processes that generate the correlation between the FB and the atoms, and possibly answer questions about the formation of the molecules. In this model, these processes are mediated by the interplay between the repulsion between localised energy states corresponding to the molecules and the probability of overlapping between atoms and localised energy states, which has a more realistic origin than the spin-flip processes from the Kondo descrition. The AM gives the possibility to look for alternative mechanisms to understand how the spectrum of excitations is affected in the crossover problem depending on the FB, and the consequences from correlations in the configuration of the ground state, as well as, dynamical processes that take place as we move away from the resonance. Also, it opens the possibility to look for a precise interpretation of the unitary limit, where regular perturbation theory becomes inapplicable [176]. Besides these possibilities, the AM has been solved exactly under some approximations by Bethe ansatz [185, 186] and very robust methods such as the Renormalization Group Theory [187, 188] can be applied. This type of methods have been designed to understand the non-perturbative region of models of this kind where different parameters move the system towards fixed points in the phase space and where contributions from different energy scales need to be considered. The possibility of using the well known results and techniques to tackle the AM may prove fruitful in the BCS-BEC crossover problem. This because, in the usual formulation there is no adequate framework to solve the problem of determining the characteristics of the ground state and the behaviour of the excitations due to correlations. These reasons strongly motivated us to study an alternative formulation to extended BCS mean field type theories which could be able to address some of the characteristic features of this problem.

In this Chapter, we will study single impurity models, in connection with the possi-

bility of using them to gain some insight on the dynamical processes that take place due to the interaction between FB and Cooper pairs and the basic fermionic nature of atoms in the BCS-BEC crossover problem. Our aim is to have a Hamiltonian theory that can describe the physics near the unitary limit, on both sides of the crossover. This Hamiltonian theory should provide a description to the formation of the Feshbach bosons and have the possibility of answering questions such as, the appearance of the pseudo-gap regime in the system, the role of non-condensed Cooper-pairs and effect of the FB. To this end, we will show for the first time, how a typical Hamiltonian used in the crossover problem, i.e. the two-channel model, and the AM relate using results from perturbation theory by means of canonical transformations. Also, we will establish the relationship between the parameters of the two models and give the regime where the crossover corresponds to in the equivalent magnetic impurity picture. Finally, we will use our results to understand some of the features seen in recent experiments with ^{6}Li and ^{40}K, and possibly give an explanation to the origin of the pseudo-gap contribution with our framework.

4.1 Models of the BCS-BEC crossover and their relationship

In order to get some insight in the relevant properties of the BCS-BEC crossover problem it proves useful to introduce the reader to the behaviour of the crossover. We do this by means of the extended BCS mean-field approach, as well as the two channel hybrid model. At the end of the section we will formally establish the equivalence of these two models in the broad resonance limit.

Based on the concepts by Leggett and Eagles [156, 157] one can formulate the problem in terms of the single channel model of the BCS-BEC crossover[1]. In this model one assumes that the fermions interact by a contact pseudo-potential with a strength given by the low energy two-body scattering amplitude (S-wave interaction). The interaction being of contact nature has in principle a range r_0 that is assumed to be negligible in the region of interest. Because we use a Feshbach resonance to control the scattering amplitude the scattering length depends on an applied external magnetic field B.

The single channel model can be approximated in momentum space, in the subspace of states in the centre of mass of motion as,

$$\mathcal{H}_{1ch} = \sum_{\mathbf{k},\sigma} (\epsilon(\mathbf{k}) - \mu_a)\, a^\dagger_{\mathbf{k},\sigma} a_{\mathbf{k},\sigma} + \frac{\lambda}{\mathcal{V}} \sum_{\mathbf{q},\mathbf{k}} a^\dagger_{-\mathbf{q},\downarrow} a^\dagger_{\mathbf{q},\uparrow} a_{\mathbf{k},\uparrow} a_{-\mathbf{k},\downarrow}, \tag{4.2}$$

where the single channel model interaction is,

$$\lambda = \frac{4\pi\hbar^2 a_{\mathrm{bg}}}{m_a} \left(1 - \frac{\Delta B}{B - B_0}\right),$$

where, $\mathbf{k}$ and $\mathbf{q}$ are the momenta, σ the index corresponding to the spin, the dispersion relation is $\epsilon(\mathbf{k}) = \hbar^2|\mathbf{k}|^2/(2m_a)$ and a_{bg} is the background scattering length, the scattering length at zero magnetic field. The background scattering length is approximately equal to the magnitude of the scattering length of the interaction potential of the lowest energy state when the magnetic field B is zero. The field where the Feshbach resonance occurs

[1] The Hamiltonian in real space in terms of fields is in the Introduction (1.3).

is B_0, m_a the mass of the atom, μ_a is the chemical potential of the fermionic fields a, ΔB the width of the resonance measured with respect to B_0 and the position of zero of the scattering length [2] , and the so-called quantization volume is denoted by $\mathcal{V}$. The quantization volume is the region in space where the density is different from zero, the effective size of the system. The above Hamiltonian is nothing more than the BCS Hamiltonian [59]. Here the interaction has been described in terms of a short range pseudo-potential characterised by the scattering length in the low energy limit and is controlled by the magnetic field. In order to have a convergent theory in limit where the scattering length becomes infinity an implicit regularisation must be employed in the sum over momenta. This regularisation is performed by subtracting an infinite contribution to the inverse of the scattering length such that the scattering amplitude derived from the two-body T-matrix has the right pole structure to have a bound state. The single channel model with zero total momentum pairs in the limit where we do a mean field approximation and we regularise the interaction to keep the integrals that describe the variation between the gap in the system and the chemical potential convergent is often referred to as the extended BCS mean-field theory [3] [51]. In order to analyse the system one performs the mean-field solution of the model which can be done easily by substituting the BCS ansatz in (4.2) while doing mean-field decoupling,

$$|\mathrm{BCS}\rangle = \prod_{\mathbf{k}} \left(u_{\mathbf{k}} + v_{\mathbf{k}} a^{\dagger}_{\mathbf{k},\uparrow} a^{\dagger}_{-\mathbf{k},\downarrow} \right) |0\rangle,$$

where $|0\rangle$ is the filled Fermi sea, $u_{\mathbf{k}}$ and $v_{\mathbf{k}}$ are variational parameters and correspond to the probability amplitudes of a pair of fermions with opposite momenta to be empty or occupied. The variational parameters obey the constraint $u^2_{\mathbf{k}} + v^2_{\mathbf{k}} = 1$, because they are probability amplitudes. Then it follows to use the Bogoliubov procedure for the quadratic Hamiltonian one obtains, and use the relationship between amplitudes of the BCS ansatz to minimise the energy. Thus, the variational parameters are related as follows [44],

$$u^2_{\mathbf{k}} = \frac{1}{2}\left(1 + \frac{\epsilon(\mathbf{k}) - \mu_a}{\sqrt{(\epsilon(\mathbf{k}) - \mu_a)^2 + \Delta^2_{\mathbf{k}}}}\right),$$

$$v^2_{\mathbf{k}} = \frac{1}{2}\left(1 - \frac{\epsilon(\mathbf{k}) - \mu_a}{\sqrt{(\epsilon(\mathbf{k}) - \mu_a)^2 + \Delta^2_{\mathbf{k}}}}\right),$$

$$u_{\mathbf{k}} v_{\mathbf{k}} = \frac{\Delta_{\mathbf{k}}}{2\sqrt{(\epsilon(\mathbf{k}) - \mu_a)^2 + \Delta^2_{\mathbf{k}}}}.$$

[2] ΔB is negative if the zero of the scattering length is at a field lower than the resonance (^{6} Li case, $a_{\mathrm{bg}} < 0$ and $\Delta B < 0$), positive if at a higher field (^{40}K case, , $a_{\mathrm{bg}} > 0$ and $\Delta B > 0$). The significance of this detail has to do with the fact that the ^{40}K system would have a Fermi liquid point when the scattering length is zero, by this we mean that at higher fields the system is a Fermi liquid. For ^{6}Li we would have a non-interacting Bose system limit at zero scattering length, and the system beyond this point would be a pure BEC.

[3] The exact solution of (4.2) is actually mean-field.

The equations for the number of particles N and the gap $\Delta_{\mathbf{k}}$ are,

$$\Delta_{\mathbf{k}} = \frac{\lambda}{\mathcal{V}} \sum_{\mathbf{k}} u_{\mathbf{k}} v_{\mathbf{k}}, \tag{4.3}$$

$$N = 2 \sum_{\mathbf{k}} v_{\mathbf{k}}^2, \tag{4.4}$$

where, $u_{\mathbf{k}} v_{\mathbf{k}} = \langle a^{\dagger}_{\mathbf{k},\uparrow} a^{\dagger}_{-\mathbf{k},\downarrow} \rangle = \langle a_{-\mathbf{k},\downarrow} a_{\mathbf{k},\uparrow} \rangle$. These lead to the well know equations [51, 156, 157] for the gap[4] (4.5) and the number of particles (4.6) ,

$$\int_0^{\infty} \left(\frac{1}{\sqrt{x}} - \frac{\sqrt{x}}{\sqrt{(x-\tilde{\mu})^2 + \tilde{\Delta}^2}} \right) \mathrm{dx} = \frac{\pi}{k_F a} \tag{4.5}$$

$$\int_0^{\infty} \left(\sqrt{x} - \frac{\sqrt{x}(x-\tilde{\mu})}{\sqrt{(x-\tilde{\mu})^2 + \tilde{\Delta}^2}} \right) \mathrm{dx} = \frac{4}{3} \tag{4.6}$$

where the dimensionless chemical potential is $\tilde{\mu} = \mu_a / \epsilon_F$, the dimensionless gap is $\tilde{\Delta} = \Delta / \epsilon_F$, the Fermi energy $\epsilon_F = \hbar^2 k_F^2 / (2 m_a)$, with k_F the Fermi momentum. The dimensionless parameter $1/(k_F a)$ controls the behaviour in the crossover so that in the weak coupling limit $1/(k_F a) \to -\infty$ (BCS) and in the strong coupling limit $1/(k_F a) \to \infty$ (BEC). In the above equations the interaction has been regularised to make the integrals in (4.5) and (4.6) convergent. Namely the coupling of the interaction term is modified as follows,

$$\frac{\mathcal{V}}{\lambda} \to \frac{\mathcal{V}}{\lambda} - \sum_{\mathbf{k}} \frac{1}{2\epsilon(\mathbf{k})}.$$

The regularisation amounts to integrating out the high energy modes in the gap equation (4.5) [51]. The solution of equations (4.5) and (4.6) is show in Fig. 4.2, where we have also included the condensate fraction which can be calculated from [189]:

$$\frac{n_0}{n} = \frac{3\pi}{16} \frac{\tilde{\Delta}^2}{\mathrm{Im}\sqrt{\tilde{\mu} + i\tilde{\Delta}}}$$

In the BEC limit ($1/(k_F a) \to \infty$) where we have a gas of tightly bound molecules, the solution of the above equations gives the correspondence between the chemical potential and the energy of a bound state: $E_b = -2\mu_a = \hbar^2/(m_a a^2)$. In the BCS limit, the gap has the usual dependence on the interaction parameter given by $\Delta = 8\mu_a \exp(-\pi/(2k_F|a|))$. The size of the Cooper-pair can be estimated [189] by using i.e. Pippard's coherence length $\xi = 4/(\pi k_F \tilde{\Delta})$, so as we move from the BCS limit to the BEC limit the Cooper-pairs become "smaller" collapsing to the tightly bound molecules. In the BCS limit $\Delta \to 0$, and the pairs are separated in space on a macroscopic scale.

One unphysical feature of the single channel model is that it only supports one bound state independently on how strong the attraction is [171]. Therefore, it could be more

[4] In the derivation of the gap equation we have assumed that the gap is constant, such that $\Delta_{\mathbf{k}} \approx \Delta =$ const. in the region of interest. Also we have taken the limit where: $1/\mathcal{V} \sum_{\mathbf{k}} \approx 1/(2\pi)^3 \int \mathrm{d}\mathbf{k}$.

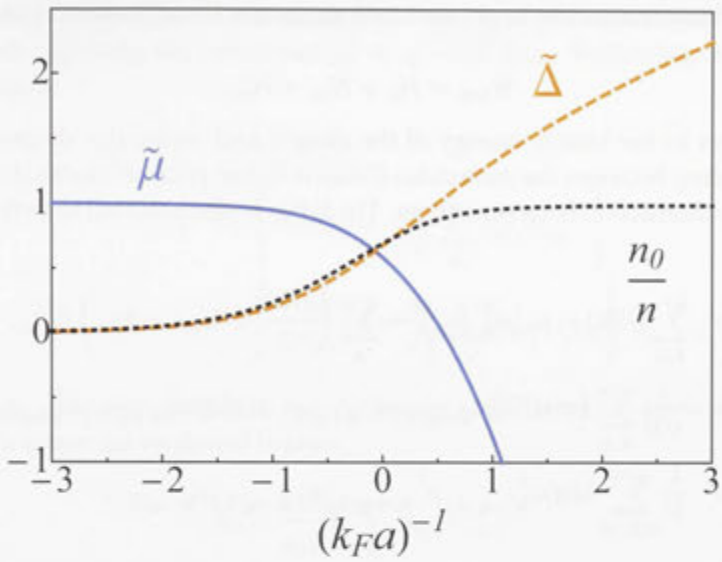

Figure 4.2: The parameters of the extended BCS mean-field theory, $\tilde{\mu} = \mu/\epsilon_F$, $\tilde{\Delta} = \Delta/\epsilon_F$ and the condensate fraction, n_0/n.

suitable for the analysis of the BCS side of the resonance. Also, the two-body scattering amplitude doesn't have the characteristics of scattering via a resonant state. Considering that a resonance is a positive energy state with finite lifetime, the Hamiltonian (4.2) only has true bound states,thus the description is insufficient [52]. One may ask if this scheme of regularisation and mean-field approximation is justified at all very close to the resonance where the formation of the molecules is actually taking place, and if so up to which point? Still, it is true that the qualitative agreement in both BEC and BCS limits with experiment is surprisingly good considering the interpolation nature of the theory. Another problem, comes from the fact that the extended BCS mean-field theory has only zero total momentum pairs and forbids density fluctuations. This has the consequence of incorrectly describing the low energy excitations of the system, eliminating the Bogoliubov-Anderson mode, which should exist for superfluidity to be present, as seen in the experiments [51, 161]. The absence of the collective Bogoliubov-Anderson mode implies that the leading corrections to the ground state energy of (4.2) in powers of $k_F a$ are incorrect from the start [51].

In order to treat the problem of the bound state in the BEC side of the resonance and verify the validity of the assumption of only considering the atoms and not the molecules, a single channel, a number of multi-channel models were proposed [181, 190–193]. The channels in these models refer to the lowest energy hyperfine states of the system close to the Feshbach resonance. The most simple of these is a model based on the possible interaction between molecules in a non-degenerate configuration formed due to the Feshbach resonance on the BEC side and the atoms in the BCS side. This hybrid atomic-molecular Hamiltonian, contains the relevant features of the crossover while having a

well defined bound state, virtual bound states and resonant states. Some analytic results can be obtained in certain limits, i.e. in the limit of an infinitely narrow resonance [52]. The so-called "two-channel hybrid", or atom-molecule Hamiltonian [5] can be written as follows [181],

$$\mathcal{H}_{2ch} = \mathcal{H}_0 + \mathcal{H}_{ba} + \mathcal{H}_{aa}, \tag{4.7}$$

where, $\mathcal{H}_0$ refers to the kinetic energy of the atomic and molecular degrees of freedom, $\mathcal{H}_{ba}$ is the coupling between the molecules (bosons b) and pairs of atoms (fermions a) and $\mathcal{H}_{aa}$ defines the interaction between atoms. The latter is also referred to as the background interaction.

$$\begin{aligned}
\mathcal{H}_0 &= \sum_{\mathbf{k},\sigma} \left(\epsilon(\mathbf{k}) - \mu_a\right) a^\dagger_{\mathbf{k},\sigma} a_{\mathbf{k},\sigma} + \sum_{\mathbf{k}} \left(\frac{\epsilon(\mathbf{k})}{2} + \delta_{\text{bare}} - 2\mu_a\right) b^\dagger_{\mathbf{k}} b_{\mathbf{k}}, \\
\mathcal{H}_{ba} &= \frac{1}{\sqrt{\mathcal{V}}} \sum_{\mathbf{k},\mathbf{q}} \left(g(\mathbf{q})^* b^\dagger_{\mathbf{q}} a_{\mathbf{k}+\mathbf{q}/2,\uparrow} a_{-\mathbf{k}+\mathbf{q}/2,\downarrow} + g(\mathbf{q}) a^\dagger_{-\mathbf{k}+\mathbf{q}/2,\downarrow} a^\dagger_{\mathbf{k}+\mathbf{q}/2,\uparrow} b_{\mathbf{q}} \right), \\
\mathcal{H}_{aa} &= \frac{1}{\mathcal{V}} \sum_{\mathbf{k},\mathbf{k}',\mathbf{q}} \lambda(\mathbf{q}) a^\dagger_{\mathbf{k}'+\mathbf{q}/2,\downarrow} a^\dagger_{-\mathbf{k}'+\mathbf{q}/2,\uparrow} a_{-\mathbf{k}-\mathbf{q}/2,\uparrow} a_{\mathbf{k}-\mathbf{q}/2,\downarrow},
\end{aligned}$$

where, $\epsilon(\mathbf{k})$ is the kinetic energy of the atoms, μ_a is the chemical potential of the atoms, δ_{bare} is the microscopic detuning from the Feshbach resonance. This detuning is introduced by the application of the external magnetic field close to the Feshbach resonance. The couplings g and λ are the interaction strengths between the molecules and the atoms, and the atoms, they depend on the scattering length. Note that the above Hamiltonian does not have a molecular interaction term, since we have assumed that the density is low enough such that molecules do not interact with each other, and the gas is cold enough such that this kind of interactions are energetically unfavourable. As mentioned previously, the above Hamiltonian has all the basic ingredients of a well defined theory for the crossover, but in order to find an alternative picture it further requires some simplifications. We need an alternative picture because the Hamiltonian as it is can't answer questions regarding the formation of the molecules, and on the BCS-side of the resonance their effect is usually not considered.

In the limit when only one bound state exists, corresponding to the centre of mass momenta mode $\mathbf{q} = 0$ in (4.7), and letting $\delta_{\text{bare}} - 2\mu_a \to \delta(B)$ we have,

$$\begin{aligned}
\mathcal{H}_{2ch} &\approx \sum_{\mathbf{k},\sigma} \left(\epsilon(\mathbf{k}) - \mu\right) a^\dagger_{\mathbf{k},\sigma} a_{\mathbf{k},\sigma} + \delta(B) b^\dagger_0 b_0 \\
&+ \frac{g_0}{\sqrt{\mathcal{V}}} \sum_{\mathbf{k}} \left(b^\dagger_0 a_{\mathbf{k},\uparrow} a_{-\mathbf{k},\downarrow} + a^\dagger_{-\mathbf{k},\downarrow} a^\dagger_{\mathbf{k},\uparrow} b_0 \right). \\
&+ \frac{\lambda_{\text{bg}}}{\mathcal{V}} \sum_{\mathbf{q},\mathbf{k}} a^\dagger_{-\mathbf{q},\downarrow} a^\dagger_{\mathbf{q},\uparrow} a_{\mathbf{k},\uparrow} a_{-\mathbf{k},\downarrow}
\end{aligned} \tag{4.8}$$

where $\delta(B) = \Delta\mu(B - B_0)$, the difference in magnetic moments between the two lowest hyperfine states (the states of the two atoms and the molecule) is $\Delta\mu$ and the Feshbach resonance is situated at B_0, while $\lambda_{\text{bg}} = 4\pi\hbar^2 a_{\text{bg}}/m$, is the background interaction. The

[5] The Hamiltonian in real space in terms of fields is in the Introduction (1.4).

Hamitonian in (4.8) corresponds to the situation where if the temperature is low enough b_0 corresponds to an homogenous molecular condensate. The two channel model (4.8) may be related to the single channel model by looking at the equation of motion of the operator b_0 and imposing the constraint $g_0 = \sqrt{-\delta(B)\lambda_{\text{res}}}$. Following the results from [52], then we have,

$$\begin{aligned}
\partial_t b_0 &= -i\left[b_0, \mathcal{H}_{2ch}\right]_- \\
&= -i\left\{\delta(B) b_0 + \frac{g_0}{\sqrt{\mathcal{V}}}\sum_{\mathbf{k}} a_{\mathbf{k},\uparrow} a_{-\mathbf{k},\downarrow}\right\} \\
&= -i\left\{-\frac{g_0^2}{\lambda_{\text{res}}} b_0 + \frac{g_0}{\sqrt{\mathcal{V}}}\sum_{\mathbf{k}} a_{\mathbf{k},\uparrow} a_{-\mathbf{k},\downarrow}\right\},
\end{aligned}$$

because g_0 is the only relevant scale, the stationary solution of the above equation gives the following relation for enslaved bosons,

$$b_0 = \frac{\lambda_{\text{res}}}{g_0\sqrt{\mathcal{V}}}\sum_{\mathbf{k}} a_{\mathbf{k},\uparrow} a_{-\mathbf{k},\downarrow}, \tag{4.9}$$

with $g_0 = \sqrt{4\pi\hbar^2 a_{\text{bg}}\Delta\mu\Delta B/m}$. The interaction in the single channel model is given by, $\lambda = \lambda_{\text{bg}} + \lambda_{\text{res}}$, with $\lambda_{\text{res}} = -\lambda_{\text{bg}}\Delta B/(B - B_0)$, the contribution due to the Feshbach resonance. Using (4.9) in (4.8) we have $\mathcal{H}_{2ch} \to \mathcal{H}_{1ch}$. We call the bosons enslaved because they can effectively be defined in terms of the atom pairs with opposite momentum. In the broad resonance limit, the above mapping suggests the possibility that the single channel model could describe the physics of the system very well. The broad resonance limit is defined as: $k_F r_0 \ll 1$ with the range of the interaction defined as $r_0 = 8\pi\hbar^4/(m^2 g_0^2)$. The interpretation of r_0 comes from the fact that the two-body s-wave scattering cross section of the two-channel model is given by [50, 52, 169]:

$$f_0(k) \approx -\frac{1}{a^{-1} - r_0 k^2/2 + ik},$$

from the above expression it is clear the when $|a| \to \infty$, and $r_0 \to 0$, the effective interaction strength is given by $\lambda_{\text{eff}} \sim k_F |f_0(k_F)| = 1$, therefore the name unitary limit. When $k_F r_0 \to \infty$, this is the infinitely narrow resonance limit. One can relate the gap to the mean value of the molecular condensate with (4.3) as:

$$\langle b_0^\dagger b_0\rangle \approx \frac{\lambda_{\text{res}}^2\mathcal{V}}{\lambda^2 g_0^2}\Delta^2 = \varphi\tilde{\Delta}^2, \tag{4.10}$$

where,

$$\varphi = \varphi_0\left(\frac{\Delta B}{\Delta B + B_0 - B}\right)^2 = \varphi_0\left(1 - \frac{k_F a_{\text{bg}}}{k_F a}\right)^2,$$

a dimensionless function of the magnetic field, at unitarity $\varphi_0 = \epsilon_F^2\mathcal{V}/(\Delta\mu\Delta B\lambda_{\text{bg}})$. However, φ diverges at $B = B_0 + \Delta B$, thus could be thought of being unphysical near this point. In the case of ^{40}K because $\Delta B > 0$ the divergence is in the BCS side and we would expect the system to be absent of molecules, still we know that the gap vanishes expo-

nentially as we approach the limit $1/k_F a \to -\infty$ thus the gap falls faster that φ and we have that the molecules disappear. In the case of ^{6}Li things are "easier" to interpret since we expect a pure BEC, but still the number of molecules should be finite and in fact if we had no losses, half the number of fermions. Therefore, this identification is problematic and clearly the point $B = B_0 + \Delta B$ should be studied more carefully in the BEC side of the resonance. On the other hand, we may argue that the approximation to represent the variation of the scattering length in terms of the magnetic field ceases to be valid away from the Feshbach resonance. Therefore a more accurate expression for $a(B)$ most be used such that we have the correct behaviour in the BEC limit, depending on the substance under study, i.e. ^{6}Li or ^{40}K. Since we have a molecular condensate one can write $b_0 \approx \sqrt{N_b}\tilde{b}_0$, where N_b is the number of molecules and $\tilde{b}_0$ refers to a single molecular state. In the BEC limit $N_b \to N/2$ and $\langle \tilde{b}_0^\dagger \tilde{b}_0 \rangle \to 1$, thus we have the following condition,

$$\lim_{(k_F a)^{-1} \to \infty} \varphi \tilde{\Delta}^2 = \frac{N}{2}. \tag{4.11}$$

Since we know from the solution of (4.5) and (4.6) that the gap increases in the BEC side, we arrive at a contradiction, because the gap should go as $\tilde{\Delta} \sim (k_F a)^2 \to 0$ in the BEC limit from using (4.11). This gives some understanding of the partial success of the simple extended mean-field picture in the asymptotic BCS limit, and motivates the possibility to modify theories of this kind to address the problem in the strongly interacting region. Still, one must bear in mind that in the problem with a medium or a small size resonance one should include more channels in the theory to analyse the problem even qualitatively [52, 181]. The approach that we will follow here differs from that of modifying the single channel model and we refer the reader to the vast literature in the subject, see for example the relevant sections of [19, 51, 63] and references there in.

4.2 Magnetic impurity models

In the early 1960's the search for theories and mechanisms to describe and understand the behaviour seen in non-magnetic metals with magnetic impurities motivated the development of new descriptions such as the one given by Kondo model [61] and the Anderson model [62]. The relevance of these models for ultracold atoms comes from the fact that under the approximation of having only one molecular bound state while neglecting the atom-atom interaction in the two-channel hybrid model, the BCS-BEC crossover problem is equivalent to the anisotropic Kondo model [181]. In this context we will summarise the well known characteristics of the Kondo model, and we will show that by means of a canonical transformation the Anderson model will allow us to include the terms necessary to consider the atom-atom interaction missing in the Kondo model mapping of the two-cannel model. This will allow us to extend region of validity of the mapping to an equivalent magnetic impurity problem and study the crossover in both BEC and BCS side of the Feshbach resonance. With this in mind, we will also summarise the parameter regimes of the Anderson model from well know results [184], we will review the well known results of the Schrieffer-Wolff canonical transformation that maps the Kondo model and the Anderson model [194].

The Kondo model considers the interaction between the conduction electrons in the

non magnetic metal with the spins of magnetic impurities, which can take any allowed quantum number and don't interact with each other. The Kondo model is the following [6],

$$\mathcal{H}_{\mathrm{K}} = \sum_{\mathbf{k},\sigma} \epsilon_{\mathbf{k}} n_{c_{\mathbf{k},\sigma}} + \sum_{\mathbf{k},\mathbf{q}} \left(J^{z}_{\mathbf{k},\mathbf{q}} S^{z} \left(c^{\dagger}_{\mathbf{k},\uparrow} c_{\mathbf{q},\uparrow} - c^{\dagger}_{\mathbf{k},\downarrow} c_{\mathbf{q},\downarrow} \right) + J^{+}_{\mathbf{k},\mathbf{q}} S^{+} c^{\dagger}_{\mathbf{k},\downarrow} c_{\mathbf{q},\uparrow} + J^{-}_{\mathbf{k},\mathbf{q}} S^{-} c^{\dagger}_{\mathbf{k},\uparrow} c_{\mathbf{q},\downarrow} \right), \tag{4.12}$$

where $c^{\dagger}$ (c) creates (destroys) a conduction electron or fermion carrier, and the occupation of the electrons is $n_{c_{\mathbf{k},\sigma}} = c^{\dagger}_{\mathbf{k},\sigma} c_{\mathbf{k},\sigma}$. The operators S^{ν} are the spin components of the impurity, and they obey: $\left[S^{-}, S^{+}\right]_{-} = 2S^{z}$, such that: $S^{+} = S^{x} + iS^{y}$ and $S^{-} = S^{x} - iS^{y}$. The sub-indices $\mathbf{k}$ and $\mathbf{q}$ denote momenta and σ's spin. The energy of the conduction electrons relative to the Fermi energy is given by $\epsilon_{\mathbf{k}}$ and the $J^{\nu}_{\mathbf{k},\mathbf{q}}$ are the interaction strengths for different spin, $\nu \in \{x, y, z\}$. When all the J's have the same value ($J^{\nu} = J \ \forall \ \nu$), the model is referred to as *isotropic* while if the $J's$ are different it is called *anisotropic*. The sign of the J's determines if the coupling is anti-ferromagnetic ($J > 0$) or ferromagnetic ($J < 0$). This meaning that the spins tend to align in the same direction (ferromagnetic) maximising their magnetic moment or the they minimise the energy by forming opposite spin pair configurations (anti-ferromagnetic) to minimise their magnetic moment. The relationship to the two-channel hybrid model follows from identifying that the spins correspond to the Feshbach bosons and the conduction electrons are analogous to the free atoms. Therefore, a spin-flip corresponds to the creation of a FB and a particle-hole excitation to a Cooper-pair, see Fig. 4.3 (right). Because the spins do not commute, the interaction of the spins with the fermion carriers has the effect of flipping the local spins introducing local correlations. This changes the contribution to the energy due to interactions, the self-energy Σ of the fermion carriers and therefore the collective excitations of the system have a finite life-time which leads to have a contribution to the resistivity. The resistivity is defined as,

$$\varrho \sim \mathrm{Im}[\Sigma]$$

The self energy Σ can be defined by using the Dyson equation and the interacting $\mathcal{G}$ and the non-interacting $\mathcal{G}_0$ Green's functions as [44],

$$\Sigma = \mathcal{G}^{-1} - \mathcal{G}_0^{-1}$$

When $J \neq 0$, Kondo did a perturbation theory calculation of the energy of (4.12) to third-order and a minimum in the resistivity appears which depends on the temperature [61]. This phenomena is now called the *Kondo effect*. The resistivity of the system is then given by,

$$\varrho(T) = \varrho(0) \left(1 - 4J\rho(\epsilon_F) \ln \left(\frac{k_B T}{D} \right) \right) + bT^5$$

The Kondo term is the J term, the temperature independent part $\varrho(0)$, and the b term is due to phonons. The density of states at the Fermi level is $\rho(\epsilon_F)$ and D is the bandwidth, such that:

$$\rho(\epsilon) = \begin{cases} \rho(\epsilon_F), & \text{for} \quad -D \leq \epsilon \leq D, \\ 0, & \text{elsewhere.} \end{cases}$$

[6] In the old days, this model was called the s-d model, and was originally introduced by Zener [195].

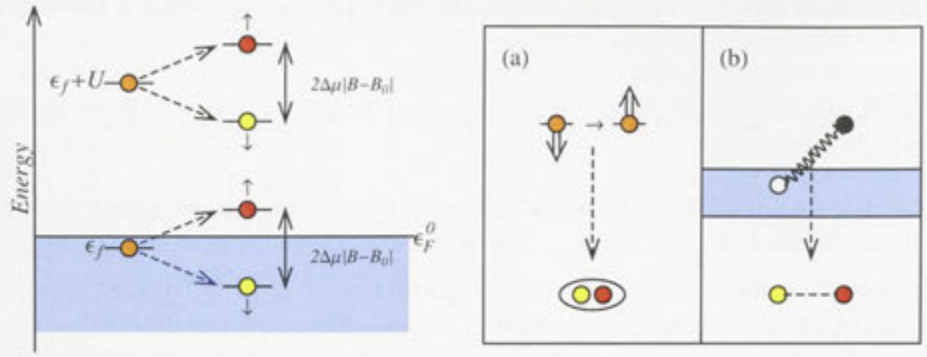

Figure 4.3: Left Panel: Energy diagram for for the position of magnetic impurity energy levels ϵ_f and $\epsilon_f + U$. The effect of the detuning with respect to unitarity, induces Zeeman splitting in the equivalent single impurity picture. The spin up states (red) correspond to the configuration that minimises the energy for positive detuning (BCS side of the resonance) and the spin down states (yellow) correspond to negative detuning (BEC side of the resonance).Right Panel: The equivalence in representations between the magnetic impurity models and the crossover problem. A molecular bound state, Feshbach boson, is equivalent to the spin-flip process in the impurity level (a). A Cooper-pair is equivalent to a particle hole excitation of a fermion carrier in the impurity model (b).

which means that the density of states is considered constant and equal to its value at the Fermi level over the energy span $2D$.

As one decrease the temperature there is a critical temperature called the *Kondo temperature* T_K where the perturbation theory used to to derive the resistance minimum breaks down. At this energy scale, high energy processes in the self-energy become dominant and the theory diverges. This is called the *Kondo problem*, here the theory needs to be modified because the resistivity and other quantities become infinity as we approach $T = T_K$, this being un-physical. Renormalization Group Theory [196] was devised as a way to solve divergency problems of this kind, when suddenly all energy scales become relevant. The Kondo temperature T_K is given by [60, 184],

$$k_B T_K \sim D \exp\left(-\frac{1}{2|J|\rho(\epsilon_F)}\right). \tag{4.13}$$

The Kondo temperature signals the energy scale where the interaction becomes non-perturbative as we decrease temperature.

In contrast to the Kondo model, the Anderson model is based on the assumption that the fermion carriers in the dilute magnetic alloy interact with other "localised" electrons. This interaction is controlled by the Coulomb repulsion of the two localised electrons of opposite spin and the probability of overlap of their orbitals with the conduction electrons, i. e. the hybridisation. The Anderson model is thought to have a more realistic description of the processes that occur in the system [60]. In the BCS-BEC crossover problem because we have neutral atoms there is no Coulomb repulsion but instead we

have the energy that takes to have a doubly occupied impurity and this is proportional to the difference in magnetic moments from the two lowest hyperfine states and the width of the resonance. As we move away from the resonance the detuning from the resonance shifts the local chemical potential of the impurities depending on their spin inducing a Zeeman type splitting, see Fig. 4.3 (left).

Still, the Kondo model has the essential ingredients to solve the problem of the minimum in the resistivity seen in experiments. The Anderson model solves the problem of explaining the *ferromagnetism* seen in dilute magnetic alloys, and provides a picture on how to interpret the flipping of the spins that leads to correlations in the Kondo model. The ferromagnetic phase in the AM represents the formation of the Feshbach Boson in the mapping to the BCS-BEC crossover problem. The AM is written as follows,

$$\mathcal{H}_{\mathrm{AM}} = \mathcal{H}_0 + \mathcal{H}_V,$$

where,

$$\begin{aligned} \mathcal{H}_0 &= \sum_{\mathbf{k},\sigma} \epsilon_{\mathbf{k}} n_{c_{\mathbf{k},\sigma}} + \epsilon_f \sum_{\sigma} n_{f_\sigma} + U n_{f_\uparrow} n_{f_\downarrow}, \\ \mathcal{H}_V &= \sum_{\mathbf{k},\sigma} V_{\mathbf{k}} \left(f_\sigma^\dagger c_{\mathbf{k},\sigma} + c_{\mathbf{k},\sigma}^\dagger f_\sigma \right), \end{aligned}$$

where $f^\dagger$ (f) creates (destroys) a magnetic impurity with number operators $n_{f_\sigma} = f_\sigma^\dagger f_\sigma$. The energy cost of having a doubly occupied impurity is U and the hybridisation is V which is proportional to the probability of of overlap between the localised impurities and the conduction electrons. The impurity energy levels are ϵ_f and $\epsilon_f + U$. In the limit where $U = 0$, the AM is sometimes referred to as the Fano-Anderson model [60] and can be solved exactly by the Green's function technique, its solution for the case $U \neq 0$ can be found exactly in the limit where $V_{\mathbf{k}} = V$ =constant by means of Bethe ansatz [7] [185, 186] and it was first solved for all parameter regimes using Renormalisation Group theory [187, 188].

In the AM picture the localised electrons can jump to the conduction band because of the hybridisation, and vice-versa. This induces the possibility of occupation of the localised state by a conduction electron by Pauli blocking the state with the same spin polarisation. If $U = 0$ then the process of "flipping" happens without any preferred sequence. Still, if $U \neq 0$ then there is an energy cost to populate the state by two electrons. Therefore, hopping on and off the localised energy state becomes correlated, for one electron of a certain spin to populate the localised state from the conduction band the localised electron with the same spin must leave. This then gives the appearance of flipping the spin, while there is no flipping actually taking place. In the BCS-BEC crossover picture the creation of a Cooper-pair and a Feshbach boson occur in an analogous way. Depending on the energy cost to have a doubly occupied impurity a FB will be created and as this happens a Cooper-pair disappears, then a free atom interacts with the

[7] The solution using Bethe ansatz of models of the type of the Anderson model or the Kondo model can be done in the limit where the system is isotropic with constant hybridisation and when the dispersion relation can be linearised provided that the Fermi energy is much larger than all other energy scales. In this limit the system is quasi-one dimensional and these kinds of models are integrable.

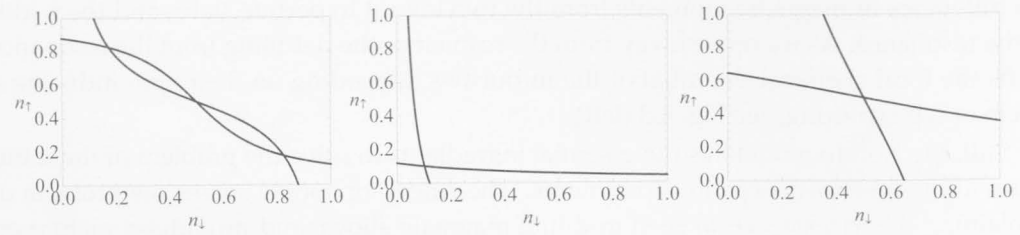

Figure 4.4: Graphical solution of the equations 4.14, with parameters $\{x, y\}$ for $\{\frac{1}{2}, 5\}$ (left), $\{-\frac{1}{2}, 5\}$ (middle), $\{\frac{1}{2}, 1\}$ (right). The solutions are magnetic with valence one (left), non-magnetic with valence different from one (middle) and non-magnetic with valence one (right).

localised fermion generating a Cooper-pair. Once the Cooper-pair is formed and when another free fermion interacts with the occupied impurity level a FB is formed and the cycle starts again.

The solution in mean-field for $U \neq 0$ gives some qualitative behaviour, one approximates the interaction term as,

$$U n_{f_\uparrow} n_{f_\downarrow} \approx U\langle n_{f_\uparrow}\rangle n_{f_\downarrow} + U\langle n_{f_\downarrow}\rangle n_{f_\uparrow} - U\langle n_{f_\uparrow}\rangle\langle n_{f_\downarrow}\rangle,$$

where $\langle\cdot\rangle$ is the ground state average. The above approximation allows to solve the model as shown by Anderson [62]. The regimes of the model are controlled by the solution of the following well known system of equations for the expectation value of the impurity populations of opposite spins [62],

$$\begin{aligned} \cot(\pi n_\uparrow) &= y n_\downarrow - yx, \\ \cot(\pi n_\downarrow) &= y n_\uparrow - yx, \end{aligned} \tag{4.14}$$

with, $x = (\epsilon_F - \epsilon_f - V)/U$, $y = U/\Gamma$, and $\Gamma = \pi\rho(\epsilon_F)V^2$. Plots of the equations for the magnetic and paramagnetic cases can be seen in Fig. 4.4. One can see in the left plot of Fig. 4.4 that the magnetic regime has 3 points where the two curves for $n_\uparrow$ and $n_\downarrow$, intersect, two of them (the extrema) are the magnetic solutions ($n_\uparrow \neq n_\downarrow$) and the one in the middle is the non magnetic one ($n_\downarrow = n_\uparrow$). One can check that the energy is minimised for the magnetic solution, if it exists. As one changes the parameters of the model the three mean-field solutions collapse to a single solution, which is always non-magnetic but can have integer or non-integer valence ($n_f = n_\uparrow + n_\downarrow$).

The model is *symmetric* [184] when the impurity levels are placed symmetrically with respect to the Fermi level. Therefore, the model has particle-hole symmetry and $\epsilon_f = -U/2$. In this case then $n_f = 1$, always. If the model is *asymmetric*, then there is no particle-hole symmetry, and $\epsilon_f \neq -U/2$. In this case the valence n_f can take non-integer values, having fluctuations [60].

Assuming that we have a macroscopic sample, the solution where $n_\uparrow \neq n_\downarrow$ [8] , gives

[8] In the zero temperature limit at the microscopic level this criteria is an artefact of mean-field where one

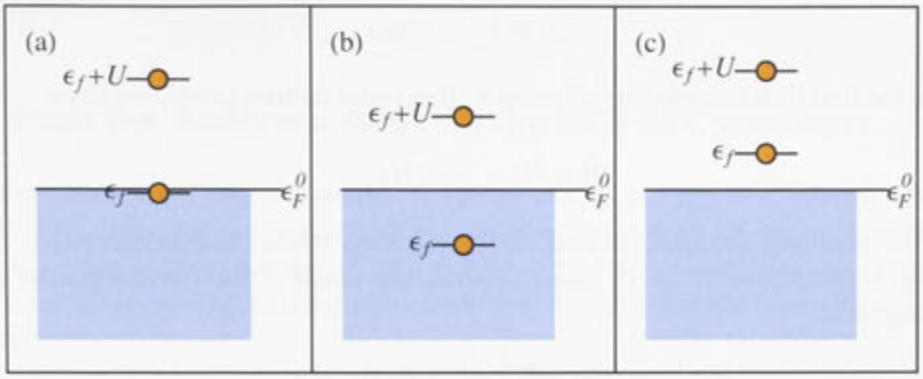

Figure 4.5: The Anderson model regimes depending on the impurity level ϵ_f and the interaction U for $V = 0$, mixed valence regime (a), magnetic regime (b) and the non-magnetic regime [Reproduced after [184]].

qualitatively the regime where the magnetisation in the system is different from zero and develops a local moment. This is the Kondo limit of the model.

In order to further understand the model is useful to look at the solutions when the hybridisation is zero, as discussed in [184]. The possible regimes of the model in this limit are controlled by value of U and the position of the impurity level relative to the Fermi energy. In the case when one of the impurity levels is at the Fermi energy or very close to it while the value U is large, we are in the valence fluctuation regime [Fig. 4.5 (a)]. When one of the impurity levels is below and the other one above the Fermi energy while U is large then we are in the magnetic or Kondo regime [Fig. 4.5 (b)]. The remaining configuration is when both impurity levels are well above or below the Fermi level; then the system is non magnetic [Fig. 4.5 (c)]. As the hybridisation is turned on, the picture becomes more subtle and one needs to take care properly on how the effective impurity levels are defined [184, 197]. In BCS-BEC crossover problem, the Kondo regime is when we have a FB in the BEC side of the resonance. As we move towards the BCS limit the system is in a crossover moving from the Kondo limit to the valence fluctuation regime and deep in the BCS regime to the configuration when both impurity levels are above or below the Fermi level.

The hybridisation V turns on the scattering on and off the localised energy states and U regulates the correlations, these in combination with the value of ϵ_f give a rich variety of physics. The full solution of all the different regimes according to the parameters was done by Krishna-murthy, Wilkins and Wilson [187, 188].

The AM can be related by a canonical transformation to the Kondo Hamiltonian. This procedure gives the equivalence in the limit of large U of the AM [60, 184]. The following well known canonical transformation is used [194],

$$\tilde{\mathcal{H}} = e^{\mathcal{S}} \mathcal{H} e^{-\mathcal{S}},$$

has broken the symmetry between different spins.

where, to construct $\mathcal{S}$, we impose,

$$\left[\mathcal{S}, \mathcal{H}_0\right]_- = -\mathcal{H}_V.$$

Then to the first order, neglecting all other higher order commutators, we have:

$$\tilde{\mathcal{H}} = \mathcal{H}_0 + \frac{1}{2}\left[\mathcal{S}, \mathcal{H}_V\right]_-.$$

Using the resulting commutator and taking the limit where double occupancy of the impurity is forbidden ($U \gg 0$), one can write the result of the transformation in the following form:

$$\begin{aligned} \tilde{\mathcal{H}}_{\mathrm{AM}} &= \tilde{\mathcal{H}}_0 + \sum_{\mathbf{k},\mathbf{q}} J_{\mathbf{k},\mathbf{q}} \vec{S}_c(\mathbf{k},\mathbf{q}) \cdot \vec{S}_f \\ &- \sum_{\mathbf{k},\mathbf{q}} \left(W_{\mathbf{k},\mathbf{q}} + \frac{J_{\mathbf{k},\mathbf{q}}}{4} \Psi_f^\dagger \Psi_f \right) \Psi_{c_\mathbf{k}}^\dagger \Psi_{c_\mathbf{q}}, \end{aligned} \tag{4.15}$$

where the second term has the form of the spin-fermion carrier interaction of the Kondo model. In the above, we have defined, $J_{\mathbf{k},\mathbf{q}} = 2V_\mathbf{k}V_\mathbf{q}Z_\mathbf{k}$, $W_{\mathbf{k},\mathbf{q}} = V_\mathbf{k}V_\mathbf{q}A_\mathbf{k}$, with

$$\begin{aligned} A_\mathbf{k} &= -\frac{1}{\epsilon_\mathbf{k} - \epsilon_f}, \\ Z_\mathbf{k} &= -\frac{U}{(\epsilon_\mathbf{k} - \epsilon_f)(\epsilon_\mathbf{k} - \epsilon_f - U)} = -\frac{1}{\epsilon_\mathbf{k} - \epsilon_f - U} - A_\mathbf{k}, \end{aligned} \tag{4.16}$$

and the spin operators are,

$$\begin{aligned} \vec{S}_f &= \frac{1}{2} \sum_{j\in\{x,y,z\}} \left(\Psi_f^\dagger \sigma^j \Psi_f \right) \hat{\mathrm{e}}_j, \\ \vec{S}_c(\mathbf{k},\mathbf{q}) &= \frac{1}{2} \sum_{j\in\{x,y,z\}} \left(\Psi_{c_\mathbf{k}}^\dagger \sigma^j \Psi_{c_\mathbf{q}} \right) \hat{\mathrm{e}}_j, \end{aligned}$$

where σ^j are the Pauli matrices. The unitary vectors in Cartesian coordinates are denoted by $\hat{\mathrm{e}}_j$, and the "spinors" $\Psi_\xi^\dagger$ and Ψ_ξ are defined as follows:

$$\Psi_\xi^\dagger = \left(\xi_\uparrow^\dagger, \xi_\downarrow^\dagger\right), \quad \Psi_\xi = \begin{pmatrix} \xi_\uparrow \\ \xi_\downarrow \end{pmatrix}$$

The interaction strength and the impurity levels are renormalized in $\tilde{\mathcal{H}}_0$ to $\tilde{U} = U + \sum_\mathbf{k} J_{\mathbf{k},\mathbf{k}}$ and $\tilde{\epsilon}_f = \epsilon_f + \sum_\mathbf{k} W_{\mathbf{k},\mathbf{k}}$ (see the Appendix B for details). In the limit when $|\mathbf{k}| \approx k_F$, neglecting the renormalisation in $\mathcal{H}_0$ while transforming the electron states to include the last term, we arrive to the situation when only the term with the spins of the Hamiltonian (4.15) adds to $\mathcal{H}_0$. This limit gives the Kondo model. Then it follows that the Kondo coupling $J^\nu = J$ in (4.12) is given by:

$$J = -\frac{V_{k_F}^2 U}{\epsilon_f (\epsilon_f + U)}. \tag{4.17}$$

For the symmetric Anderson model is $J = 4V_{k_F}^2/U$, and the coupling is antiferromagnetic.

4.3 From the Anderson model to the BCS-BEC crossover

In this section we will show how the Anderson model and the two channel model of the BCS-BEC crossover can be mapped to each other in the limit where it only exists one molecular state or Feshbach boson. We will give the relationship between parameters of the equivalent pictures of these two crossovers. We consider the following Anderson model,

$$\mathcal{H}_{\mathrm{AM}} = \mathcal{H}_0 + \mathcal{H}_V,$$

where,

$$\begin{aligned} \mathcal{H}_0 &= \sum_{\mathbf{k},\sigma} \epsilon_{\mathbf{k}} n_{c_{\mathbf{k},\sigma}} + \sum_{\sigma} \epsilon_{f_\sigma} n_{f_\sigma} + U n_{f_\uparrow} n_{f_\downarrow}, \\ \mathcal{H}_V &= \sum_{\mathbf{k},\sigma} V \left(f_\sigma^\dagger c_{\mathbf{k},\sigma} + c_{\mathbf{k},\sigma}^\dagger f_\sigma \right), \end{aligned}$$

$c^\dagger$ (c) creates (destroys) a fermion carrier which is a projected representation of the atom $a^\dagger$ (a) creation (annihilation) operator, $f^\dagger$ (f) creates (destroys) a fermionic impurity which corresponds to an atom with the energy necessary to form a FB. They have number operators, $n_{f_\sigma} = f_\sigma^\dagger f_\sigma$ and $n_{c_{\mathbf{k},\sigma}} = c_{\mathbf{k},\sigma}^\dagger c_{\mathbf{k},\sigma}$. The sub-indices k's denote momenta and σ's spin . The energy of a carrier relative to the Fermi energy is given by $\epsilon_{\mathbf{k}}$, the energy required for double occupancy of the impurity is U, the hybridisation is V. The impurity energy levels at zero field are ϵ_f and $\epsilon_f + U$, while in this model the impurity energy levels for opposite spins are modified by a detuning such that, $\epsilon_{f_\sigma} = \epsilon_f + \mathrm{sgn}(\sigma)\delta(B)$ and $\delta(B)$ is the detuning with respect to the Feshbach resonance. This means that there is a shift in the impurity energy levels of different spin [see Fig. 4.3]. A similar Hamiltonian has also been considered in the study of quantum dots coupled to ferromagnetic leads [198]. We can perform a canonical transformation as follows,

$$\tilde{\mathcal{H}} = e^{\mathcal{S}} \mathcal{H}_{\mathrm{AM}} e^{-\mathcal{S}} = \mathcal{H}_0 + \sum_{n=1}^{\infty} \left[\frac{1}{n!} - \frac{1}{(n+1)!} \right] \mathcal{H}_n, \tag{4.18}$$

with,

$$\mathcal{H}_n = \overbrace{[\mathcal{S}, [\mathcal{S}, [\mathcal{S}, \dots [\mathcal{S}}^{n \text{ times}}, \mathcal{H}_V]_- \dots]_-]_-]_-$$

while,

$$[\mathcal{S}, \mathcal{H}_0]_- = -\mathcal{H}_V.$$

From Section 4.2 we know that, in a first order expansion, the first two terms of $\tilde{\mathcal{H}}$ reproduce the Kondo Hamiltonian [60]. This is equivalent to second order Rayleigh-Schrödinger perturbation theory [199]. If we go to higher orders, we have the generation of terms with BCS-like symmetry [200–202] which will allow us to relate the AM and the BCS-BEC crossover problem including the background interaction between atoms. We

consider $\mathcal{H}_0$ and the first two odd terms of $\mathcal{H}_n$ that have the correct symmetry in (4.18) [199]. Then, equivalent to sixth order perturbation theory, in the large U limit, taking $\epsilon_{\mathbf{k}} \approx \epsilon_{\mathbf{k}_F} = \epsilon = \text{const.}$, while considering the sum over $\mathbf{k}$ close to the Fermi momentum, we have the following (see the Appendix B for details),

$$\tilde{\mathcal{H}}_{\text{eff}} = \tilde{\mathcal{H}}_0 + \tilde{\mathcal{H}}_{c-c} + \tilde{\mathcal{H}}_{s-c}, \tag{4.19}$$

where the effective carrier-carrier interaction is:

$$\tilde{\mathcal{H}}_{c-c} = \tilde{\lambda} \sum_{\sigma} \sum_{\mathbf{k},\mathbf{q},\mathbf{k}_1,\mathbf{k}_2} c^{\dagger}_{\mathbf{k},-\sigma} c_{\mathbf{q},-\sigma} c^{\dagger}_{\mathbf{k}_1,\sigma} c_{\mathbf{k}_2,\sigma}, \tag{4.20}$$

and the effective spin-carrier interaction is:

$$\tilde{\mathcal{H}}_{s-c} = \sum_{\sigma} \sum_{\mathbf{k},\mathbf{q}} \left\{ \tilde{\gamma}_1 n_{f_{-\sigma}} c^{\dagger}_{\mathbf{k},\sigma} c_{\mathbf{q},\sigma} + \tilde{J} c^{\dagger}_{\mathbf{k},\sigma} c_{\mathbf{q},-\sigma} f^{\dagger}_{-\sigma} f_{\sigma} \right\}, \tag{4.21}$$

with,

$$\begin{aligned} \tilde{\lambda} &= -V^4 A^3, \\ \tilde{J} &= V^2 A \left(2V^2 A^2 - 1\right), \\ \tilde{\gamma}_1 &= -\tilde{J}, \end{aligned}$$

and $A = -(\epsilon - \epsilon_f)^{-1}$. Next, we take the limit where $\mathbf{k}_1 \approx \mathbf{q}$ and $\mathbf{k}_2 \approx \mathbf{k}$, considering only scattering processes between fermions of opposite spin with the same momentum and pairs of holes with the same momentum. At the same time, we neglect the γ_1 term in (4.21), which is equivalent to imposing, $c^{\dagger}_{\mathbf{k},\downarrow} c_{\mathbf{q},\downarrow} \approx c^{\dagger}_{\mathbf{k},\uparrow} c_{\mathbf{q},\uparrow}$, making the model anisotropic and having no Kondo J_z component. Thus, the effective Hamiltonian is [9] :

$$\tilde{\mathcal{H}}_{\text{eff}} = \sum_{\sigma} \sum_{\mathbf{k},\mathbf{q}} \left\{ \tilde{\epsilon}\, c^{\dagger}_{\mathbf{k},\sigma} c_{\mathbf{k},\sigma} + \frac{\tilde{\lambda}}{\mathcal{V}} c^{\dagger}_{\mathbf{k},-\sigma} c_{\mathbf{q},-\sigma} c^{\dagger}_{\mathbf{q},\sigma} c_{\mathbf{k},\sigma} + \tilde{J} c^{\dagger}_{\mathbf{k},\sigma} c_{\mathbf{q},-\sigma} f^{\dagger}_{-\sigma} f_{\sigma} \right\}, + \sum_{\sigma} \tilde{\epsilon}_{f_\sigma} n_{f_\sigma}. \tag{4.22}$$

where, $\tilde{\epsilon} = \epsilon + V^2 A \left(V^2 A^2 - 1\right)$ and $\tilde{\epsilon}_{f_\sigma} = \epsilon_{f_\sigma} + V^2 A \left(1 - V^2 A^2\right)$. Similar results, obtained via canonical transformations, have been used to analyse the periodic Anderson model in three dimensions [201], and the two band model for the high-Tc superconductivity [202].

Using the above equations, the effective Hamiltonian can be related to the two-channel hybrid model of the BCS-BEC crossover problem language as follows. We start by relating the impurity operators to their spin representation and this to its approximate equivalent bosonic representation. We interpret f_σ ($f^{\dagger}_{\sigma}$) as the annihilation (creation) operator of the spin σ component of the FB composed of two fermions, $\tilde{b}_0 \to S^- \to f^{\dagger}_{\downarrow} f_{\uparrow}$, and $\tilde{b}^{\dagger}_0 \to S^+ \to f^{\dagger}_{\uparrow} f_{\downarrow}$, while $n_{f_\uparrow} - n_{f_\downarrow} = S^z \to \tilde{b}^{\dagger}_0 \tilde{b}_0$. We consider that a FB can be represented by $\tilde{b}_0$ and restrict the sector of Hilbert space of the bound state to the one of two levels with an empty or occupied molecular state, with a single particle[10]. Then we

[9] Where the volume factor $1/\mathcal{V}$ comes from eliminating the sums over $\mathbf{k}_1$ and $\mathbf{k}_2$, in the $\tilde{\lambda}$ term.

[10] The molecular condensate operator in (4.8) is $b_0 \approx \sqrt{N_b}\tilde{b}_0$, in this section we work with one molecule.

have[11]:

$$\tilde{\mathcal{H}}_{\text{eff}} = \sum_{\mathbf{k},\sigma} \tilde{\epsilon}\, c^{\dagger}_{\mathbf{k},\sigma} c_{\mathbf{k},\sigma} + \delta(B)\tilde{b}^{\dagger}_{0}\tilde{b}_{0} + \frac{\tilde{J}}{\sqrt{\mathcal{V}}} \sum_{\mathbf{k}} \left(\tilde{b}^{\dagger}_{0} c^{\dagger}_{\mathbf{k},\uparrow} c_{\mathbf{k},\downarrow} + c^{\dagger}_{\mathbf{k},\downarrow} c_{\mathbf{k},\uparrow} \tilde{b}_{0} \right) + \frac{2\tilde{\lambda}}{\mathcal{V}} \sum_{\mathbf{k},\mathbf{q}} c^{\dagger}_{\mathbf{k},\downarrow} c_{\mathbf{q},\downarrow} c^{\dagger}_{\mathbf{q},\uparrow} c_{\mathbf{k},\uparrow},$$

where the term $\sum_{\sigma}(\epsilon_f + V^2 A\left(1 - V^2 A^2\right)) n_{f_\sigma}$ has been omitted since it only shifts the energy and we have taken the limit where $\mathbf{k} \approx \mathbf{q}$ in the $\tilde{J}$ term. Following the same procedure as in [181], it follows to identify the fermion carrier operators with a suitable spin representation. This can be done by the following pseudo spins,

$$c^{\dagger}_{\mathbf{k},\uparrow} c_{\mathbf{k},\downarrow} \equiv \sigma^{+}_{\mathbf{k}}, \quad c^{\dagger}_{\mathbf{k},\downarrow} c_{\mathbf{k},\uparrow} \equiv \sigma^{-}_{\mathbf{k}}, \quad c^{\dagger}_{\mathbf{k},\uparrow} c_{\mathbf{k},\uparrow} - c^{\dagger}_{\mathbf{k},\downarrow} c_{\mathbf{k},\downarrow} \equiv \sigma^{z}_{\mathbf{k}},$$

with $\sigma^{j}_{\mathbf{k}}$ the Pauli matrices. We can relate the above pseudo spin representation to the so called symmetrised atom-pair operators d. Then the remaining terms in the Hamiltonian can be written in terms of the fermionic atom creation and annihilation operators. With the following constraint on the algebra, $\left[d_{\mathbf{k}}, d^{\dagger}_{\mathbf{k}}\right]_{-} \approx \sigma^{z}_{\mathbf{k}}$. Thus,

$$d^{\dagger}_{\mathbf{k}} \approx \frac{1}{2}(\sigma^{x}_{\mathbf{k}} - i\sigma^{y}_{\mathbf{k}}) \equiv \sigma^{-}_{\mathbf{k}} \quad \text{and} \quad d_{\mathbf{k}} \approx \frac{1}{2}(\sigma^{x}_{\mathbf{k}} + i\sigma^{y}_{\mathbf{k}}) \equiv \sigma^{+}_{\mathbf{k}}.$$

It follows that the symmetrised atom-pair operators can be defined as,

$$d_{\mathbf{k}} = \frac{1}{\sqrt{2}} \left(a_{-\mathbf{k},\downarrow} a_{\mathbf{k},\uparrow} + a_{\mathbf{k},\downarrow} a_{-\mathbf{k},\uparrow} \right),$$

$$d^{\dagger}_{\mathbf{k}} = \frac{1}{\sqrt{2}} \left(a^{\dagger}_{\mathbf{k},\uparrow} a^{\dagger}_{-\mathbf{k},\downarrow} + a^{\dagger}_{-\mathbf{k},\uparrow} a^{\dagger}_{\mathbf{k},\downarrow} \right).$$

Therefore, $d_{\mathbf{k}}$ and $d^{\dagger}_{\mathbf{k}}$ obey (in terms of the atom operators a):

$$\left[d^{\dagger}_{\mathbf{k}}, d_{\mathbf{k}}\right]_{-} = \frac{1}{2} \left(n_{a_{\mathbf{k}}} + n_{a_{-\mathbf{k}}} - 2 \right), \tag{4.23}$$

where, $a^{\dagger}_{\xi,\uparrow} a_{\xi,\uparrow} + a^{\dagger}_{\xi,\downarrow} a_{\xi,\downarrow} = n_{a_\xi} \in \{0, 1, 2\}$. Next we restrict n_{a_ξ}, such that, $n_{a_{\mathbf{k}}} + n_{a_{-\mathbf{k}}} \in \{0, 4\}$, empty or doubly occupied, in which case the representation in pseudo spins is meaningful [182]. One has for the anti-commutator of the d's,

$$\begin{aligned} \left[d_{\mathbf{k}}, d^{\dagger}_{\mathbf{k}}\right]_{+} &= \frac{1}{2} \left(n_{a_{\mathbf{k}}} + n_{a_{-\mathbf{k}}} - 2 \right) \\ &+ a^{\dagger}_{\mathbf{k},\uparrow} a^{\dagger}_{-\mathbf{k},\downarrow} a_{\mathbf{k},\downarrow} a_{-\mathbf{k},\uparrow} + a^{\dagger}_{-\mathbf{k},\uparrow} a^{\dagger}_{\mathbf{k},\downarrow} a_{-\mathbf{k},\downarrow} a_{\mathbf{k},\uparrow} \\ &- a^{\dagger}_{-\mathbf{k},\downarrow} a_{-\mathbf{k},\downarrow} a^{\dagger}_{\mathbf{k},\uparrow} a_{\mathbf{k},\uparrow} - a^{\dagger}_{-\mathbf{k},\uparrow} a_{-\mathbf{k},\uparrow} a^{\dagger}_{-\mathbf{k},\downarrow} a_{-\mathbf{k},\downarrow}. \end{aligned}$$

In the limit of empty or double occupancy we have,

$$\left[d_{\mathbf{k}}, d^{\dagger}_{\mathbf{k}}\right]_{+} = \mathbb{1}_{\mathbf{k}},$$

where $\mathbb{1}$ is the identity matrix, in this basis, $\mathbb{1}_{\mathbf{k}} = \sum_{\sigma} a^{\dagger}_{\mathbf{k},\sigma} a_{\mathbf{k},\sigma} - \sigma^{z}_{\mathbf{k}}$. Next, using the

[11] Where the volume factor, $1/\sqrt{\mathcal{V}}$ comes from eliminating the sum over $\mathbf{q}$, in the $\tilde{J}$ term.

relationship with the c's we have the following equations from the commutator and anti-commutator of the d's,

$$\begin{aligned} n_{c_{\mathbf{k},\uparrow}} - n_{c_{\mathbf{k},\downarrow}} &= -\sigma^z_{\mathbf{k}}, \\ n_{c_{\mathbf{k},\uparrow}} + n_{c_{\mathbf{k},\downarrow}} - 2n_{c_{\mathbf{k},\downarrow}} n_{c_{\mathbf{k},\uparrow}} &= \mathbb{1}_{\mathbf{k}}, \end{aligned}$$

where the solutions are,

$$n_{c_{\mathbf{k},\uparrow}} = \frac{1}{2}\left(\mathbb{1}_{\mathbf{k}} - \sigma^z_{\mathbf{k}}\right), \quad \text{and} \quad n_{c_{\mathbf{k},\downarrow}} = \frac{1}{2}\left(\mathbb{1}_{\mathbf{k}} + \sigma^z_{\mathbf{k}}\right).$$

Therefore, we have that,

$$\sum_{\mathbf{k},\sigma} \tilde{\epsilon} n_{c_{\mathbf{k},\sigma}} = \sum_{\mathbf{k},\sigma} \tilde{\epsilon} a^\dagger_{\mathbf{k},\sigma} a_{\mathbf{k},\sigma} + \text{constant},$$

for the kinetic energy of the atoms. The term in (4.19) that comes from the carrier-carrier interaction transforms as follows,

$$c^\dagger_{\mathbf{k},\downarrow} c_{\mathbf{q},\downarrow} c^\dagger_{\mathbf{q},\uparrow} c_{\mathbf{k},\uparrow} = -\sigma^-_{\mathbf{k}} \sigma^+_{\mathbf{q}} \approx -d^\dagger_{\mathbf{k}} d_{\mathbf{q}} \to -2a^\dagger_{\mathbf{k},\downarrow} a^\dagger_{-\mathbf{k},\uparrow} a_{-\mathbf{q},\uparrow} a_{\mathbf{q},\downarrow},$$

where we used: $c^\dagger_{\mathbf{k},\downarrow} c_{\mathbf{k},\uparrow} \approx d^\dagger_{\mathbf{k}} \to \sqrt{2} a^\dagger_{\mathbf{k},\downarrow} a^\dagger_{-\mathbf{k},\uparrow}$. Here we can readily identify that a Cooper-pair corresponds to a particle-hole excitation in the impurity picture [see Fig. 4.3]. Alternatively we can perform a canonical transformation and obtain the following correspondence between the c's and the a's,

$$\begin{aligned} c^\dagger_{\mathbf{k},\downarrow} &\to \frac{2^{1/4}}{2}\left(a^\dagger_{-\mathbf{k},\downarrow} + a^\dagger_{\mathbf{k},\uparrow}\right) + \frac{2^{1/4}}{2}\left(a^\dagger_{\mathbf{k},\downarrow} - a^\dagger_{-\mathbf{k},\uparrow}\right), \\ c_{\mathbf{k},\uparrow} &\to \frac{2^{1/4}}{2}\left(a^\dagger_{-\mathbf{k},\downarrow} + a^\dagger_{\mathbf{k},\uparrow}\right) - \frac{2^{1/4}}{2}\left(a^\dagger_{\mathbf{k},\downarrow} - a^\dagger_{-\mathbf{k},\uparrow}\right), \\ c_{\mathbf{k},\downarrow} &\to \frac{2^{1/4}}{2}\left(a_{-\mathbf{k},\downarrow} + a_{\mathbf{k},\uparrow}\right) + \frac{2^{1/4}}{2}\left(a_{\mathbf{k},\downarrow} - a_{-\mathbf{k},\uparrow}\right), \\ c^\dagger_{\mathbf{k},\uparrow} &\to \frac{2^{1/4}}{2}\left(a_{-\mathbf{k},\downarrow} + a_{\mathbf{k},\uparrow}\right) - \frac{2^{1/4}}{2}\left(a_{\mathbf{k},\downarrow} - a_{-\mathbf{k},\uparrow}\right). \end{aligned}$$

With the above, we can write the effective Hamiltonian as follows:

$$\begin{aligned} \tilde{\mathcal{H}}_{\text{eff}} &= \sum_{\mathbf{k},\sigma} \tilde{\epsilon} a^\dagger_{\mathbf{k},\sigma} a_{\mathbf{k},\sigma} + \delta(B) \tilde{b}^\dagger_0 \tilde{b}_0 + \frac{\tilde{J}\sqrt{2}}{\sqrt{\mathcal{V}}} \sum_{\mathbf{k}} \left(\tilde{b}^\dagger_0 a_{\mathbf{k},\uparrow} a_{-\mathbf{k},\downarrow} + a^\dagger_{-\mathbf{k},\downarrow} a^\dagger_{\mathbf{k},\uparrow} \tilde{b}_0\right) \\ &\quad - \frac{2\tilde{\lambda}}{\mathcal{V}} \sum_{\mathbf{q},\mathbf{k}} a^\dagger_{\mathbf{k},\downarrow} a^\dagger_{-\mathbf{k},\uparrow} a_{-\mathbf{q},\uparrow} a_{\mathbf{q},\downarrow}. \end{aligned} \tag{4.24}$$

where, the a's correspond to the fermion atoms and the $\tilde{b}_0$'s to the molecular bound state in the center of mass frame of reference. This is the so called two-channel hybrid model used in the BCS-BEC crossover problem in the limit where we have one bound state as seen from comparison with (4.8). From this correspondence, we can identify, $\tilde{\epsilon} = \epsilon(\mathbf{k}) - \mu$, $\tilde{J}\sqrt{2} = g_0$ and $-2\tilde{\lambda} = \lambda_{\text{bg}}$, with the parameters from the crossover problem: $g_0 = \sqrt{\lambda_{\text{bg}} \Delta\mu \Delta B}$ and $\lambda_{\text{bg}} = 4\pi\hbar^2 a_{\text{bg}}/m$.

At this point, we have established the connection between the AM and the BCS-BEC crossover problem. Since, we can map between the two models in the above limits, we can rewrite the parameters of the AM in terms of $\tilde{J}$ and $\tilde{\lambda}$ from the ultra-cold gas system. To this end we need to solve the following system of equations:

$$\begin{aligned} \frac{\tilde{J}}{\sqrt{\mathcal{V}}} &= Vx(2x^2-1), \\ \frac{\tilde{\lambda}}{\mathcal{V}} &= -Vx^3, \end{aligned} \tag{4.25}$$

where, $x = VA$, and we scaled the coupling coefficients properly, so that the equations are in the units of energy. Close to the Fermi energy, $A \approx 1/\epsilon_f$. We have for the parameters of the equivalent impurity problem,

$$\begin{aligned} V &\approx \frac{g_0^{3/2}}{2^{1/4}\mathcal{V}^{1/4}\sqrt{|\lambda_{\mathrm{bg}}|}} \\ \epsilon_f &\approx -\frac{g_0^2}{|\lambda_{\mathrm{bg}}|} \\ \epsilon &= \bar{\epsilon} - \epsilon_f \end{aligned} \tag{4.26}$$

From our equations it is evident that if one would consider the background interaction to be zero then one would have a divergent hybridisation which would be unphysical, and the identification with a Kondo-like model questionable. Thus including the interaction between atoms fixes this problem. The last parameter to be determined for the AM is the interaction energy of the impurity U. We consider U to be given by the maximum value it can have in terms of the relationship with $\tilde{J}$, from the Kondo limit of the symmetric Anderson model, therefore,

$$U \sim \frac{4V^2\sqrt{\mathcal{V}}}{\tilde{J}} = \frac{2g_0^2}{|\lambda_{\mathrm{bg}}|} = 2|\Delta\mu\Delta B|.$$

From the estimation of ϵ_f and U, we can see that at unitarity the AM is *symmetric*, $\epsilon_f = -U/2$ and as we move to the BCS side the AM becomes *asymmetric*. The results are consistent with Falco and Stoof that obtain the Kondo model at unitarity [181]. Because the hybridisation depends explicitly on the quantization volume $\mathcal{V}$, we estimate it following the same procedure as in [203], we have then,

$$\mathcal{V} = \frac{8\pi}{15}\left(\frac{8\pi\hbar^2|a_{bg}|\rho_0}{m^2\omega^2}\right)^{3/2},$$

where ρ_0 is the peak density and $\omega/2\pi$ is the trapping frequency. The trapping frequency for a fixed Fermi energy depends implicitly on the number of atoms. For typical parameters of ^{6}Li and ^{40}K the estimation of the hybridisation as a perturbation parameter breaks down, because of the dependence on the trapping frequency in the quantization volume. But the proper perturbation parameter is $x = VA$. In order to verify this, we need to consider the full commutator expansion in (4.18). This expansion has been calculated to infinite order by Chan and Gulacsi [200]. The resulting equations for the coupling

parameters when the value of U is large are:

$$\begin{aligned} \frac{\tilde{J}}{\sqrt{\mathcal{V}}} &= -2Vx F(2\sqrt{2}x) \\ \frac{\tilde{\lambda}}{\mathcal{V}} &= 2Vx(F(2\sqrt{2}x) - F(2x)), \end{aligned} \tag{4.27}$$

where,

$$F(x) = \frac{\sin x}{x} + \frac{\cos x - 1}{x^2}.$$

The equations (4.27) reduce to (4.25) when $x \to 0$. Therefore, the proper perturbation parameter is x and the solutions we obtain from taking the first two odd terms in the series in (4.18) hold provided $|x| < 1$. There are infinitely many solutions of (4.27) for V and x for fixed $\tilde{J}$ and $\tilde{\lambda}$, due to the oscillatory nature of $F(x)$. The solution that corresponds to $x < 0$ closest to zero corresponds to the solution from the third order expansion, for small $|x|$. Using experimentally relevant parameters we have verified that the condition for using the third order expansion ($|x| < 1$) is fulfilled with the available data of ^{6}Li and ^{40}K.

In the mapping of the two-channel model to the Anderson model, we can trace back the origin of the the interaction between atoms with different spin projections in the two-channel model to the interplay between V and U. The probability amplitude of hoping V of an effective particle or hole and the difference in energy U between the two projections of the localised energy state of the impurity, generates by means of the canonical transformation the expansion that explicitly exhibits the correlation between the localised energy levels representing the Feshbach boson $f \sim \tilde{b}_0$ and the atoms $c \sim a$. The impurity or molecule induces higher order scattering processes that effectively induce correlations between the atoms in the c representation as in the regular picture of the generation of multi-particle processes of the Anderson model [60].

4.4 Anderson model physics in the crossover

In order to know the regime where the BCS-BEC crossover problem corresponds to the AM, we need to know the hybridisation parameter, $\Gamma = \pi\rho(\epsilon_F^0)V^2$. The hybridisation parameter is the energy width of the impurity level assuming that the density of states that represents the impurity state is a Lorentzian or Cauchy distribution [184]. To estimate the value of Γ, we use the semiclassical approximation of the density of states per particle of a non-interacting Fermi gas in a harmonic potential [204, 205], $\rho(\epsilon) = r\epsilon^2/(\hbar^3\omega^3 N)$, where ω is the angular trap frequency, and the proportionality constant is $r = 1$, which is fixed by the relation:

$$\int_0^{\epsilon_F^0} \rho(\epsilon)\mathrm{d}\epsilon = 1$$

. It follows that: $\epsilon_F^0 = \hbar\omega(3N)^{1/3}$, with N being the number of atoms. Then we have $\rho(\epsilon_F^0) = 3/\epsilon_F^0$. Therefore, the angular trap frequency can be defined as: $\omega = \epsilon_F^0/\hbar(3N)^{1/3}$ and we can parametrize in terms of the number of particles for fixed Fermi energy.

For ^{6}Li, typical experimental values are $\epsilon_F^0 \sim .58\mu$K, $N \sim 10^6 - 10^{10}$ and $\rho_0 \sim 7.6 \times 10^{18}$ m^{-3} with $\lambda_{\mathrm{bg}}/\epsilon_F^0 \sim -13.7\mathcal{V}/N$, and $g_0/\epsilon_F^0 = 7.83\times 10^2\sqrt{\mathcal{V}/N}$. Then we have: $V/\epsilon_F^0 \sim$

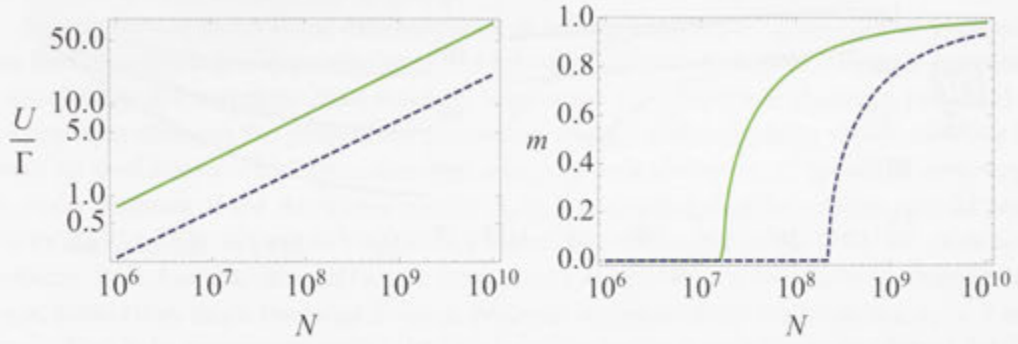

Figure 4.6: The ratio of U and the hybridisation parameter, U/Γ at unitarity, as a function of the number of atoms N (left). The magnetisation m at unitarity as a function of the number of atoms N (right). The solid (green) curves correspond to the parameters of ^{6}Li while the dashes (blue) correspond to ^{40}K, see main text.

$4.9 \times 10^4/N^{1/4}$, and $U/\epsilon_F^0 = 2|\epsilon_f|/\epsilon_F^0 \sim 3.2 \times 10^3$.

In the case of ^{40}K we have $\epsilon_F^0 \sim 2.16\mu$K, $\rho_0 = 3\times10^{19}$ m^{-3}, $\lambda_{\rm bg}/\epsilon_F^0 \sim 4.8\times10^4\mathcal{V}/N$, and $g_0/\epsilon_F^0 = 2.8\times10^3\sqrt{\mathcal{V}/N}$. Then , $V/\epsilon_F^0 \sim 1.8\times10^3/N^{1/4}$, and $U/\epsilon_F^0 = 2|\epsilon_f|/\epsilon_F^0 \sim 8.9\times10^4$.

The regime of the system is controlled by the impurity level ϵ_f and the ratio $U/\Gamma = 4\sqrt{\mathcal{V}}\epsilon_F^0/(3\sqrt{2}\pi g_0)$, as seen in Fig. 4.6. The ratio U/Γ is dependent on the width of the resonance, the background scattering length, and the number of atoms for a fixed Fermi energy. With these parameters and at the unitary limit ($B = B_0$) we can see that the situation corresponds to the *symmetric single impurity Anderson model*. As we move towards the BCS side of the resonance the model becomes *asymmetric*. Depending on these quantities the system will go between being frozen, developing a local moment, in the valence fluctuation, or in the empty impurity regime [184, 188, 197]. The magnitude of the aforementioned quantity suggests that Anderson model physics are very relevant in the BCS-BEC crossover near unitarity, note that in the estimation of parameters we have considered the broad resonances of ^{6}Li and ^{40}K. Because the ratio U/ϵ_F^0 is much larger than one, this length scale dominates the behaviour in the crossover region, and the equivalent Kondo temperature can be very large relative to ϵ_F^0, which is the temperature scale of the system. Therefore different energy length scales are relevant and we are indeed in the region of the Kondo Problem. Because of this, we take the mean-field solution of the AM and use the results that have been extracted from the renormalization group solution and the Bethe ansatz to have a qualitative understanding of the behaviour. The Kondo temperature for the AM is [184]:

$$k_B T_K = U\left(\frac{\Gamma}{2U}\right)^{1/2} \exp\left(\frac{-\pi|\epsilon_f||\epsilon_f + U|}{2U\Gamma}\right) \tag{4.28}$$

Using our equations (4.26) we have that at unitarity as we increase the number of atoms, $k_B T_K$ decreases being the same order of magnitude as ϵ_F^0 for large N [see Fig. 4.7 (left, dashed lines)]. For different particle numbers, as we change the magnetic field in the BCS

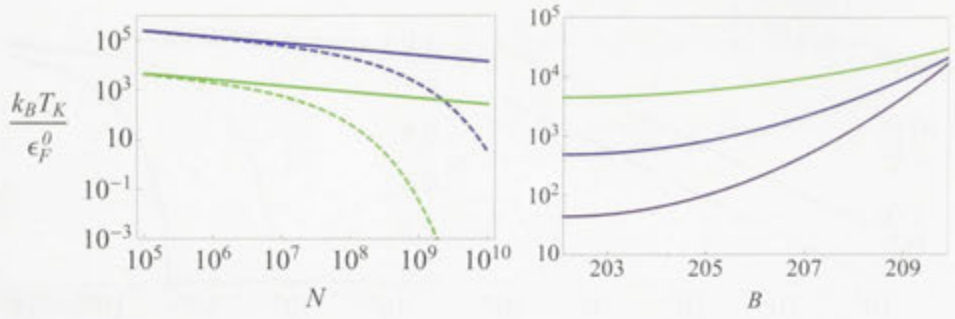

Figure 4.7: The Kondo temperature relative to the Fermi energy. Left Panel: The Kondo temperature as a function of the number of atoms at the resonance (dashes), and when $m = 0$ (solid), where blue corresponds to ^{40}K and green to ^{6}Li. Right Panel: Kondo Temperature for ^{40}K at fixed particle number as a function of the magnetic field on the BCS side of the resonance, $B_0 = 202.1$G. We consider $N = 5 \times 10^8$(purple), 2×10^9(blue), 5×10^9(green).

side of the resonance the Kondo temperature increases having a maximum when one of the impurity levels is at the Fermi level, see Fig. 4.7 (left, solid lines) .

Since the possible regimes depend on both the width of the resonance and the background scattering length, the range of number of particles to observe the crossover between Anderson model regimes would be extended for a narrow resonance, and U/Γ varies in magnitude over a larger scale. The energy difference between the two impurity levels U, is proportional to the width of the resonance. Therefore, the consideration of single occupancy of the impurity is valid for a broad resonance, and in the limit of a narrow resonance we would recover a system with a higher ratio U/Γ, because $U/\Gamma \sim |\Delta\mu\Delta B|^{-1/2}$. In the unitary limit the impurity level $\epsilon_f = -U/2$, while U is large and can be of the same order of magnitude of Γ for experimentally relevant number of atoms $N \sim 10^6 - 10^9$, in the case of ^{6}Li. Therefore, as we move from unitarity to the BCS side with these parameters, the system is moving towards the valence fluctuation regime of the AM, defined as the regime where: $-\epsilon_f \ll \Gamma \ll U$ see [188]. The calculations using mean-field theory suggest this behaviour, as seen from the dependency of the magnetisation m on the number of particles plotted in Fig. 4.6. Clearly the plots show that m increases as a function of the particle number moving to the Kondo regime, towards saturation $m = 1$. As one decreases the number of atoms, Γ increases and the system moves towards the frozen impurity regime, which is equivalent in the symmetric AM to the strong coupling regime [187, 188]. The valence at unitarity is always one independent of the number of particles, because the AM is symmetric.

The AM in the valence fluctuation regime physically corresponds to the situation where depending on the number of atoms, the system evolves from the formation of the FB to having degeneracy between states for free particles (empty impurity) and the molecule (occupied impurity state). This fact is relevant to recent experiments [160, 163, 167, 168], where a contribution of non-condensed pairs has been measured. This suggests that the valence fluctuation mechanism is complementary to other ap-

proaches employed to understand the formation of the so-called "preformed pairs", non-condensed Cooper-pairs, in strongly interacting fermion systems.

As one moves away from the resonance at a fixed number of atoms, the only parameter that changes is the impurity level of each spin, effectively a local chemical potential. If we change the magnetic field from its resonant value, the local chemical potential of the impurity changes the position of the lowest energy of the impurity which can now be either be well below $-U/2$ (negative detuning) or well above $-U/2$ (positive detuning). From the regimes of the Anderson model (4.5), it is implied that the system should saturate in the magnetic regime below the resonance, to correspond to the BCS-BEC crossover problem. Still, here the description in terms of the Anderson model needs to consider the corrections away from the large U limit, because configurations with valence $n_f > 1$ can occur. This is in agreement with what we would expect from our results plotted for the Kondo temperature [see Fig. 4.7]. This implies that the magnetisation is different from zero and maximal, equivalent to have a FB in the system on average at the resonance. In contrast, as one moves to positive detuning the system moves towards to partially magnetic and non-magnetic regimes with the highest impurity level moving towards Fermi level and then well below the Fermi level. This fact signifies that there is less than one FB in the system on average, and the system moves away to the valence fluctuation regime and later to the empty impurity regime [188]. As one would expect, the system is partially magnetic away from the resonance while the magnetisation is maximal at the resonance in the mean-field picture, thus we are in the Kondo limit of the AM at unitarity. Since U/Γ is proportional to $N^{1/2}$, as one decreases the number of atoms one moves away from the Kondo regime of the AM [187, 188] in the BEC side close to unitarity, see Fig. 4.6.

The behaviour of the system in the strongly interacting region of the crossover with the parameters of ^{6}Li and ^{40}K is shown in Fig. 4.8. In order to understand this region we have used the mean-field solution of the Anderson model [62]. Here we show the region where mapping to the AM is valid, which is for the valency: $0 \leq n_f \leq 1$, for the mean-field solution the upper limit is when $B = B_0$. One can see that, as we move towards the BCS side of the crossover, we are equivalently moving across different parameter regimes of the single impurity Anderson model. The formation of the FB is conveniently represented by the magnetisation in the system in mean-field approximation. We can see that in the unitarity limit the occupation of the molecules grows to a saturation value where for fields $B < B_0$ the mapping ceases to be valid. In the BCS side of the resonance the system becomes non-magnetic, reaching the minimum in magnetisation for $B \approx B_0 + |\Delta B|$, here there is no FB on average. The discontinuous change in the slope, in Figs. 4.8, when there is no FB on average in the valence is probably an artefact of the mean-field solution of the Anderson model. One would expect things to be smooth concerning n_f in a more sophisticated solution scheme. On the other hand, we would expect the transition to the magnetic regime qualitatively the same. The limit where the valence in mean-field is one, corresponds to the symmetric Anderson model, because $\epsilon_f = -U/2$, here the system has its maximum magnetisation in mean-field.

Away from unitarity, using the renormalization group results from [187, 188], one can deduce the following facts. For moderate and experimentally relevant particle numbers, $\Gamma \ll U$, starting at unitarity, the system moves from being the symmetric AM to become asymmetric as we move from the resonance. The system moves from the Kondo regime, to the mixed valence regime as we increase the magnetic field. Once there is no FB on

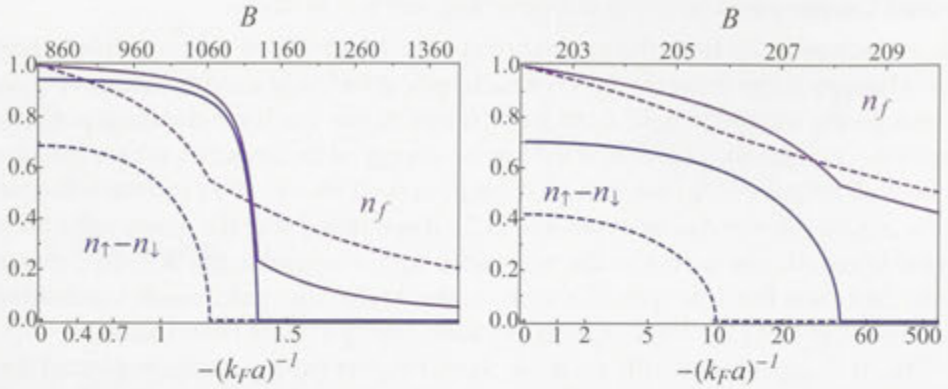

Figure 4.8: The magnetisation equivalent to the average occupation of the molecular state $\langle \tilde{b}_0^\dagger \tilde{b}_0 \rangle = m = n_\uparrow - n_\downarrow$ and the valence $n_f = n_\uparrow + n_\downarrow$ from the mean-field solution of the AM Eq. (4.14) [62]. Left Panel: The behaviour for the parameters of ^{6}Li, with $N = 10^8$ (dashes) and 5×10^8 (solid), $B_0 = 834$G. Right Panel: Results for ^{40}K, we have considered $N = 5 \times 10^8$ (dashes) and 3×10^9 (solid), $B_0 = 202.1$G. Note the limit where $1/k_F a \to -\infty$ for ^{40}K is $B = 209.9$.

average, the highest impurity level starts to move below the Fermi level and then the system starts to move towards the frozen impurity regime. The frozen impurity regime is defined as $n_f = 0$, with the lowest energy level being the one with no impurity. As the impurity energy reaches U above a certain critical energy, the system moves from the frozen impurity regime towards the empty orbital regime. In the empty orbital regime all the impurity configurations have the same probability, thus this is the regime dominated by thermal fluctuations at high temperature. In this region, the mapping between the two-channel model and the AM breaks down because all the configurations for the impurity fillings must be considered, not only $n_f \leq 1$. Same situation happens for fields lower than B_0, where the mean-field solution of the AM would predict a decrease in the magnetisation moving towards the doubly populated impurity limit, $n_f = 2$, thus the model is un-physical. Away from the resonance in the BEC side, the description based on the single impurity breaks down since we expect the number of molecules to grow and ultimately achieve the conversion to a molecular gas. Therefore, depending on the density and temperature the interaction among molecules needs to be taken into account and Bose-Einstein condensation should also be considered. In addition, the mapping to a singly occupied molecular state by means of pseudo-spins is implicitly taken in the mapping by truncating the Hilbert space, and occupation numbers of the impurity larger than one are thus un-physical. However, we think that by including higher spin states, equivalent to additional modes occupied and/or degeneracy some progress could be made, and a degenerate Anderson model [184], lifting the constraint on the Hilbert space should be more adequate to describe the situation, while still being in the dilute limit. Still, to describe the superfluid behaviour seen across the resonance interactions between molecules should be included at some level, i.e see [44, 204].

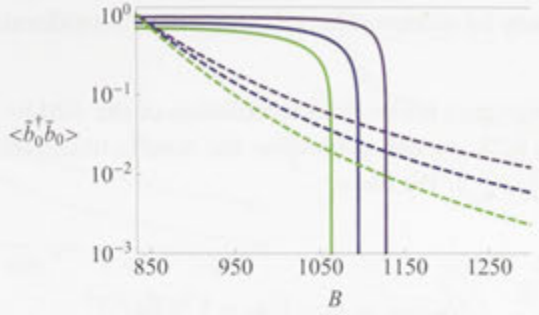

Figure 4.9: The mean occupation of the Feshbach boson $\langle \tilde{b}_0^\dagger \tilde{b}_0 \rangle$ in the BCS side of the Feshbach resonance for ^{6}Li. The solid lines are the solutions using the Anderson model mean-field and the dashes correspond to using the formula (4.29) with Δ from the extended BCS mean-field approach. Parameters are: $N = 5 \times 10^7$(green), 1×10^8(blue), 1×10^9(purple), in (4.29) we have considered: $N_b/N = 1 \times 10^{-6}$(green), 1.2×10^{-6}(blue), 1.4×10^{-6}(purple).

4.4.1 Comparison between single-channel predictions and the Anderson model mapping

We use the relationship given by (4.10), to relate the gap to the occupation of one Feshbach molecule using the solution of (4.5) and (4.6) in the BCS side of the resonance, namely we have,

$$\langle \tilde{b}_0^\dagger \tilde{b}_0 \rangle \approx \frac{\varphi \tilde{\Delta}^2}{N_b}, \tag{4.29}$$

where

$$\varphi = \varphi_0 \left(\frac{\Delta B}{\Delta B + B_0 - B} \right)^2 = \varphi_0 \left(1 - \frac{k_F a_{\rm bg}}{k_F a} \right)^2,$$

with, $\varphi_0 = \epsilon_F^2 \mathcal{V}/(\Delta\mu \Delta B \lambda_{\rm bg})$ and the number of FB's given by N_b. We fix the concentration of of molecules such that $r_b = N_b/N \ll 1$. We can tune the concentration, by fixing it at the unitary limit, to have a qualitative comparison with the solution of one molecule given by the Anderson model, see Fig. 4.9. We find that as we move deeper towards the BCS side of the resonance the solution given by the standard BCS framework predicts always a finite number of molecules that asymptotically approach zero. On the other hand the AM solution predicts, as noted before, a critical field $B = B_c \sim B_0 + |\Delta B|$ for which above the mean occupation of the FB is zero. This discrepancy most likely has to do with the fact that we have used the mean-field solution of the AM in our estimations, and the full renormalization group approach should be used, this requires further investigation.

In order to further compare the results from the AM approach a desirable quantity to know would be the equivalent of the gap. Still, since a single impurity cannot possible open a gap in the many-body system we can analyse what happens to the fermions near the impurity levels and calculate a local "gap" seen only by fermions with energy close to the impurity energy levels. In order to estimate this "gap" we need to calculate $\langle a_{-\mathbf{k},\uparrow} a_{\mathbf{k},\downarrow} \rangle \approx \langle c_{\mathbf{k},\uparrow}^\dagger c_{\mathbf{k},\downarrow} \rangle / \sqrt{2}$. Basically, we need to calculate the expectation value of a spin-flip process of a fermion carrier. In general these process are instantaneous and in

the thermodynamic limit their average should be zero. Still, close to the impurity energy levels some progress may be achieved by relaxing some considerations.

Using the Green's function mean-field calculation of the AM by means of the method of equations of motion [62], we can generalise the results to calculate the corresponding Green's function for $\langle c^\dagger_{\mathbf{k},\uparrow} c_{\mathbf{k},\downarrow}\rangle$. We have,

$$G_{\mathbf{k}\sigma,\mathbf{k}\sigma'} = \delta_{\sigma,\sigma'}\left(G_0 + V^2 G_0^2 G_f^\sigma\right), \tag{4.30}$$

where,

$$G_0 = \frac{1}{\omega - \epsilon(\mathbf{k})}, \qquad G_f^\sigma = \frac{1}{\omega - E_\sigma + i\Gamma},$$

with $E_\sigma = \epsilon_f + U n_{-\sigma}$. Here G_0 is the non-interacting Green's function and $G_f^\sigma \equiv G_{f\sigma,f\sigma}$ corresponds to the energy state σ of the impurity. The Green's function is defined as [206]:

$$G_{\mathbf{k}\sigma,\mathbf{q}\sigma'} = -i\int_{-\infty}^{\infty} dt e^{i(\omega+i\eta)(t-t')}\theta(t-t')\langle\left[c_{\mathbf{k},\sigma}(t), c^\dagger_{\mathbf{q},\sigma'}(t')\right]_+\rangle$$

The problem with (4.30) is that is zero strictly if $\sigma \neq \sigma'$. Still, if we relax the constraint due to the canonical anti-commutation relations and write the following,

$$G_{\mathbf{k}\uparrow,\mathbf{k}\downarrow} = \lim_{\eta\to 0}\eta\left(G_0 + V^2 G_0^2 G_f^\uparrow\right), \tag{4.31}$$

using that,

$$2G_0^2 G_f \approx \frac{\delta(\epsilon(\mathbf{k}) - E_\uparrow)}{\nu\epsilon_F}\left(G_f^\uparrow - G_0 - \nu\epsilon_F G_0^2\right),$$

with $\nu \approx (\epsilon(\mathbf{k}) - E_\uparrow)/\epsilon_F$. We let $\eta \to \nu \to 0$ and we obtain,

$$\langle c^\dagger_{\mathbf{k},\uparrow} c_{\mathbf{k},\downarrow}\rangle = -\frac{1}{\pi}\int_{-\infty}^{\epsilon_F} \mathrm{Im}\left(G_{\mathbf{k}\uparrow,\mathbf{k}\downarrow}\right) d\omega \tag{4.32}$$

$$= \frac{V^2}{\epsilon_F}\left(n_\uparrow - \theta(\epsilon_F - \epsilon(\mathbf{k}))\right)\delta(\epsilon(\mathbf{k}) - E_\uparrow) \tag{4.33}$$

Using the density of states, It follows that,

$$\sum_{\mathbf{k}}\langle c^\dagger_{\mathbf{k},\uparrow} c_{\mathbf{k},\downarrow}\rangle \approx \frac{V^2}{\epsilon_F}\int_{-\infty}^{\infty}\left(n_\uparrow - \theta(\epsilon_F - \epsilon)\right)\delta(\epsilon - E_\uparrow)\rho(\epsilon)d\epsilon \tag{4.34}$$

$$\approx \frac{V^2\rho(\epsilon_F)}{\epsilon_F} n_\uparrow \tag{4.35}$$

we can calculate similarly for $\langle c^\dagger_{\mathbf{k},\downarrow} c_{\mathbf{k},\uparrow}\rangle$. We let,

$$\Delta \approx \frac{V^2|\lambda|}{2\sqrt{2\epsilon_F}\mathcal{V}}\sum_{\mathbf{k}}\left(\langle c^\dagger_{\mathbf{k},\downarrow} c_{\mathbf{k},\uparrow}\rangle + \langle c^\dagger_{\mathbf{k},\uparrow} c_{\mathbf{k},\downarrow}\rangle\right) \tag{4.36}$$

$$\approx \frac{V^2|\lambda|\rho(\epsilon_F)}{2\sqrt{2\epsilon_F}\mathcal{V}}\left(n_\uparrow + n_\downarrow\right), \tag{4.37}$$

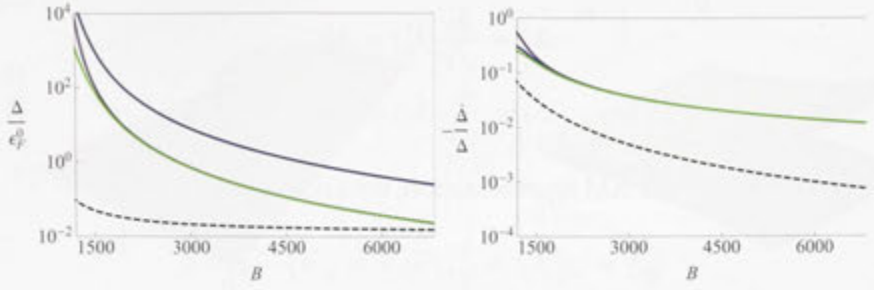

Figure 4.10: The gap Δ/ϵ_F^0 and its logaritmic derivative $-1/\Delta\partial_B\Delta$ for ^{6}Li. Parameters are: $N = 5\times10^7$(green), 1×10^8(blue), 1×10^9(purple) using (4.37) also is shown the solution from the extended BCS mean-field (black, dashes).

In the BCS limit $n_\uparrow = n_\downarrow = n_f/2$ therefore,

$$\frac{\Delta}{\epsilon_F} \propto \frac{|\lambda|}{\mathcal{V}} n_f \rho(\epsilon_F) \to 0,$$

consistent with the extended BCS mean-field result. However, a closer analysis with the parameters of ^{6}Li shows [see Fig. 4.10] that the valence doesn't decrease fast enough as compared to the BCS solution. We can see that as we increase the magnetic field $B > B_0$ the change in the gap decreases, and the gap itself decreases qualitatively with the same behaviour of the of the BCS solution. Still, the qualitative agreement is lost in the case of ^{40}K since we approach the point where the scattering length is zero (what we call a Fermi point) too fast for the valence to have a significant effect. Better agreement should be possible with a better approximation for the dependency of the Feshbach resonance on B deep into the BCS regime for ^{40}K in principle this might be an artefact of the simple form used. Also, the interaction strength for the equivalent "gap" must be properly renormalized since in our simple estimation we have used the divergent expression for the interaction at unitarity, this could be cured by including effects beyond mean-field in the Anderson model. Due to our results, a pausible strategy would be to treat the Feshbach bosons and the Cooper pairs in an independent manner, as we consider in the next section.

4.4.2 Possible origin of the pseudo-gap

Now we move back to the crossover language and use the single impurity solution for a dilute ensemble of FB. We independently determine the contribution from the Cooper pairs and the Feshbach bosons. If we apply the mean-field decoupling scheme to Eq. (4.8), while considering an ensemble of N_b Feshbach bosons in the lowest state such that the interaction in the two channel model is scaled as $\tilde{g}_0 = g_0 N_b$. This is equivalent to N_b single impurity contributions. As a result we will obtain the following Hamiltonian:

$$\mathcal{H}_{\text{eff}} \approx \sum_{\mathbf{k},\sigma} \left(\epsilon(\mathbf{k}) - \mu_a\right) a^\dagger_{\mathbf{k},\sigma} a_{\mathbf{k},\sigma} + + \sum_{\mathbf{k}} \left(\Delta_b^* a_{\mathbf{k},\uparrow} a_{-\mathbf{k},\downarrow} + \Delta_b a^\dagger_{-\mathbf{k},\downarrow} a^\dagger_{\mathbf{k},\uparrow}\right).$$

where,

$$\Delta_b^* = \frac{\tilde{g}_0}{\sqrt{\mathcal{V}}}\langle \tilde{b}_0^\dagger \rangle + \Delta_{\text{BCS}}^*,$$
$$\Delta_b = \frac{\tilde{g}_0}{\sqrt{\mathcal{V}}}\langle \tilde{b}_0 \rangle + \Delta_{\text{BCS}}.$$

On the other hand, from the AM representation, we know that,

$$\langle \tilde{b}_0^\dagger \rangle = \langle f_\downarrow^\dagger f_\uparrow \rangle \approx \frac{1}{2}\sqrt{n_f + m}\sqrt{n_f - m + 2},$$
$$\langle \tilde{b}_0 \rangle = \langle f_\uparrow^\dagger f_\downarrow \rangle \approx \frac{1}{2}\sqrt{n_f - m}\sqrt{n_f + m + 2},$$

where, $m = n_\uparrow - n_\downarrow$, $n_f = n_\uparrow + n_\downarrow$, depend on the interaction strengths of the single impurity problem. Here we are assuming that the molecules are very far apart, and we can define a collection of isotropic sets of molecules and "Fermi seas". In addition,

$$\Delta_{\text{BCS}} = \frac{\lambda}{\mathcal{V}}\sum_{\mathbf{k}}\langle a_{\mathbf{k},\uparrow} a_{-\mathbf{k},\downarrow} \rangle,$$

is the usual BCS gap equation. In this theory we have assumed that the mean occupation of the molecular state is independent of the gap, contrary to the BCS extended mean-field scenario and the regular two channel equivalence of section 4.1, see (4.10). Then, diagonalising the Hamiltonian, we have:

$$\mathcal{H}_{\text{eff}} = \sum_{\mathbf{k},\sigma} E_{\mathbf{k}} \gamma_{\mathbf{k},\sigma}^\dagger \gamma_{\mathbf{k},\sigma} + \text{constant},$$

where the γ's are the Bogoliubov modes and the dispersion relation for the excitations is given by $E_{\mathbf{k}} = \sqrt{(\epsilon(\mathbf{k}) - \mu_b)^2 + |\Delta_b|^2}$. On the BCS side of the resonance, we have:

$$E_{\mathbf{k}} = \sqrt{(\epsilon(\mathbf{k}) - \mu_a)^2 + \frac{g_0 N_b}{\sqrt{\mathcal{V}}}(\langle \tilde{b}_0 \rangle + \langle \tilde{b}_0^\dagger \rangle)\Delta_{\text{BCS}} + \frac{g_0^2 N_b^2}{4\mathcal{V}}\langle \tilde{b}_0^\dagger \rangle \langle \tilde{b}_0 \rangle + \Delta_{\text{BCS}}^2}, \tag{4.38}$$

where, without loss of generality, $\Delta_{\text{BCS}} \in \mathcal{R}$. One can see that if $\Delta_{\text{BCS}} = 0$ (no superfluid, $T > T_c$), there is a pseudo-gap contribution to the excitations given by the valence and the magnetisation so that: $\Delta_{pg}^2 = g_0^2 N_b^2 \sqrt{(n_f^2 - m^2)((n_f + 2)^2 - m^2)}/(4\mathcal{V})$, as the one seen in experiments [167, 168]. From our analisys in the previous sections this contribution can be attributed to valence fluctuations and the average population of the FB. At unitarity, since $n_f = 1$ the pseudo-gap contribution only depends on the average population of the FB, see Fig. 4.11. As we increase the number of atoms N, m saturates to one and the contribution vanishes [see Fig. 4.6 (right)]. Moving away from unitarity the pseudo-gap depends on both the magnetisation and the valence which in general has fluctuations, $n_f \neq$Integer. These results are relevant since in the regular treatment using the single channel model there is no way to obtain a contribution for the pseudo gap, because the molecules vanish as the Cooper pairs disappear and the usual BCS gap is zero.

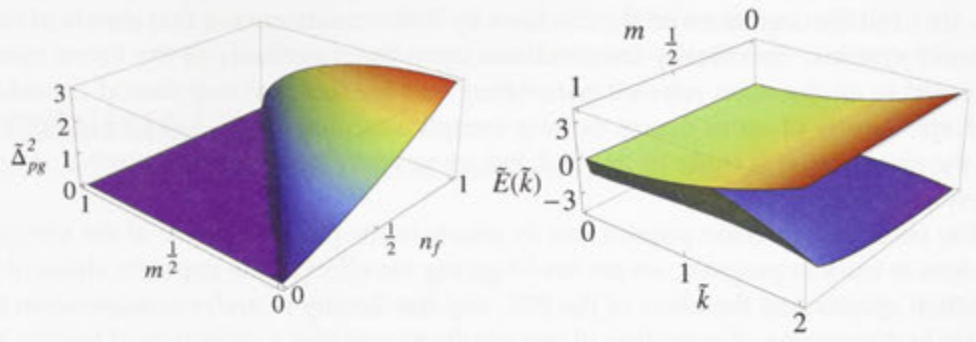

Figure 4.11: Left: The pseudo gap contribution to the dispersion relation $\tilde{\Delta}_{pg} = \mathrm{Re}(\Delta_{pg})4\mathcal{V}/(g_0^2 N_b^2)$. Right: The scaled dispersion relation $\tilde{E}(\tilde{k}) = (\mu_a \pm E(\tilde{k}))/\epsilon_F^0$ for non-interacting fermions (upper branch) and the strongly interacting fermions at unitarity (lower branch) as a function of the magnetisation equivalent to the average occupation of the molecular state $\langle \tilde{b}_0^\dagger \tilde{b}_0 \rangle = m = n_\uparrow - n_\downarrow$ and the scaled momentum $\tilde{k} = k/k_F$. Parameters are: $g_0^2 N_b^2/(4\mathcal{V}) = 10$, $\mu_a/\epsilon_F^0 = 1.5$, and $n_f = 1$.

4.5 Outstanding problems

The remaining question is how do the valence and the magnetisation change as a function of temperature, so far the calculations were performed at $T = 0$. From what we know about the AM, one would expect that the valence and the magnetisation start to drop significantly at a temperature, $T^* = E^*/k_B$ not necessarily T_c. This should depend on the effective energy level of the impurity closest to the Fermi level [184]. From our results at unitarity in mean-field approximation of the AM [see Fig. 4.6], we can see that the magnetisation is strongly dependent on the number of atoms or, alternatively the Fermi energy. As one increases the particle number the magnetisation increases, the while as we move the effective energy level of the impurity, the magnetisation and the valence are suppressed. These processes being opposites suggest that there should be a regime where they compensate each other. This regime would probably represent the boundary for the suppression of the magnetisation and the valence. It seems that one would need to go beyond the large U limit that we have considered (where the mapping is valid) and consider the effect of additional terms from the Schrieffer-Wolff transformation [194, 200] (4.18) to determine the relationship with effective parameters of the crossover considering excitations and part of the spectrum.

On the other hand, the single impurity picture should become less reliable as one increases the density or moves towards the BEC side, since we would expect the FB's to interact with each other. Therefore, it is possible that the situation could be pictured in a more realistic manner in terms of the *periodic Anderson model* (PAM) [207, 208], where more than one impurity is considered and there is interaction among them. This model has been shown to have a non-Fermi liquid ground state for certain parameter regimes [209]. This is relevant since in strongly interacting Fermi systems, like the one under consideration, the normal state might not be a Fermi liquid [19]. For moderate particle numbers, where the single impurity picture should be reliable, one would hope to be

able to use AM and all the results from the exact solution by Tsvelick and Wiegmann [185, 186], but the conditions on the solutions by Bethe ansatz are not that simple in these ultracold systems. Specifically the condition upon the magnitude of the Fermi energy compared to all the other relevant parameters and the fact that one should consider a quadratic density of states due to the trap complicates matters. Thus, one would hope that the usual methods could be applied, but up to which point requires further investigation on its own.

The study of Anderson physics and its effects in the phase diagram of the ultracold fermions is work in progress, we are investigating the effect of the impurity states in the excitation spectra and the effect of the BEC and the density is under consideration too. We are in the process of extending of our results to consider a collection of bosons and the BEC, instead of one molecule, along the lines of what has been done in the study of mixed valence compounds [207, 210] with the proper modifications.

4.6 Summary of results

In our work on this topic we have managed to address the possibility of using an alternative fermionic formulation to the single channel model of the BCS-BEC crossover problem having a well defined Hamiltonian theory near the unitary limit that can be treated exactly in some limits. Our work extends the application of the mapping of the two-channel model to the Kondo model in the unitary limit in the limit of one molecule, using the Anderson model to move towards the BCS side of the Feshbach resonance. We have achieved a way to describe the formation of a Feshbach boson and at the level of mean-field theory, interpret the effect of pre-formed pairs as a consequence of valence fluctuations in the equivalent impurity picture of the Anderson model. Finally using the AM we were able to give a possible interpretation to the emergence of the pseudo gap in the BCS-side of the resonance at the Hamiltonian level, in the limit that the molecules could be considered non-interacting, for small molecule numbers in a single mode.

Chapter 5

Conclusions

As described in the Introduction, the purpose of this thesis has been to study effects of many-body interactions on the formation and behaviour of localised states in ultracold atomic systems. We have analysed systems where atomic interactions and localisation effects play a fundamental role in the macroscopic behaviour of ultracold atoms. The study of the model systems presented in this thesis is motivated by possible applications. First, the control of interaction effects in the behaviour of collective states suggests the possibility to employ these states in quantum computing [32] and atomtronics [38–40, 211]. Secondly, the study of ultracold systems can be used to explain analogous behaviour in solid state systems. Third, the possibility to manipulate interactions and use their effect in applications of interferometry and metrology [64, 212]. We now summarise the major results of this thesis and provide an outlook for future possible directions of research on the basis of these results.

To address the question regarding the effects of the many-body interaction beyond the mean-field approximation in the transition from delocalised to localised states in a Bose-Josephson junction, we performed the direct diagonalization of the Bose-Hubbard model in the two mode approximation in the limit of large number of atoms in Chapter 2. We found that the nonlinear interaction between atoms induces the relaxation to stationary states. The property of stationarity was found by analysing behaviour of the populations and the transition from delocalised to self-trapped states in a symmetric double-well potential in the basis of energy eigenstates. In relation with the relaxation to stationary states we found the preferred basis of the system, depending of the interaction, and its relation with the emergence of decoherence in the one-body reduced density matrix.

The next system we have analysed in Chapter 2, was the BEC inside a high finesse cavity. In this system atoms of different angular momentum of hyperfine states couple to the lowest photon mode inside the cavity. We analysed the system in the limit where the ground state energy has negligible change as the number of photons is increased. We worked in a truncated Hilbert space, where we constructed the ground state phase diagram. From the ground state phase diagram it appears that the transition to the super-radiant state in the absence of interaction between atoms for strong interaction between photons and atoms can be identified with a localised to delocalised transition, thus giving an alternative point of view to the quantum phase transition of the Dicke model [57]. We found that, as the interaction between atoms increases, the system is in a crossover from the super-radiant state to a state where as a function of the energy shows quantisation of the population of the atoms, and suppression of quantum fluctuations. A surprising finding was that, in the limit of strong atom-photon interaction, the system shows a different

kind of quantisation, this time in the fluctuations of the population and the fluctuations of the tunnelling correlations. We found that, in general, the interaction with the photon field enhances quantum fluctuations inducing transitions of the atoms from the localised to the delocalised regimes.

Moving from purely bosonic systems, in Chapter 3 we have considered Bose-Fermi mixtures. First, we considered the effect of fermions on the macroscopic quantum self-trapping (MQST) phenomenon. We considered experimentally relevant values of parameters for the ^{87}Rb-^{40}K mixture using mean-field approximation for the equations of motion of the system. We found that, depending on the nature of the inter-species interaction, MQST occurs for smaller separations between the double-well minima for attraction and the opposite for repulsion. We found agreement between our variational calculations and the numerical solution of the evolution of the wave function for the BEC localised in one of the wells. The onset of MQST is affected by the fermions in the system because the interactions narrow and widen the wave function of the BEC for attraction and repulsion, respectively. The expected experimental signal of the effect due to fermions was obtained where one can clearly discriminate between both the enhancement and suppression of the MQST regime.

In the second part of Chapter 3, we considered a Bose-Fermi mixture in a three-site ring configuration. We considered a system in the limit of small number of atoms of each species where the fermion filling was equal or less than one. We constructed the ground state phase diagram of the system depending on the intra- and inter-species interaction between atoms by directly diagonalising the Bose-Fermi-Hubbard model. The system is particle-hole symmetric in the fermion filling, such that $1/3$ filling for inter-species attraction corresponds to $2/3$ filling for inter-species repulsion and vice-versa. The ground state phase diagram is strongly dependent on the inter-species interaction that promotes configurations with in-homogenous states. Besides from the states with the regular Mott-Insulator symmetry of the pure Bose system, we found new insulating states characterised by in-homogenous configurations of bosons and strong quantum fluctuations.

The third part of Chapter 3 was devoted to the study of a simplified model with the necessary ingredients of a topological insulator. We considered a system with four sites, two three-site rings with interacting bosons and fermions and a position dependent hopping depending on an artificial vector potential. This vector potential breaks the particle-hole symmetry between fermion fillings and changes the structure of the ground state phase diagram. As a consequence of this symmetry breaking, an additional region with insulating characteristics appears in the case of inter-species attraction for $3/4$ filling of fermions. On the other hand, for $1/4$ filling of fermions in the case of inter-species repulsion, a region appears with the superfluid component of the system being enhanced. These regions in the phase diagram are characterised by enhanced quantum fluctuations.

In Chapter 4, we considered a strongly interacting Fermi system. We studied the BCS-BEC crossover and its relation to magnetic impurity models. We found the equivalent representation of the problem in terms of localised energy states and particle-hole excitations for the Feshbach bosons and the Cooper-pairs respectively. We were able to map the two-channel model of the BCS-BEC crossover to the single impurity Anderson model. We used the results of the mapping to extend the impurity model equivalency to the Kondo model beyond the unitary limit into the BCS-side of the Feshbach resonance

where the Anderson model holds. We analysed the formation of the Feshbach bosons, equivalent to the magnetisation in the system, as a function of the magnetic detuning with respect to the Feshbach resonance. We considered experimentally relevant parameters of ^{6}Li and ^{40}K. We found that a pseudo-gap forms depending on the number of the Feshbach bosons in the system and the valence fluctuations of the equivalent magnetic impurity picture. Finally, we identified the parameter regimes of the Anderson model in the BCS-BEC crossover.

In this thesis new major results can be summarised as follows:

- The establishment of the relation between stationary states and decoherence originated from many-body interactions in double well bosonic systems.
- The suppression or enhancement of localisation related phenomena (Superfluid and Mott-Insulator states or Macroscopic Quantum Self-trapping) in Bose-Fermi mixtures due to the presence of fermions and the interplay with many-body interactions in few site systems.
- The mapping of the BCS-BEC crossover problem to a magnetic impurity problem in the BCS side of a Feshbach resonance, and the possible origin of the pseudo gap in strongly interacting ultracold fermion systems.

In all these systems the emergence of quantum fluctuations has profound consequences in the ground state configurations and the role of localised states. The properties of delocalised states of the BEC in the double-well potential and the control of the nonlinear interaction can be used for interferometry using BEC's [212–215]. Recently, a nonlinear atom interferometer surpassed the classical precision limit [212]. Our results connected with the relaxation to stationary states could be used to interpret the results seen in recent experiments in the dynamics of tuneable superfluid junctions in atom chips [216].

The new insulating states found in few-atom systems, such as the three-site ring, could be used for quantum information processing, since they are protected by an energy gap and different state configurations can be created depending on the interactions. It remains to be seen up to how resilient these states are to decoherence. The natural extension of these systems is to consider more sites and other geometries where might be possible to generate circuits with new properties. These systems could also be used to study quantum magnetism [217–219] where, in the strongly interacting regime, the spins of the atoms have effective interactions that can give rise to frustrated configurations. Our simplified model of a topological insulator can be used as a basis to understand more complicated geometries and investigate the role of interaction in the configurations of the system and its relation to topological invariants [155].

The new approach that we have suggested for the treatment of the BCS-BEC crossover problem can be used to construct models taking into account the interaction between Feshbach bosons and the possible role these might have in the formation of non-Fermi liquid ground states in strongly interacting Fermi systems. We have found a well defined Hamiltonian representation to describe the BCS crossover where we can identify effective degrees of freedom that induce correlations in the ground state due to the many-body interaction. The techniques used for the study of this system could be applied to other systems of ultracold gases in optical lattices, such as the Bose-Fermi mixture in the

super-solid state [220] or Fermi-Fermi mixtures, providing alternative means to find the properties of the ground state and the effect of interactions in the spectrum of excitations.

Finally, the BEC in a cavity [85] and Bose-Fermi mixtures in optical lattices [220–222] are systems where super-solid behaviour is currently being investigated. The investigation of the properties of this phase and the interplay with other quantum phenomena has just started to attract the attention of the researchers, therefore new experimental and theoretical developments are on their way.

Variational solution of coupling parameters for a Bose-Fermi mixture

The dynamics of the system (3.9) and the population imbalance characterizing a self-trapped state (3.10) are determined by the interaction dependent coupling parameters, C_j, C_{01}, and the mode energies, μ_j. To compute them, we use the variational method with the trial function given by Eq. (3.11). The mode energies are found from the following functional:

$$\mu_j = -\frac{2}{n_j} \max \left[\int_{\mathbb{R}} \mathrm{d}x \, \mathcal{L}[\Phi_j] \Big|_{\mu_j=0} \right], \tag{A.1}$$

where the Lagrangian density $\mathcal{L}[\Phi_j]$ corresponding to the equations of motion (3.7) for each nonlinear mode can be separated in three parts: $\mathcal{L} = \mathcal{L}_k + \mathcal{L}_b + \mathcal{L}_f$, The kinetic energy contribution ($\mathcal{L}_k$), the bosonic ($\mathcal{L}_b$) and the fermionic ($\mathcal{L}_f$) mean field contributions are:

$$\begin{aligned} \mathcal{L}_k &= -\frac{1}{2}\left(\frac{\mathrm{d}\Phi}{\mathrm{d}x}\right)^2, \\ \mathcal{L}_b &= \frac{1}{2}\left(\mu - (|x| - x_0)^2\right)\Phi^2 - \frac{\sigma}{4}\Phi^4, \\ \mathcal{L}_f &= -\frac{u_1}{2}\rho_f(x)\Phi^2. \end{aligned}$$

With the trial function (3.11), and the fermionic density $\rho_f(x)$ is extracted from the numerical computations, all the components of the Lagrangian density except from $\mathcal{L}_f$, can be calculated analytically:

$$\int_{\mathbb{R}} \mathrm{d}x \, \mathcal{L}_k[\Phi_{0,1}] = \pm \frac{A_{0,1}^2 \sqrt{\pi}}{2a_{0,1}^3} \left(\left(2x_0^2 - a_{0,1}^2\right) w_{0,1} \mp a_{0,1}^2 \right),$$

$$\int_{\mathbb{R}} \mathrm{d}x\ \mathcal{L}_b[\Phi_0] = \mu_0 a_0 A_0^2 \sqrt{\pi}\,(1+w_0) \tag{A.2}$$

$$+ \frac{\sigma a_0 A_0^4 \sqrt{\pi}}{2\sqrt{2}} \left(1 + 3w_0^2 + 4w_0^{3/2}\right) \tag{A.3}$$

$$+ \frac{a_0 A_0^2 \sqrt{\pi}}{2} \left(4x_0^2 \mathrm{erf}\left(\frac{x_0}{a_0}\right) - a_0^2 - 4x_0^2 \right. \tag{A.4}$$

$$\left. - \left(a_0^2 + 2x_0^2\right) w_0 + \frac{8x_0 a_0}{\sqrt{\pi}} w_0 \right), \tag{A.5}$$

$$\int_{\mathbb{R}} \mathrm{d}x\ \mathcal{L}_b[\Phi_1] = \mu_1 a_1 A_1^2 \sqrt{\pi}\,(1-w_1) \tag{A.6}$$

$$+ \frac{\sigma a_1 A_1^4 \sqrt{\pi}}{2\sqrt{2}} \left(1 + 3w_1^2 - 4w_1^{3/2}\right) \tag{A.7}$$

$$+ \frac{a_1 A_1^2 \sqrt{\pi}}{2} \left(4x_0^2 \mathrm{erf}\left(\frac{x_0}{a_1}\right) - a_1^2 - 4x_0^2 \right. \tag{A.8}$$

$$\left. + \left(a_1^2 + 2x_0^2\right) w_1 \right), \tag{A.9}$$

where, $w_{0,1} = \exp(-x_0^2/a_{0,1}^2)$, and the square amplitudes, $A_{0,1}^2 = n_{0,1}/(2a_{0,1}\sqrt{\pi}(1 \pm w_{0,1}))$. The coupling coefficients C_0, C_1, and C_{01} can now be computed explicitly as a function of the widths a_0 and a_1:

$$C_0 = \frac{1 + 3w_0^2 + 4w_0^{3/2}}{2\sqrt{2\pi} a_0 \left(1 + w_0\right)^2}, \tag{A.10}$$

$$C_1 = \frac{1 + 3w_1^2 - 4w_1^{3/2}}{2\sqrt{2\pi} a_1 \left(1 - w_1\right)^2}, \tag{A.11}$$

$$C_{01} = \frac{q w_0^{-\gamma_1} w_1^{-\gamma_0} + w_0^{-1} w_1^{-1} - 2\left(w_0^{-\gamma_1} - w_1^{-\gamma_0} + 1\right)}{2\sqrt{\pi\left(a_0^2 + a_1^2\right)}\left(w_0^{-1} + 1\right)\left(w_1^{-1} - 1\right)} \tag{A.12}$$

where, $\gamma_{0,1} = a_{0,1}^2/(a_0^2 + a_1^2)$ and $q = \exp(-2x_0^2/(a_0^2 + a_1^2))$. The computation of all quantities follows from numerically minimizing the functional (A.1) with all numerical constants fixed, and $a_{0,1}$ as variational parameters. In the limit of $r_{fb} \to 0$ our variational results are consistent with the numerical results for the pure BEC system presented in [56].

Canonical transformations

B.1 The Schrieffer-Wolf transformation to first order

Let the single impurity Anderson (AM) be,

$$\mathcal{H}_{\mathrm{AM}} = \mathcal{H}_0 + \mathcal{H}_V,$$

where,

$$\begin{aligned} \mathcal{H}_0 &= \sum_{\mathbf{k},\sigma} \epsilon_{\mathbf{k}} n_{c_{\mathbf{k},\sigma}} + \epsilon_f \sum_{\sigma} n_{f_\sigma} + \frac{U}{2} \sum_{\sigma} n_{f_\sigma} n_{f_{-\sigma}}, \\ \mathcal{H}_V &= \sum_{\mathbf{k},\sigma} V_{\mathbf{k}} \left(f_\sigma^\dagger c_{\mathbf{k},\sigma} + c_{\mathbf{k},\sigma}^\dagger f_\sigma \right), \end{aligned}$$

with the number operators, $n_{f_\sigma} = f_\sigma^\dagger f_\sigma$ and $n_{c_{\mathbf{k},\sigma}} = c_{\mathbf{k},\sigma}^\dagger c_{\mathbf{k},\sigma}$. The sub-indices k's denote momenta and σ's spin projection. The onsite repulsion is given by U, the hybrization between the conduction electrons and the impurity is V and the energy of the impurity is given by ϵ_f. I perform a canonical transformation,

$$\tilde{\mathcal{H}} = \mathrm{e}^{\mathcal{S}} \mathcal{H} \mathrm{e}^{-\mathcal{S}}, \tag{B.1}$$

the cannonical transformation acts like a rotation over the Hilbert space, where,

$$\mathcal{S} = \sum_{\mathbf{k},\sigma} V_{\mathbf{k}} \left(A_{\mathbf{k}} + Z_{\mathbf{k}} n_{f_{-\sigma}} \right) \left(f_\sigma^\dagger c_{\mathbf{k},\sigma} - c_{\mathbf{k},\sigma}^\dagger f_\sigma \right),$$

where the $A_{\mathbf{k}}$ and $Z_{\mathbf{k}}$ are determined depending on the the perturbation parameter of the model. The canonical transformation (B.1), is equivalent to applying perturbation theory for V. This reads,

$$\tilde{\mathcal{H}} = \mathcal{H}_0 + \frac{1}{2}\left[\mathcal{S}, \mathcal{H}_V\right]_- + \frac{1}{3}\left[\mathcal{S}, \left[\mathcal{S}, \mathcal{H}_V\right]_-\right]_- + \frac{1}{8}\left[\mathcal{S}, \left[\mathcal{S}, \left[\mathcal{S}, \mathcal{H}_V\right]_-\right]_-\right]_- + \cdots \tag{B.2}$$

with the condition to remove[1] $\mathcal{H}_V$ from the expansion of $\mathcal{H}$,

$$\mathcal{H}_V - \left[\mathcal{H}_0, \mathcal{S}\right]_- = 0. \tag{B.3}$$

[1] I use the convention, $\left[A, B\right]_\pm = AB \pm BA$

I have:

$$\begin{aligned}\left[\mathcal{H}_0,\mathcal{S}\right]_- &= -\sum_{\mathbf{k},\mathbf{q},\sigma,\gamma} V_{\mathbf{q}}\left(A_{\mathbf{k}}+Z_{\mathbf{k}}n_{f_{-\sigma}}\right)\left[\left(f_\sigma^\dagger c_{\mathbf{k},\sigma}-c_{\mathbf{k},\sigma}^\dagger f_\sigma\right),H_0\right]_- \\ &- \sum_{\mathbf{k},\mathbf{q},\sigma,\gamma} V_{\mathbf{q}}Z_{\mathbf{k}}\left[n_{f_{-\sigma}},H_0\right]_-\left(f_\sigma^\dagger c_{\mathbf{k},\sigma}-c_{\mathbf{k},\sigma}^\dagger f_\sigma\right), \qquad \text{(B.4)}\end{aligned}$$

with,

$$H_0=\epsilon_{\mathbf{q}}n_{c_{\mathbf{q},\gamma}}+\epsilon_f n_{f_\gamma}+\frac{U}{2}n_{f_\gamma}n_{f_{-\gamma}},$$

and I have used the convention that if there is no explicit dependence of an index in the elements of the sum, the sum for that index is discarded. Since,

$$\left[n_{f_{-\sigma}},\mathcal{H}_0\right]_-=0,$$

because,

$$\left[n_{f_\sigma},n_{f_\gamma}\right]_-=\left[n_{c_{\mathbf{k},\sigma}},n_{f_\gamma}\right]_-=\left[n_{c_{\mathbf{k},\sigma}},n_{c_{\mathbf{q},\gamma}}\right]_-=0.$$

The requirement on the commutation of the number operators imply that for c and f,

$$\left[c^\dagger,f^\dagger\right]_+=\left[c,f\right]_+=\left[c^\dagger,f\right]_+=\left[f^\dagger,c\right]_+=0,$$

while, the following commutator algebra gives exactly the same answer in all the computations of the first order regarding the elimination of the hybridiazation, and the commutation of number operators,

$$\left[c^\dagger,f^\dagger\right]_-=\left[c,f\right]_-=\left[c^\dagger,f\right]_-=\left[f^\dagger,c\right]_-=0.$$

Still the final result regarding the ordering of operators and the form in first order expansion depends on this choice we will denote by $\kappa=\pm1$ corresponding to either choice in the final answer. I employed the following identities:

$$\begin{aligned}\left[A,BC\right]_- &= \left[A,B\right]_\pm C-B\left[C,A\right]_\pm \\ \left[AB,CD\right]_- &= A\left[B,C\right]_\pm D-\left[C,A\right]_\pm BD+CA\left[B,D\right]_\pm-C\left[D,A\right]_\pm B\end{aligned}$$

It follows that the second term in (B.4) is identically zero. The commutator in the first term of (B.4) gives:

$$\begin{aligned}\left[\left(f_\sigma^\dagger c_{\mathbf{k},\sigma}-c_{\mathbf{k},\sigma}^\dagger f_\sigma\right),H_0\right]_- &= \delta_{\sigma,\gamma}\delta_{\mathbf{k},\mathbf{q}}\epsilon_{\mathbf{q}}\left(f_\sigma^\dagger c_{\mathbf{q},\gamma}+c_{\mathbf{q},\gamma}^\dagger f_\sigma\right) \\ &- \delta_{\sigma,\gamma}\epsilon_f\left(f_\gamma^\dagger c_{\mathbf{k},\sigma}+c_{\mathbf{k},\sigma}^\dagger f_\gamma\right) \\ &- Un_{f_{-\sigma}}\left(f_\sigma^\dagger c_{\mathbf{k},\sigma}+c_{\mathbf{k},\sigma}^\dagger f_\sigma\right).\end{aligned}$$

I used the following results:

$$\begin{aligned}
\left[f_\sigma^\dagger c_{\mathbf{k},\sigma}, n_{c_{\mathbf{q},\gamma}}\right]_- &= f_\sigma^\dagger \left[c_{\mathbf{k},\sigma}, n_{c_{\mathbf{q},\gamma}}\right]_- = \delta_{\sigma,\gamma}\delta_{\mathbf{k},\mathbf{q}} f_\sigma^\dagger c_{\mathbf{q},\gamma}, \\
\left[c_{\mathbf{k},\sigma}^\dagger f_\sigma, n_{c_{\mathbf{q},\gamma}}\right]_- &= \left[c_{\mathbf{k},\sigma}^\dagger, n_{c_{\mathbf{q},\gamma}}\right]_- f_\sigma = -\delta_{\sigma,\gamma}\delta_{\mathbf{k},\mathbf{q}} c_{\mathbf{q},\gamma}^\dagger f_\sigma, \\
\left[f_\sigma^\dagger c_{\mathbf{k},\sigma}, n_{f_\gamma}\right]_- &= \left[f_\sigma^\dagger, n_{f_\gamma}\right]_- c_{\mathbf{k},\sigma} = -\delta_{\sigma,\gamma} f_\gamma^\dagger c_{\mathbf{k},\sigma}, \\
\left[c_{\mathbf{k},\sigma}^\dagger f_\sigma, n_{f_\gamma}\right]_- &= c_{\mathbf{k},\sigma}^\dagger \left[f_\sigma, n_{f_\gamma}\right]_- = \delta_{\sigma,\gamma} c_{\mathbf{k},\sigma}^\dagger f_\gamma,
\end{aligned}$$

and the usual anti-commutation relations for fermions of the same kind, c or f, using the Kronecker deltas in the corresponding summations, I then have for (B.4),

$$\left[\mathcal{H}_0, \mathcal{S}\right]_- = -\sum_{\mathbf{k},\sigma} V_\mathbf{k} \left(A_\mathbf{k} + Z_\mathbf{k} n_{f_{-\sigma}}\right) \left(\epsilon_\mathbf{k} - \epsilon_f - U n_{f_{-\sigma}}\right) \left(f_\sigma^\dagger c_{\mathbf{k},\sigma} + c_{\mathbf{k},\sigma}^\dagger f_\sigma\right).$$

From the condition (B.3), I have the following set of equations:

$$\begin{aligned}
A_\mathbf{k} \left(\epsilon_\mathbf{k} - \epsilon_f\right) + 1 &= 0, \\
-(A_\mathbf{k} + Z_\mathbf{k})U + \left(\epsilon_\mathbf{k} - \epsilon_f\right) Z_\mathbf{k} &= 0,
\end{aligned}$$

where, I have used that for fermions, $n_\xi^2 = n_\xi$. The solutions for the coefficients of $\mathcal{S}$ can be written as:

$$\begin{aligned}
A_\mathbf{k} &= -\frac{1}{\epsilon_\mathbf{k} - \epsilon_f}, \\
Z_\mathbf{k} &= -\frac{U}{\left(\epsilon_\mathbf{k} - \epsilon_f\right)\left(\epsilon_\mathbf{k} - \epsilon_f - U\right)} = -\frac{1}{\epsilon_\mathbf{k} - \epsilon_f - U} - A_\mathbf{k},
\end{aligned} \tag{B.5}$$

fullfiling the condition for $\mathcal{S}$ to be dimensionless. It follows to compute for first order,

$$\begin{aligned}
\left[\mathcal{S}, \mathcal{H}_V\right]_- &= \sum_{\mathbf{k},\mathbf{q},\sigma,\gamma} V_\mathbf{q} V_\mathbf{k} \left(A_\mathbf{k} + Z_\mathbf{k} n_{f_{-\sigma}}\right) \left[f_\sigma^\dagger c_{\mathbf{k},\sigma} - c_{\mathbf{k},\sigma}^\dagger f_\sigma, f_\gamma^\dagger c_{\mathbf{q},\gamma} + c_{\mathbf{q},\gamma}^\dagger f_\gamma\right]_- \\
&+ \sum_{\mathbf{k},\mathbf{q},\sigma,\gamma} V_\mathbf{q} V_\mathbf{k} Z_\mathbf{k} \left[n_{f_{-\sigma}}, f_\gamma^\dagger c_{\mathbf{q},\gamma} + c_{\mathbf{q},\gamma}^\dagger f_\gamma\right]_- \left(f_\sigma^\dagger c_{\mathbf{k},\sigma} - c_{\mathbf{k},\sigma}^\dagger f_\sigma\right).
\end{aligned} \tag{B.6}$$

The commutators needed are:

$$\begin{aligned}
\left[f_\sigma^\dagger c_{\mathbf{k},\sigma} - c_{\mathbf{k},\sigma}^\dagger f_\sigma, f_\gamma^\dagger c_{\mathbf{q},\gamma} + c_{\mathbf{q},\gamma}^\dagger f_\gamma\right]_- &= \delta_{\sigma,\gamma} \left(\delta_{\mathbf{k},\mathbf{q}} \left(f_\sigma^\dagger f_\gamma + f_\gamma^\dagger f_\sigma\right) - \left(c_{\mathbf{q},\gamma}^\dagger c_{\mathbf{k},\sigma} + c_{\mathbf{k},\sigma}^\dagger c_{\mathbf{q},\gamma}\right)\right), \\
\left[n_{f_{-\sigma}}, f_\gamma^\dagger c_{\mathbf{q},\gamma} + c_{\mathbf{q},\gamma}^\dagger f_\sigma\right]_- &= \delta_{-\sigma,\gamma} \left(f_{-\sigma}^\dagger c_{\mathbf{q},\gamma} - c_{\mathbf{q},\gamma}^\dagger f_{-\sigma}\right),
\end{aligned}$$

where, I have used the following computations:

$$
\begin{aligned}
\left[f_\sigma^\dagger c_{\mathbf{k},\sigma}, f_\gamma^\dagger c_{\mathbf{q},\gamma}\right]_- &= 0, \\
\left[c_{\mathbf{k},\sigma}^\dagger f_\sigma, c_{\mathbf{q},\gamma}^\dagger f_\gamma\right]_- &= 0, \\
\left[f_\sigma^\dagger c_{\mathbf{k},\sigma}, c_{\mathbf{q},\gamma}^\dagger f_\gamma\right]_- &= f_\sigma^\dagger \left[c_{\mathbf{k},\sigma}, c_{\mathbf{q},\gamma}^\dagger\right]_+ f_\gamma - c_{\mathbf{q},\gamma}^\dagger \left[f_\gamma, f_\sigma^\dagger\right]_+ c_{\mathbf{k},\sigma} = \delta_{\sigma,\gamma}\left(\delta_{\mathbf{k},\mathbf{q}} f_\sigma^\dagger f_\gamma - c_{\mathbf{q},\gamma}^\dagger c_{\mathbf{k},\sigma}\right), \\
\left[c_{\mathbf{k},\sigma}^\dagger f_\sigma, f_\gamma^\dagger c_{\mathbf{q},\gamma}\right]_- &= c_{\mathbf{k},\sigma}^\dagger \left[f_\sigma, f_\gamma^\dagger\right]_+ c_{\mathbf{q},\gamma} - f_\gamma^\dagger \left[c_{\mathbf{q},\gamma}, c_{\mathbf{k},\sigma}^\dagger\right]_+ f_\sigma = \delta_{\sigma,\gamma}\left(c_{\mathbf{k},\sigma}^\dagger c_{\mathbf{q},\gamma} - \delta_{\mathbf{k},\mathbf{q}} f_\gamma^\dagger f_\sigma\right), \\
\left[n_{f_{-\sigma}}, f_\gamma^\dagger c_{\mathbf{q},\gamma}\right]_- &= \left[n_{f_{-\sigma}}, f_\gamma^\dagger\right]_- c_{\mathbf{q},\gamma} = \delta_{-\sigma,\gamma} f_{-\sigma}^\dagger c_{\mathbf{q},\gamma}, \\
\left[n_{f_{-\sigma}}, c_{\mathbf{q},\gamma}^\dagger f_\gamma\right]_- &= c_{\mathbf{q},\gamma}^\dagger \left[n_{f_{-\sigma}}, f_\gamma\right]_- = -\delta_{-\sigma,\gamma} c_{\mathbf{q},\gamma}^\dagger f_{-\sigma}.
\end{aligned}
$$

Now, I write for (B.6),

$$
\begin{aligned}
\left[\mathcal{S}, \mathcal{H}_V\right]_- &= \sum_{\mathbf{k},\mathbf{q},\sigma} V_\mathbf{q} V_\mathbf{k} \left(A_\mathbf{k} + Z_\mathbf{k} n_{f_{-\sigma}}\right)\left(2\delta_{\mathbf{k},\mathbf{q}} n_{f_\sigma} - c_{\mathbf{q},\gamma}^\dagger c_{\mathbf{k},\sigma} - c_{\mathbf{k},\sigma}^\dagger c_{\mathbf{q},\gamma}\right) \\
&+ \sum_{\mathbf{k},\mathbf{q},\sigma} V_\mathbf{q} V_\mathbf{k} Z_\mathbf{k} \left(f_{-\sigma}^\dagger c_{\mathbf{q},-\sigma} - c_{\mathbf{q},-\sigma}^\dagger f_{-\sigma}\right)\left(f_\sigma^\dagger c_{\mathbf{k},\sigma} - c_{\mathbf{k},\sigma}^\dagger f_\sigma\right) \\
&= 2\sum_{\mathbf{k},\mathbf{q},\sigma} V_\mathbf{q} V_\mathbf{k} \left(A_\mathbf{k} + Z_\mathbf{k} n_{f_{-\sigma}}\right)\left(\delta_{\mathbf{k},\mathbf{q}} n_{f_\sigma} - c_{\mathbf{k},\sigma}^\dagger c_{\mathbf{q},\sigma}\right) \\
&+ 2\sum_{\mathbf{k},\mathbf{q},\sigma} V_\mathbf{q} V_\mathbf{k} Z_\mathbf{k} \left(c_{\mathbf{k},\sigma}^\dagger c_{\mathbf{q},-\sigma} f_{-\sigma}^\dagger f_\sigma\right) \\
&+ \kappa \sum_{\mathbf{k},\mathbf{q},\sigma} V_\mathbf{q} V_\mathbf{k} Z_\mathbf{k} \left(c_{\mathbf{k},\sigma}^\dagger c_{\mathbf{q},-\sigma}^\dagger f_{-\sigma} f_\sigma + f_\sigma^\dagger f_{-\sigma}^\dagger c_{\mathbf{q},-\sigma} c_{\mathbf{k},\sigma}\right),
\end{aligned}
\tag{B.7}
$$

where in the last equality, I used the symmetry in momentum indices. We define, $J_{\mathbf{k},\mathbf{q}} = 2V_\mathbf{k} V_\mathbf{q} Z_\mathbf{k}$, $W_{\mathbf{k},\mathbf{q}} = V_\mathbf{k} V_\mathbf{q} A_\mathbf{k}$, and we can write the transformed Hamiltonian as,

$$
\begin{aligned}
\tilde{\mathcal{H}}_{\mathrm{AM}} &= \mathcal{H}_0 + \sum_{\mathbf{k},\mathbf{q},\sigma} \left(W_{\mathbf{k},\mathbf{q}} + \frac{J_{\mathbf{k},\mathbf{q}}}{2} n_{f_{-\sigma}}\right)\left(\delta_{\mathbf{k},\mathbf{q}} n_{f_\sigma} - c_{\mathbf{k},\sigma}^\dagger c_{\mathbf{q},\sigma}\right) \\
&+ \sum_{\mathbf{k},\mathbf{q},\sigma} \frac{J_{\mathbf{k},\mathbf{q}}}{2} \left(c_{\mathbf{k},\sigma}^\dagger c_{\mathbf{q},-\sigma} f_{-\sigma}^\dagger f_\sigma\right) \\
&+ \kappa \sum_{\mathbf{k},\mathbf{q},\sigma} \frac{J_{\mathbf{k},\mathbf{q}}}{4} \left(c_{\mathbf{k},\sigma}^\dagger c_{\mathbf{q},-\sigma}^\dagger f_{-\sigma} f_\sigma + f_\sigma^\dagger f_{-\sigma}^\dagger c_{\mathbf{q},-\sigma} c_{\mathbf{k},\sigma}\right),
\end{aligned}
$$

Now using the following identity,

$$
\sum_{\mathbf{k},\mathbf{q},\sigma} \left(c_{\mathbf{k},\sigma}^\dagger c_{\mathbf{q},-\sigma} f_{-\sigma}^\dagger f_\sigma\right) = 2\sum_{\mathbf{k},\mathbf{q}} \vec{S}_c(\mathbf{k},\mathbf{q}) \cdot \vec{S}_f - \frac{1}{2}\sum_{\mathbf{k},\mathbf{q},\sigma} \left(n_{f_\sigma} - n_{f_{-\sigma}}\right) c_{\mathbf{k},\sigma}^\dagger c_{\mathbf{q},\sigma},
$$

where,

$$\begin{aligned} 2\vec{S}_f &= \sum_{j\in\{x,y,z\}} \left(\Psi^\dagger_f \sigma^j \Psi_f\right) \hat{\mathrm{e}}_j, \\ 2\vec{S}_c(\mathbf{k},\mathbf{q}) &= \sum_{j\in\{x,y,z\}} \left(\Psi^\dagger_{c_\mathbf{k}} \sigma^j \Psi_{c_\mathbf{q}}\right) \hat{\mathrm{e}}_j, \end{aligned}$$

with σ^j the Pauli matrices,

$$\sigma^x = \begin{pmatrix} 0 & 1 \\ 1 & 0 \end{pmatrix}, \qquad \sigma^y = \begin{pmatrix} 0 & -i \\ i & 0 \end{pmatrix}, \qquad \sigma^z = \begin{pmatrix} 1 & 0 \\ 0 & -1 \end{pmatrix},$$

while the unitary vectors in cartesian coordinates are denoted by $\hat{\mathrm{e}}_j$, and the "spinors" $\Psi^\dagger_\xi$ and Ψ_ξ are defined as follows,

$$\begin{aligned} \Psi^\dagger_\xi &= \left(\xi^\dagger_\uparrow, \xi^\dagger_\downarrow\right) \\ \Psi_\xi &= \left(\xi_\uparrow, \xi_\downarrow\right)^{\mathrm{T}} \end{aligned}$$

The Hamiltonian to first order can be re-written as:

$$\begin{aligned} \tilde{\mathcal{H}}_{\mathrm{AM}} &= \mathcal{H}_0 + \sum_{\mathbf{k},\mathbf{q}} J_{\mathbf{k},\mathbf{q}} \vec{S}_c(\mathbf{k},\mathbf{q}) \cdot \vec{S}_f \\ &+ \frac{\kappa}{4} \sum_{\mathbf{k},\mathbf{q},\sigma} J_{\mathbf{k},\mathbf{q}} \left(c^\dagger_{\mathbf{k},\sigma} c^\dagger_{\mathbf{q},-\sigma} f_{-\sigma} f_\sigma + f^\dagger_\sigma f^\dagger_{-\sigma} c_{\mathbf{q},-\sigma} c_{\mathbf{k},\sigma} \right) \\ &- \sum_{\mathbf{k},\mathbf{q},\sigma} \left(W_{\mathbf{k},\mathbf{q}} + \frac{J_{\mathbf{k},\mathbf{q}}}{4} N_f \right) c^\dagger_{\mathbf{k},\sigma} c_{\mathbf{q},\sigma} \\ &+ \sum_{\mathbf{k},\sigma} \left(W_{\mathbf{k},\mathbf{k}} + \frac{J_{\mathbf{k},\mathbf{k}}}{2} n_{f_{-\sigma}} \right) n_{f_\sigma}, \end{aligned}$$

w where, $N_f = n_{f_\uparrow} + n_{f_\downarrow}$. Note that equivalently, one can write:

$$\begin{aligned} N_f &= \left(\Psi^\dagger_f \Psi_f\right), \\ \sum_\sigma c^\dagger_{\mathbf{k},\sigma} c_{\mathbf{q},\sigma} &= \left(\Psi^\dagger_{c_\mathbf{k}} \Psi_{c_\mathbf{q}}\right), \end{aligned}$$

with this equivalencies one can directly identify that under the transformations: $\kappa = -1$, $A \to -A$, $Z \to -Z$, which imply $J \to -J$, $W \to -W$, one recovers exactly the result given by Schrieffer and Wolff. Their interpretation for the additional terms from $\mathcal{H}_0$ in $\tilde{\mathcal{H}}_{\mathrm{AM}}$ is that, the first term is an s-d exchange interaction term, the second one is called the two particle channel term, the third one is referred to as, the direct (spin-independent) s-d interaction, and the last one renormalizes U and ϵ_f.

B.2 The Schrieffer-Wolf transformation to second order

The next order of the canonical transformation can be computed by starting from the first order commutation,

$$\begin{aligned}
\left[\mathcal{S},\mathcal{H}_V\right]_- &= \sum_{\mathbf{k},\mathbf{q},\sigma}\left(2W_{\mathbf{k},\mathbf{q}}+J_{\mathbf{k},\mathbf{q}}n_{f_{-\sigma}}\right)\left(\delta_{\mathbf{k},\mathbf{q}}n_{f_\sigma}-c^\dagger_{\mathbf{k},\sigma}c_{\mathbf{q},\sigma}\right)\\
&+ \sum_{\mathbf{k},\mathbf{q},\sigma}J_{\mathbf{k},\mathbf{q}}\left(c^\dagger_{\mathbf{k},\sigma}c_{\mathbf{q},-\sigma}f^\dagger_{-\sigma}f_\sigma\right)\\
&+ \sum_{\mathbf{k},\mathbf{q},\sigma}\frac{J_{\mathbf{k},\mathbf{q}}}{2}\left(c^\dagger_{\mathbf{k},\sigma}c^\dagger_{\mathbf{q},-\sigma}f_{-\sigma}f_\sigma+f^\dagger_\sigma f^\dagger_{-\sigma}c_{\mathbf{q},-\sigma}c_{\mathbf{k},\sigma}\right),
\end{aligned}$$

I will use the anticommutation algebra,

$$\left[c^\dagger,f^\dagger\right]_+=\left[c,f\right]_+=\left[c^\dagger,f\right]_+=\left[f^\dagger,c\right]_+=0,$$

For the second order I need to compute, $\left[\mathcal{S},\left[\mathcal{S},\mathcal{H}_V\right]_-\right]_-=C_1+C_2+C_3$, with,

$$\begin{aligned}
C_1 &= \left[\mathcal{S},\sum_{\mathbf{k},\mathbf{q},\sigma}\left(2W_{\mathbf{k},\mathbf{q}}+J_{\mathbf{k},\mathbf{q}}n_{f_{-\sigma}}\right)\left(\delta_{\mathbf{k},\mathbf{q}}n_{f_\sigma}-c^\dagger_{\mathbf{k},\sigma}c_{\mathbf{q},\sigma}\right)\right]_-\\
C_2 &= \left[\mathcal{S},\sum_{\mathbf{k},\mathbf{q},\sigma}J_{\mathbf{k},\mathbf{q}}\left(c^\dagger_{\mathbf{k},\sigma}c_{\mathbf{q},-\sigma}f^\dagger_{-\sigma}f_\sigma\right)\right]_-\\
C_3 &= \left[\mathcal{S},\sum_{\mathbf{k},\mathbf{q},\sigma}\frac{J_{\mathbf{k},\mathbf{q}}}{2}\left(c^\dagger_{\mathbf{k},\sigma}c^\dagger_{\mathbf{q},-\sigma}f_{-\sigma}f_\sigma+f^\dagger_\sigma f^\dagger_{-\sigma}c_{\mathbf{q},-\sigma}c_{\mathbf{k},\sigma}\right)\right]_-
\end{aligned}$$

I will use the following identities,

$$\begin{aligned}
\left[A,BC\right]_- &= \left[A,B\right]_\pm C-B\left[C,A\right]_\pm\\
\left[AB,CD\right]_- &= A\left[B,C\right]_\pm D-\left[C,A\right]_\pm BD+CA\left[B,D\right]_\pm-C\left[D,A\right]_\pm B
\end{aligned}$$

For the first term I have, $C_1=\sum_{\mathbf{k}_1,\mathbf{k},\mathbf{q}}\sum_{\sigma,\gamma}V_{\mathbf{k}_1}\alpha_1$,

$$\begin{aligned}
\alpha_1 &= \left[\left(A_{\mathbf{k}_1}+Z_{\mathbf{k}_1}n_{f_{-\gamma}}\right)\left(f^\dagger_\gamma c_{\mathbf{k}_1,\gamma}-c^\dagger_{\mathbf{k}_1,\gamma}f_\gamma\right),\left(2W_{\mathbf{k},\mathbf{q}}+J_{\mathbf{k},\mathbf{q}}n_{f_{-\sigma}}\right)\left(\delta_{\mathbf{k},\mathbf{q}}n_{f_\sigma}-c^\dagger_{\mathbf{k},\sigma}c_{\mathbf{q},\sigma}\right)\right]_-\\
&= J_{\mathbf{k},\mathbf{q}}\left(A_{\mathbf{k}_1}+Z_{\mathbf{k}_1}n_{f_{-\gamma}}\right)\lambda_1\left(\delta_{\mathbf{k},\mathbf{q}}n_{f_\sigma}-c^\dagger_{\mathbf{k},\sigma}c_{\mathbf{q},\sigma}\right)\\
&- Z_{\mathbf{k}_1}\left(2W_{\mathbf{k},\mathbf{q}}+J_{\mathbf{k},\mathbf{q}}n_{f_{-\sigma}}\right)\lambda_2\left(f^\dagger_\gamma c_{\mathbf{k}_1,\gamma}-c^\dagger_{\mathbf{k}_1,\gamma}f_\gamma\right)\\
&+ \left(2W_{\mathbf{k},\mathbf{q}}+J_{\mathbf{k},\mathbf{q}}n_{f_{-\sigma}}\right)\left(A_{\mathbf{k}_1}+Z_{\mathbf{k}_1}n_{f_{-\gamma}}\right)\lambda_3
\end{aligned}$$

where,

$$\begin{aligned}
\lambda_1 &= \left[f_\gamma^\dagger c_{\mathbf{k}_1,\gamma} - c_{\mathbf{k}_1,\gamma}^\dagger f_\gamma, n_{f_{-\sigma}}\right]_- \\
&= -\delta_{-\sigma,\gamma}\left(f_{-\gamma}^\dagger c_{\mathbf{k}_1,\gamma} + c_{\mathbf{k}_1,\gamma}^\dagger f_{-\gamma}\right), \\
\lambda_2 &= \left[\delta_{\mathbf{k},\mathbf{q}} n_{f_\sigma} - c_{\mathbf{k},\sigma}^\dagger c_{\mathbf{q},\sigma}, n_{f_{-\sigma}}\right]_- \\
&= 0, \\
\lambda_3 &= \left[f_\gamma^\dagger c_{\mathbf{k}_1,\gamma} - c_{\mathbf{k}_1,\gamma}^\dagger f_\gamma, \delta_{\mathbf{k},\mathbf{q}} n_{f_\sigma} - c_{\mathbf{k},\sigma}^\dagger c_{\mathbf{q},\sigma}\right]_- \\
&= -\delta_{\sigma,\gamma}\left\{\delta_{\mathbf{k},\mathbf{q}}\left(f_\sigma^\dagger c_{\mathbf{k}_1,\gamma} + c_{\mathbf{k}_1,\gamma}^\dagger f_\sigma\right) + \delta_{\mathbf{k},\mathbf{k}_1}\left(f_\gamma^\dagger c_{\mathbf{q},\sigma} + c_{\mathbf{q},\sigma}^\dagger f_\gamma\right)\right\},
\end{aligned}$$

After some algebra and adding over γ we can write C_1 as,

$$\begin{aligned}
C_1 &= -\sum_\sigma \sum_{\mathbf{k}_1,\mathbf{k},\mathbf{q}} \Big(B_1 + B_2 c_{\mathbf{k},-\sigma}^\dagger c_{\mathbf{q},-\sigma} + B_3 n_{f_{-\sigma}} \\
&+ B_4 n_{f_{-\sigma}} c_{\mathbf{k},-\sigma}^\dagger c_{\mathbf{q},-\sigma}\Big)\left(f_\sigma^\dagger c_{\mathbf{k}_1,\sigma} + c_{\mathbf{k}_1,\sigma}^\dagger f_\sigma\right),
\end{aligned} \tag{B.8}$$

with,

$$\begin{aligned}
B_1 &= 2V_{\mathbf{k}_1}\left(\delta_{\mathbf{k}_1,\mathbf{q}} W_{\mathbf{k},\mathbf{k}} A_{\mathbf{k}_1} + \delta_{\mathbf{k}_1,\mathbf{k}} W_{\mathbf{k}_1,\mathbf{q}} A_{\mathbf{q}}\right), \\
B_2 &= -V_{\mathbf{k}_1} J_{\mathbf{k},\mathbf{q}} A_{\mathbf{k}_1}, \\
B_3 &= V_{\mathbf{k}_1}\left(\delta_{\mathbf{k},\mathbf{q}} J_{\mathbf{k},\mathbf{q}}\left(A_{\mathbf{k}_1} + Z_{\mathbf{k}_1}\right) + \delta_{\mathbf{k}_1,\mathbf{q}}\left(2W_{\mathbf{k},\mathbf{k}} Z_{\mathbf{k}_1} + J_{\mathbf{k},\mathbf{k}}\left(A_{\mathbf{k}_1} + Z_{\mathbf{k}_1}\right)\right)\right. \\
&+ \left.\delta_{\mathbf{k}_1,\mathbf{k}}\left(2W_{\mathbf{k}_1,\mathbf{q}} Z_{\mathbf{q}} + J_{\mathbf{k}_1,\mathbf{q}}\left(A_{\mathbf{q}} + Z_{\mathbf{q}}\right)\right)\right), \\
B_4 &= -V_{\mathbf{k}_1} J_{\mathbf{k},\mathbf{q}} Z_{\mathbf{k}_1},
\end{aligned}$$

We continue with the next term and write $C_2 = \sum_{\mathbf{k}_1,\mathbf{k},\mathbf{q}} \sum_{\sigma,\gamma} V_{\mathbf{k}_1} J_{\mathbf{k},\mathbf{q}} \alpha_2$, where,

$$\begin{aligned}
\alpha_2 &= \Big[\Big(A_{\mathbf{k}_1} + Z_{\mathbf{k}_1} n_{f_{-\gamma}}\Big)\left(f_\gamma^\dagger c_{\mathbf{k}_1,\gamma} - c_{\mathbf{k}_1,\gamma}^\dagger f_\gamma\right), c_{\mathbf{k},\sigma}^\dagger c_{\mathbf{q},-\sigma} f_\sigma^\dagger f_{-\sigma}\Big]_- \\
&= Z_{\mathbf{k}_1}\left[n_{f_{-\gamma}}, c_{\mathbf{k},\sigma}^\dagger c_{\mathbf{q},-\sigma} f_\sigma^\dagger f_{-\sigma}\right]_-\left(f_\gamma^\dagger c_{\mathbf{k}_1,\gamma} - c_{\mathbf{k}_1,\gamma}^\dagger f_\gamma\right) \\
&+ \Big(A_{\mathbf{k}_1} + Z_{\mathbf{k}_1} n_{f_{-\gamma}}\Big)\left[f_\gamma^\dagger c_{\mathbf{k}_1,\gamma} - c_{\mathbf{k}_1,\gamma}^\dagger f_\gamma, c_{\mathbf{k},\sigma}^\dagger c_{\mathbf{q},-\sigma} f_\sigma^\dagger f_{-\sigma}\right]_-
\end{aligned}$$

After some algebra and adding over γ we can write C_2 as,

$$\begin{aligned}
C_2 &= \sum_{\mathbf{k}_1,\mathbf{k},\mathbf{q}} \sum_\sigma V_{\mathbf{k}_1} J_{\mathbf{k},\mathbf{q}} \Big(\Big(A_{\mathbf{k}_1} + Z_{\mathbf{k}_1}\Big(n_{f_\sigma} + n_{f_{-\sigma}}\Big)\Big) c_{\mathbf{k},-\sigma}^\dagger c_{\mathbf{k}_1,-\sigma} \\
&- \delta_{\mathbf{k},\mathbf{k}_1}\Big(A_{\mathbf{k}_1} + Z_{\mathbf{k}_1} n_{f_\sigma}\Big) n_{f_{-\sigma}}\Big)\left(f_\sigma^\dagger c_{\mathbf{q},\sigma} + c_{\mathbf{q},\sigma}^\dagger f_\sigma\right) \\
&- \sum_{\mathbf{k}_1,\mathbf{k},\mathbf{q}} \sum_\sigma V_{\mathbf{k}_1} J_{\mathbf{k},\mathbf{q}} Z_{\mathbf{k}_1}\left(c_{\mathbf{k},-\sigma}^\dagger c_{\mathbf{k}_1,-\sigma} f_\sigma^\dagger c_{\mathbf{q},\sigma} + \delta_{\mathbf{q},\mathbf{k}_1} n_{f_{-\sigma}} c_{\mathbf{k},\sigma}^\dagger f_\sigma\right).
\end{aligned} \tag{B.9}$$

The last term remains and we write $C_3 = \sum_{\mathbf{k}_1,\mathbf{k},\mathbf{q}} \sum_\sigma V_{\mathbf{k}_1} J_{\mathbf{k},\mathbf{q}} \alpha_3$, where,

$$\begin{aligned}
\alpha_3 &= \left[\left(A_{\mathbf{k}_1} + Z_{\mathbf{k}_1} n_{f_{-_\gamma}} \right) \left(f_\gamma^\dagger c_{\mathbf{k}_1,\gamma} - c_{\mathbf{k}_1,\gamma}^\dagger f_\gamma \right), \left(c_{\mathbf{k},\uparrow}^\dagger c_{\mathbf{q},\downarrow}^\dagger f_\downarrow f_\uparrow + \text{h.c.} \right) \right]_- \\
&= Z_{\mathbf{k}_1} \left[n_{f_{-_\gamma}}, \left(c_{\mathbf{k},\uparrow}^\dagger c_{\mathbf{q},\downarrow}^\dagger f_\downarrow f_\uparrow + \text{h.c.} \right) \right]_- \left(f_\gamma^\dagger c_{\mathbf{k}_1,\gamma} - c_{\mathbf{k}_1,\gamma}^\dagger f_\gamma \right) \\
&+ \left(A_{\mathbf{k}_1} + Z_{\mathbf{k}_1} n_{f_{-_\gamma}} \right) \left[f_\gamma^\dagger c_{\mathbf{k}_1,\gamma} - c_{\mathbf{k}_1,\gamma}^\dagger f_\gamma, \left(c_{\mathbf{k},\uparrow}^\dagger c_{\mathbf{q},\downarrow}^\dagger f_\downarrow f_\uparrow + \text{h.c.} \right) \right]_-
\end{aligned}$$

After some algebra and rearranging the terms in the summations we can write C_3 as,

$$\begin{aligned}
C_3 &= \sum_{\mathbf{k}_1,\mathbf{k},\mathbf{q}} \sum_\sigma V_{\mathbf{k}_1} J_{\mathbf{k},\mathbf{q}} \left(Z_{\mathbf{k}_1} n_{f_{-_\sigma}} c_{\mathbf{k},-\sigma}^\dagger c_{\mathbf{k}_1,-\sigma} \right. \\
&+ \left. \left(A_{\mathbf{k}_1} + Z_{\mathbf{k}_1} n_{f_\sigma} \right) \left(\delta_{\mathbf{k},\mathbf{k}_1} n_{f_{-_\sigma}} - c_{\mathbf{k},-\sigma}^\dagger c_{\mathbf{k}_1,-\sigma} \right) \right) \left(f_\sigma^\dagger c_{\mathbf{q},\sigma} + c_{\mathbf{q},\sigma}^\dagger f_\sigma \right) \\
&- \sum_{\mathbf{k}_1,\mathbf{k},\mathbf{q}} \sum_\sigma V_{\mathbf{k}_1} J_{\mathbf{k},\mathbf{q}} Z_{\mathbf{k}_1} \left(c_{\mathbf{k},-\sigma}^\dagger c_{\mathbf{k}_1,-\sigma} c_{\mathbf{q},\sigma}^\dagger f_\sigma + \delta_{\mathbf{k},\mathbf{k}_1} n_{f_{-_\sigma}} f_\sigma^\dagger c_{\mathbf{q},\sigma} \right)
\end{aligned} \tag{B.10}$$

The sum of C_2 and C_3 can be simplified and yields,

$$C_2 + C_3 = \sum_{\mathbf{k}_1,\mathbf{k},\mathbf{q}} \sum_\sigma V_{\mathbf{k}_1} J_{\mathbf{k},\mathbf{q}} Z_{\mathbf{k}_1} \left(\left(2 n_{f_{-_\sigma}} - 1 \right) c_{\mathbf{k},-\sigma}^\dagger c_{\mathbf{k}_1,-\sigma} - \delta_{\mathbf{k},\mathbf{k}_1} n_{f_{-_\sigma}} \right) \left(f_\sigma^\dagger c_{\mathbf{q},\sigma} + c_{\mathbf{q},\sigma}^\dagger f_\sigma \right) \tag{B.11}$$

So finally we can write,

$$\begin{aligned}
\left[\mathcal{S}, \left[\mathcal{S}, \mathcal{H}_V \right]_- \right]_- &= \sum_\sigma \sum_{\mathbf{k}_1,\mathbf{k},\mathbf{q}} \left(a_1 + a_2 n_{f_{-_\sigma}} + a_3 c_{\mathbf{k},-\sigma}^\dagger c_{\mathbf{q},-\sigma} \right. \\
&+ \left. a_4 n_{f_{-_\sigma}} c_{\mathbf{k},-\sigma}^\dagger c_{\mathbf{q},-\sigma} \right) \left(f_\sigma^\dagger c_{\mathbf{k}_1,\sigma} + c_{\mathbf{k}_1,\sigma}^\dagger f_\sigma \right),
\end{aligned} \tag{B.12}$$

where,

$$\begin{aligned}
a_1 &= -2 V_{\mathbf{k}_1} \left(\delta_{\mathbf{k}_1,\mathbf{q}} W_{\mathbf{k},\mathbf{k}} A_{\mathbf{k}_1} + \delta_{\mathbf{k}_1,\mathbf{k}} W_{\mathbf{k}_1,\mathbf{q}} A_{\mathbf{q}} \right), \\
a_2 &= -V_{\mathbf{k}_1} \left(\delta_{\mathbf{k},\mathbf{q}} J_{\mathbf{k},\mathbf{q}} \left(A_{\mathbf{k}_1} + Z_{\mathbf{k}_1} \right) + \delta_{\mathbf{k}_1,\mathbf{q}} \left(2 W_{\mathbf{k},\mathbf{k}} Z_{\mathbf{k}_1} + J_{\mathbf{k},\mathbf{k}} \left(A_{\mathbf{k}_1} + Z_{\mathbf{k}_1} \right) \right) \right. \\
&+ \left. \delta_{\mathbf{k}_1,\mathbf{k}} \left(2 W_{\mathbf{k}_1,\mathbf{q}} Z_{\mathbf{q}} + J_{\mathbf{k}_1,\mathbf{q}} \left(A_{\mathbf{q}} + Z_{\mathbf{q}} \right) \right) \right) - V_{\mathbf{q}} J_{\mathbf{k},\mathbf{k}_1} Z_{\mathbf{q}}, \\
a_3 &= V_{\mathbf{k}_1} J_{\mathbf{k},\mathbf{q}} A_{\mathbf{k}_1} - V_{\mathbf{q}} J_{\mathbf{k},\mathbf{k}_1} Z_{\mathbf{q}}, \\
a_4 &= V_{\mathbf{k}_1} J_{\mathbf{k},\mathbf{q}} Z_{\mathbf{k}_1} + 2 V_{\mathbf{q}} J_{\mathbf{k},\mathbf{k}_1} Z_{\mathbf{q}},
\end{aligned}$$

B.3 The Schrieffer-Wolf transformation to third order

We start by using the second order commutation result of the previous section, for the third order I need to compute, $\left[\mathcal{S},\left[\mathcal{S},\left[\mathcal{S},\mathcal{H}_V\right]_-\right]_-\right]_- = D_1 + D_2 + D_3 + D_4$, with,

$$\begin{aligned}
D_1 &= \sum_{\sigma}\sum_{\mathbf{k}_1,\mathbf{k},\mathbf{q}} a_1\left[\mathcal{S},\left(f_\sigma^\dagger c_{\mathbf{k}_1,\sigma} + c_{\mathbf{k}_1,\sigma}^\dagger f_\sigma\right)\right]_- \\
D_2 &= \sum_{\sigma}\sum_{\mathbf{k}_1,\mathbf{k},\mathbf{q}} a_2\left[\mathcal{S}, c_{\mathbf{k},-\sigma}^\dagger c_{\mathbf{q},-\sigma}\left(f_\sigma^\dagger c_{\mathbf{k}_1,\sigma} + c_{\mathbf{k}_1,\sigma}^\dagger f_\sigma\right)\right]_- \\
D_3 &= \sum_{\sigma}\sum_{\mathbf{k}_1,\mathbf{k},\mathbf{q}} a_3\left[\mathcal{S}, n_{f_{-\sigma}}\left(f_\sigma^\dagger c_{\mathbf{k}_1,\sigma} + c_{\mathbf{k}_1,\sigma}^\dagger f_\sigma\right)\right]_- \\
D_4 &= \sum_{\sigma}\sum_{\mathbf{k}_1,\mathbf{k},\mathbf{q}} a_4\left[\mathcal{S}, n_{f_{-\sigma}} c_{\mathbf{k},-\sigma}^\dagger c_{\mathbf{q},-\sigma}\left(f_\sigma^\dagger c_{\mathbf{k}_1,\sigma} + c_{\mathbf{k}_1,\sigma}^\dagger f_\sigma\right)\right]_-
\end{aligned}$$

Using the result from first order, I have for D_1,

$$\begin{aligned}
D_1 &= 2\sum_{\sigma}\sum_{\mathbf{k}_2,\mathbf{k}_1,\mathbf{k},\mathbf{q}} V_{\mathbf{k}_2} a_1 \left\{\left(A_{\mathbf{k}_2} + Z_{\mathbf{k}_2} n_{f_{-\sigma}}\right)\left(\delta_{\mathbf{k}_2,\mathbf{k}_1} n_{f_\sigma} - c_{\mathbf{k}_1,\sigma}^\dagger c_{\mathbf{k}_2,\sigma}\right)\right. \\
&+ Z_{\mathbf{k}_2}\left(c_{\mathbf{k}_2,\sigma}^\dagger c_{\mathbf{k}_1,-\sigma} f_{-\sigma}^\dagger f_\sigma\right) \\
&+ \left.\frac{Z_{\mathbf{k}_2}}{2}\left(c_{\mathbf{k}_2,\sigma}^\dagger c_{\mathbf{k}_1,-\sigma}^\dagger f_{-\sigma} f_\sigma + f_\sigma^\dagger f_{-\sigma}^\dagger c_{\mathbf{k}_1,-\sigma} c_{\mathbf{k}_2,\sigma}\right)\right\},
\end{aligned} \tag{B.13}$$

The remaining terms can be rewritten as,

$$\begin{aligned}
D_2 &= \sum_{\sigma}\sum_{\mathbf{k}_1,\mathbf{k},\mathbf{q}} a_2\left\{\left[\mathcal{S}, n_{f_{-\sigma}}\right]_-\left(f_\sigma^\dagger c_{\mathbf{k}_1,\sigma} + c_{\mathbf{k}_1,\sigma}^\dagger f_\sigma\right)\right. \\
&+ \left. n_{f_{-\sigma}}\left[\mathcal{S},\left(f_\sigma^\dagger c_{\mathbf{k}_1,\sigma} + c_{\mathbf{k}_1,\sigma}^\dagger f_\sigma\right)\right]_-\right\}, \\
D_3 &= \sum_{\sigma}\sum_{\mathbf{k}_1,\mathbf{k},\mathbf{q}} a_3\left\{\left[\mathcal{S}, c_{\mathbf{k},-\sigma}^\dagger c_{\mathbf{q},-\sigma}\right]_-\left(f_\sigma^\dagger c_{\mathbf{k}_1,\sigma} + c_{\mathbf{k}_1,\sigma}^\dagger f_\sigma\right)\right. \\
&+ \left. c_{\mathbf{k},-\sigma}^\dagger c_{\mathbf{q},-\sigma}\left[\mathcal{S},\left(f_\sigma^\dagger c_{\mathbf{k}_1,\sigma} + c_{\mathbf{k}_1,\sigma}^\dagger f_\sigma\right)\right]_-\right\}, \\
D_4 &= \sum_{\sigma}\sum_{\mathbf{k}_1,\mathbf{k},\mathbf{q}} a_4\left\{\left[\mathcal{S}, n_{f_{-\sigma}} c_{\mathbf{k},-\sigma}^\dagger c_{\mathbf{q},-\sigma}\right]_-\left(f_\sigma^\dagger c_{\mathbf{k}_1,\sigma} + c_{\mathbf{k}_1,\sigma}^\dagger f_\sigma\right)\right. \\
&+ \left. n_{f_{-\sigma}} c_{\mathbf{k},-\sigma}^\dagger c_{\mathbf{q},-\sigma}\left[\mathcal{S},\left(f_\sigma^\dagger c_{\mathbf{k}_1,\sigma} + c_{\mathbf{k}_1,\sigma}^\dagger f_\sigma\right)\right]_-\right\}.
\end{aligned}$$

For the first two commutators of the remaining terms, one has,

$$\begin{aligned}
\left[\mathcal{S}, n_{f_{-\sigma}}\right]_- &= -\sum_{\mathbf{k}_2} V_{\mathbf{k}_2}\left(A_{\mathbf{k}_2} + Z_{\mathbf{k}_2} n_{f_\sigma}\right)\left(f_{-\sigma}^\dagger c_{\mathbf{k}_2,-\sigma} + c_{\mathbf{k}_2,-\sigma}^\dagger f_{-\sigma}\right), \\
\left[\mathcal{S}, c_{\mathbf{k},-\sigma}^\dagger c_{\mathbf{q},-\sigma}\right]_- &= \sum_{\mathbf{k}_2} V_{\mathbf{k}_2}\left(A_{\mathbf{k}_2} + Z_{\mathbf{k}_2} n_{f_\sigma}\right)\left(\delta_{\mathbf{k}_2,\mathbf{k}} f_{-\sigma}^\dagger c_{\mathbf{q},-\sigma} + \delta_{\mathbf{k}_2,\mathbf{q}} c_{\mathbf{k},-\sigma}^\dagger f_{-\sigma}\right) \\
&\approx \sum_{\mathbf{k}_2} \delta_{\mathbf{k}_2,\mathbf{k}} V_{\mathbf{k}_2}\left(A_{\mathbf{k}_2} + Z_{\mathbf{k}_2} n_{f_\sigma}\right)\left(f_{-\sigma}^\dagger c_{\mathbf{q},-\sigma} + c_{\mathbf{q},-\sigma}^\dagger f_{-\sigma}\right),
\end{aligned}$$

the term with $n_{f_{-\sigma}} c^{\dagger}_{\mathbf{k},-\sigma} c_{\mathbf{q},-\sigma}$, yields,

$$\begin{aligned}
\left[\mathcal{S}, n_{f_{-\sigma}} c^{\dagger}_{\mathbf{k},-\sigma} c_{\mathbf{q},-\sigma}\right]_- &= \left[\mathcal{S}, n_{f_{-\sigma}}\right]_- c^{\dagger}_{\mathbf{k},-\sigma} c_{\mathbf{q},-\sigma} + n_{f_{-\sigma}} \left[\mathcal{S}, c^{\dagger}_{\mathbf{k},-\sigma} c_{\mathbf{q},-\sigma}\right]_- \\
&\approx \sum_{\mathbf{k}_2} V_{\mathbf{k}_2} \left(A_{\mathbf{k}_2} + Z_{\mathbf{k}_2} n_{f_\sigma}\right) \left\{ c^{\dagger}_{\mathbf{k},-\sigma} c_{\mathbf{q},-\sigma} \right. \\
&+ \left. \delta_{\mathbf{k}_2,\mathbf{k}} \left(n_{f_{-\sigma}} - 1\right) \right\} \left(f^{\dagger}_{-\sigma} c_{\mathbf{q},-\sigma} + c^{\dagger}_{\mathbf{q},-\sigma} f_{-\sigma}\right)
\end{aligned}$$

we will use the next identity,

$$\begin{aligned}
\left(f^{\dagger}_{-\sigma} c_{\mathbf{k}_2,-\sigma} + c^{\dagger}_{\mathbf{k}_2,-\sigma} f_{-\sigma}\right) \left(f^{\dagger}_{\sigma} c_{\mathbf{k}_1,\sigma} + c^{\dagger}_{\mathbf{k}_1,\sigma} f_{\sigma}\right) &\equiv \left(c^{\dagger}_{\mathbf{k}_2,\sigma} c^{\dagger}_{\mathbf{k}_1,-\sigma} f_{-\sigma} f_{\sigma} + f^{\dagger}_{\sigma} f^{\dagger}_{-\sigma} c_{\mathbf{k}_1,-\sigma} c_{\mathbf{k}_2,\sigma}\right) \\
&- \left(c^{\dagger}_{\mathbf{k}_2,-\sigma} c_{\mathbf{k}_1,\sigma} f^{\dagger}_{\sigma} f_{-\sigma} + c^{\dagger}_{\mathbf{k}_1,\sigma} c_{\mathbf{k}_2,-\sigma} f^{\dagger}_{-\sigma} f_{\sigma}\right)
\end{aligned}$$

Using the above for D_2 after some algebra we have,

$$\begin{aligned}
D_2 &= 2 \sum_{\sigma} \sum_{\mathbf{k}_2,\mathbf{k}_1,\mathbf{k},\mathbf{q}} V_{\mathbf{k}_2} a_2 \left\{ \left(A_{\mathbf{k}_2} + Z_{\mathbf{k}_2}\right) \left(\delta_{\mathbf{k}_2,\mathbf{k}_1} n_{f_\sigma} n_{f_{-\sigma}} - n_{f_\sigma} c^{\dagger}_{\mathbf{k}_1,\sigma} c_{\mathbf{k}_2,\sigma} \right.\right. \\
&+ \left.\left. c^{\dagger}_{\mathbf{k}_1,\sigma} c_{\mathbf{k}_2,-\sigma} f^{\dagger}_{-\sigma} f_{\sigma}\right) - \frac{A_{\mathbf{k}_2}}{2} \left(c^{\dagger}_{\mathbf{k}_2,\sigma} c^{\dagger}_{\mathbf{k}_1,-\sigma} f_{-\sigma} f_{\sigma} + f^{\dagger}_{\sigma} f^{\dagger}_{-\sigma} c_{\mathbf{k}_1,-\sigma} c_{\mathbf{k}_2,\sigma}\right) \right\}
\end{aligned}$$

Thus, next term D_3 can be written as,

$$\begin{aligned}
D_3 &= \sum_{\sigma} \sum_{\mathbf{k}_2,\mathbf{k}_1,\mathbf{k},\mathbf{q}} V_{\mathbf{k}_2} a_3 \left\{ \delta_{\mathbf{k}_2,\mathbf{k}_1} A_{\mathbf{k}_2} n_{f_\sigma} n_{f_{-\sigma}} \right. \\
&+ \delta_{\mathbf{k}_2,\mathbf{k}_1} Z_{\mathbf{k}_2} n_{f_\sigma} c^{\dagger}_{\mathbf{k},-\sigma} c_{\mathbf{q},-\sigma} - A_{\mathbf{k}_2} c^{\dagger}_{\mathbf{k},-\sigma} c_{\mathbf{q},-\sigma} c^{\dagger}_{\mathbf{k}_1,\sigma} c_{\mathbf{k}_2,\sigma} \\
&- Z_{\mathbf{k}_2} n_{f_{-\sigma}} c^{\dagger}_{\mathbf{k},-\sigma} c_{\mathbf{q},-\sigma} c^{\dagger}_{\mathbf{k}_1,\sigma} c_{\mathbf{k}_2,\sigma} - \delta_{\mathbf{k},\mathbf{k}_2} \left(A_{\mathbf{k}_2} + Z_{\mathbf{k}_2}\right) c^{\dagger}_{\mathbf{k}_1,\sigma} c_{\mathbf{q},-\sigma} f^{\dagger}_{-\sigma} f_{\sigma} \\
&+ \left. \delta_{\mathbf{k},\mathbf{k}_2} \left(A_{\mathbf{k}_2} + Z_{\mathbf{k}_2}\right) \left(c^{\dagger}_{\mathbf{k}_1,\sigma} c^{\dagger}_{\mathbf{q},-\sigma} f_{-\sigma} f_{\sigma} + f^{\dagger}_{\sigma} f^{\dagger}_{-\sigma} c_{\mathbf{q},-\sigma} c_{\mathbf{k}_1,\sigma}\right) \right\}
\end{aligned}$$

we have after some simplifications for D_4,

$$D_4 = \sum_{\sigma} \sum_{\mathbf{k}_2,\mathbf{k}_1,\mathbf{k},\mathbf{q}} V_{\mathbf{k}_2} a_4 \left(A_{\mathbf{k}_2} + Z_{\mathbf{k}_2}\right) \left(\delta_{\mathbf{k}_2,\mathbf{k}_1} n_{f_\sigma} n_{f_{-\sigma}} c^{\dagger}_{\mathbf{k},-\sigma} c_{\mathbf{q},-\sigma} - n_{f_{-\sigma}} c^{\dagger}_{\mathbf{k},-\sigma} c_{\mathbf{q},-\sigma} c^{\dagger}_{\mathbf{k}_1,\sigma} c_{\mathbf{k}_2,\sigma}\right).$$

We have that the third oder expansion gives the following,

$$\begin{aligned}
\left[\mathcal{S}, \left[\mathcal{S}, \left[\mathcal{S}, \mathcal{H}_V\right]_-\right]_-\right]_- &= \sum_{\sigma} \sum_{\mathbf{k},\mathbf{q},\mathbf{k}_1,\mathbf{k}_2} \left\{ b_1 n_{f_\sigma} + b_2 c^{\dagger}_{\mathbf{k}_1,\sigma} c_{\mathbf{k}_2,\sigma} \right. \\
&+ b_3 n_{f_\sigma} n_{f_{-\sigma}} + b_4 n_{f_{-\sigma}} c^{\dagger}_{\mathbf{k}_1,\sigma} c_{\mathbf{k}_2,\sigma} \\
&+ b_5 c^{\dagger}_{\mathbf{k},-\sigma} c_{\mathbf{q},-\sigma} c^{\dagger}_{\mathbf{k}_1,\sigma} c_{\mathbf{k}_2,\sigma} + b_6 n_{f_\sigma} n_{f_{-\sigma}} c^{\dagger}_{\mathbf{k}_1,\sigma} c_{\mathbf{k}_2,\sigma} \\
&+ b_7 n_{f_{-\sigma}} c^{\dagger}_{\mathbf{k},-\sigma} c_{\mathbf{q},-\sigma} c^{\dagger}_{\mathbf{k}_1,\sigma} c_{\mathbf{k}_2,\sigma} + b_8 c^{\dagger}_{\mathbf{k}_2,\sigma} c_{\mathbf{k}_1,-\sigma} f^{\dagger}_{-\sigma} f_{\sigma} \\
&+ \left. b_9 \left(c^{\dagger}_{\mathbf{k}_2,\sigma} c^{\dagger}_{\mathbf{k}_1,-\sigma} f_{-\sigma} f_{\sigma} + f^{\dagger}_{\sigma} f^{\dagger}_{-\sigma} c_{\mathbf{k}_1,-\sigma} c_{\mathbf{k}_2,\sigma}\right) \right.
\end{aligned}$$

with,

$$\begin{aligned}
b_1 &= 2\delta_{\mathbf{k}_1,\mathbf{k}_2} V_{\mathbf{k}_2} A_{\mathbf{k}_2} a_1, \\
b_2 &= -2V_{\mathbf{k}_2} A_{\mathbf{k}_2} a_1, \\
b_3 &= 2\delta_{\mathbf{k}_1,\mathbf{k}_2} V_{\mathbf{k}_2} \left(\left(A_{\mathbf{k}_2} + Z_{\mathbf{k}_2} \right) a_1 + Z_{\mathbf{k}_2} a_2 \right), \\
b_4 &= V_{\mathbf{k}_2} \left(\delta_{\mathbf{k},\mathbf{q}} A_{\mathbf{k}_2} a_3 - Z_{\mathbf{k}_2} a1 - \left(A_{\mathbf{k}_2} + Z_{\mathbf{k}_2} \right) a_2 \right), \\
b_5 &= -V_{\mathbf{k}_2} A_{\mathbf{k}_2} a_3, \\
b_6 &= \delta_{\mathbf{k}_1,\mathbf{k}_2} V_{\mathbf{k}_2} \left(A_{\mathbf{k}_2} + Z_{\mathbf{k}_2} \right) a_4, \\
b_7 &= -V_{\mathbf{k}_2} \left(Z_{\mathbf{k}_2} a_3 + \left(A_{\mathbf{k}_2} + Z_{\mathbf{k}_2} \right) a_4 \right), \\
b_8 &= 2V_{\mathbf{k}_2} \left(Z_{\mathbf{k}_2} a_1 - \left(A_{\mathbf{k}_2} + Z_{\mathbf{k}_2} \right) a_2 - \delta_{\mathbf{k}_2,\mathbf{k}} \left(A_{\mathbf{k}_2} + Z_{\mathbf{k}_2} \right) a_3 \right), \\
b_9 &= V_{\mathbf{k}_2} \left(Z_{\mathbf{k}_2} a_1 - \left(A_{\mathbf{k}_2} + Z_{\mathbf{k}_2} \right) a_2 + \delta_{\mathbf{k}_2,\mathbf{k}} \left(A_{\mathbf{k}_2} + Z_{\mathbf{k}_2} \right) a_3 \right),
\end{aligned}$$

with,

$$\begin{aligned}
a_1 &= -2V_{\mathbf{k}_1} \left(\delta_{\mathbf{k}_1,\mathbf{q}} W_{\mathbf{k},\mathbf{k}} A_{\mathbf{k}_1} + \delta_{\mathbf{k}_1,\mathbf{k}} W_{\mathbf{k}_1,\mathbf{q}} A_{\mathbf{q}} \right), \\
a_2 &= V_{\mathbf{k}_1} J_{\mathbf{k},\mathbf{q}} A_{\mathbf{k}_1} - V_{\mathbf{q}} J_{\mathbf{k},\mathbf{k}_1} Z_{\mathbf{q}}, \\
a_3 &= -V_{\mathbf{k}_1} \left(\delta_{\mathbf{k},\mathbf{q}} J_{\mathbf{k},\mathbf{q}} \left(A_{\mathbf{k}_1} + Z_{\mathbf{k}_1} \right) + \delta_{\mathbf{k}_1,\mathbf{q}} \left(2W_{\mathbf{k},\mathbf{k}} Z_{\mathbf{k}_1} + J_{\mathbf{k},\mathbf{k}} \left(A_{\mathbf{k}_1} + Z_{\mathbf{k}_1} \right) \right) \right. , \\
&+ \left. \delta_{\mathbf{k}_1,\mathbf{k}} \left(2W_{\mathbf{k}_1,\mathbf{q}} Z_{\mathbf{q}} + J_{\mathbf{k}_1,\mathbf{q}} \left(A_{\mathbf{q}} + Z_{\mathbf{q}} \right) \right) \right) - V_{\mathbf{q}} J_{\mathbf{k},\mathbf{k}_1} Z_{\mathbf{q}}, \\
a_4 &= V_{\mathbf{k}_1} J_{\mathbf{k},\mathbf{q}} Z_{\mathbf{k}_1} + 2V_{\mathbf{q}} J_{\mathbf{k},\mathbf{k}_1} Z_{\mathbf{q}},
\end{aligned}$$

and $J_{\mathbf{k},\mathbf{q}} = 2V_{\mathbf{k}} V_{\mathbf{q}} Z_{\mathbf{k}}$, $W_{\mathbf{k},\mathbf{q}} = V_{\mathbf{k}} V_{\mathbf{q}} A_{\mathbf{k}}$.In the limit where $U \to \infty$, we have that,

$$\begin{aligned}
\left[\mathcal{S}, \left[\mathcal{S}, \left[\mathcal{S}, \mathcal{H}_V \right]_- \right]_- \right]_- &= \sum_{\sigma} \sum_{\mathbf{k}_2,\mathbf{k}_1,\mathbf{k},\mathbf{q}} \left\{ b_1 n_{f_\sigma} + b_2 c^\dagger_{\mathbf{k}_1,\sigma} c_{\mathbf{k}_2,\sigma} + b_4 n_{f_{-\sigma}} c^\dagger_{\mathbf{k}_1,\sigma} c_{\mathbf{k}_2,\sigma} \right. \\
&+ \left. \left(b_5 + b_7 \right) c^\dagger_{\mathbf{k},-\sigma} c_{\mathbf{q},-\sigma} c^\dagger_{\mathbf{k}_1,\sigma} c_{\mathbf{k}_2,\sigma} + b_8 c^\dagger_{\mathbf{k}_2,\sigma} c_{\mathbf{k}_1,-\sigma} f^\dagger_{-\sigma} f_\sigma \right\}
\end{aligned}$$

Bibliography

[1] S. F. Caballero-Benitez, V. Romero-Rochín, and R. Paredes. Intrinsic decoherence in an ultracold Bose gas confined in a double-well potential. *J. Phys. B: At. Mol. Opt. Phys.*, 43(9):095301, 2010.

[2] S. F. Caballero-Benítez, V. Romero-Rochín, and R. Paredes. Delocalization to self-trapping transition of a Bose fluid confined in a double-well potential: an analysis via one- and two-body correlation properties. *J. Phys. B: At. Mol. Opt. Phys.*, 43(11):115301, 2010.

[3] S. F. Caballero-Benítez, E. A. Ostrovskaya, M. Gulácsí, and Y. S. Kivshar. Macroscopic quantum self-trapping of an ultracold Bose–Fermi mixture in a double-well potential. *J. Phys. B: At. Mol. Opt. Phys.*, 42(21):215308, 2009.

[4] S. F. Caballero-Benítez and E. A. Ostrovskaya. A three-site bose–fermi ring with a few atoms. *J. Phys. B: At. Mol. Opt. Phys.*, 44(13):135301, 2011.

[5] V. I. Balykin, V. G. Minogin, and V. S. Letokhov. Electromagnetic trapping of cold atoms. *Rep. Prog. Phys.*, 63(9):1429, 2000.

[6] N. Masuhara, J. M. Doyle, J. C. Sandberg, D. Kleppner, T. J. Greytak, H. F. Hess, and G. P. Kochanski. Evaporative Cooling of Spin-Polarized Atomic Hydrogen. *Phys. Rev. Lett.*, 61(8):935, 1988.

[7] E. L. Raab, M. Prentiss, A. Cable, S. Chu, and D. E. Pritchard. Trapping of Neutral Sodium Atoms with Radiation Pressure. *Phys. Rev. Lett.*, 59(23):2631, 1987.

[8] F. Dalfovo, S. Giorgini, L. P. Pitaevskii, and S. Stringari. Theory of Bose-Einstein condensation in trapped gases. *Rev. Mod. Phys.*, 71(3):463, 1999.

[9] K. Huang. *Statistical Mechanics*. Wiley, second edition, 1987.

[10] M. H. Anderson, J. R. Ensher, M. R. Matthews, C. E. Wieman, and E. A. Cornell. Observation of Bose-Einstein Condensation in a Dilute Atomic Vapor. *Science*, 269(5221):198, 1995.

[11] C. C. Bradley, C. A. Sackett, J. J. Tollett, and R. G. Hulet. Evidence of Bose-Einstein Condensation in an Atomic Gas with Attractive Interactions. *Phys. Rev. Lett.*, 75(9):1687, 1995.

[12] K. B. Davis, M. O. Mewes, M. R. Andrews, N. J. van Druten, D. S. Durfee, D. M. Kurn, and W. Ketterle. Bose-Einstein Condensation in a Gas of Sodium Atoms. *Phys. Rev. Lett.*, 75(22):3969, 1995.

[13] I. Bloch. Ultracold quantum gases in optical lattices. *Nat. Phys.*, 1(1):23, 2005.

[14] E. Cornell. Very Cold Indeed: The Nanokelvin Physics of Bose-Einstein Condensation. *J. Res. Natl. Inst. Stand. Technol.*, 101:419, 1996.

[15] W. S. Bakr, J. I. Gillen, A. Peng, S. Folling, and M. Greiner. A quantum gas microscope for detecting single atoms in a Hubbard-regime optical lattice. *Nature*, 462(7269):74, 2009.

[16] P. Würtz, T. Langen, T. Gericke, A. Koglbauer, and H. Ott. Experimental Demonstration of Single-Site Addressability in a Two-Dimensional Optical Lattice. *Phys. Rev. Lett.*, 103(8):080404, 2009.

[17] J. Hubbard. Electron Correlations in Narrow Energy Bands. *Proc. R. Soc. Lond. A, Mathematical and Physical Sciences*, 276:238, 1963.

[18] M. P. A. Fisher, P. B. Weichman, G. Grinstein, and D. S. Fisher. Boson localization and the superfluid-insulator transition. *Phys. Rev. B*, 40(1):546, 1989.

[19] Q. Chen, J. Stajic, S. Tan, and K. Levin. BCS-BEC crossover: From high temperature superconductors to ultracold superfluids. *Phys. Rep.*, 412(1):1, 2005.

[20] F. Alet, A. M. Walczak, and M. P. A. Fisher. Exotic quantum phases and phase transitions in correlated matter. *Phys. A: Stat. and Theor. Phys.*, 369(1):122, 2006.

[21] S. Sachdev. Quantum magnetism and criticality. *Nat. Phys.*, 4(3):173, 2008.

[22] G. G. Batrouni, R. T. Scalettar, G. T. Zimanyi, and A. P. Kampf. Supersolids in the Bose-Hubbard Hamiltonian. *Phys. Rev. Lett.*, 74(13):2527, 1995.

[23] G. V. Chester. Speculations on Bose-Einstein Condensation and Quantum Crystals. *Phys. Rev. A*, 2(1):256, 1970.

[24] M. E. Fisher and D. R. Nelson. Spin Flop, Supersolids, and Bicritical and Tetracritical Points. *Phys. Rev. Lett.*, 32(24):1350, 1974.

[25] A. J. Leggett. Can a Solid Be "Superfluid"? *Phys. Rev. Lett.*, 25(22):1543, 1970.

[26] Y. J. Lin, R. L. Compton, K. Jimenez-Garcia, J. V. Porto, and I. B. Spielman. Synthetic magnetic fields for ultracold neutral atoms. *Nature*, 462(7273):628, 2009.

[27] Y.-J. Lin, R. L. Compton, A. R. Perry, W. D. Phillips, J. V. Porto, and I. B. Spielman. Bose-Einstein Condensate in a Uniform Light-Induced Vector Potential. *Phys. Rev. Lett.*, 102(13):130401, 2009.

[28] V. W. Scarola and S. Das Sarma. Emulating non-Abelian topological matter in cold-atom optical lattices. *Phys. Rev. A*, 77(2):023612, 2008.

[29] T. D. Stanescu, V. Galitski, and S. Das Sarma. Topological states in two-dimensional optical lattices. *Phys. Rev. A*, 82(1):013608, 2010.

[30] T. D. Stanescu, V. Galitski, J. Y. Vaishnav, C. W. Clark, and S. Das Sarma. Topological insulators and metals in atomic optical lattices. *Phys. Rev. A*, 79(5):053639, 2009.

[31] A. Y. Kitaev. Fault-tolerant quantum computation by anyons. *Ann. Phys.*, 303(1):2, 2003.

[32] C. Nayak, S. H. Simon, A. Stern, M. Freedman, and S. Das Sarma. Non-Abelian anyons and topological quantum computation. *Rev. Mod. Phys.*, 80(3):1083, 2008.

[33] M. Gustavsson, E. Haller, M. J. Mark, J. G. Danzl, R. Hart, A. J. Daley, and H.-C. Nägerl. Interference of interacting matter waves. *New J. Phys.*, 12(6):065029, 2010.

[34] C. Gross, T. Zibold, E. Nicklas, J. Estève, and M. K. Oberthaler. Nonlinear atom interferometer surpasses classical precision limit. *Nature*, 464(7292):1165, 2010.

[35] M. F. Riedel, P. Böhi, Y. Li, T. W. Hänsch, A. Sinatra, and P. Treutlein. Atom-chip-based generation of entanglement for quantum metrology. *Nature*, 464(7292):1170, 2010.

[36] S. Will, T. Best, U. Schneider, L. Hackermuller, D.-S. Luhmann, and I. Bloch. Time-resolved observation of coherent multi-body interactions in quantum phase revivals. *Nature*, 465(7295):197, 2010.

[37] H. J. Briegel, D. E. Browne, W. Dur, R. Raussendorf, and M. Van den Nest. Measurement-based quantum computation. *Nat. Phys.*, 5:19, 2009.

[38] A. Benseny, S. Fernández-Vidal, J. Bagudà, R. Corbalán, A. Picón, L. Roso, G. Birkl, and J. Mompart. Atomtronics with holes: Coherent transport of an empty site in a triple-well potential. *Phys. Rev. A*, 82(1):013604, 2010.

[39] R. A. Pepino, J. Cooper, D. Z. Anderson, and M. J. Holland. Atomtronic Circuits of Diodes and Transistors. *Phys. Rev. Lett.*, 103(14):140405, 2009.

[40] R. A. Pepino, J. Cooper, D. Meiser, D. Z. Anderson, and M. J. Holland. Open quantum systems approach to atomtronics. *Phys. Rev. A*, 82(1):013640, 2010.

[41] W. H. Zurek. Decoherence and the Transition from Quantum to Classical. *Physics Today*, 44(10):36, 1991.

[42] W. H. Zurek. Decoherence, einselection, and the quantum origins of the classical. *Rev. Mod. Phys.*, 75(3):715, 2003.

[43] S. Sachdev. *Quantum Phase Transitions*. Cambridge University Press, 1999.

[44] A. L. Fetter and J. D. Walecka. *Quantum Theory of Many-Particle Systems*. Dover, New York, 2003.

[45] D. Jaksch, C. Bruder, J. I. Cirac, C. W. Gardiner, and P. Zoller. Cold Bosonic Atoms in Optical Lattices. *Phys. Rev. Lett.*, 81(15):3108, 1998.

[46] M. Albiez, R. Gati, J. Fölling, S. Hunsmann, M. Cristiani, and M. K. Oberthaler. Direct observation of tunneling and nonlinear self-trapping in a single bosonic Josephson junction. *Phys. Rev. Lett.*, 95(1):010402, 2005.

[47] C. Chin, R. Grimm, P. Julienne, and E. Tiesinga. Feshbach resonances in ultracold gases. *Rev. Mod. Phys.*, 82(2):1225, 2010.

[48] J. Fortágh and C. Zimmermann. Magnetic microtraps for ultracold atoms. *Rev. Mod. Phys.*, 79(1):235, 2007.

[49] C. Monroe, W. Swann, H. Robinson, and C. Wieman. Very cold trapped atoms in a vapor cell. *Phys. Rev. Lett.*, 65(13):1571, 1990.

[50] R. A. Duine and H. T. C. Stoof. Atom-molecule coherence in Bose gases. *Phys. Rep.*, 396(3):115, 2004.

[51] I. Bloch, J. Dalibard, and W. Zwerger. Many-body physics with ultracold gases. *Rev. Mod. Phys.*, 80(3):885, 2008.

[52] V. Gurarie and L. Radzihovsky. Resonantly paired fermionic superfluids. *Ann. Phys.*, 322(1):2, 2007.

[53] C. W. Gardiner. Particle-number-conserving bogoliubov method which demonstrates the validity of the time-dependent gross-pitaevskii equation for a highly condensed bose gas. *Phys. Rev. A*, 56(2):1414, 1997.

[54] A. J. Leggett. Bose-Einstein condensation in the alkali gases: Some fundamental concepts. *Rev. Mod. Phys.*, 73(2):307, 2001.

[55] M. Salerno. Matter-wave quantum dots and antidots in ultracold atomic Bose-Fermi mixtures. *Phys. Rev. A*, 72(6):063602, 2005.

[56] E. A. Ostrovskaya, Y. S. Kivshar, M. Lisak, B. Hall, F. Cattani, and D. Anderson. Coupled-mode theory for Bose-Einstein condensates. *Phys. Rev. A*, 61(3):031601, 2000.

[57] R. H. Dicke. Coherence in Spontaneous Radiation Processes. *Phys. Rev.*, 93(1):99, 1954.

[58] A. Smerzi, S. Fantoni, S. Giovanazzi, and S. R. Shenoy. Quantum Coherent Atomic Tunneling between Two Trapped Bose-Einstein Condensates. *Phys. Rev. Lett.*, 79(25):4950, 1997.

[59] J. Bardeen, L. N. Cooper, and J. R. Schrieffer. Theory of Superconductivity. *Phys. Rev.*, 108(5):1175, 1957.

[60] G. D. Mahan. *Many Particle Physics*. Plenum, New York, 3rd edition, 2000.

[61] J. Kondo. Resistance Minimum in Dilute Magnetic Alloys. *Prog. Theor. Phys.*, 32(1):37, 1964.

[62] P. W. Anderson. Localized Magnetic States in Metals. *Phys. Rev.*, 124(1):41, 1961.

[63] S. Giorgini, L. P. Pitaevskii, and S. Stringari. Theory of ultracold atomic Fermi gases. *Rev. Mod. Phys.*, 80(4):1215, 2008.

[64] A. D. Cronin, J. Schmiedmayer, and D. E. Pritchard. Optics and interferometry with atoms and molecules. *Rev. Mod. Phys.*, 81(3):1051, 2009.

[65] D. Ananikian and T. Bergeman. Gross-Pitaevskii equation for Bose particles in a double-well potential: Two-mode models and beyond. *Phys. Rev. A*, 73(1):013604, 2006.

[66] J. Eilbeck. The discrete self-trapping equation. *Physica D*, 16:318, 1985.

[67] R. Franzosi, V. Penna, and R. Zecchina. Quantum dynamics of coupled bosonic wells within the Bose-Hubbard picture. *Int. J. Mod. Phys. B*, 14:943, 2000.

[68] L. Fu and J. Liu. Quantum entanglement manifestation of transition to nonlinear self-trapping for Bose-Einstein condensates in a symmetric double well. *Phys. Rev. A*, 74(6):063614, 2006.

[69] M. Holthaus and S. Stenholm. Coherent control of the self-trapping transition. *Eur. Phys. J. B*, 20(3):451, 2001.

[70] G. J. Milburn, J. Corney, E. M. Wright, and D. F. Walls. Quantum dynamics of an atomic Bose-Einstein condensate in a double-well potential. *Phys. Rev. A*, 55(6):4318, 1997.

[71] R. Paredes. Tunneling of ultracold Bose gases in multiple wells. *Phys. Rev. A*, 73(3):033616, 2006.

[72] R. Paredes and E. Neri. Quantum dynamics of a Bose gas in finite n -well potentials in one dimension. *J. Phys. B: At. Mol. Opt. Phys.*, 42(3):035301, 2009.

[73] S. Raghavan, A. Smerzi, S. Fantoni, and S. R. Shenoy. Coherent oscillations between two weakly coupled Bose-Einstein condensates: Josephson effects, π oscillations, and macroscopic quantum self-trapping. *Phys. Rev. A*, 59(1):620, 1999.

[74] A. P. Tonel, J. Links, and A. Foerster. Behaviour of the energy gap in a model of Josephson coupled Bose–Einstein condensates. *J. Phys. A: Gen. Phys.*, 38(31):6879, 2005.

[75] A. P. Tonel, J. Links, and A. Foerster. Quantum dynamics of a model for two Josephson-coupled Bose–Einstein condensates. *J. Phys. A: Gen. Phys.*, 38(6):1235, 2005.

[76] B. Wu and J. Liu. Commutability between the Semiclassical and Adiabatic Limits. *Phys. Rev. Lett.*, 96(2):020405, 2006.

[77] B. A. Malomed, I. M. Skinner, P. L. Chu, and G. D. Peng. Symmetric and asymmetric solitons in twin-core nonlinear optical fibers. *Phys. Rev. E*, 53(4):4084, 1996.

[78] A. W. Snyder, D. J. Mitchell, L. Poladian, D. R. Rowland, and Y. Chen. Physics of nonlinear fiber couplers. *J. Opt. Soc. Am. B*, 8(10):2102, 1991.

[79] C. Ottaviani, V. Ahufinger, R. Corbalán, and J. Mompart. Adiabatic splitting, transport, and self-trapping of a Bose-Einstein condensate in a double-well potential. *Phys. Rev. A*, 81(4):043621, 2010.

[80] Q. Xie and W. Hai. Quantum entanglement and classical bifurcations in a coupled two-component Bose-Einstein condensate. *Eur. Phys. J. D*, 39(2):277, 2006.

[81] A. Sacchetti. Universal Critical Power for Nonlinear Schrödinger Equations with a Symmetric Double Well Potential. *Phys. Rev. Lett.*, 103(19):194101, 2009.

[82] G. L. Salmond, C. A. Holmes, and G. J. Milburn. Dynamics of a strongly driven two-component Bose-Einstein condensate. *Phys. Rev. A*, 65(3):033623, 2002.

[83] F. T. Arecchi, E. Courtens, R. Gilmore, and H. Thomas. Atomic Coherent States in Quantum Optics. *Phys. Rev. A*, 6(6):2211, 1972.

[84] J. M. Radcliffe. Some properties of coherent spin states. *J. Phys. A: Gen. Phys.*, 4(3):313, 1971.

[85] K. Baumann, C. Guerlin, F. Brennecke, and T. Esslinger. Dicke quantum phase transition with a superfluid gas in an optical cavity. *Nature*, 464(7293):1301, 2010.

[86] O. Castaños, R. López-Peña, J. G. Hirsch, and E. López-Moreno. Classical and quantum phase transitions in the Lipkin-Meshkov-Glick model. *Phys. Rev. B*, 74(10):104118, 2006.

[87] P. Ribeiro, J. Vidal, and R. Mosseri. Exact spectrum of the Lipkin-Meshkov-Glick model in the thermodynamic limit and finite-size corrections. *Phys. Rev. E*, 78(2):021106, 2008.

[88] S. Zöllner, H.-D. Meyer, and P. Schmelcher. Ultracold few-boson systems in a double-well trap. *Phys. Rev. A*, 74(5):053612, 2006.

[89] R. Gati and M. K. Oberthaler. A bosonic Josephson junction. *J. Phys. B: At. Mol. Opt. Phys.*, 40(10):R61, 2007.

[90] A. Auerbach. *Interacting Electrons and Quantum Magnetism*. Springer-Verlag, New York, 1994.

[91] E. Davis. *Quantum Theory of Open Systems*. Academic Press, London, 1976.

[92] F. Haake. *Quantum Satistics and Solid State Physics*. Springer, Berlin, 1973.

[93] R. Kubo, M. Toda, and N. Hashitsume. *Statistical Physics II*. Springer, Berlin, 1985.

[94] A. Redfield. John S. Waugh, Editor: Advances in Magnetic Resonance, Vol. 1. . *B. der Bun. phys. Chem.*, 70(9-10):1181, 1965.

[95] V. Romero-Rochin and I. Oppenheim. Relaxation properties of two-level systems in condensed phases. *Phys. A: Stat. and Theor. Phys.*, 155(1):52, 1989.

[96] M. Schlosshauer. *Decoherence and the Quantum -to- Classical transition*. Springer, Berlin, 2008.

[97] M. O. Scully and M. S. Zubairy. *Quantum Optics*. Cambridge University Press, New York, 1997.

[98] L. van Hove. Quantum-mechanical perturbations giving rise to statistical transport equation. *Physica*, 21:517, 1955.

[99] L. van Hove. The approach to equilibrium in quantum statistics- A perturbation treatment to general order. *Physica*, 23:441, 1957.

[100] R. Zwanzig. *Lectures in Theoretical Physics*. Interscience, New York, 1961.

[101] L. Landau and L. Lifshitz. *Statistical Physics, Part I*. Pergamon, Oxford, 1980.

[102] E. Joos. Why do we observe a classical spacetime? *Phys. Lett. A*, 116(1):6, 1986.

[103] E. Joos and H. D. Zeh. The emergence of classical properties through interaction with the environment. *Z. Phys. B Cond. Mat.*, 59:223, 1985. 10.1007/BF01725541.

[104] J. R. Anglin and A. Vardi. Dynamics of a two-mode Bose-Einstein condensate beyond mean-field theory. *Phys. Rev. A*, 64(1):013605, 2001.

[105] N. Bar-Gill, G. Kurizki, M. Oberthaler, and N. Davidson. Dynamic control and probing of many-body decoherence in double-well Bose-Einstein condensates. *Phys. Rev. A*, 80(5):053613, 2009.

[106] D. A. R. Dalvit, J. Dziarmaga, and W. H. Zurek. Decoherence in Bose-Einstein condensates: Towards bigger and better Schrödinger cats. *Phys. Rev. A*, 62(1):013607, 2000.

[107] G. Gordon. Dynamical decoherence control of multi-partite systems. *J. Phys. B: At. Mol. Opt. Phys.*, 42(22):223001, 2009.

[108] Y. P. Huang and M. G. Moore. Creation, detection, and decoherence of macroscopic quantum superposition states in double-well Bose-Einstein condensates. *Phys. Rev. A*, 73(2):023606, 2006.

[109] Y. Khodorkovsky, G. Kurizki, and A. Vardi. Bosonic Amplification of Noise-Induced Suppression of Phase Diffusion. *Phys. Rev. Lett.*, 100(22):220403, 2008.

[110] J. Ruostekoski and D. F. Walls. Nondestructive optical measurement of relative phase between two Bose-Einstein condensates. *Phys. Rev. A*, 56(4):2996, 1997.

[111] J. Ruostekoski and D. F. Walls. Bose-Einstein condensate in a double-well potential as an open quantum system. *Phys. Rev. A*, 58(1):R50, 1998.

[112] W. Wang, L. B. Fu, and X. X. Yi. Effect of decoherence on the dynamics of Bose-Einstein condensates in a double-well potential. *Phys. Rev. A*, 75(4):045601, 2007.

[113] M. Castagnino, S. Fortin, R. Laura, and O. Lombardi. A general theoretical framework for decoherence in open and closed systems. *Classical and Quantum Gravity*, 25(15):154002, 2008.

[114] M. Castagnino, S. Fortin, and O. Lombardi. Decoherence as a relative phenomenon: a generalization of the spin-bath model. arXiv:0907.1933.

[115] S. Zöllner, H.-D. Meyer, and P. Schmelcher. Correlations in ultracold trapped few-boson systems: Transition from condensation to fermionization. *Phys. Rev. A*, 74(6):063611, 2006.

[116] G. Chen, Z. Chen, and J.-Q. Liang. Ground-state properties for coupled Bose-Einstein condensates inside a cavity quantum electrodynamics. *EPL (Europhysics Letters)*, 80(4):40004, 2007.

[117] Y. Colombe, T. Steinmetz, G. Dubois, F. Linke, D. Hunger, and J. Reichel. Strong atom-field coupling for bose-einstein condensates in an optical cavity on a chip. *Nature*, 450(7167):272, 2007.

[118] J. Larson and J.-P. Martikainen. Ultracold atoms in a cavity-mediated double-well system. *Phys. Rev. A*, 82(3):033606, 2010.

[119] J. Larson, B. Damski, G. Morigi, and M. Lewenstein. Mott-insulator states of ultracold atoms in optical resonators. *Phys. Rev. Lett.*, 100(5):050401, 2008.

[120] R. Jordens, N. Strohmaier, K. Gunter, H. Moritz, and T. Esslinger. A Mott insulator of fermionic atoms in an optical lattice. *Nature*, 455(7210):204, 2008.

[121] M. Köhl, H. Moritz, T. Stöferle, K. Günter, and T. Esslinger. Fermionic Atoms in a Three Dimensional Optical Lattice: Observing Fermi Surfaces, Dynamics, and Interactions. *Phys. Rev. Lett.*, 94(8):080403, 2005.

[122] U. Schneider, L. Hackermüller, S. Will, T. Best, I. Bloch, T. A. Costi, R. W. Helmes, D. Rasch, and A. Rosch. Metallic and Insulating Phases of Repulsively Interacting Fermions in a 3D Optical Lattice. *Science*, 322(5907):1520, 2008.

[123] G. K. Campbell, J. Mun, M. Boyd, P. Medley, A. E. Leanhardt, L. G. Marcassa, D. E. Pritchard, and W. Ketterle. Imaging the Mott Insulator Shells by Using Atomic Clock Shifts. *Science*, 313(5787):649, 2006.

[124] N. Gemelke, X. Zhang, C.-L. Hung, and C. Chin. In situ observation of incompressible Mott-insulating domains in ultracold atomic gases. *Nature*, 460(7258):995, 2009.

[125] F. Gerbier, S. Fölling, A. Widera, O. Mandel, and I. Bloch. Probing number squeezing of ultracold atoms across the superfluid-mott insulator transition. *Phys. Rev. Lett.*, 96(9):090401, 2006.

[126] M. Greiner, O. Mandel, T. Esslinger, T. W. Hansch, and I. Bloch. Quantum phase transition from a superfluid to a Mott insulator in a gas of ultracold atoms. *Nature*, 415(6867):39, 2002.

[127] J. Mun, P. Medley, G. K. Campbell, L. G. Marcassa, D. E. Pritchard, and W. Ketterle. Phase Diagram for a Bose-Einstein Condensate Moving in an Optical Lattice. *Phys. Rev. Lett.*, 99(15):150604, 2007.

[128] I. B. Spielman, W. D. Phillips, and J. V. Porto. Condensate fraction in a 2d bose gas measured across the mott-insulator transition. *Phys. Rev. Lett.*, 100(12):120402, 2008.

[129] B. D. Josephson. Possible new effects in superconductive tunnelling. *Phys. Lett.*, 1(7):251, 1962.

[130] P. W. Anderson. Considerations on the Flow of Superfluid Helium. *Rev. Mod. Phys.*, 38(2):298, 1966.

[131] L. Jiang, G. K. Brennen, A. V. Gorshkov, K. Hammerer, M. Hafezi, E. Demler, M. D. Lukin, and P. Zoller. Anyonic interferometry and protected memories in atomic spin lattices. *Nat. Phys.*, 4(6):482, 2008.

[132] C. Ospelkaus, S. Ospelkaus, K. Sengstock, and K. Bongs. Interaction-Driven Dynamics of ^{40}K $-^{87}$ Rb Fermion-Boson Gas Mixtures in the Large-Particle-Number Limit. *Phys. Rev. Lett.*, 96(2):020401, 2006.

[133] F. Ferlaino, C. D'Errico, G. Roati, M. Zaccanti, M. Inguscio, G. Modugno, and A. Simoni. Feshbach spectroscopy of a $K-Rb$ atomic mixture. *Phys. Rev. A*, 73(4):040702, 2006.

[134] G. Roati, F. Riboli, G. Modugno, and M. Inguscio. Fermi-Bose Quantum Degenerate ^{40}K $-^{87}$ Rb Mixture with Attractive Interaction. *Phys. Rev. Lett.*, 89(15):150403, 2002.

[135] F. Schreck, L. Khaykovich, K. L. Corwin, G. Ferrari, T. Bourdel, J. Cubizolles, and C. Salomon. Quasipure Bose-Einstein Condensate Immersed in a Fermi Sea. *Phys. Rev. Lett.*, 87(8):080403, 2001.

[136] C. Silber, S. Günther, C. Marzok, B. Deh, P. W. Courteille, and C. Zimmermann. Quantum-Degenerate Mixture of Fermionic Lithium and Bosonic Rubidium Gases. *Phys. Rev. Lett.*, 95(17):170408, 2005.

[137] C. A. Stan, M. W. Zwierlein, C. H. Schunck, S. M. F. Raupach, and W. Ketterle. Observation of Feshbach Resonances between Two Different Atomic Species. *Phys. Rev. Lett.*, 93(14):143001, 2004.

[138] C. Lee, T. J. Alexander, and Y. S. Kivshar. Melting of Discrete Vortices via Quantum Fluctuations. *Phys. Rev. Lett.*, 97(18):180408, 2006.

[139] K. B. Blagoev and K. S. Bedell. Luttinger Theorem in One Dimensional Metals. *Phys. Rev. Lett.*, 79(6):1106, 1997.

[140] J. M. Luttinger. Fermi surface and some simple equilibrium properties of a system of interacting fermions. *Phys. Rev.*, 119(4):1153, 1960.

[141] M. Zaccanti, C. D'Errico, F. Ferlaino, G. Roati, M. Inguscio, and G. Modugno. Control of the interaction in a Fermi-Bose mixture. *Phys. Rev. A*, 74(4):041605, 2006.

[142] W. H. Press, B. P. Flannery, S. A. Teukolsky, and E. T. Vetterling. *Numerical Recipes in C: The Art of Scientific Computing*. Cambridge University Press, Cambridge, 1992.

[143] M. Cramer, J. Eisert, and F. Illuminati. Inhomogeneous Atomic Bose-Fermi Mixtures in Cubic Lattices. *Phys. Rev. Lett.*, 93(19):190405, 2004.

[144] I. Brouzos, S. Zöllner, and P. Schmelcher. Correlation versus commensurability effects for finite bosonic systems in one-dimensional lattices. *Phys. Rev. A*, 81(5):053613, 2010.

[145] P. Zin, B. Oleś, and K. Sacha. Huge quantum particle number fluctuations in a two-component Bose gas in a double-well potential. arXiv:1004.1541v1 (2010).

[146] I. Brouzos, S. Zöllner, and P. Schmelcher. Correlation versus commensurability effects for finite bosonic systems in one-dimensional lattices. *Phys. Rev. A*, 81(5):053613, 2010.

[147] L. D. Carr and M. J. Holland. Quantum phase transitions in the Fermi–Bose Hubbard model. *Phys. Rev. A*, 72(3):031604, 2005.

[148] D.-S. Lühmann, K. Bongs, K. Sengstock, and D. Pfannkuche. Localization and delocalization of ultracold bosonic atoms in finite optical lattices. *Phys. Rev. A*, 77(2):023620, 2008.

[149] F. Zhou and C. Wu. Quantum dynamics, particle delocalization and instability of Mott states: the effect of fermion–boson conversion on Mott states. *New J. Phys.*, 8(8):166, 2006.

[150] F. D. M. Haldane. Model for a Quantum Hall Effect without Landau Levels: Condensed-Matter Realization of the "Parity Anomaly". *Phys. Rev. Lett.*, 61(18):2015, 1988.

[151] G. Juzeliūnas and P. Öhberg. Slow Light in Degenerate Fermi Gases. *Phys. Rev. Lett.*, 93(3):033602, 2004.

[152] A. S. Sørensen, E. Demler, and M. D. Lukin. Fractional Quantum Hall States of Atoms in Optical Lattices. *Phys. Rev. Lett.*, 94(8):086803, 2005.

[153] S.-L. Zhu, H. Fu, C.-J. Wu, S.-C. Zhang, and L.-M. Duan. Spin Hall Effects for Cold Atoms in a Light-Induced Gauge Potential. *Phys. Rev. Lett.*, 97(24):240401, 2006.

[154] F. Hébert, F. Haudin, L. Pollet, and G. G. Batrouni. Mott insulators and correlated superfluids in ultracold Bose-Fermi mixtures. *Phys. Rev. A*, 76(4):043619, 2007.

[155] A. Kitaev. Anyons in an exactly solved model and beyond. *Ann. Phys.*, 321(1):2, 2006.

[156] D. M. Eagles. Possible pairing without superconductivity at low carrier concentrations in bulk and thin-film superconducting semiconductors. *Phys. Rev.*, 186(2):456, 1969.

[157] A. J. Leggett. *in Modern trends in the theory of condensed matter : proceedings of the XVI Karpacz Winter School of Theoretical Physics*. Springer-Verlag, Berlin ; New York :, 1980.

[158] S. Jochim, M. Bartenstein, A. Altmeyer, G. Hendl, S. Riedl, C. Chin, J. Hecker Denschlag, and R. Grimm. Bose-Einstein Condensation of Molecules. *Science*, 302(5653):2101, 2003.

[159] C. A. Regal, M. Greiner, and D. S. Jin. Observation of Resonance Condensation of Fermionic Atom Pairs. *Phys. Rev. Lett.*, 92(4):040403, 2004.

[160] C. Chin, M. Bartenstein, A. Altmeyer, S. Riedl, S. Jochim, J. H. Denschlag, and R. Grimm. Observation of the Pairing Gap in a Strongly Interacting Fermi Gas. *Science*, 305(5687):1128, 2004.

[161] M. W. Zwierlein, J. R. Abo-Shaeer, A. Schirotzek, C. H. Schunck, and W. Ketterle. Vortices and superfluidity in a strongly interacting Fermi gas. *Nature*, 435(7045):1047, 2005.

[162] A. A. Abrikosov. On the Magnetic Properties of Superconductors of the Second Group. *Soviet Physics JETP*, 5(6):1174, 1957.

[163] J. Kinast, A. Turlapov, J. E. Thomas, Q. Chen, J. Stajic, and K. Levin. Heat Capacity of a Strongly Interacting Fermi Gas. *Science*, 307(5713):1296, 2005.

[164] H. Heiselberg. Fermi systems with long scattering lengths. *Phys. Rev. A*, 63(4):043606, 2001.

[165] T.-L. Ho. Universal Thermodynamics of Degenerate Quantum Gases in the Unitarity Limit. *Phys. Rev. Lett.*, 92(9):090402, 2004.

[166] H. Hu, P. D. Drummond, and X.-J. Liu. Universal thermodynamics of strongly interacting Fermi gases. *Nat. Phys.*, 3(7):469, 2007.

[167] J. P. Gaebler, J. T. Stewart, T. E. Drake, D. S. Jin, A. Perali, P. Pieri, and G. C. Strinati. Observation of pseudogap behaviour in a strongly interacting Fermi gas. *Nat. Phys.*, 6(8):569, 2010.

[168] J. T. Stewart, J. P. Gaebler, and D. S. Jin. Using photoemission spectroscopy to probe a strongly interacting Fermi gas. *Nature*, 454(7205):744, 2008.

[169] S. Giorgini, L. P. Pitaevskii, and S. Stringari. Theory of ultracold atomic Fermi gases. *Rev. Mod. Phys.*, 80(4):1215, 2008.

[170] E. Burovski, N. Prokof'ev, B. Svistunov, and M. Troyer. Critical Temperature and Thermodynamics of Attractive Fermions at Unitarity. *Phys. Rev. Lett.*, 96(16):160402, 2006.

[171] P. Nozières and S. Schmitt-Rink. Bose condensation in an attractive fermion gas: From weak to strong coupling superconductivity. *J. Low Temp. Phys.*, 59(3):195, 1985.

[172] A. Bulgac, J. E. Drut, and P. Magierski. Quantum Monte Carlo simulations of the BCS-BEC crossover at finite temperature. *Phys. Rev. A*, 78(2):023625, 2008.

[173] J. Carlson, S.-Y. Chang, V. R. Pandharipande, and K. E. Schmidt. Superfluid Fermi Gases with Large Scattering Length. *Phys. Rev. Lett.*, 91(5):050401, 2003.

[174] S. Y. Chang, V. R. Pandharipande, J. Carlson, and K. E. Schmidt. Quantum Monte Carlo studies of superfluid Fermi gases. *Phys. Rev. A*, 70(4):043602, 2004.

[175] R. Jáuregui, R. Paredes, and G. T. Sánchez. BEC-BCS crossover of a trapped Fermi gas without using the local density approximation. *Phys. Rev. A*, 76(1):011604, 2007.

[176] A. Perali, P. Pieri, and G. C. Strinati. Quantitative Comparison between Theoretical Predictions and Experimental Results for the BCS-BEC Crossover. *Phys. Rev. Lett.*, 93(10):100404, 2004.

[177] K. Huang and C. N. Yang. Quantum-Mechanical Many-Body Problem with Hard-Sphere Interaction. *Phys. Rev.*, 105(3):767, 1957.

[178] T. D. Lee and C. N. Yang. Many-Body Problem in Quantum Mechanics and Quantum Statistical Mechanics. *Phys. Rev.*, 105(3):1119, 1957.

[179] T. D. Lee and C. N. Yang. Many-body problem in quantum mechanics and quantum statistical mechanics. *Phys. Rev.*, 105(3):1119, 1957.

[180] A. Bulgac, J. E. Drut, and P. Magierski. Spin 1/2 Fermions in the Unitary Regime: A Superfluid of a New Type. *Phys. Rev. Lett.*, 96(9):090404, 2006.

[181] G. M. Falco and H. T. C. Stoof. Dressed molecules in resonantly interacting ultracold atomic Fermi gases. *Phys. Rev. A*, 75(2):023612, 2007.

[182] P. W. Anderson. Random-Phase Approximation in the Theory of Superconductivity. *Phys. Rev.*, 112(6):1900, 1958.

[183] A. A. Abrikosov. Electron Scattering on Magnetic Impurities in Metals. *Physics*, 2:5, 1965.

[184] A. C. Hewson. *The Kondo Problem to Heavy Fermions*. Cambridge University Press, Cambridge, 1993.

[185] A. M. Tsvelick and P. B. Wiegmann. Exact solution of the Anderson model. II. Thermodynamic properties at finite temperatures. *J. Phys. C: Solid State Phys.*, 16(12):2321, 1983.

[186] P. B. Wiegmann and A. M. Tsvelick. Exact solution of the Anderson model: I. *J. Phys. C: Solid State Phys.*, 16(12281), 1983.

[187] H. R. Krishna-murthy, J. W. Wilkins, and K. G. Wilson. Renormalization-group approach to the Anderson model of dilute magnetic alloys. I. Static properties for the symmetric case. *Phys. Rev. B*, 21(3):1003, 1980.

[188] H. R. Krishna-murthy, J. W. Wilkins, and K. G. Wilson. Renormalization-group approach to the Anderson model of dilute magnetic alloys. II. Static properties for the asymmetric case. *Phys. Rev. B*, 21(3):1044, 1980.

[189] G. Ortiz and J. Dukelsky. BCS-to-BEC crossover from the exact BCS solution. *Phys. Rev. A*, 72(4):043611, 2005.

[190] P. D. Drummond and K. V. Kheruntsyan. Coherent molecular bound states of bosons and fermions near a Feshbach resonance. *Phys. Rev. A*, 70(3):033609, 2004.

[191] M. Holland, S. J. J. M. F. Kokkelmans, M. L. Chiofalo, and R. Walser. Resonance Superfluidity in a Quantum Degenerate Fermi Gas. *Phys. Rev. Lett.*, 87(12):120406, 2001.

[192] Y. Ohashi and A. Griffin. BCS-BEC Crossover in a Gas of Fermi Atoms with a Feshbach Resonance. *Phys. Rev. Lett.*, 89(13):130402, 2002.

[193] E. Timmermans, K. Furuya, P. W. Milonni, and A. K. Kerman. Prospect of creating a composite Fermi-Bose superfluid. *Phys. Lett. A*, 285(3-4):228, 2001.

[194] J. R. Schrieffer and P. A. Wolff. Relation between the Anderson and Kondo Hamiltonians. *Phys. Rev.*, 149(2):491, 1966.

[195] C. Zener. Interaction Between the d Shells in the Transition Metals. *Phys. Rev.*, 81(3):440, 1951.

[196] K. G. Wilson. The renormalization group: Critical phenomena and the Kondo problem. *Rev. Mod. Phys.*, 47(4):773, 1975.

[197] F. D. M. Haldane. Scaling Theory of the Asymmetric Anderson Model. *Phys. Rev. Lett.*, 40(6):416, 1978.

[198] J. Martinek, M. Sindel, L. Borda, J. Barnasacute, J. König, G. Schön, and J. von Delft. Kondo Effect in the Presence of Itinerant-Electron Ferromagnetism Studied with the Numerical Renormalization Group Method. *Phys. Rev. Lett.*, 91(24):247202, 2003.

[199] M. Wagner. *Unitary Transformations in Solid State Physics.* Amsterdam: North-Holland, 1986.

[200] R. Chan and M. Gulácsi. The exact Schrieffer–Wolff transformation. *Phil. Mag.*, 84(12):1265, 2004.

[201] R. Y. Chang. *Canonical Perturbative Approach to Strongly Correlated Systems.* PhD thesis, Australian National University, 2004.

[202] J. Zaanen and A. M. Olesacute. Canonical perturbation theory and the two-band model for high-T_{c} superconductors. *Phys. Rev. B*, 37(16):9423, 1988.

[203] M. J. Davis, S. J. Thwaite, M. K. Olsen, and K. V. Kheruntsyan. Pairing mean-field theory for the dynamics of dissociation of molecular Bose-Einstein condensates. *Phys. Rev. A*, 77(2):023617, 2008.

[204] D. A. Butts and D. S. Rokhsar. Trapped Fermi gases. *Phys. Rev. A*, 55(6):4346, 1997.

[205] L. Salasnich. Ideal quantum gases in D-dimensional space and power-law potentials. *J. Math. Phys.*, 41(12):8016, 2000.

[206] H. Bruus and K. Flensberg. *Many-Body Quantum Theory in Condensed Matter Physics.* Oxford University Press, 2004.

[207] P. Coleman. New approach to the mixed-valence problem. *Phys. Rev. B*, 29(6):3035, 1984.

[208] C. M. Varma and Y. Yafet. Magnetic susceptibility of mixed-valence rare-earth compounds. *Phys. Rev. B*, 13(7):2950, 1976.

[209] Z. Gulácsi and D. Vollhardt. Exact Insulating and Conducting Ground States of a Periodic Anderson Model in Three Dimensions. *Phys. Rev. Lett.*, 91(18):186401, 2003.

[210] F. D. M. Haldane. New model for the mixed-valence phenomenon in rare-earth materials. *Phys. Rev. B*, 15(5):2477, 1977.

[211] T. Lahaye, T. Pfau, and L. Santos. Mesoscopic Ensembles of Polar Bosons in Triple-Well Potentials. *Phys. Rev. Lett.*, 104(17):170404, 2010.

[212] C. Gross, T. Zibold, E. Nicklas, J. Estève, and M. K. Oberthaler. Nonlinear atom interferometer surpasses classical precision limit. *Nature*, 464(7292):1165, 2010.

[213] G. B. Jo, Y. Shin, S. Will, T. A. Pasquini, M. Saba, W. Ketterle, D. E. Pritchard, M. Vengalattore, and M. Prentiss. Long Phase Coherence Time and Number Squeezing of Two Bose-Einstein Condensates on an Atom Chip. *Phys. Rev. Lett.*, 98(3):030407, 2007.

[214] T. Schumm, S. Hofferberth, L. M. Andersson, S. Wildermuth, S. Groth, I. Bar-Joseph, J. Schmiedmayer, and P. Kruger. Matter-wave interferometry in a double well on an atom chip. *Nat. Phys.*, 1(1):57, 2005.

[215] Y. Shin, G. B. Jo, M. Saba, T. A. Pasquini, W. Ketterle, and D. E. Pritchard. Optical Weak Link between Two Spatially Separated Bose-Einstein Condensates. *Phys. Rev. Lett.*, 95(17):170402, 2005.

[216] L. J. LeBlanc, A. B. Bardon, J. McKeever, M. H. T. Extavour, D. Jervis, J. H. Thywissen, F. Piazza, and A. Smerzi. Dynamics of a tunable superfluid junction. arXiv:1006.3550v2.

[217] M. Freedman, C. Nayak, and K. Shtengel. Extended Hubbard Model with Ring Exchange: A Route to a Non-Abelian Topological Phase. *Phys. Rev. Lett.*, 94(6):066401, 2005.

[218] P. Fulde, K. Penc, and N. Shannon. Fractional charges in pyrochlore lattices. *Ann. Phys.*, 11(12):892, 2002.

[219] R. Moessner and S. L. Sondhi. Resonating Valence Bond Phase in the Triangular Lattice Quantum Dimer Model. *Phys. Rev. Lett.*, 86(9):1881, 2001.

[220] I. Titvinidze, M. Snoek, and W. Hofstetter. Supersolid Bose-Fermi Mixtures in Optical Lattices. *Phys. Rev. Lett.*, 100(10):100401, 2008.

[221] H. P. Büchler and G. Blatter. Supersolid versus Phase Separation in Atomic Bose-Fermi Mixtures. *Phys. Rev. Lett.*, 91(13):130404, 2003.

[222] P. P. Orth, D. L. Bergman, and K. Le Hur. Supersolidity of cold-atom Bose-Fermi mixtures in optical lattices. *Phys. Rev. A*, 80(2):023624, 2009.